Constraints on microbial pesticide degradation in soils

Dissertation to obtain the doctoral degree of Agricultural Sciences

(Dr. sc. agr.)

Faculty of Agricultural Sciences

University of Hohenheim

Institute of Soil Science and Land Evaluation

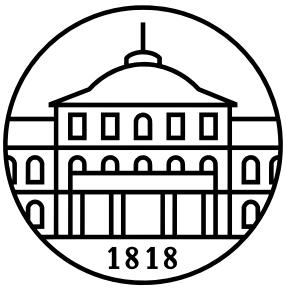

submitted by

Johannes Wirsching

from Kottweil-Berglen, Baden-Würrtemberg, Germany

2023

This thesis was accepted as a doctoral dissertation in fulfillment of the requirements for the degree "Doktor der Agrarwissenschaften" by the Faculty of Agricultural Sciences at the University of Hohenheim on 20th of October 2022.

Date of examination:	20th of April 2023
Dean of Faculty:	Prof. Dr. Ralf Vögele

Eximation committee

Head of comittee:	Prof. Dr. Uwe Ludewig
1st examiner and reviewer:	Prof. Dr. Elen Kandeler
2nd examiner and reviewer:	Prof. Dr. Marcus Andreas Horn
3nd examiner:	Prof. Dr. Georg Cadisch

Contents

List of Figures

List of Tables

1 Summary

Pesticides are an essential component of intensified agriculture and have contributed significantly to the increase in food production observed in recent decades. Since 1960,

pesticide use has increased by a factor of fifteen to twenty, representing a market value of $40 billion in 2016. Soil monitoring campaigns to track pesticide contamination of croplands across Europe are quantifying pesticide residues whose residence times in soils exceed expected values. Diffuse contamination by pesticide residues raises concerns about soil functions, soil biodiversity, and food safety, as well as the transport of contaminants by wind and water to surface waters or to adjacent, organically managed croplands. Data on the frequency of occurrence and concentrations of pesticide residues in soil demonstrate a discrepancy between the determination of persistence and subsequent approval and their actual fate in soil. This raises the question of whether degradability of individual organic compounds has been adequately studied. Microbiological degradation is the most important process for reducing pesticide loads in soils. A reliable estimate of pesticide residence time requires an expanded understanding of the factors limiting microbial degradation. Degradation of anthropogenic organic chemicals in soils occurs much more slowly than would be expected based on their physicochemical properties. While processes that determine the fate of pesticides in soil have often been studied at different spatial and temporal scales, reasons for discrepancies between the observed complete degradation of pesticides under laboratory conditions and their persistence in the field remain unclear. This thesis addresses this challenge by focusing on the central question of why inherently biodegradable compounds in soils display increased persistence under field conditions. Organic contaminants in low but detectable and environmentally significant concentrations could remain in the soil once available concentrations fall below a threshold where bioenergetic growth restrictions come into play. In addition, potential microbial and biophysical limitations and environmental factors such as soil temperature and soil moisture are often examined separately in current degradation studies. Combinations of temperature and soil moisture changes associated with different concentration levels have been less well examined, resulting in an incomplete understanding of the degradation process. Another key factor in the demonstrated discrepancy between predicted and actual

persistence in the field could be due to laboratory experiments that cannot account for field-scale processes. Therefore, degradation rates determined in laboratory experiments cannot be confidently extrapolated to the field scale. This thesis presents new results on concentration-dependent degradation of pesticides, extends our understanding of the influencing variables of temperature and soil moisture, and highlights the importance of soil structure and precipitation events for the transport and subsequent microbial degradation of pesticides in a field experiment.

In order to identify additional degradation processes, three studies were conducted in this thesis, using either a highly mobile (2-methyl-4-chlorophenoxyacetic acid; MCPA) or an immobile herbicide (*N*-phosphonomethylglycine; glyphosate) as a model compound. In the first study, microbial degradation of 30, 50, 100, 500, 1000, 5000, and 20000 $\mu g\,kg^{-1}$ ^{14}C-labeled MCPA was examined in an incubation experiment (37 days) to determine a concentration threshold below which MCPA degradation ceases. To quantify the abundances of microorganisms involved in MCPA degradation as well as their degradation activity, copy numbers of the *tfdA* gene (DNA) and transcripts (mRNA) were determined by quantitative real-time PCR. DT_{50} values derived from the cumulative ^{14}C mineralization curves were used as parameters for the degradation rates. Quantification of microbial activity revealed an increase in gene expression between 1,000 and 5,000 $\mu g\,kg^{-1}$. An actual increase in *tfdA*-harboring microorganisms could only be detected at a concentration of 20,000 $\mu g\,kg^{-1}$. Concentrations of $\geq$ 1,000 $\mu g\,kg^{-1}$ were associated with delayed mineralization during the first five days. This can be attributed to inefficient MCPA degradation in the initial phase; the substrate concentration exceeded the available degradation potential and could only be converted more rapidly after a subsequent increase in degraders. Degradation of concentrations of $\leq$ 1,000 $\mu g\,kg^{-1}$ followed first-order kinetics, independent of microbial abundance. Consequently, contrary to our hypothesis, the persistence of pesticides at low concentrations cannot be explained by the absence of functional gene expression, yet this study extends previous understanding

of MCPA degradation by providing evidence for concentration-dependent dynamics of degradation and regulation of the *tfdA* gene.

In the second part of this thesis, the roles of soil temperature (10°C and 20°C) and soil moisture content (pF 1.8 and pF 3.5) in the degradation of two MCPA concentrations, 1 and 20 $mg\,kg^{-1}$, were examined by applying the microbiological analyses presented in the first study. An incubation experiment (28 days) and gene-based modeling to support data interpretation found that under colder (10°C) and drier conditions (pF 3.5), microbial MCPA degradation was limited to a greater extent at 20 $mg\,kg^{-1}$ than at 1 $mg\,kg^{-1}$. Under limiting conditions, there was a metabolic shift toward anabolic utilization of MCPA-derived carbon (C), reflected in increased carbon use efficiency (CUE), and ^{14}C mineralization was no longer linearly related to the actual MCPA dissipation. This discrepancy was determined from the DT_{50} values derived from the ^{14}C-mineralization curves, which predict a longer residence time compared to total MCPA dissipation. Moreover, it was shown that the influence of environmental conditions on microbial degradation strongly depends on the initial MCPA concentration and that DT_{50} values should be derived from the total MCPA decline.

The third study examined the translocation of ^{13}C-labeled glyphosate in a 21-day field experiment following simulated rain events along shrinkage cracks formed in a clay-rich soil after a preceding dry period. Microbial degradation potential and activity in a 50 cm deep profile were assessed by quantifying the functional genes *goxA* and *sarc*, which are involved in the degradation of glyphosate to AMPA or sarcosine, respectively. In addition, the incorporation of ^{13}C into phospholipid fatty acids as biomarkers for $Gram^-$ and $Gram^+$ bacteria and fungi allowed us to draw conclusions about the participation of the main soil microbial groups in degradation. The occurrence of preferential flow pathways was identified as the dominant transport pathway for highly sorptive glyphosate in conjunction with simulated rainfall events. In contrast to bulk soil samples, in which degradation of glyphosate to AMPA dominated, enhanced degradation to sarcosine was

observed in shrinkage cracks. In both soil compartments, significantly more involvement of fungi than of Gram$^+$ bacteria was observed during the initial phase of glyphosate degradation. This ratio shifted over time toward Gram$^+$ bacteria, which eventually dominated glyphosate degradation. Gram$^-$ bacteria had a constant but comparatively lower degradation participation rate. Our results suggest a succession of the three microbial groups involved in glyphosate degradation, with fungi initiating glyphosate degradation and facilitating further degradation by bacteria.

This dissertation identified further important regulatory mechanisms for microbially mediated pesticide degradation. The previously unknown concentration-dependent degradation dynamics and the concentration-dependent influence of limiting environmental conditions on microbial degradation emphasize the importance of studies using a realistic concentration range. Evidence of deep transport of a highly sorptive pesticide such as glyphosate primarily via preferential flow pathways into the subsoil with lower degradation dynamics underscores the need to include processes that can only be verified in field studies as part of risk assessments. The results of this thesis suggest that the biodegradation rates of pesticides are not homogeneous at field scales and may account in part for the discrepancy between complete degradation of pesticides under laboratory conditions and their persistence in the field. Laboratory studies in which soil samples are pooled and mixed to obtain a single "representative" sample can provide a simplified understanding of the process, but the complexity, particularly that of soil heterogeneity, of pesticide distribution and microbial degradation associated with prevailing climatic conditions, requires calibration of previously used methods in field studies and possibly at landscape, watershed, or regional scales. The scale-dependent degradation aspect will become even more important in the future; as soil properties and processes that control the toxicological aspects of contaminants include temperature and moisture, and changes associated with climate change will lead to an increase in extreme precipitation, longer dry periods, and soil erosion.

2 Zusammenfassung

Pestizide sind ein wesentlicher Bestandteil der intensivierten Landwirtschaft und haben erheblich zu dem in den letzten Jahrzehnten beobachteten Anstieg der Nahrungsmittelproduktion beigetragen. Seit 1960 ist der Einsatz von Pestiziden um das Fünfzehn- bis Zwanzigfache gestiegen, was einem Marktwert von 40 Milliarden Dollar im Jahr 2016 entspricht. Im Rahmen von Bodenmonitoring-Kampagnen zur Erfassung der Pestizidbelastung von Anbauflächen in ganz Europa werden Pestizidrückstände quantifiziert, deren Verweildauer in Böden die Erwartungswerte überschreiten und auf eine mögliche Akkumulation hinweisen. Die diffuse Kontamination von Böden durch Pestizidrückstände gibt Anlass zu Bedenken hinsichtlich der Bodenfunktionen, der biologischen Vielfalt des Bodens und der Lebensmittelsicherheit sowie des Transports von Schadstoffen durch Wind- und Wassererosion in Oberflächengewässer oder angrenzende, ökologisch bewirtschaftete Anbauflächen. Die Daten über die Häufigkeit des Auftretens und die Höhe der Konzentrationen von Pestizidrückständen belegen eine Diskrepanz zwischen der in Vorstudien ermittelten Verweilzeit und der späteren Zulassung und werfen die Frage auf, ob die Abbaubarkeit einzelner, organischer Verbindungen hinreichend untersucht wurde. Der mikrobiologische Abbau ist der wichtigste Prozess zur Verringerung der Pestizidbelastung in Böden. Eine zuverlässigere Abschätzung der Persistenz von Pestiziden erfordert ein erweitertes Verständnis der begrenzenden Faktoren des mikrobiellen Abbaus. Obgleich die Prozesse, die den Verbleib von Pestiziden im Boden kontrollieren, häufig auf verschiedenen räumlichen und zeitlichen Ebenen untersucht wurden, ist die Diskrepanz zwischen dem vollständigen Abbau von Pestiziden unter Laborbedingungen und ihrer Persistenz im Feld noch immer nicht abschließend geklärt. Die vorliegende Dissertation behandelt die zentrale Frage, warum biologisch abbaubare Verbindungen in Böden unter Feldbedingungen eine erhöhte Persistenz aufweisen. Organische Schadstoffe in geringen, aber nachweisbaren und umweltrelevanten Konzentrationen könnten im Boden verbleiben, sobald die verfügbaren Konzentrationen unter einen Schwellenwert fallen, bei

dem bioenergetische Wachstumsbeschränkungen zum Tragen kommen. Darüber hinaus werden potenzielle mikrobielle und biophysikalische Beschränkungen und Umweltfaktoren wie Bodentemperatur und Bodenwassergehalt in aktuellen Abbaustudien häufig getrennt untersucht, nicht aber eine Kombination von Temperatur- und Bodenwassergehaltsänderungen auf den Abbau von umweltrelevanter Pestizidkonzentrationen, was zu einem bislang unvollständigen Verständnis des Abbauprozesses beitragen kann. Ein weiteres Schlüsselelement für die Inkongruenz zwischen vorhergesagter und in Feldstudien ermittelter Persistenz könnte auf die Art und den Umfang der Abbaustudien zurückzuführen sein. In Laborexperimenten ermittelte Abbauprozesse lassen sich nicht ohne weiteres auf den Feldmaßstab übertragen. Aus diesen Gründen werden in dieser Thesis neue Ergebnisse zum konzentrationsabhängigen Abbau von Pestiziden vorgestellt, das Verständnis der Einflussgrößen Temperatur und Bodenwassergehalt erweitert und die Bedeutung von Bodenstruktur und Niederschlags-ereignissen für den Transport und den anschließenden mikrobiellen Abbau in einem Feldexperiment hervorgehoben.

Um weitere Abbauprozesse zu entschlüsseln, wurden in dieser Dissertation drei Studien mit einem hochmobilen (2-Methyl-4-Chlorphenoxyessigsäure; MCPA) beziehungsweise einem immobilen Herbizid (*N*-Phosphonomethylglycin; Glyphosat) als Modellverbindung durchgeführt. In der ersten Studie wurde in einem Inkubationsversuch (37 Tage) der mikrobielle Abbau von 30, 50, 100, 500, 1000, 5000 und 20000 $\mu g\,kg^{-1}$ ^{14}C-markiertem MCPA untersucht. Auf diese Weise sollte eine Konzentrationsschwelle bestimmt werden, unterhalb derer funktionale Gene, die an dem Abbauweg beteiligt sind, nicht mehr exprimiert werden und der MCPA Abbau zum Stillstand kommt. Um die Häufigkeit der Mikroorganismen, die am MCPA-Abbau beteiligt sind und deren Abbauaktivität zu quantifizieren, wurden die Kopienzahl des *tfdA*-Gens (DNA) und die Transkripte (mRNA) durch quantitative Echtzeit-PCR bestimmt. Die aus der kumulativen ^{14}C-Mineralisierungskurve abgeleiteten DT_{50}-Werte wurden als Parameter für die Abbaugeschwindigkeit herangezogen. Die Quantifizierung der mikrobiellen Aktivität, ergab

einen Anstieg der Genexpression zwischen 1,000 und 5,000 µg kg^{-1}. Ein tatsächlicher Anstieg der *tfdA*-tragenden Mikroorganismen konnte erst bei einer Konzentration von 20,000 µg kg^{-1} festgestellt werden. Konzentrationen von ≥1,000 µg kg^{-1} waren in den ersten fünf Tagen mit einer verzögerten Mineralisierung verbunden. Ursache hierfür war ein ineffizienter MCPA-Abbau in der Anfangsphase, da die Substratkonzentration das vorhandene Abbaupotenzial überstieg und erst nach einer anschließenden Erhöhung der mikrobiellen Abbauer schneller umgesetzt werden konnte. Der Abbau von Konzentrationen von ≤1,000 µg kg^{-1} folgte einer Kinetik erster Ordnung, unabhängig von der vorhandenen mikrobiellen Abundanz. Folglich kann die Persistenz von Pestiziden in niedrigen Konzentrationen nicht durch das Fehlen einer funktionellen Genexpression erklärt werden. Trotz der widerlegten Hypothese eines durch die Genexpression beschränkten MCPA-Abbaus unterhalb einer bestimmten Konzentrationsschwelle erweitert diese Studie das bisherige Verständnis des MCPA-Abbaus, indem sie Beweise für eine konzentrationsabhängige Abbaudynamik und die Regulierung des *tfdA*-Gens liefert.

Im zweiten Teil dieser Arbeit wird die Rolle der Bodentemperatur (10°C und 20°C) und des Bodenwassergehalts (pF 1.8 und pF 3.5) für den Abbau von zwei MCPA-Konzentrationen von 1 und 20 mg kg^{-1} anhand der in der ersten Studie vorgestellten mikrobiologischen Analysen untersucht. Ein Inkubationsexperiment (28 Tage) und eine genbasierte Modellierung zur Unterstützung der Dateninterpretation ergaben, dass unter kälteren (10°C) und trockeneren Bedingungen (pF 3.5) der mikrobielle MCPA-Abbau bei 20 mg kg^{-1} in einem stärkeren Maße eingeschränkt war als bei 1 mg kg^{-1}. Unter limitierenden Bedingungen kam es zu einer Verschiebung des Stoffwechsels hin zu einer anabolen Nutzung von MCPA-abgeleitetem Kohlenstoff, was sich in einer erhöhten Kohlenstoffnutzungseffizienz (engl. carbon use efficiency (CUE)) niederschlug, so dass die ^{14}C-Mineralisierung nicht mehr in einem linearen Verhältnis zur tatsächlichen MCPA-Abnahme stand. Diese Diskrepanz ist aus den ^{14}C-Mineralisierungskurven abgeleiteten DT_{50}-Werten ersichtlich, die eine längere Verweilzeit im Vergleich zur gesamten MCPA-

Abnahme vorhersagen. Die Studie kommt zu dem Schluss, dass die Größenordnung der Wechselwirkung zwischen Bodentemperatur und Wassergehalt und dem mikrobiellen Abbau in erster Linie von der Ausgangskonzentration abhängt, und empfiehlt, die Verweilzeit aus der tatsächlichen MCPA-Abnahme abzuleiten.

Die dritte Studie untersuchte die Verlagerung von ^{13}C-markiertem Glyphosat nach simulierten Regenereignissen entlang von Trockenrissen, die sich in einem tonhaltigen "Gleysol" (World Reference Base for Soil Resources) nach einer vorangegangenen Trockenperiode in einem 21-tägigen Feldversuch gebildet hatten. Das mikrobielle Abbaupotenzial und die Aktivität in einem 50 cm tiefen Profil wurden durch Quantifizierung der funktionellen Gene *goxA* und *sarc* bewertet, die einerseits am Abbau von Glyphosat zu AMPA oder Sarkosin beteiligt sind. Darüber hinaus ermöglichte der Einbau von ^{13}C in Phospholipid-Fettsäure als Biomarker für Gram$^-$ und Gram$^+$-Bakterien und Pilze Rückschlüsse auf die Abbaubeteiligung. Das Auftreten von präferentiellen Fließwegen konnte als dominierender Transportweg für hoch sorptives Glyphosat in Verbindung mit simuliertem Niederschlag identifiziert werden. Im Gegensatz zu Massenbodenproben, in denen der Abbau von Glyphosat zu AMPA dominierte, wurde in Trockenrissen ein verstärkter Abbau zu Sarkosin beobachtet. In beiden Bodenkompartimenten wurde in der Anfangsphase des Glyphosatabbaus eine signifikante Beteiligung von Pilzen gegenüber Gram$^+$-Bakterien beobachtet. Dieses Verhältnis verschob sich im Laufe der Zeit in Richtung Gram$^+$-Bakterien, die schließlich den Glyphosatabbau dominierten. Gram$^-$-Bakterien zeigten eine konstante, aber vergleichsweise geringere Abbaubeteiligung. Unsere Ergebnisse deuten auf eine Sukzession der drei am Glyphosatabbau beteiligten mikrobiellen Gruppen hin, wobei Pilze den Glyphosatabbau einleiten und den weiteren Abbau durch Bakterien erleichtern.

In dieser Dissertation wurden weitere wichtige Regulationsmechanismen für den mikrobiell vermittelten Abbau von Pestiziden aufgedeckt. Die unbekannte konzentrationsabhängige Abbaudynamik und der konzentrationsgesteuerte Einfluss begrenzender Umwelt-

faktoren auf den mikrobiellen Abbau unterstreichen die Bedeutung von Untersuchungen in realistischen Konzentrationsbereichen. Der Nachweis des Tiefentransports eines stark sorptiven Pestizids wie Glyphosat über präferentielle Fließwege als Hauptweg und eine geringere Abbaudynamik im Unterboden unterstreicht die Notwendigkeit, Prozesse, die nur in Feldstudien nachzuweisen sind, auch im Hinblick auf die Risikobewertung zu erfassen. Aus den Befunden der vorliegender Doktorarbeit kann geschlussfolgert werden, dass die biologischen Abbauraten von Pestiziden im Feldmaßstab nicht homogen sind und teilweise für die Diskrepanz zwischen dem vollständigen Abbau von Pestiziden unter Laborbedingungen und ihrer Persistenz im Feld verantwortlich sein könnten. Laborstudien, bei denen Bodenproben zusammengeführt und gemischt werden, um eine einzige "repräsentative" Probe zu erhalten, können ein vereinfachtes Verständnis des Prozesses vermitteln, doch die Komplexität, insbesondere die Heterogenität des Bodens in Bezug auf die Verteilung von Pestiziden und den mikrobiellen Abbau in Verbindung mit den vorherrschenden klimatischen Bedingungen, erfordert eine Kalibrierung der bisher verwendeten Methoden für die Risikobewertung von Pestiziden, auch in Feldversuchen und möglicherweise auf Landschafts-, Wassereinzugs- oder regionaler Ebene. Der Aspekt des maßstabsabhängigen Abbaus von Pestiziden wird in Zukunft an Bedeutung gewinnen, da zu den Bodeneigenschaften und -prozessen, welche die toxikologischen Eigenschaften von Schadstoffen kontrollieren, auch Temperatur und Feuchtigkeit gehören und die mit dem Klimawandel einhergehenden Veränderungen zu einer Zunahme von extremen Niederschlägen, längeren Trockenperioden und Bodenerosion führen werden.

3 General Introduction

3.1 Pesticide exposure and environmental risk

Soils are reactive landscape elements that serve as buffer zones to prevent or minimize direct pollutant inputs to groundwater and drinking water reservoirs. Agricultural soils are particularly important because they are exposed to high inputs of agrochemicals in industrialized countries (Hedlund et al., 2020). Pesticides have been used to regulate pests, weeds, or diseases (Cooper and Dobson, 2007; Popp et al., 2013) on cropland and in conventional agriculture for more than 50 years and have contributed significantly to increased food production in recent decades (Silva et al., 2019b). Nearly 500 active ingredients are registered today in the European Union (EU) (EC, 2020a), and global pesticide use is estimated to have increased to 3.5 million tons by 2020 (Sharma et al., 2019). Regardless of the undeniable benefits of widespread use of pesticides in agriculture, high application rates and their negative effects on non-target organisms raise serious environmental and health concerns (FAO, 2017). Pesticide application in the field is difficult to confine to target plants or pathogenic organisms, and a considerable fraction of the amount applied - up to 50% - reaches the soil surface (Fenner et al., 2013). Subsequent abiotic transport processes such as wind erosion, leaching, or runoff direct the movement of pesticides into soil-adjacent environmental compartments (air and water; (Gavrilescu, 2005)). Therefore, to minimize these risks, it is important to fully understand pesticides' turnover processes in the soil to comprehensively assess their fate.

3.1.1 Legacy effect of pesticide application on soils

Off-site pesticide transport can impair ecosystem functions and numerous pesticide residues are frequently found in water (Casado et al., 2019), food, animal feed Authority et al. (2020), and humans (Bevan et al., 2017). A large-scale soil sampling campaign (Silva et al., 2019a), provided the first study with a more comprehensive overview of

pesticide residues from 317 soil samples collected in 11 EU countries in 2015. Only 17% of the agricultural topsoils studied contained no pesticides, while 25% of the soils contained specific pesticide residues, and 58% contained a mixture of several pesticides (Silva et al., 2019a). Glyphosate and its metabolite AMPA, DDE pp. (metabolite of the long-banned DDT), and the broad-spectrum fungicides boscalid, epoxiconazole, and tebuconazole were the most commonly found compounds with the highest concentrations in soil samples. However, from the study of Silva et al. (2019a), it was not clear from which agricultural management system the samples had originated or whether these results were due to short-term contamination or accumulated residues.

A drawback addressed in the study by Riedo et al. (2021), in which 100 agricultural soils under organic and conventional management were compared in terms of the number and concentrations of pesticide residues. Even after 20 years of organic management, up to 16 different pesticide residues were detected, including herbicides linuron, napropamide, but also atrazine, which has been banned for 30 years (Riedo et al., 2021). Since no direct pesticide applications occurred in the organically managed fields for at least three years, the study by Riedo et al. (2021) indicated that the pesticides had either remained in the soil much longer than expected or that the contamination came indirectly from neighboring conventional fields (Sarmah et al., 2004). Considering the half-lives of the pesticides and their maximum application doses, only traces of five pesticides (boscalid, epoxiconazole, fluopicolide, flusilazole, and S-metolachlor TP) should have been detectable after ten years (Riedo et al., 2021). Residence times of pesticides well above predicted concentrations indicate long-term accumulation in soil, threatening soil health and a wide range of microbially mediated ecosystem services.

3.1.2 Risks of pesticides to soil life and microbially-related ecological functions

Important ecosystem services affected by the presence of agrochemicals include soil processes such as phosphorus (P), carbon (C), and nitrogen (N) cycling, and soil quality

indices such as arbuscular mycorrhizal fungi (AMF), community-level physiological profiles (CLPP), alkaline phosphatase (AlP) and dehydrogenase (DH) activities (Nivelle et al., 2018).

Arbuscular mycorrhizal fungi (AMF) establish a symbiosis with plants to obtain C in exchange for P (Karpouzas et al., 2014). They promote plant growth by facilitating N (Veresoglou et al., 2012) and P uptake (Goverde et al., 2000) and improving ecosystem resilience to nutrient deficiencies, drought, and biotic stresses such as herbivory (Koricheva et al., 2009). The study by (Riedo et al., 2021) has now provided evidence that AMF abundance is reduced to a greater extent by current pesticide residues than by mineral fertilizers, and that pesticide management appears to be more important than management practices.

Considering the toxicity of pesticides or pesticide mixtures in general to non-target organisms, glyphosate (*N*-phosphonomethylglycine) has received special attention. Since its introduction in 1974, it has gained a strong foothold in the herbicide market and is now the most widely used herbicide for weed control (Duke, 2018). Glyphosate, as a non-selective herbicide, inhibits the activity of 5-enolpyruvylshikimate-3-phosphate synthase (EPSPS), an enzyme found in plants but also in certain bacteria and fungal strains that produce the class I version of EPSPS (Padgette et al., 1995; Funke et al., 2006). Conversely, microorganisms containing a gene encoding class II EPSPS display glyphosate tolerance Priestman et al. (2005). This selection pressure caused by glyphosate application is reflected in a shift in the microbial community. Newman et al. (2016) demonstrated that even at the recommended application dose, the composition of phospholipid fatty acids in the rhizosphere changed. RNA sequencing analyses indicated that in glyphosate-treated soils carbohydrate and amino acid metabolism and iron acquisition were down-regulated in the rhizosphere (Newman et al., 2016), consistent with reduced availability of iron (Cakmak et al., 2009). Small differences in the sensitivity of soil and rhizosphere microorganisms to glyphosate can lead to significant changes in

plant or animal pathogens (Van Der Heijden et al., 2016). Glyphosate application can shift the balance between pathogenic *Fusarium spp.* and antagonistic microorganisms such as *Pseudomonas fluorescens* in favour of root pathogens (Zobiole et al., 2011).

Current pesticide approval protocols consider only a limited number of environmental and health indicators and non-target organisms Geissen et al. (2021). Data on the long-term effects of pesticide residue mixtures on non-standard and native species and communities are not yet available (Pereira et al., 2009; Van Bruggen et al., 2018; Wang et al., 2020). Soil contamination assessment is particularly important as organic agriculture develops rapidly in Europe. According to EU regulations, in order to prevent pesticide contamination, pesticide approval is based on predicted environmental concentrations determined in preliminary studies (PECs; (Silva et al., 2019a)). Such PEC values are calculated based on worst-case conditions. Consideration is given to recommended application doses, application frequency, a standard soil bulk density of 1.5 $\mathrm{g\,m^{-3}}$ and tillage depth of 5 cm for permanent crops and 20 cm for annual crops, typical interception by plants, and the half-life of the active ingredient in soil determined from laboratory or field studies (Ockleford et al., 2017). Evidence of accumulating pesticide residues suggests that the applied risk assessment is inadequate.

3.2 Pesticide degradation in soils - a general overview

The actual degradation of pesticides in soil is controlled by interactions between microbial and physicochemical processes, the chemical properties of the pesticide, and the environmental boundary conditions. Taking glyphosate as an example, the most relevant processes that pesticides undergo in the soil are shown in Figure 1.

3.2.1 Sorption, immobilization, and bioavailability

The mobility, bioavailability, and consequent leaching of pesticides in soil depends on their sorption properties. A strongly sorptive compound leads to immobilization in the

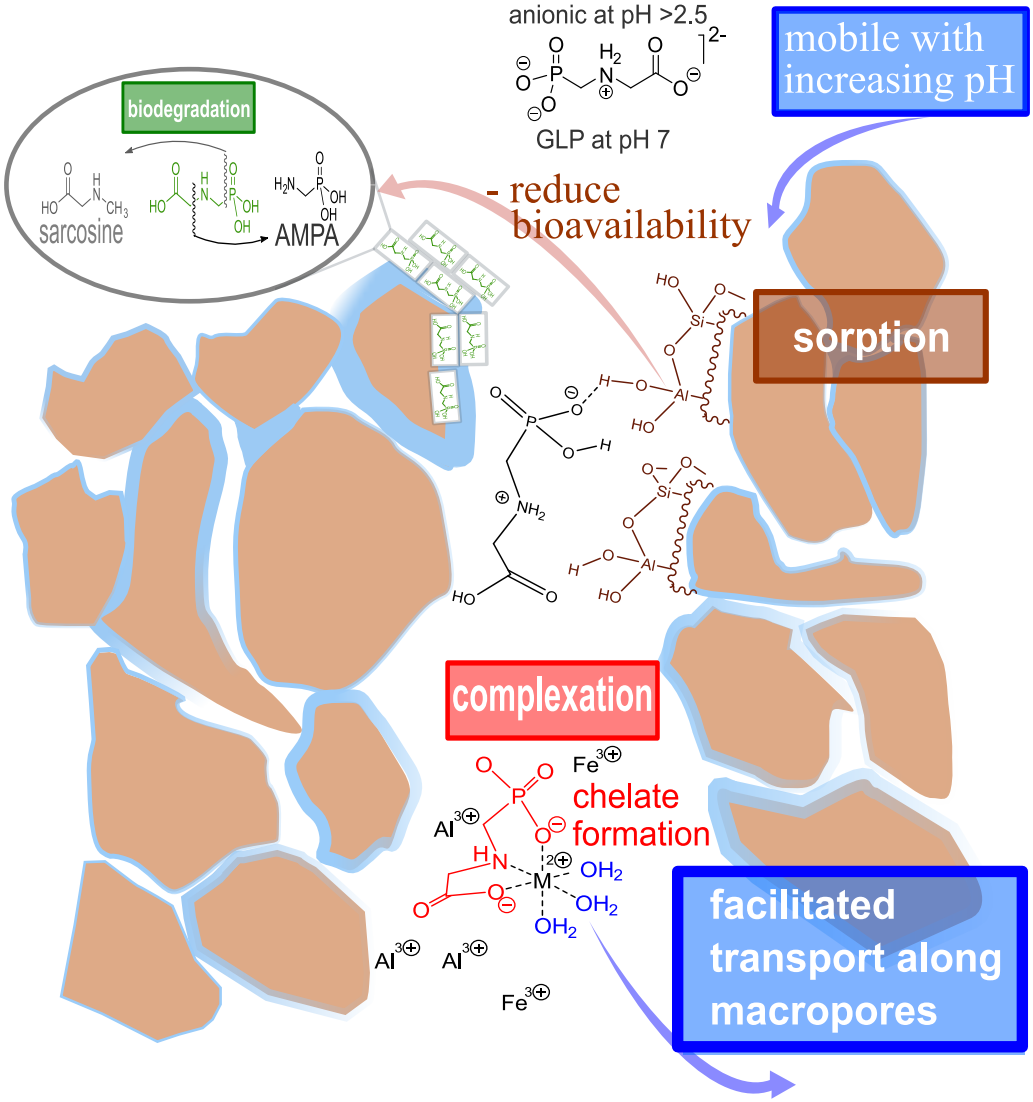

Figure 1: Glyphosate initially consists of three functional groups: a carboxyl group, an amino group, and a phosphonic group. At pH 2, it is a neutral molecule with positive and negative charges at different locations within the same molecule. As pH increases, glyphosate is in an anionic state along with negatively charged mineral surfaces, which reduces its sorption capacity. Glyphosate can also form complexes with dissolved and adsorbed doubly charged metal ions, particularly iron and aluminum oxides; this complex formation can lead to particle-facilitated transport and translocation to greater depths.

soil matrix, while a weakly sorbed compound can be easily translocated (Borggaard and Gimsing, 2008). In this thesis, the focus is on microbial degradability of MCPA

and glyphosate, which could not be more different in terms of their sorption properties. MCPA is weakly adsorbed in contrast to glyphosate; its Freundlich adsorption coefficients range from 0.7 to 27.2 (Jensen et al., 2004) and for glyphosate from 0.6 to 5.0 $\times$ 10^5 $mg^{(1-nF)} \cdot L^{nF}$ kg (Vereecken, 2005). Once MCPA esters enter the soil, they are quickly hydrolyzed to salts or free acids (Hornsby et al., 1995). Subsequently, they are in an anionic state (Morton et al., 2020). The actual proportion of anions and neutral molecules depends on the soil pH (Kah and Brown, 2006) and the pK_a value (the acid dissociation constant) of the herbicide. MCPA has a pK_a value of 3.09 (Mackay et al., 2006); at pH of 4, 89% of the compound is present in anionic form, 11% is present in neutral form, and at pH 7, 100% is in anionic form (Paszko et al., 2016). MCPA is thus a weak acid that is highly soluble and mobile except under very acidic conditions (Bailey et al., 2017).

Compared to MCPA, glyphosate has unique sorption properties. A small molecule with three polar functional groups (carboxyl, amino, and phosphonate group; (Borggaard and Gimsing, 2008)) as compared to MCPA, which has only one carboxyl group (Paszko et al., 2016), it is strongly sorbed to soil minerals (Borggaard and Gimsing, 2008). Like MCPA, glyphosate is present as an anion in the range of typical soil pH values (4-8; (Barja and dos Santos Afonso, 2005)).

The main sorbents in soil for glyphosate are trivalent aluminum and iron oxides, poorly ordered aluminum silicates (allophane), and the edge of phyllosilicates, especially goethite (α-FeOOH), which has been verified in numerous studies (Gimsing and Borggaard, 2001; Sheals et al., 2002; Dideriksen and Stipp, 2003).

High humic and fulvic acid contents, characteristic of soils with high organic matter content (OM), have been reported to increase the sorption potential of MCPA (Hiller et al., 2012) and glyphosate (Dollinger et al., 2015).

Liming of agricultural soils in conjunction with pesticide application to suppress rushes (Morton et al., 2020) increases soil pH (Blake and Goulding, 2002). MCPA and glyphosate then dissociate into the anionic forms (Paszko et al., 2016), decreasing their affinity for

OM (Werner et al., 2013) and thus reducing their adsorptive capacity in the soil (Paszko, 2011).

Dideriksen and Stipp (2003) reported competitive sorption behavior of glyphosate with phosphorus (P) at soil binding sites and Hiller et al. (2012) reported this as well for MCPA. In the presence of phosphorus, their sorption potentials are reduced, enhancing leachability.

Sorption strength limits microbial degradation (Jensen et al., 2004) by reducing the concentration of the pesticide in solution. Microorganisms in soil (with the exception of fungi) can only utilize soluble substrate (Kuzyakov, 2010) as a source of energy and C for growth. The ratio of sorbed to dissolved substrate is a criterion for the behavior of the pesticide in soil (Bailey and White, 1970). This ratio, therefore, is key to soil bioavailability and accumulation (Greer and Shelton, 1992). High sorption or low desorption of glyphosate has been associated with lower mineralization (about 15%), indicating limited bioavailability of glyphosate, while MCPA was mineralized to 72% in the topsoil at the same time (Sørensen et al., 2006).

3.2.2 Environmental boundary conditions

Water flow can accelerate microbial degradation of pesticides by facilitating the encounter of spatially separated pesticides and bacterial degradation products at the millimeter scale (Pinheiro et al., 2018). In addition, higher soil water content supports diffusive transport of pesticides along the soil pore network (Dechesne et al., 2010). Therefore, rainfall intensities are important because heavy rainfall can promote faster pollutant transport by reaching deeper soil layers than low intensity rainfall (Manzoni et al., 2012b). Glyphosate and MCPA degradation are both impaired under anaerobic conditions (Vink and Van Der Zee, 1997; Sørensen et al., 2006), such as those in soil under heavy rainfall. Oxidoreductases utilizing O_2 as a terminal electron acceptor are involved in the degradation of glyphosate (Wolińska and Stępniewska, 2012). In the first step of

MCPA degradation, the α-ketoglutarate-dependent dioxygenase uses α-ketoglutarate and molecular oxygen (O_2) as co-substrate and iron as a prosthetic group for conversion to MCP (4-chloro-2-methylphenol) (Baelum et al., 2006; Guengerich, 2015). Soil temperature and soil nutrient content also affect the degradation of MCPA and glyphosate, as these factors regulate the growth and activity of soil microbial communities (Kah and Brown, 2006).

3.2.3 Field-scale pesticide degradation constraints - the known unknown

Degradation experiments are used to determine degradation pathways, formation of main metabolites, and degradation endpoints. Standard endpoints are the DT_{50} and DT_{90} values, which describe how long it takes for 50% to 90% of a pesticide to dissipate. They can be performed under controlled laboratory conditions or under near-natural conditions in field experiments. Laboratory experiments using soil microcosms are a simplified representation of the processes in nature. Their advantage is that factors affecting pesticide turnover can be studied separately in a manipulated experiment. Their disadvantage is the preparation of the soil microcosms. Homogenization of samples for water content adjustment and pesticide addition eliminates the spatial separation of substrate and soil microorganisms. Therefore, conclusions drawn from these experiments cannot be readily extrapolated to the field scale (Herrero-Hernández et al., 2015). Currently, one of the biggest gaps in our knowledge is how the spatial distribution of pesticide microbial degraders impedes pesticide degradation, especially considering that certain pesticide degrader microhabitats may represent only 1% of the total soil volume (Pallud et al., 2004). In undisturbed soils, pesticide-degrading microorganisms are heterogeneously distributed and form hotspots with enhanced C turnover (Kuzyakov and Blagodatskaya, 2015). This spatial concentration of microorganisms at the mm scale can reduce the potential encounters of degraders with pesticides (Pallud et al., 2004). How far the degradation dynamics can diverge when a pesticide is applied to a part of the soil with

low or high degradation potential is illustrated by the study of Vieublé Gonod et al. (2006) in which either 2% or 75% of 2,4-D (2,4-dichlorophenoxyacetic acid), also a phenoxy, was converted in a three-day incubation period. But microbial distribution is only one aspect of further pesticide degradation; the distribution of pesticide concentration in the soil profile alone could determine the degradation dynamics. Numerous studies (Helweg, 1987a; Helweg et al., 1998a; Bælum et al., 2006, 2008a; Nicolaisen et al., 2008a) have proven that microbial growth on pesticides as a substrate source commences only above a certain concentration threshold, i.e., the degradation potential for a given pesticide in soil is increased only above a certain concentration threshold. At low pesticide concentrations, the energy derived from the microbial degradation of some pesticides might not be sufficient to meet their cellular energy requirements, resulting in pesticide persistence despite microbial accessibility (Huang and Chang, 1998). Adjacent areas of high and low pesticide concentrations are connected by the soil pore system. The higher pesticide turnover in hot spots leads to a concentration gradient. This concentration gradient drives diffusive transport from neighboring, less active zones toward the area where concentration is declining. In heterogeneous soils, where pesticides and degraders are either initially separated (Pinheiro et al., 2018) or pesticides are locally depleted by rapid degradation at hot spots, diffusive transport often becomes the rate-limiting factor (Johnson et al., 2013; Babey et al., 2017). Thus, soil water content as a solvent is critical (Schroll et al., 2006) for further degradation of low molar concentrations of pesticides in interaction with soil temperature, which regulates microbial activity (Helweg, 1993a). However, advective transport processes also bring substrate and degraders into contact even when the two were originally separated and, according to Pinheiro et al. (2015a), are more effective in removing the limitations of biological accessibility for pesticide degradation than diffusive transport alone. Therefore, at the field scale, not only soil water content is crucial for microbial pesticide degradation but also the frequency and intensity of rainfall events. However, the opposite effect between pesticide and microbial pesticide degraders

is possible if heavy rainfall events in structured soils result in translocation of pesticides to less microbially active soil depths via preferential flow pathways. Vertical transport of dissolved or particle-bound pesticides after precipitation events depends on soil structure (Franklin et al., 2021), which is difficult to assess due to heterogenic distribution and shape of macropores (e.g., biopores or macropores of non-biological origin), and may only be investigated in comprehensive field studies. This spatial dimension of pesticide degradation, in the form of the distribution of pesticides in the soil profile and their subsequent degradation in isolated hotspots, may also help explain the differences in expected and actual residence times.

3.3 Objectives

The objective of this thesis is to improve our knowledge of the fate of pesticides in soils and to identify processes that may close the gap between expected and often prolonged observed residence times under natural conditions. Three possible mechanisms controlling pesticide degradation were investigated. First, whether limited microbial degradation at low pesticide concentrations could explain the discrepancy between total degradation observed in laboratory experiments and actual persistence in the environment was examined. Second, the influence of environmental factors (temperature and soil moisture) on selected MCPA concentrations was addressed. Finally, microbial glyphosate degradation was evaluated in the field following a simulated rainfall event to address soil structure variability as a determinant of pesticide degradation.

The first objective was to investigate in a short-term laboratory incubation experiment (37 days) whether metabolic demand exceeds catabolic energy yield during degradation of low pesticide concentrations and if degradation ceases below a certain concentration threshold. It was hypothesized that:

H1: Degradation is impeded as soon as available pesticide concentrations fall below a threshold value that triggers the expression of relevant functional genes.

H2: There are different concentration thresholds for the onset of activity and growth of microorganisms involved in degradation.

H3: The decrease in microbial growth as pesticide concentration decreases will be reflected in reduced carbon use efficiency (CUE) during pesticide degradation.

These results should provide useful information on the microbial degradation kinetics of pesticide residues at realistic concentrations ranging from 30 to 20000 µg kg^{-1} and could also define the concentration threshold above which microbial activity and growth of microorganisms involved in MCPA degradation will occur. According to this information, two concentrations (1 and 20 µg kg^{-1}) were selected for the subsequent experiment.

To examine how environmental conditions affect microbial degradation, a short-term incubation experiment (28 days) was carried out to investigate the interactions of temperature (10 and 20 °C), soil moisture (pF 1.8 and 3.5), and the combination of both factors on the microbial degradation of 1 and 20 mg kg^{-1}, ^{14}C-labeled MCPA. The objective was not only to investigate whether environmental factors delay or enhance pesticide degradation, but also to assess the partitioning of ^{14}C between biomass production and $^{14}CO_2$ respiration, i.e., carbon use efficiency (CUE) (Manzoni et al., 2012b). CUE reflects the microbial balance between catabolism and anabolism, in which high CUE implies a much higher biomass gain while lower CUE results from C loss through respiration or excretion (Manzoni et al., 2012b). Since CUE is highly dependent on soil temperature and water content, the direct physiological responses of microbial pesticide degraders during C turnover can be studied. It was hypothesized that:

H4: At reduced temperature and soil moisture we will observe a higher CUE and an increase in ^{14}C content in the microbial biomass.

H5: This C redistribution may result in a substantial overestimation of pesticide half-life if derived only from ^{14}C mineralization curves compared to the actual MCPA decline.

H6: The effect size will be more pronounced at higher initial concentrations.

This experimental set-up will not only reveal the extent to which pesticide degradation is affected by the expected variations in temperature and soil moisture content during the spraying season in central Europe, but the determination of CUE will also make it possible, for the first time in the context of pesticide degradation, to follow C allocation into anabolic and catabolic processes. The intention of the field experiment was to distinguish separate processes that are elusive at the laboratory scale. For instance, soil structure could play a crucial role as an influencing variable, i.e., via occurrence of preferential flow pathways as the predominant transport route for highly sorptive glyphosate in conjunction with rainfall events. The objective was to follow the distribution of glyphosate in a highly structured soil after a simulated rain event of 24 L m^{-2} and to evaluate the spatial heterogeneity of microbial degradation in topsoil, subsoil, shrinkage cracks, and bulk soil samples.

H7: In structured soils, preferential flow pathways facilitate depth displacement of even highly sorptive pesticides.

H8: Microbial degradation in the soil profile is heteorogeneously distributed and declines with increasing soil depth.

These results will shed light on the heterogeneous distribution of microbial pesticide degradation in the soil profiles studied and provide a possible explanation for why residence times might be higher under natural conditions.

3.4 General approach

3.4.1 Assessment of pesticide degradation in soils

Microbial degradation is the primary route for complete removal of pesticides, from the environment and results in the production of microbial biomass, mineralization compounds

(e.g., CO_2), metabolites, and unextracted residues (Wang et al., 2016). Nevertheless, photocatalytic conversion of MCPA when an aqueous solution was irradiated to 4-chloro2-methylphenol and 4-chloro-2-methylphenyl formate was observed by Zertal et al. (2001). (Barrett and McBride, 2005) reported abiotic glyphosate degradation mediated by the manganese dioxide mineral birnessite. MCPA was selected to study the concentration, temperature, and soil moisture dependency of pesticide degradation because, unlike glyphosate, microbial degradation is not limited by increased sorption and rate-limiting bioavailability, and only the selected variables should determine degradation. In contrast, glyphosate was used in the field experiment to illustrate the translocation of a highly sorptive herbicide in structured soils after a heavy rain event.

3.4.2 Microbial degradation of MCPA

MCPA (4-chloro-2-methylophenoxy-acetic acid) is closely related to 2,4-D (2,4-dichlorophenoxyacetic acid) and belongs to the phenoxyacetic herbicides. Since its introduction

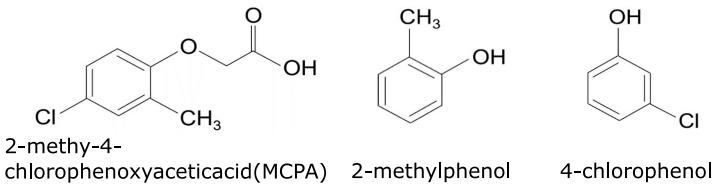

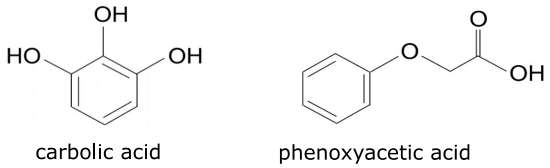

Figure 2: Structural formulas of MCPA and its possible degradation products (2-methylphenol, 4-chlorophenol, carbolic acid and phenoxyacetic acid).

nearly 50 years ago it has become one of the most widely used herbicides in the world (Morton et al., 2020). MCPA is a systemic, selective herbicide against broadleaf weeds. It

causes excessive DNA, RNA, and protein synthesis in the meristem, leading to uninhibited growth and eventual death of the plant (Peterson, 1967). In the soil, MCPA is degraded into 2-methylphenol, 4-chlorophenol, carbolic acid, and phenoxyacetic acid ((McManus et al., 2014); Figure 2).

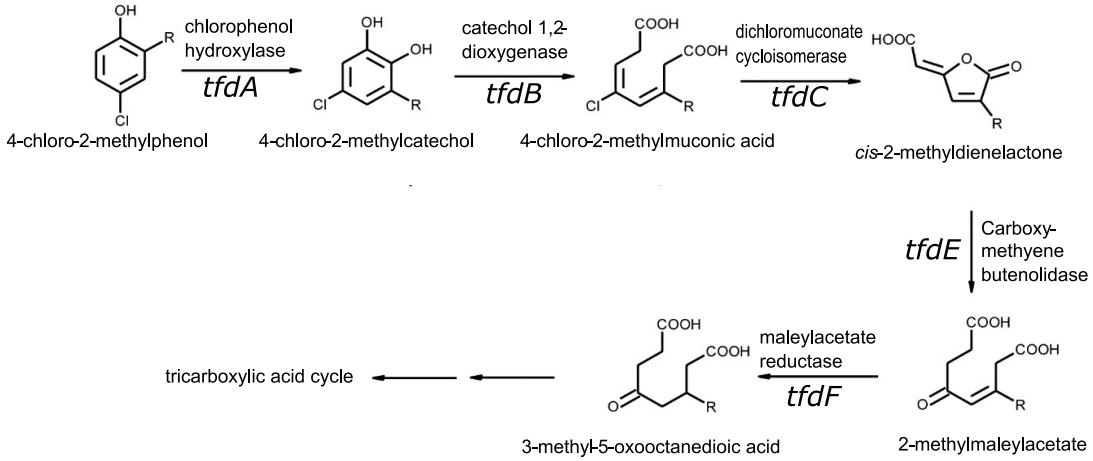

Figure 3: Degradation pathway of 4-chloro-2-methylphenol (major metabolite of MCPA) by soil bacteria, adapted from Paszko et al. (2016)

In the first step of degradation, the ether bond of MCPA is cleaved into 4-chloro-2-methylphenol as an intermediate compound (Rodríguez-Cruz et al., 2010). In the next steps, hydroxyl groups are introduced into the phenolic compounds to form the corresponding catechins, which are then cleaved and finally introduced into the citric acid cycle ((Arora and Bae, 2014); Figure 3). *TfdABCDEF* genes (Figure 3) translate the responsible enzymes located on the plasmid pJP4 discovered by Pemberton (1979) in *Cupriavidus necator*, and make it possible to utilize MCPA as a sole C source. In both laboratory studies, MCPA degradation was assessed after the initial rate-limiting degradation step from MCPA to MCP by quantifying microbial degradation potential and activity based on *tfdA DNA* and *tfdA RNA* transcript abundances. In addition, the *cadA* gene was quantified, which encodes an enzyme similar to 2,4,5-trichlorophenoxyacetic acid (2,4,5-T)-oxygenase that facilitates the conversion of phenoxyacetate to phenol

(Danganan et al., 1994). However, in the present thesis, the *cadA* gene showed no response to the application of MCPA. Degradation kinetics were determined by fitting a kinetic model to cumulative ^{14}C-mineralization curves to derive DT_{50} values. In addition, ^{14}C incorporation into microbial biomass was quantified and CUE was calculated based on the ratio of ^{14}C mineralization to total ^{14}C uptake. The actual MCPA decline was quantified after hot water methanol extraction (1:1) and subsequent measurement by HPLC-MS/MS (tandem mass spectrometry; Agilent 6490 iFunnel Triple Quadrupole (QqQ)).

3.4.3 Microbial degradation of glyphosate

In the soil, glyphosate is degraded either into AMPA via the cleavage of the C-N bond by glyphosate oxidoreductase, or into sarcosine via the immediate cleavage of the C-P bond by C-P lyase ((Zhan et al., 2018); Figure 5).

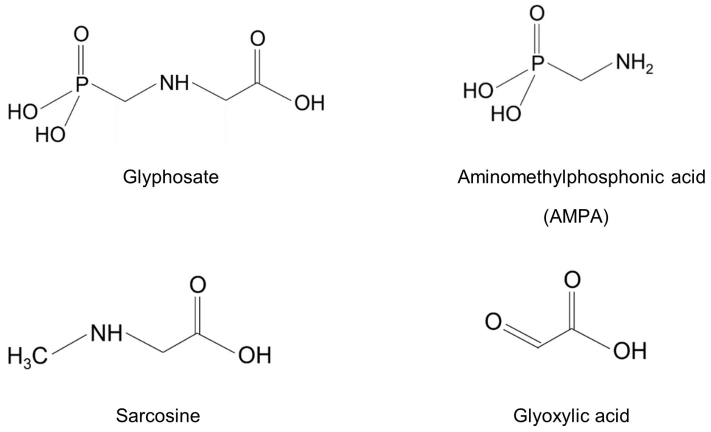

Figure 4: Structural formulae of glyphosate and its metabolites (aminomethylphosphonic acid (AMPA), sarcosine and glyoxylic acid).

The most common degradation pathway for glyphosate in bacteria involves cleavage of the C-N bond by a glyphosate oxidoreductase, producing AMPA either as a final product or as an intermediate that is further degraded (Zhan et al., 2018). In a co-

metabolic glyphosate degradation, microorganisms utilize glyphosate as the sole source of phosphorus after the cleavage of AMPA (Pipke and Amrhein, 1988). However, there are strains that can utilize glyphsoate as either the sole source of phosphorus, nitrogen, or nitrogen and phosphorus (Obojska et al., 1999; Krzyśko-Lupicka et al., 1997).

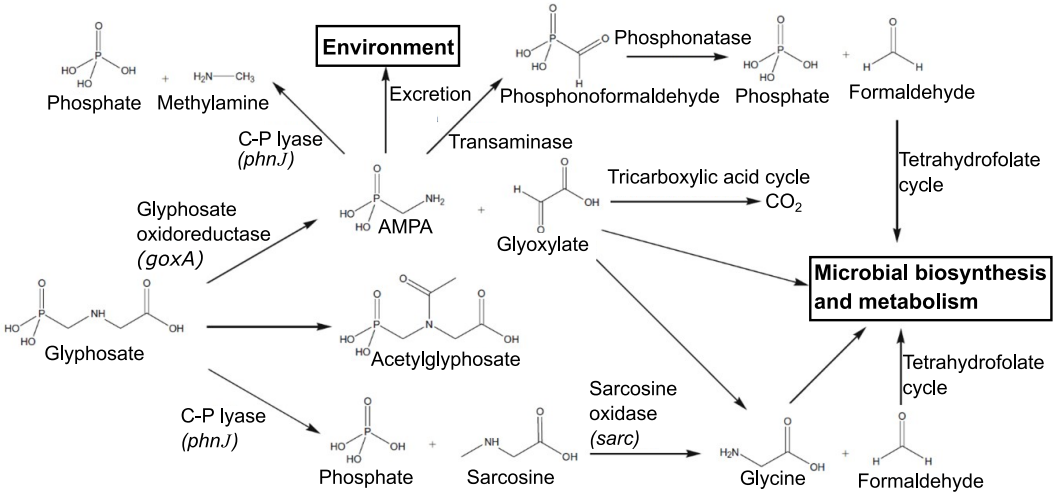

Figure 5: Glyphosate degradation pathways adapted from Zhan et al. (2018).

The gene sequences of glyphosate oxidoreductase (*goxA*), the enzyme responsible for the cleavage of the C-N bond to yield AMPA and glyoxylate, was recently identified in *Ochrobactrum sp. G-1* and these sequences are presented in this thesis as a newly designed primer pair. The C-P lyase pathway, which is crucial for further mineralization of AMPA or for the first step of glyphosate degradation to sarcosine (Sviridov et al., 2015), is encoded in the operon phnCDEFGHIJKLMNOP. Considerable conservative evolution in the aligned sequences of the *phnJ* protein compared with other Phn proteins suggests that it is the key enzyme of the glyphosate degradation pathway (Morales et al., 2020). Since no specific *phnJ* sequence could be assigned to glyphosate degradation, the functional gene *sarc*, following González-Valenzuela and Dussán (2018), was used in addition to *goxA*, an indicator for the AMPA pathway, to follow glyphosate degradation to sarcosine.

Sarc encodes the necessary sarcosine oxidase in the second glyphosate degradation step, in which sarcosine is converted to glycine (Figure 5). Participation of the three major microbial groups in glyphosate degradation - Gram-positive, Gram-negative bacteria, and fungi - was assessed by the incorporation of ^{13}C into the indicative phospholipid fatty acids. GLP-$^{13}C_3$,^{15}N and AMPA-^{13}C,^{15}N residues in soil samples were quantified using an extraction protocol followed by CE-MS analysis as described by Wimmer et al. (2022).

4 Biodegradation of Pesticides at the Limit: Kinetics and Microbial Substrate Use at Low Concentrations

This chapter includes the following publication:

1. Wirsching, J., Pagel, H., Ditterich, F., Uksa, M., Werneburg, M., Zwiener, C.,Berner, D., Kandeler, E., & Poll, C., (2020). "Biodegradation of Pesticides at theLimit: Kinetics and Microbial Substrate Use at Low Concentrations." Frontiers in Microbiology 11, 1476. doi:10.3389/fmicb.2020.02107.

4.1 Abstract

The objective of our study was to test whether limited microbial degradation at low pesticide concentrations could explain the discrepancy between overall degradability demonstrated in laboratory tests and their actual persistence in the environment. Studies on pesticide degradation are often performed using unrealistically high application rates seldom found in natural environments. Nevertheless, biodegradation rates determined for higher pesticide doses cannot necessarily be extrapolated to lower concentrations. In this context, we wanted to (i) compare the kinetics of pesticide degradation at different concentrations in arable land and (ii) clarify whether there is a concentration threshold below which the expression of the functional genes involved in the degradation pathway is inhibited without further pesticide degradation taking place. We set up an incubation experiment for four weeks using ^{14}C-ring labeled 2-methyl-4-chlorophenoxyacetic acid (MCPA) as a model compound in concentrations from 30 to 20,000 µg kg^{-1} dry weight. To quantify the abundance of putative microorganisms involved in MCPA degradation and their degradation activity, tfdA gene copy numbers (DNA) and transcripts (mRNA) were determined by quantitative real-time PCR. Mineralization dynamics of MCPA derived-C were analyzed by monitoring $^{14}CO_2$ production and ^{14}C assimilation by soil microorganisms. We identified two different concentration thresholds for growth and

activity with respect to MCPA degradation using *tfdA* gene and mRNA transcript abundance as growth and activity indices, respectively. The *tfdA* gene expression started to increase between 1,000 and 5,000 µg kg^{-1} dry weight, but an actual increase in *tfdA* sequences could only be determined at a concentration of 20,000 µg. Accordingly, we observed a clear shift from catabolic to anabolic utilization of MCPA-derived C in the concentration range of 1,000 to 5,000 µg kg^{-1}. Concentrations >1,000 µg kg^{-1} were mainly associated with delayed mineralization, while concentrations <1,000 µg kg^{-1} showed rapid absolute dissipation. The persistence of pesticides at low concentrations cannot, therefore, be explained by the absence of functional gene expression. Nevertheless, significant differences in the degradation kinetics of MCPA between low and high pesticide concentrations illustrate the need for studies investigating pesticide degradation at environmentally relevant concentrations.

4.2 Introduction

Pesticide application is the dominant pest control method utilized by farmers in Germany, with an average application rate of 2.8 kg ha^{-1} on arable land (Baumgarten et al., 2008). However, the behavior and ecotoxicological effects of many pesticides in the environment have not been adequately clarified (Sarmah et al., 2004; Carvalho, 2017). After application of pesticides, a considerable fraction ends up in the soil, where filtering functions, such as immobilization by clay minerals and organic matter (Sun et al., 2010), chemical and microbial degradation provide important ecosystem services for groundwater and surface water protection (Keesstra et al., 2012). Despite pesticide biodegradation, which is considered as the most important degradation pathway (Nowak et al., 2011b), remnants of multiple pesticides (including their metabolites), persist at low but detectable and environmentally relevant concentrations in soils. As a result, soils shift from serving as sinks of pesticides to secondary sources (Miglioranza et al., 2002).

Silva et al. (2019a) discovered that only 17% of 317 tested agricultural topsoils in the European Union (EU) contained no pesticides. While 25% of soils contained specific pesticide residues, 58% contained a mixture of several pesticides in medium and maximum concentrations of 0.02 to 0.04 mg kg^{-1} and 0.31 to 0.41 mg kg^{-1}, respectively (Silva et al., 2019a).

There is growing evidence that numerous organic pollutants persist in soil, even though they are fully biodegradable under optimal laboratory conditions (e.g., 2,4-dichlorophenoxyacetic acid; (Nowak et al., 2011b; Fenner et al., 2013)). Processes effective in the field can be elusive at the laboratory scale. For example, pesticide residues may be bound to soil organic matter (SOM), especially due to the formation of hydrophobic SOM particles (Goebel et al., 2011; Kaestner et al., 2014), making the pesticide inaccessible to microbes. If the pesticide is bioavailable and degraders are present, diffusion may limit microbial uptake of a compound (Dechesne et al., 2010). However, microbial pesticide decomposers may not be present or the heterogeneous distribution of pesticides and their degraders may result in low degradation rates (Dechesne et al., 2010)). Pesticide molecules in inactive zones will be degraded either only in the case of new colonization by microbes or by mass transfer to adjacent zones (Dechesne et al., 2010).

The selected concentration range can also result in a difference between measured total mineralization in laboratory experiments and the fate of pesticide residues in the field. Most studies focus on relatively high concentrations, always with the maximum permitted application amount in mind, which ranges from 0.5 mg to 50 mg kg^{-1} (Jensen et al., 2004; Bælum et al., 2006; Jacobsen et al., 2008; Nicolaisen et al., 2008a; Rosenbom et al., 2014). These concentrations, however, exist only immediately after application or occur in the event of accidental spillage resulting in local point infiltration (Helweg et al., 1998a).

Currently, the microbial degradation of higher pesticide concentrations is well characterized. Degradation is often associated with the stimulation of microbial growth and metabolic

mineralization, leading to the typical sigmoidal form of the degradation curves with a significant delay, exponential increase and saturation phase (Fomsgaard, 1997a). This process can be described by a logistic function including a zero and first-order term in which, at some point, substrate availability becomes the limiting factor, and the curves begin to asymptote (Brunner and Focht, 1984; Fomsgaard and Kristensen, 1999a). However, this process of degradation requires microbial utilization of pesticides as both energy and C sources (Duo-Sen and Shui-Ming, 1987a). In contrast, fewer pesticide degradation studies in the range of 40–80 $\mu g\,kg^{-1}$ have been published (Mueller et al., 1992; Helweg, 1993a; Helweg et al., 1998a)). Fomsgaard (1997a) demonstrated that degradation rates observed at higher concentrations cannot necessarily be transferred to degradation behavior at lower concentrations.

Fundamentally different preconditions influence microbial degradation at low pesticide concentrations. When pesticide concentrations are low, the distance between the molecule and the microorganisms increases, minimizing the probability of contact (Coche et al., 2018)). Degradation of low pesticide concentrations often follows first-order kinetics (Jacobsen and Pedersen, 1991; Helweg et al., 1998a) without microbial uptake as an energy or C source (Fomsgaard and Kristensen, 1999a). This lack of energetic use of pesticides at low concentrations may explain their incomplete microbial degradation. At low concentrations, the trade-off between gaining energy from the degradation of organic compounds and the energy and resources required for the expression of specialized enzymes involved in the degradation pathway could become negative. Microbes may also not be able to break down the pesticide, not because of energy limitations, but because no growth substrate (C) is available at the required concentration. Consequently, as concentrations of pesticides fall below a certain threshold, the growth of degrading microbes as well as the expression of related functional genes may be restricted (Egli, 2010).

One approach to address this topic is the use of model compounds such as 2-methyl-4-

chlorophenoxyacetic acid (MCPA), as used in our study. Their degradation pathways and the protocols for detection of the relevant functional genes are well-known. The purpose of our study was to test whether the absence of functional gene expression under conditions of gradual energy or C limitation can explain the formation of pesticide residues in soil. We also wanted to correlate dynamic gene expression with alterations in MCPA degradation kinetics. We hypothesized that (1) degradation is impeded as soon as available pesticide concentrations fall below a threshold value that triggers the expression of relevant functional genes, (2) there are two different concentration thresholds for initiation of activity and growth of the microorganisms involved in degradation, and (3) the shift in growth and activity of degrader organisms with decreasing pesticide concentration is directly linked to changes in their metabolic utilization of the pesticide. To test these hypotheses, we set up a microcosm experiment using ^{14}C-ring MCPA at concentrations from 30 to 20,000 µg kg^{-1} soil. By quantifying the abundance of the *tfdA* gene coding for the enzyme of the initial degradation step in which MCPA is converted into 4-chloro-2-methylphenol (MCP), we obtained an indicator for changes in the abundance of microorganisms carrying the *tfdA*-degradation pathway. Based on this indicator, we determined the threshold concentrations above which an increase in microbial abundance was possible (Bælum et al., 2006; Ditterich et al., 2013a). In addition, we quantified *tfdA* gene expression (mRNA) as an activity index to clarify whether different thresholds for growth and gene expression exist. Furthermore, we monitored the ^{14}C flux in CO_2 and microbial biomass as an indicator of the shift between anabolic and catabolic use of MCPA, to derive microbial carbon use efficiency (CUE).

4.3 Materials and Methods

4.3.1 Study site and Soil Sampling

Soil for the experiment was taken from a study site located in the middle of the Ammer catchment between Herrenberg and Tübingen (48°33´24.664´´, 8°52´31.259´´)

in southwest Germany. The parent rock of the study site is composed of Muschelkalk dips below mudstones, dolomites, and thin coal beds of Lettenkeuper. These layers are covered by thick loess layers that enable intense agriculture. We took soil samples in June 2016 from an Ap horizon (0–5 cm) of a silty Luvisol (World Reference Base for Soil Resources, (Table 1)). The sampled soil was in a dry condition with volumetric water content of 10%. Pesticide application was restricted to chloridazon and metamitron; MCPA had not been applied previously at this site. After sampling, the soil was sieved (<2 mm), homogenized, and stored at -20°C.

Table 1: Chemical and physical soil properties

Soil Horizon	Depth	pH	C_{org}	Nitrogen	Phosphate	Sand	Silt	Clay
Ap	[cm]	[$CaCl_2$]	[mg g^{-1}]	[mg g^{-1}]	[mg g^{-1}]	[%]	[%]	[%]
	0-5	6.48	18.4	2.1	1.038	2.26	72.04	23.8

4.3.2 Experimental Design

The experimental design consisted of eight MCPA concentration treatments with three replicates each (0, 30, 50, 100, 500, 1,000, 5,000, 20,000 mg kg^{-1} soil), resulting in 24 microcosms per set. We selected these concentrations after the aforementioned publication of Silva et al. (2019a) to account for possible MCPA concentrations directly after application as well as a depth-dependent dilution. At a soil density of 1.2 g cm^{-3} and a recommended application rate of 2.0 g ha^{-1}, 16.6 mg kg^{-1} would be present in the first centimeter of soil almost immediately after application. If we neglect the convective transport of MCPA, e.g., via preferential flow pathways, a further average dilution to 1.6 mg kg^{-1} follows over the first ten centimeters.

Three sets (24 microcosm × three) were spiked with ^{14}C-ring labeled MCPA to follow MCPA mineralization and utilization by soil microorganisms. These samples were destructively sampled after 8, 15, and 37 days. Additionally, one set of 24 microcosms contained only unlabeled MCPA, from which a series of subsamples for ^{14}C-

free RNA/DNA co-extraction and MCPA quantification was taken and stored at 80°C until analysis (Table 2). Final concentrations of ^{14}C MCPA in the microcosms were adjusted by mixing 15 kBq of labeled MCPA (purity 99%, specific activity 50–60 mCi/mmol; BIOTREND Chemikalien GmbH, Germany) with increasing levels of unlabeled MCPA (analytical grade MCPA 99.2% purity, Sigma-Aldrich, Germany). Briefly, soil equivalent to 50 g dry soil was weighed into plastic cups and soil moisture was adjusted by using a mixture of MCPA, deionized water, and trace amounts of ^{14}C-labeled MCPA, to a volumetric water content of 25%. Soil moisture was maintained throughout the test. After thorough mixing of the applied solution with the soil, the cores were placed in the microcosms, which were then made airtight and frozen at -20°C.

Table 2: Sampling schedule

Analyses	Sampling time
^{14}C mineralization	1, 2, 5, 7, 10, 13, 15, 17, 20, 22, 24, 27, 29, 31, 34, and 37 d
$^{14}C_{mic}$	8, 15, and 37 d
MCPA concentration	0, 5, 9, 14, 21, and 37 d
DNA/RNA measurement	0, 5, 9, 14, 21 and 37 d

4.3.3 MCPA dissipation

After thawing, 2 g was mixed with 10 ml of methanol/H_2O_{deion} (1:1 by volume) and placed on a horizontal shaker for 10 min at 200 rev min^{-1}. Samples were then incubated in a water bath at +50°C for 60 min. Finally, the samples were shaken again for 10 min at 200 rev min^{-1} and centrifuged at 2,500 g for 10 min. The supernatant was transferred to brown vials with a 0.45 m syringe filter.

Prior to HPLC-QqQ-MS/MS analysis, extracts were sonicated and vortexed for 5 min. Using a 1,260 Infinity system from Agilent Technologies, 1 µL of sample was injected onto a reversed phase column (Agilent Poroshell 120 C18, 2.1 mm internal diameter, 100 mm length, 2.7 m particle size) at a temperature of 40°C. MCPA was eluted isocratically within 5 min using 50% water and acetonitrile (both acidified with 0.1% formic acid)

at a flow rate of 0.4 $L\,min^{-1}$. After chromatographic separation, MCPA was detected by tandem mass spectrometry using an Agilent 6490 iFunnel Triple Quadrupole (QqQ) instrument. The analyte was ionized by negative electrospray (ESI), applying 12 $L\,min^{-1}$ sheath gas (N_2) at 400°C, 16 $L\,min^{-1}$ drying gas (N_2) at 150°C, 30 psi nebulizer pressure, 4.2 kV capillary voltage, and 1.2 kV nozzle voltage. MS/MS experiments were conducted by MRM (Multi Reaction Monitoring) using N_2 as collision gas and collision energy (CE) dependent mass transitions (MCPA: quantifier 198.9/140.9 at 10 eV, qualifier: 198.9/34.9 at 45 eV). The limit of quantification (LOQ) was defined at 13 $\mu g\,kg^{-1}$ MCPA in soil.

4.3.4 Measurement and Model-Based Evaluation of MCPA Mineralization

The $^{14}CO_2$ evolution of the microcosms was determined via titration (DIN EN ISO 16072:2011-09). Vials attached to the undersides of the microcosm lids contained 2 mL of 1 M NaOH, which acted as a CO_2 trap. The respiration rate was measured in an aliquot of 0.5 ml, which was treated with 0.5 ml of 1 M $BaCl_2$ and two drops of phenolphthalein prior to being titrated against 0.1 mol HCl. The neutralization reaction endpoint was indicated by a colorless, completely transparent solution. For analysis of $^{14}CO_2$ from microbial respiration, 1 ml of NaOH from the microcosm was mixed with 4 ml scintillation vial fluid (Rotiszint Eco Plus, Carl Roth GmbH + Co. KG) in a 5 ml scintillation vial (LDPE). The decay rate in Becquerel (Bq) was measured on a scintillation counter (Wallac 1411, liquid scintillation counter, United States). To account for interfering substances, a quenching adaptation with ^{14}C-aqueous standards was used to improve the accuracy of the actual counts per second (cps) for the entire energy band.

To derive the half-life of MCPA mineralization for each concentration treatment, analytical solutions of a kinetic model (Eq. 1) based on Duo-Sen and Shui-Ming (1987) and extended by Fomsgaard and Kristensen (1999) were fitted to cumulative $^{14}CO_2$ data. The reference value used to calculate the half-life refers to the maximum mineralizable ^{14}C content in the soil. It does not include the immediate ^{14}C assimilation by microorganisms.

Briefly, the full model describes the formation of $^{14}CO_2$ by two processes: direct mineralization of MCPA and formation of microbial biomass (first term in Eq. 1) and first-order mineralization of MCPA-derived ^{14}C that had been incorporated into SOM (second term in Eq. 1). The analytical solution of the full model reads as follows:

$$C = C_0 \left(1 - \frac{k_1 C_0}{(k_1 + k^* C_0) \cdot e^{k_1 \cdot t} - k^* C_0}\right) + S_0(1 - e^{-k_2 t}) \tag{1}$$

where C is MCPA-derived $^{14}CO_2$ (% of initially applied MCPA), C0 is the total mineralizable MCPA (% of initially applied MCPA), S0 is the total mineralizable MCPA-derived ^{14}C in SOM (% of initially applied MCPA), and k_1 (d^{-1}), k^* ($\%^{-1}$ d^{-1}) and k_2 (d^{-1}) are rate constants. For simplification and to provide meaningful parameter constraints for non-linear regression, we reparametrized the model by introducing the dimensionless parameter

$$f_k = \frac{k^* C_0}{k_1} \tag{2}$$

The range of f_k is constrained as $0 \leq f_k < 1$ due to the given constrains of the original model that $k^* < 0$, $k_1 > 0$, $C_0 > 0$ and $1 + k^* C_0/k_1 > 0$ (Duo-Sen and Shui-Ming (1987a)). Substituting f_k into Eq. 1 eliminates k^* and gives:

$$\begin{aligned} C &= C_0 \left(1 - \frac{k_1}{(k_1 - f_k \dot{k}_1) \cdot e^{k_1 \cdot t} + f_k k_1}\right) + S_0(1 - e^{-k_2 t}) \\ C &= C_0 \left(1 - \frac{1}{(1 - f_k) \cdot e^{k_1 \cdot t} + f_k}\right) + S_0(1 - e^{-k_2 t}) \end{aligned} \tag{3}$$

Parameter estimation was done by non-linear least squares regression with the Levenberg-Marquardt algorithm using multiple starting values as implemented in the R-package nls.multstart (Patfield and Matheson, 2008). Half-lives were calculated by numerically solving the corresponding non-linear equation derived from Eq. 3 using Newton's method

as implemented in the R-package *nleqslv*:

$$0 = e^{k_2 T_{1/2}} - \frac{e^{k_2 T_{1/2}}(2 f_k S_0 - 2 S_0) - 2 f_k S_0}{(e^{k_2 T_{1/2}}(f_k(S_0 + C_0) - S_0 - C_0) - f_k(S_0 + C_0) + 2 C_0)} \tag{4}$$

Two simplified expressions of Eq. 3 were used if parameter estimates of the full model became highly uncertain and practically unidentifiable (as indicated by asymptotic confidence intervals):

$$C = C_0 e^{-kt} \tag{5}$$

$$C = C_0 \left(1 - \frac{1}{(1 - f_k) \cdot e^{k_1 \cdot t} + f_k}\right) \tag{6}$$

Half-lives from estimated parameters of fitted Eqs 5 and 6 were calculated according to Eqs 7 and 8, respectively (see also Duo-Sen and Shui-Ming (1987a)).

$$T_{1/2} = \frac{ln(2)}{k_1} \tag{7}$$

$$T_{1/2} = \frac{1}{k_1} ln\left(\frac{1}{1 - f_k} + 1\right) \tag{8}$$

Finally, the full model (Eq. 3) was fitted to $^{14}CO_2$ mineralization data of experiments with 30–500 µg kg^{-1} initial MCPA, first-order kinetics (Eq. 5) was fitted to data of experiments with 1,000 and 5,000 µg kg^{-1} initial MCPA, and a model version neglecting incorporation of MCPA-derived ^{14}C into SOM (Eq. 6) was fitted to the data of the experiment with 20,000 µg kg^{-1} initial MCPA. An R-script of model-based data evaluation of $^{14}CO_2$ is provided as Supplementary Material.

4.3.5 Microbial biomass (C_{mic})

^{14}C incorporation into microbial biomass C was determined using the chloroform fumigation-extraction (CFE) method adapted from Poll et al. (2010a). In short, 10 g soil was fumigated with ethanol-free chloroform for 24 h. A second 10 g of the same soil was the non-fumigated control. To extract soil organic C, 40 ml of 0.5 mol K_2SO_4 was added to each fumigated and non-fumigated sample. The samples were shaken at 200 rev min^{-1} on a horizontal shaker for 30 min and centrifuged at 4,400 g. The clear supernatant was filtered through a 20 m filter and diluted 1:4 with deionized water to avoid high salinity during detection. The supernatant was measured for organic C using a total organic C analyzer (multi-N/C 2100S, Analytic Jena AG, Jena, Germany). The C_{mic} content was determined from the difference in C content between the fumigated and non-fumigated samples using a k_{EC} factor of 0.45 (Joergensen, 1996). To determine ^{14}C content in C_{mic}, 1 ml of the CFE supernatant was mixed with 4 ml scintillation vial fluid (Rotiszint Eco Plus, Carl Roth GmbH + Co. KG) in a 5 ml scintillation vial (LDPE). The calculation of incorporated ^{14}C was carried out as described for C_{mic} content, using the difference in activity for the fumigated and non-fumigated samples, but here the undiluted supernatant was used.

4.3.6 Measuring Carbon Use Efficiency (CUE)

Carbon use efficiency was calculated on the basis of a biomass-based method described by (Manzoni et al., 2012b), which can be applied to labeled substrate.

$$CUE = \frac{^{14}C_{mic}}{^{14}C_{mic} + R_{cum}} \tag{9}$$

$^{14}C_{mic}$ = ^{14}C uptake in microbial biomass

R_{cum} = cumulative respiration rate

4.3.7 Molcular Analysis

RNA and DNA were extracted from 2 g frozen soil using the RNeasy PowerSoil Total RNA Kit for soil and the RNeasy PowerSoil DNA Elution Kit (Qiagen, Germany) in a co-extraction method following the manufacturer's protocol. For further analyses, RNA and DNA samples were stored at -80°C.

Prior to reverse transcription, residual DNA in the RNA samples was digested with Turbo DNase (TURBO DNA-free^{TM} Kit, Invitrogen, Thermo Fisher Scientific, Germany; Table 3). Each reaction contained 20 µL RNA sample, 2.4 µL 10× Turbo DNA buffer and 1.6 µL Turbo DNase.

Table 3: Primer sequence

Target sequence	Primer	qPCR conditions
16S rRNA genes*	341F: CCT ACG GGA GGC AGC AG 515R: ATT ACC GCG GCT GCT GGC A	600 s at 95°C, Cycle (35): 15 s at 95 °C , 30 s at 60°C, 30 s at 72°C, 30 s at 75°C (m.o.f) melting curve
*tfdA***	F: GAG CAC TAC GCR CTG AAY TCC CG R: GTC GCG TGC TCG AGA AG	600 s at 95°C, Cycle (40): 15 s at 95 °C , 30 s at 64°C, 30 s at 72°C, 30 s at 81°C (m.o.f) melting curve
*cadA****	F: AAG CTG CAR TTT GAR AAY GG R: MGG ATT GAA ATC CTG RTA	600 s at 95°C, Cycle (40): 15 s at 95 °C , 30 s at 55°C, 30 s at 72°C, 30 s at 80°C (m.o.f) melting curve

m.o.f - measurement of fluorescence; *López-Gutiérrez et al. (2004), **Bælum et al. (2006), ***(Kitagawa et al., 2002a)

For reverse transcription, the SuperScript^{TM} III Reverse Transcriptase Kit with Random Primers, RNase OUT (Invitrogen, Thermo Fisher Scientific, Germany), and 10 mmol dNTPs (Genaxxon, Germany) were used according to the manufacturer's protocol and reaction conditions described in Supplementary Table 4. Two subsamples of each RNA extract were used: one subsample was treated with reverse transcriptase in the second reaction step (cDNA sample); the other was supplemented with nuclease-free water instead (RNA sample) to account for DNA residues.

Real-time PCR quantification was performed on all cDNA and RNA samples. The determination of total bacteria (16S rRNA genes) and MCPA degraders (total *tfdA*

gene abundance) was carried out using an ABI Prism 7500 Fast (Applied Biosystems, Germany). qPCR conditions are described in Table 3. The qPCR efficiency ranged from 95 to 105%. The SYBR Green reaction was performed using the Power SYBR® Green Kit (Applied Biosystems, Germany) according to Ditterich et al. (2013a). Standard DNA was used for quantification with a dilution series from 10^8 copies μg^{-1} to 10^1 copies μg^{-1} for each standard. The detection limit was on the order of 10^3 copies g^{-1} dry weight.

4.3.8 Statistical Analysis

To examine the influence of the different concentration treatments on MCPA dissipation, i.e., *tfdA* gene abundance and expression, we used a mixed-effect model with repeated measurements, taking into account time as a within-subject factor. MCPA treatment was implemented as a categorical predictor. The individual microcosms were considered as a random effect. The modeling function lme is included in the package "nlme" of the statistical software R (R Core Team, 2018). Since we did not want a pairwise comparison for all MCPA treatments, we specified comparisons of interest using linear contrasts. In that way, the intercept at the lowest concentration (30 $\mu g\,kg^{-1}$ soil) was the average baseline across all levels. The comparison of parameters derived from the logistic model, such as half-life time, was carried out with Tukey's honest significant difference test, included in the package "emmeans." Test assumptions were checked visually by residual diagnostic plots (Kozak and Piepho, 2018). If two or more levels of a factor did not differ from each other, but did probably differ from another level, we unified the levels or "pooled" them together to achieve model simplification.

4.4 Results

4.4.1 MCPA Dissipation

2-Methyl-4-chlorophenoxyacetic acid dissipation was highly dependent on its initial concentration (Figure 6A).

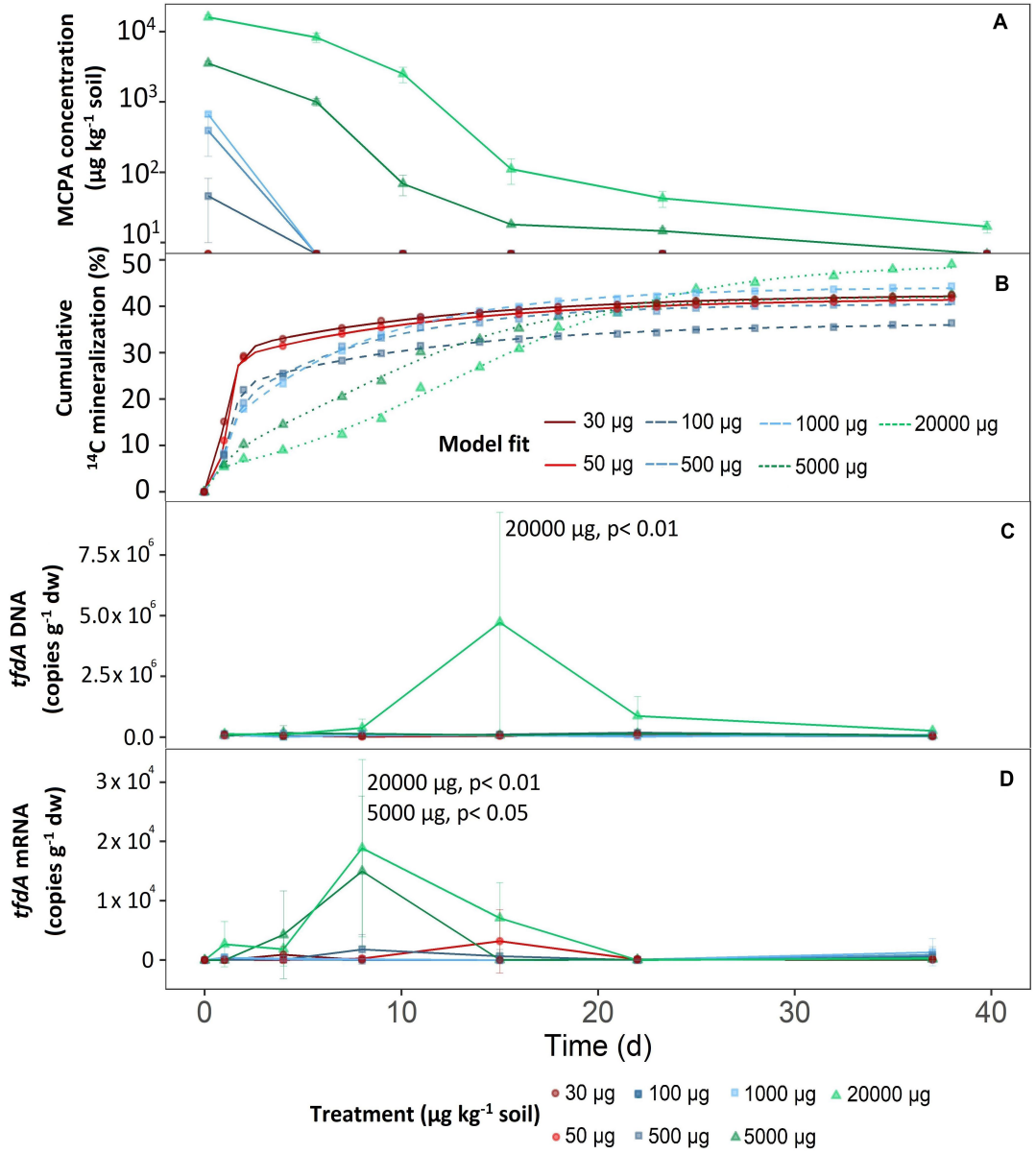

Figure 6: Mineralization of different MCPA concentrations as a function of time. (A) Decrease in MCPA concentration (detection limit, 13 µg kg^{-1} soil). (B) Mineralization of MCPA is represented by the percentage of initial ^{14}C–MCPA. Curves were fitted to the data points via a logistic model. (C) Progress curves of *tfdA* gene copy numbers in relation to dry weight. (D) Progress curves of *tfdA* gene expression in relation to dry weight. Data are presented as means ± SD. Statistically significant differences represented as significance levels of $p \leq 0.05$ and $p \leq 0.01$ ($n = 3$).

Based on MCPA dissipation, the concentration treatments could be divided into three groups. The first group consisted of the two lowest concentration treatments; 30 and 50 µg kg^{-1}. After only 1 day, extractable MCPA was below the detection limit (Figure 6A).

The mid-range group, consisting of concentration treatments from 100 to 1,000 µg kg^{-1}, also showed rapid, absolute dissipation. After eight days, no MCPA could be extracted from the soil.

On day eight and compared to the concentration range of 100 to 1,000 µg kg^{-1}, 28 and 51% of the initial concentrations of 5,000 and 20,000 µg kg^{-1} were still present, respectively. After 21 days at an initial concentration of 5,000 µg kg^{-1}, 14.7 ± 1.4 µg kg^{-1} were still detectable, and after 36 days it was no longer possible to extract MCPA from the soil. For the highest MCPA treatment (20,000 µg kg^{-1}), only 99.9% disappeared after 36 days, which meant that an absolute concentration of 16.7 ± 3.2 µg kg^{-1} remained in the soil.

4.4.2 $^{14}CO_2$ mineralization and half-life time (DT_{50})

Total mineralization (percentage of initial MCPA application), calculated according to Eq. 3, reached saturation in all treatments (Figure 6B). In the concentration range from 30 to 5,000 g, the level of saturation was about 40% (Figure 6B).

In the case of the highest concentration only, MCPA mineralization rose to a significantly higher plateau, reaching approximately 50% of initial MCPA application ($C = 51.57 \pm 2.9$; $F_{1,14} = 15.30$, $p < 0.05$).

The mineralization rate, expressed as half-life time, reflected, to some extent, the absolute MCPA reduction. A rapid degradation rate for the concentration range from 30 to 500 µg kg^{-1} was seen in the half-life time of 2 to 3 days (Figure 7). From 1,000 µg and upward, a significant deceleration of mineralization was detectable. In the case of the two highest concentrations, this resulted in half-life times of 8 and 14 days, respectively.

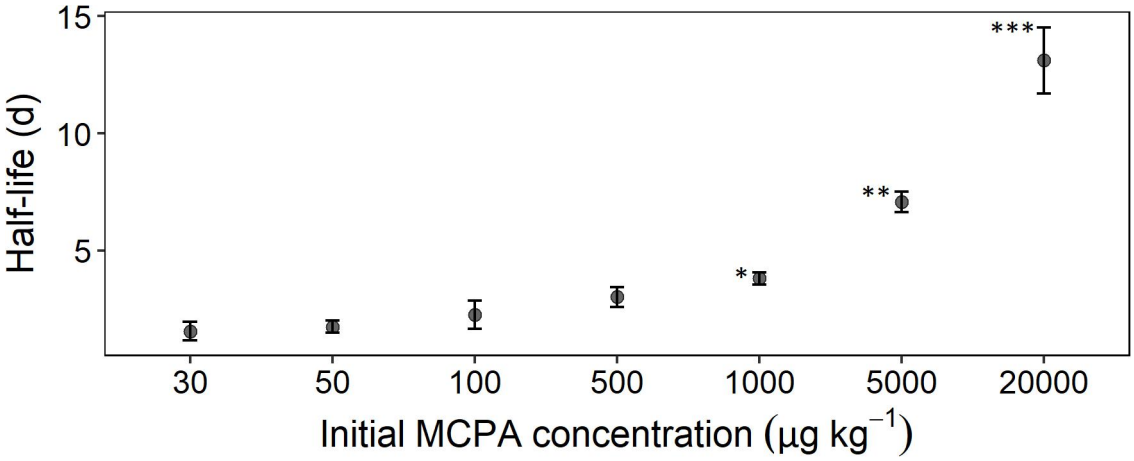

Figure 7: Half-life time as a function of initial concentration calculated according to Eq. 8. Error bars represent the standard deviation. The statistical comparison is always checked against the concentration treatment with 30 µg. Asterisks indicate p-values smaller than *p ≤ 0.05, **p ≤ 0.01, and ***p ≤ 0.001 (n = 3).

4.4.3 ^{14}C assimilation ($^{14}C_{mic}$) and carbon use efficiency (CUE)

Microbial ^{14}C uptake from the labeled MCPA increased only slightly for concentrations in the range of 30 to 1,000 µg kg^{-1} during the 37-day incubation period, remaining almost constant at 2 to 3% (Figure 8).

The MCPA treatment 20,000 µg kg^{-1} had significantly increased ^{14}C incorporation after 15 days ($F_{1,118} = 5.33$, $p < 0.05$), which was approximately 7%, and this increased to about 10% as the experiment progressed (37 days; $F_{1,118} = 19.9$, $p < 0.01$).

In comparison, at a concentration of 5,000 µg kg^{-1}, a significant increase ($F_{1,118} = 7.18$, $p < 0.05$) in ^{14}C content was observed only after 37 days (Figure 4). The CUE, calculated from the ratio of $^{14}CO_2$ respiration and ^{14}C-assimilation, was significantly higher for the two highest concentrations (CUE%, mean = 11.9 ± 4.32; $F_{1,61} = 25.15$, $p < 0.01$) compared to the lower concentrations (mean = 7.35 ± 2.71).

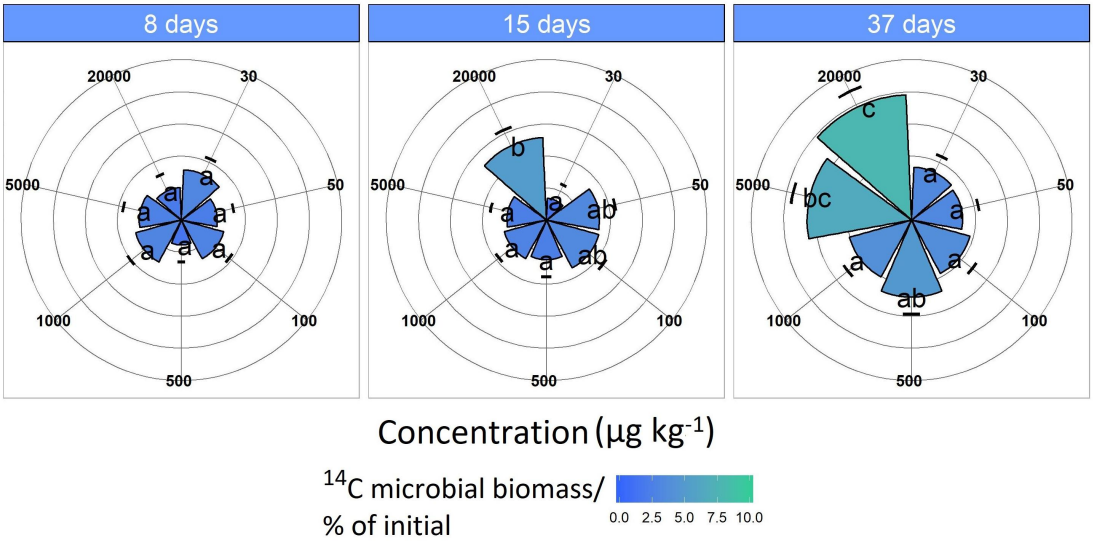

Figure 8: ^{14}C assimilation originates from the labeled MCPA as a function of time. Pie slices and the color gradient from blue to green represent the ^{14}C assimilation for each concentration. Blue indicates a minor and green a higher ^{14}C uptake. Data are presented as means ± SD. Letters indicate a statistically significant difference at $p \leq 0.05$ ($n = 3$).

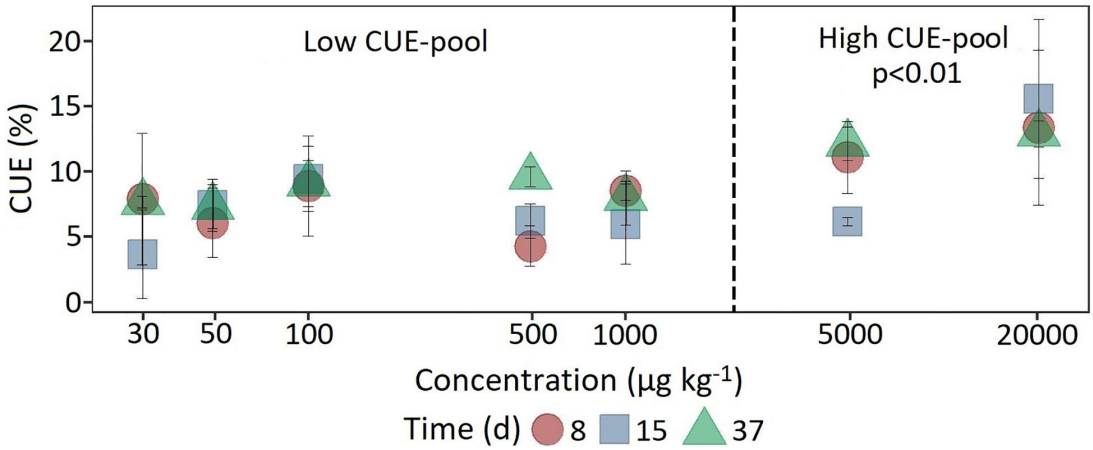

Figure 9: Dynamics of carbon use efficiency calculated from the ratio of respiration and ^{14}C assimilation at the beginning, in the middle and at the end of the experiment as a function of concentration. For statistical comparison, low (30 to 1,000 µg kg^{-1} soil) and high (5,000 to 20,000 µg kg^{-1} soil) concentration levels are pooled together based on the shift in substrate utilization between 1,000 and 5,000 µg kg^{-1} soil. Statistically significant differences are represented as significance levels of $p \leq 0.01$ ($n = 3$).

4.4.4 *TfdA* gene abundance (*tfdA* DNA) and *tfdA* transcript abundance (*tfdA* mRNA)

There were no differences in microbial abundance (16S rRNA) between the individual treatments (data not shown). Only the highest concentration of 20,000 µg kg^{-1} significantly increased *tfdA* gene copy numbers ($F_{1,107} = 14.98$, $p < 0.05$). After a short adaptation phase, *tfdA* DNA increased steadily from the fifth day onward and reached a maximum of 4.73×10^6 copy numbers g^{-1} after 15 days (Figure 6C). The fraction of *tfdA*-harboring microorganisms then decreased between the 15th and 23rd day as quickly as they had increased (Figure 6C).

Compared to the *tfdA* DNA, the *tfdA* mRNA transcript level was slightly more sensitive to MCPA addition. The concentration treatments of 5,000 ($F_{1,105} = 3.39$, $p < 0{,}05$) and 20,000 µg kg^{-1} ($F_{1,105} = 14.29$, $p < 0{,}05$) supported a significant increase in activity for the microorganisms involved in MCPA degradation compared to concentrations of less than 1,000 µg kg^{-1}. In general, *tfdA* gene expression began 4 days before copy numbers of the *tfdA* gene increased and reached a maximum of 1.5×10^4 and 1.89×10^4 copy numbers per g dry weight for the concentrations 5,000 and 20,000 µg kg^{-1}, respectively, after 8 days. Compared to the almost uniform copy number increase, activity decreased more rapidly at 5,000 µg kg^{-1} than at 20,000 µg kg^{-1}; i.e., no further *tfdA* gene expression was detected after 15 days. For the concentration of 20,000 µg kg^{-1}, *tfdA* mRNA abundance reached baseline levels after 22 days (Figure 6D).

4.5 Discussion

4.5.1 MCPA dissipation and cumulative $^{14}CO_2$-respiration

The persistence of pesticides at environmentally low concentrations has been rarely investigated, although their degradation kinetics may substantially differ from degradation at high concentrations (Fomsgaard, 1997a). The aim of this study was, therefore, to

identify shifts in degradation kinetics along a concentration gradient and to test whether the dynamics of the degrader population could explain the formation of persistent pesticide residues. Our initial hypothesis that MCPA degradation is impeded below a specific concentration threshold was not confirmed. However, we were able to group initial MCPA concentrations into two classes, with concentrations <1,000 µg kg^{-1} exhibiting rapid mineralization and concentrations >1,000 µg kg^{-1} exhibiting delayed mineralization.

Our observation that higher concentrations were associated mainly with delayed mineralization is consistent with previous studies (Helweg et al., 1998a; Fomsgaard and Kristensen, 1999a; Bælum et al., 2006; Johnsen et al., 2013). At concentrations of 5,000 and 20,000 µg kg^{-1}, the lag phase was approximately 3 to 5 days (Figures 6A,B). Three main processes for the occurrence of delayed mineralization are mentioned in the literature:

1. An unbalanced initial mRNA synthesis rate of *tfdA* and *tfdB* can lead to toxic 4-chloro-2-methylphenol levels in the cell at initial MCPA concentrations that are much higher (50 and 150 mg kg^{-1}) than applied in our study (Leveau et al., 1999a). The range of initial concentrations used in this study should, therefore, not result in significant metabolite concentrations (Jensen et al., 2004).

2. According to Fomsgaard and Kristensen (1999a)) two sequential first order processes could also be responsible for an extended lag phase at higher concentrations. First, the dissolved fraction of the pesticide is degraded. This is subsequently followed by first-order degradation of the organic matter in which the sorbed fraction of the pesticide is incorporated (Fomsgaard and Kristensen, 1999a). However, MCPA is anionic and therefore weakly adsorbed to soil colloids, usually with K_d in the range of 0.3–1 L kg^{-1} (Helweg, 1987a; Socías-Viciana et al., 1999; Hiller et al., 2006). Sorption should therefore play a minor role.

The third, and in our case most probable, explanation, is that MCPA degradation was

initially limited by the number of MCPA degraders. This presumption was supported by the increase in the number of *tfdA* genes (see below) and by the fitted modified logistic model of (Duo-Sen and Shui-Ming, 1987a). In cases where growth was seen, the curves had a sigmoidal form, reflecting the logistic growth of microorganisms. Comparable results were reported in Reffstrup et al. (1998) where the mineralization of mecoprop concentrations of 5 to 500 $mg\,kg^{-1}$ was described by an exponential form and low concentrations of 0.0005 to 0.5 $mg\,kg^{-1}$ by the zero and first-order forms of the 3/2-order model.

Concentrations of 30 to 50 $\mu g\,kg^{-1}$ showed no lag phase in MCPA mineralization, which contradicts our hypothesis that energy limitation occurs at low concentrations. An initial density of the *tfdA* gene harboring microorganisms in the range of 1.62×10^5 copy numbers g^{-1} was sufficient to convert this MCPA concentration immediately after application. We found that MCPA extraction was no longer possible after a conversion of approximately 40% of the initial applied MCPA (Figures 6A,B), which is consistent with previous studies Helweg (1993a); Helweg et al. (1998a). According to Nowak et al. (2011b), another fraction of the MCPA-C remains in the soil as biogenic residue, where degrading microorganisms utilize the C derived from the pollutant to form cellular components.

4.5.2 ^{14}C assimilation ($^{14}C_{mic}$) and carbon use efficiency (CUE)

The classification of the initial MCPA concentrations according to degradation kinetics was confirmed by differences in MCPA-derived ^{14}C assimilation. At the two high MCPA concentrations, an initially limiting MCPA degrading population was able to grow by incorporating more ^{14}C through higher CUE. Together with the modified fitted logistic model this indicates a shift from catabolic to anabolic microbial utilization of MCPA-derived C.

Transfer of the ^{14}C label to microbial biomass is a useful tool for monitoring the formation of biogenic residues and deducing a total mass balance (Kästner et al., 2016).

The difference between the original amount of MCPA-derived C minus its mineralization is often referred to as non-extractable residues (NER; (Kästner et al., 2016)). According to Nowak et al. (2011b), a significant contribution of biogenic residues to NER formation can be expected, as long as the respective pesticide can be easily degraded by microbes with significant CO_2 formation. In the present study, about 10% of MCPA-derived C remained in the soil as microbial biomass C. However, it is not possible to define exactly the origin of this ^{14}C fraction, i.e., whether it is exclusively from active microorganisms involved in degradation or if a portion of the ^{14}C has been recycled via cross feeding. Assuming that the ^{14}C is present in microorganisms that are still active, this 10% is slightly below the 20% reported in the study by Nowak et al. (2011b) in the case of 2,4-D, which nevertheless explains a considerable proportion of the mass balance. Consequently, for the concentration range from 5,000 to 20,000 µg kg^{-1} MCPA, the following estimate of the C distribution is obtained: about 50% respiration, 10% in the living biomass and 40% remaining as biogenic residues or NER.

In comparison, at concentrations below 1,000 µg, the low incorporation into living biomass (2–3%) indicated that energy use and microbial biomass build-up can also occur at low concentrations. The metabolic utilization of low MCPA concentrations is supported by a functional mechanism that is encoded in the *tfdK* gene and allows MCPA uptake against a concentration gradient; i.e., the concentration inside can be higher than that outside the cell, enabling the use of low pesticide concentrations (Leveau et al., 1998). Therefore, if an active transport system as for MCPA degradation exists, pesticides can probably be degraded even at micromolar concentrations.

4.5.3 *TfdA* gene (DNA) and transcript abundance (mRNA)

In accordance with our second hypothesis, we identified two different concentration limits for growth and activity that supported our classification of the initial MCPA concentration into groups with different residence times (Figure 7). To distinguish

between growth and activity, the number of copies of the *tfdA* gene and transcription level of mRNA synthesis were used as growth and activity indices, respectively. The observed increase in activity at the two highest MCPA concentrations coincided with the slow onset of MCPA dissipation and preceded the actual growth of *tfdA*-harboring microorganisms. Interestingly, the maximum *tfdA* mRNA level was almost identical for both concentrations 5,000 and 20,000 µg kg^{-1} (1.5×10^4 and 1.89×10^4 copy numbers g^{-1}, respectively). This observation is supported by the study of Leveau et al. (1999a), in which the maximum values of mRNA showed no significant increase from 0.1 to 1 mM 2,4-D (0.1 and 1 mM correspond to 20,000 and 200,000 µg kg^{-1}). Ledger et al. (2006) found that this could be explained by a downregulation of *tfdA* synthesis to avoid toxic intermediates. Another reason for similar synthesis maxima at two different initial concentrations may be identical cell concentrations carrying the *tfd*-degradation pathway at the beginning of MCPA degradation.

The actual differences of the higher MCPA concentrations between 5,000 and 20,000 µg kg^{-1} was due to the longer duration of activity, up to 8 days for the highest concentration treatment. This observation was also described in the study by Leveau et al. (1999a), in which a 1 mM concentration shift led to a prolongation of *tfd* expression which could be attributed to a prior decrease in the remaining MCPA to below a threshold for mRNA synthesis at 5,000 µg kg^{-1}.

The inability to detect an increase in *tfdA* gene copy numbers and transcription below 1,000 µg kg^{-1} can be attributed to several factors. On the one hand, the half-life of mRNA is on the order of minutes (Selinger et al., 2003), which means that the timing of measurement is crucial for detectability; mRNA formation may have peaked between MCPA application and the first sampling date. However, we assume that activation of mRNA synthesis requires more than 2 days, since the two highest MCPA concentrations showed a lag phase in mRNA synthesis. On the other hand, the high MCPA concentrations were associated with an increase in *tfdA* mRNA, underscoring

the coupling of gene expression with the presence of MCPA Leveau et al. (1999a). In the case of low molar concentrations, this relationship between gene expression and MCPA concentration can be decoupled; low constitutive enzyme levels would lead to the direct conversion of a small amount of MCPA Leveau et al. (1999a). Due to the rapid degradation rate at concentrations below 1,000 $\mu g\,kg^{-1}$, which could not be associated with additional *tfdA* expression to concentrations above the constituent level, our first hypothesis must be rejected.

However, we could not determine a concentration-related threshold below which the expression of relevant functional genes was inhibited and at which overall pesticide degradation did not continue. This is due to the aforementioned mechanisms that initiate immediate MCPA degradation. Active intracellular transport of low molar concentrations and constitutive gene expression together provide a degradation potential that is independent of the MCPA concentration in the soil.

4.6 Conclusion

This study focused on the biodegradation of gradually increasing pesticide concentrations using a combination of ^{14}C isotope analysis to model degradation kinetics, analysis of functional genes, and transcript abundance. We used MCPA, with a known degradation pathway, as a model compound and clearly showed that fast and slow MCPA degradation are controlled by the initial concentrations, and follow the pattern of physiological reactions. However, we had to reject our first hypothesis that below concentration threshold MCPA degradation is limited by the absence of functional gene expression.

We suggest that our results for MCPA could be extended to other compounds with low sorption affinities and uptake systems that permit transport into the cell at low molar concentrations. For components with higher sorption affinities than MCPA, different degradation mechanisms that determine fate at low concentrations may apply in soils. Further studies are therefore needed to investigate the behavior of moderately and highly

sorptive pesticides at low molar concentrations. These should address the research questions of specific gene regulation in relation to the degradation of low pesticide concentrations and the influence of spatial distribution on bioavailability at low pesticide concentrations.

4.7 Data availability statement

The raw data supporting the conclusions of this article will be made available by the authors, without undue reservation.

4.8 Author contribution

JW, EK, CP, HP, MU, and DB contributed to the conception and design of the study. JW performed the 14C mineralization, CO2 measurement and microbial biomass determination, supported by DB. JW performed the data evaluation and statistics. HP carried out the model fitting for half-life estimation and wrote the corresponding R-code. MU and FD developed the molecular biological methods. MW and CZ developed the measuring method for MCPA using LS-MS/MS. JW wrote the first draft of the manuscript. All authors contributed to the revision of the manuscript, read, and approved the submitted version.

4.9 Funding

This work was supported by the Collaborative Research Center 1253 CAMPOS (Project 6: Controls of the Fate of Agrochemicals in Soils), funded by the German Research Foundation (DFG; grant agreement SFB 1253/1). We acknowledge additional financial support by the Ellrichshausen Foundation.

4.10 Conflict of interest

The authors declare that the research was conducted in the absence of any commercial or financial relationships that could be construed as a potential conflict of interest.

4.11 Acknowledgments

We thank Dr. Andrea Riede for her dedicated support in the isotope laboratory and B.Sc. Rushan He for his excellent technical support and Kathleen Regan for English corrections.

5 Appendices

5.1 Supplementary Information for Chapter 6 (Study I)

Table 4: Reverse transcription

Reaction	Mixture	Temperature profile
reaction 1	11 µl DNA digestion sample	5 min at 65°C
(+ and - sample)	1µl random primer	>= 1 min at 4°C
	1 µl dNTPs	
reaction 2	• Preparation (+ samples):	5 min at 25°C
	4 µl 5x First Strand Buffer	60 min at 50°C
	1 µl 0.1 M DTT (100mM)	15 min at 70°C
	1 µl RNase OUT	Cool down at 4°C
	1 µl reverse transcriptase (200 U/l)	
	13 µl reaction 1	
	• Preparation (- samples):	
	4 µl 5x First Strand Buffer	
	1 µl 0.1 M DTT (100mM)	
	1 µl RNase OUT	
	1 µl DEPC water	
	13 µl reaction 1	

R-code for model fitting (half-life estimation):

https://www.frontiersin.org/articles/10.3389/fmicb.2020.02107/fullsupplementary-material

6 Temperature and soil moisture change microbial allocation of pesticide-derived C

This chapter includes the following publication:

1. Wirsching, J., Chavez-Rodriguez, L., Ditterich, F., Pagel, H., He, R., Uksa, M., Zwiener, C., Kandeler, E., & Poll, C. (2022). "Temperature and soil moisture change microbial allocation of pesticide-derived carbon." Accepted in Ecotoxicology and Environmental Safety

6.1 Graphical abstract

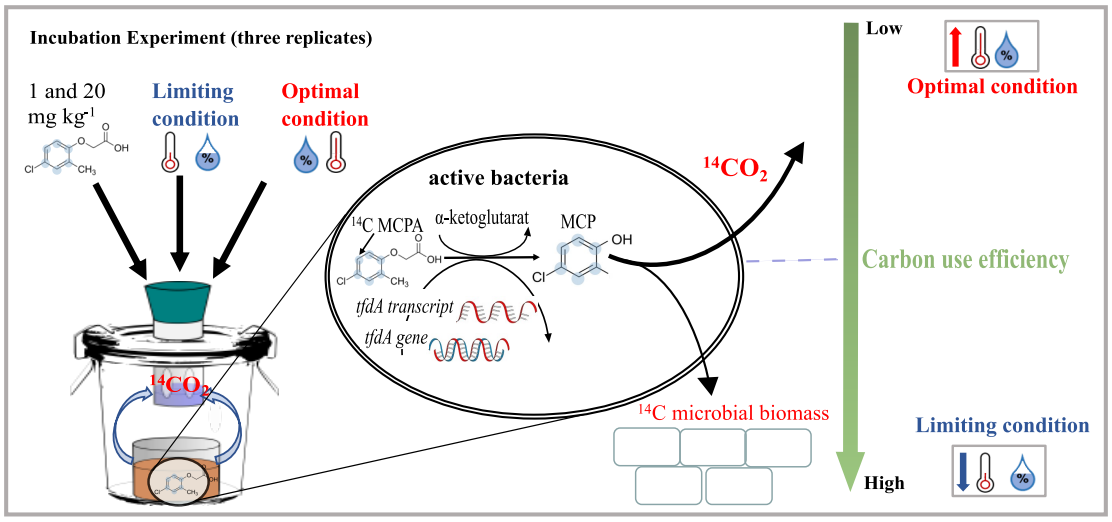

6.2 Abstract

Temperature and soil moisture are known to control pesticide mineralization. Half-lives (DT_{50}) derived from pesticide mineralization curves generally indicate longer residence times at low soil temperature and moisture, but do not indicate changes in microbial allocation of pesticide-derived C. Analysis of carbon use efficiency (CUE, formation of

biomass relative to total C uptake) can provide insights into temperature- and moisture-related physiological adaptations of pesticide degraders. We hypothesized that pesticide mineralization under changing soil moisture and temperature may not be linearly related to total pesticide turnover as drought-tolerant microbes invest C and energy in resistance mechanisms such as osmolyte formation and less maintenance energy is required at lower temperatures.

To test this hypothesis, we performed an microcosm experiment at two MCPA (2-methyl-4-chlorophenoxyacetic acid) concentrations (1 and 20 $mg\,kg^{-1}$) and defined 20°C/pF 1.8 as optimal and 10°C/pF 3.5 as limiting environmental conditions, a common range during the spray season, for pesticide degradation. A mechanistic, gene-based biological degradation model supported data interpretation.

After four weeks, mineralization reached nearly 70% under optimal conditions, but less than 25% under limiting conditions. However, the effect of limiting conditions on MCPA utilization was accompanied by increased CUE, indicating a shift towards anabolic utilization of MCPA-derived C during MCPA degradation. This is confirmed by the divergence of the mineralization-derived DT_{50} values, which indicate a longer residence time than the actual MCPA dissipation. Our results suggest that derivation of DT_{50}-values should not be based on mineralization kinetics alone, especially at low initial concentrations, as unaccounted changes in microbial allocation of pesticide-derived C may lead to overestimated residence times. In addition, our work highlights the importance of CUE for understanding the response of microbial pesticide degradation to variations in soil temperature and moisture.

6.3 Introduction

Pesticide degradation is controlled by environmental conditions such as soil temperature and soil water content. Additionally, pesticide degradation is linked to C cycling when pesticides serve as a sole C and energy source for specialized microorganisms (Pagel

et al., 2016). Thus, ^{14}C-mineralization can be considered a direct activity index for pesticide degradation (Dörfler et al., 1996), and therefore, degradation rates are often determined from mineralization of ^{14}C-labeled pesticides (Helweg, 1987b, 1993b; Schroll et al., 2006; Bouseba et al., 2009). However, assessing pesticide persistence based on ^{14}C-mineralization neglects shifts in microbial C-allocation in response to changes of soil temperature and moisture. Consequently, half-life estimates become inaccurate, and predicted concentrations of pesticide residues often do not match values measured in arable soils (Silva et al., 2019b).

Shifts in microbial C allocation alters microbial carbon use efficiency (CUE), defined as the ratio of newly synthesized biomass C to total C uptake. A low CUE is characterized by a relatively higher mineralization rate, while a high CUE is an indication of enhanced growth and potential C stabilization in soils (Manzoni et al., 2012a). Generally, CUE increases with declining temperature, indicating an increase in relative allocation of assimilated C to growth (Allison et al., 2010). Given this understanding, and despite information in the literature that a temperature increase of 10°C can accelerate pesticide mineralization by a factor of almost 2 (Thirunarayanan et al., 1985; Helweg, 1987b; Choi et al., 1988; Muskus et al., 2020), lower temperatures might not always lead to significantly decreased degradation; they may instead indicate a C redistribution within the microbial cell, where less CO_2 is emitted, as more of it is used to build additional living biomass (Allison et al., 2010).

Muskus et al. (2019a) found that a temperature drop to 10°C resulted in less mineralization of labeled ^{13}C^{15}N-glyphosate, but promoted the formation of ^{13}C non-extractable residues (NER; proteins + other remaining biomass residues (bioNER) + sorbed and sequestered starting compounds (xenoNER)). However, if BioNERs are determined at the end of an experiment, after the death of the microorganisms, information on C uptake dynamics during pesticide turnover is lost. In such a case, uptake of pesticide-derived C is only considered as an additional C reservoir and not as a driver of decomposition. The

dynamics of CUE, i.e., the proportion of the substrate that, over time, immediately goes into microbial biomass in relation to the C lost as CO_2 (Schimel and Schaeffer, 2012), could be an important addition to the conventional mineralization-based approach and provide a more accurate assessment of pesticide degradation at different temperatures.

Soil moisture is one of the most important parameters regulating biological activities in soils (Schroll et al., 2006) and serves as a solubilizer for the movement and distribution of pesticides (Chowdhury et al., 2008). According to Pinheiro et al. (2015b), below the centimeter scale, the fate of pesticides in soils depends on the spatial distribution of pesticide and degraders. In unsaturated soils, where, the contact between pesticide and microorganisms is established only by diffusion or mass flow (Jury et al., 1987) due to the heterogeneous soil matrix (Manzoni and Porporato, 2009), molecular diffusion represents the dominant mode of transport at the smallest spatial scale. Furthermore, the diffusion of dissolved substances, e.g., pesticides, is limited by the proportion of water-filled pores (Hamamoto et al., 2010); determination of water content makes it possible to compare microbial reaction rates between diffusion- and non-diffusion-limited systems (Schroll et al., 2006).

Most of the relevant literature reports that increasing water content, within a soil water potential range of -1.5 to -0.015 MPa (Schroll et al., 2006; Moyano et al., 2013), intensifies the degradation of pesticides (Griffin, 1981; Helweg, 1987b). For example, 2-methyl-4-chlorophenoxyacetic acid (MCPA) persists ten times longer in arid soils than in moist soils (Audus, 1952) due to the moisture-sensitive exponential growth of microbes (Helweg, 1987b). As aridity increases, microorganisms must invest more energy (Parr et al., 1981) in overcoming the suction tension that holds the water in the soil (Griffin, 1969). As energy requirements in drier soils may therefore increase, it is conceivable that the way microbes allocate C will have a profound impact on pesticide mineralization rates. This may mean that, due to physiological trade-offs between C-assimilation and dissimilation under drought conditions (Schimel et al., 2007), $^{14}CO_2$ mineralization may

not be linearly related to total pesticide turnover (Zeglin et al., 2013).

Specifically, drought-tolerant microbes invest heavily in the formation of extracellular enzymes to maintain carbon uptake for the synthesis of stress response compounds such as osmolytes, cryoprotectants, and chaperones (Schimel et al., 2007) to stabilize cell pressure (Manzoni et al., 2014). This would imply that pesticide mineralization is not synonymous with microbial pesticide degradation since microbial C utilization plays a decisive role. This mechanism has already been demonstrated for soil C turnover by Zeglin et al. (2013), in which soil C sequestration potential was higher under dry conditions.

Degradation rate and C allocation are affected not only by environmental conditions, but also by initial pesticide concentration (Schoen and Winterlin, 1987; Karanasios et al., 2012). Pesticide degradation at low concentrations usually follows first order kinetics and is often astonishingly fast (Helweg et al., 1998b; Fomsgaard and Kristensen, 1999b). In contrast, pesticide degradation at high concentrations is slower and accompanied by a simultaneous increase in degradation activity and genetic degradation potential (Ditterich et al., 2013b). With respect to C-allocation, in a previous study we (Wirsching et al., 2020a) demonstrated that the predominantly catabolic use of MCPA at concentrations $\leq$ 1 mg kg^{-1} shifted towards a gradually increasing anabolic metabolism at concentrations $\geq$ 5 mg kg^{-1}. If initial pesticide concentration determines C use by microbial pesticide degraders, the impacts of temperature and moisture on C allocation may also depend on pesticide concentration.

Therefore, we aimed to investigate how temperature, soil moisture and their interaction affect degradation at two MCPA concentrations (1 and 20 mg kg^{-1}), evaluate microbial allocation of MCPA-derived C, and determine whether carbon redistribution could explain a deviation of mineralization-based half-life from actual MCPA dissipation. We used ^{14}C-labeled MCPA as a model compound since it is a weakly adsorbing pesticide (Patzko, 2009) that is readily soluble in water (Fredslund et al., 2008) and highly biodegradable

(Oh et al., 1995). Another advantage of using MCPA is that the functional genes involved in MCPA degradation have been well characterized (Nicolaisen et al., 2008b) and can support our understanding of MPCA degradation dynamics.We hypothesized that at lower temperature and soil moisture i) higher CUE results in an increase in ^{14}C content in microbial biomass, and ii) this carbon redistribution may result in a substantial overestimation of pesticide half-life if derived only from ^{14}C mineralization curves. We expected that iii) the effect size would be more pronounced at higher initial concentrations.

To test these hypotheses, we determined the temporal relationship between mineralization ($^{14}CO_2$) and biomass formation ($^{14}C_{mic}$, i.e., CUE), and measured alterations in microbial degradation activity (*tfdA* mRNA) and MCPA-degrading genetic potential (*tfdA* DNA). To complement the experimentally determined CUE, we calibrated a gene-centric model using the experimental data (mineralization, *tfdA* mRNA, and *tfdA*). Based on the calibrated model, we predicted two model-based CUEs to interpret the pesticide-derived C use of specific MCPA degraders.

6.4 Materials and Methods

6.4.1 Soil origin and sampling

The study site was in the central region of the Ammer catchment in southwest Germany (48°33'24.664", 8°52'31.259"). Soil samples were taken in March 2019 from an Ap-horizon (0-30 cm) of a silty Luvisol (World Reference Basis for Soil Resources). According to farmers' records of their cropping and spraying programs going back to 1990, MCPA had never been applied to the agricultural field. The main pesticides applied were chloridazone and metamitron. After sampling, the soil was sieved (<2 mm), homogenized, and stored at -20 °C (-80 °C for mRNA samples) to prevent further biological reactions. The main characteristics of the soil are shown in Table 5.

Table 5: Chemical and physical soil properties

Soil Horizon	Depth	pH	C_{org}	Nitrogen	Phosphate	Sand	Silt	Clay
Ap	[cm]	[$CaCl_2$]	[mg g^{-1}]	[mg g^{-1}]	[mg g^{-1}]	[%]	[%]	[%]
	0-5	6.48	18.4	2.1	1.038	2.26	72.04	23.8

6.4.2 Experimental Design

The experimental setup consisted of two soil temperature (10 and 20 °C), two soil water content (pF 1.8 and 3.5), and two concentration treatments of ^{14}C ring-labeled MCPA (1 and 20 mg kg^{-1} dry weight) plus one control treatment without MPCA application. In this study, we defined 10°C, pF 3.5, and the lower MCPA concentrations as limiting conditions and 20°C, pF 1.8, and the higher MCPA concentration as optimal conditions for microbial degradation. We chose concentrations based on Wirsching et al. (2020a) because first-order degradation is very rapid at 1 mg kg^{-1} and microbial growth does not occur until 20 mg kg^{-1}. Additionally, 20 mg kg^{-1} represents typical applications of MCPA in the field.

A set of microcosms with all treatment combinations consisted of 36 samples (2 water content levels x 2 soil temperature levels x 3 MCPA concentrations (including the control) x 3 replicates). Four of these sets were prepared, yielding in total 144 microcosms (Figure S1). MCPA solution was uniformly applied to adjust gravimetric soil water content to 39.6% (pF 1.8) and 29.1% (pF 3.5). Subsequently, after thoroughly mixing the soil with the MCPA solution, cylinders (diameter = 5.6 cm, height = 4 cm) were filled with 100 g of soil and compacted to a bulk density of 1.2 g cm^{-3} (height of the soil core was 3 cm).

In three of these sets (108 microcosms), ^{14}C-ring labeled MCPA with an activity of 15 kBq (99% purity, specific activity 50-60 mCi mmol^{-1}; BIOTREND Chemikalien GmbH, Germany) was applied. One set was sacrificed at each of three time points (5, 15 and 28 days, sampling schedule Table 7) to quantify ^{14}C incorporation into microbial biomass ($^{14}C_{mic}$). Time points were selected according to the evolution of the $^{14}CO_2$ mineralization curve, i.e., in the initial lag phase (no $^{14}CO_2$ evolution), in the exponential degradation

phase (maximum $^{14}CO_2$ evolution), and in the final saturation phase (renewed decrease in $^{14}CO_2$ evolution). In the last sacrificed set, $^{14}CO_2$-respiration was measured every second day. In the fourth set (36 microcosms) only unlabeled MCPA (analytical MCPA purity 99.2%, Sigma-Aldrich, Germany) was applied. A series of subsamples (on every second day) was taken and stored at -20 °C for MCPA quantification and at -80 °C for RNA/DNA co-extraction (RNA stability can only be guaranteed at -80 °C) until the analysis.

6.4.3 MCPA dissipation

MCPA was extracted from 2 g of soil dissolved in a suspension of 10mL methanol/water (1:1) as described by Pagel et al. (2016). MCPA was quantified by HPLC-MS/MS analysis (tandem mass spectrometry; Agilent 6490 iFunnel Triple Quadrupole (QqQ), Waldbronn-Germany). The recovery of total MCPA from soil samples was greater than 98% with a detection limit of 13 $\mu g\,kg^{-1}$ (detailed information in the Supplement).

6.4.4 MCPA mineralization ($^{14}CO_2$)

To determine the MCPA-derived $^{14}CO_2$ respiration, an aliquot of 1 mL was taken every second day from a CO_2 trap containing 2 mL 1M NaOH set up in the microcosm. It was then mixed with 4 ml of scintillation liquid (Rotiszint Eco Plus, Carl Roth GmbH + Co. KG) in a 5 mL scintillation vial (LDPE). The decay rate in bequerels (Bq) was measured using a scintillation counter (Wallac 1411, Liquid Scintillation Counter, USA, detailed information in the Supplement).

The half-lives (DT_{50MIN}) derived from the cumulative mineralization curves were calculated from the estimated parameters of the fitted eqs.10 and 11 (see also Duo-Sen and Shui-Ming (1987b) and Wirsching et al. (2020a)):

$$C = C_0 \cdot \left(1 - \frac{1}{(1 - f_k) \cdot e^{k_1 \cdot t} + f_k}\right) \tag{10}$$

$$\mathrm{DT}_{50\mathrm{MIN}} = \frac{1}{k_1} \cdot \ln\left[\frac{1}{1 - f_k} + 1\right] \tag{11}$$

Where C is the MCPA-derived $^{14}CO_2$ (% of MCPA initially applied), C_0 is the total mineralizable MCPA that was not immediately incorporated into the microbial biomass or bound to the soil organic matter after application (% of MCPA initially applied), k_1 (d^{-1}) is the rate constant of MCPA degradation per day, and and f_k is a dimensionless parameter, where the range of f_k is constrained as $0 \leq f_k < 1$ (Wirsching et al., 2020a).

6.4.5 Microbial biomass (C_{mic})

Microbial biomass was estimated using the chloroform fumigation extraction method (CFE) developed by Vance et al. (1987), adapted by Poll et al. (2010b) for an additional ^{14}C determination. To obtain the ^{14}C content in C_{mic}, 1 mL of the CFE supernatant was mixed with 4 mL scintillation liquid (Rotiszint Eco Plus, Carl Roth GmbH+Co. KG) in a 5 mL scintillation vial (LDPE). Subsequently, the decay rate in Bq was determined using a scintillation counter (Wallac 1411, Liquid Scintillation Counter, USA). Calculation of the incorporated ^{14}C was performed as described for the C_{mic} content in the Supplement.

6.4.6 DNA/RNA co-extraction

For RNA and DNA extraction, 2 g frozen soil was weighed into 15 mL bead-beating tubes and extracted using the RNAeasy PowerSoil Total RNA Kit for soil (Qiagen, Germany) and the RNAeasy PowerSoil DNA Elution Kit (Qiagen, Germany) in a co-extraction method following the manufacturer's protocol. Before using the RNA-samples for Real-Time quantitative PCR (qPCR), possible remaining DNA in the RNA samples was digested using the TURBO DNA-free™ Kit (Invitrogen, Thermo Fisher Scientific, Germany, Table 8).

6.4.7 Real-Time quantitative PCR (qPCR)

For gene quantification (bacterial 16S rRNA and functional genes), qPCR assays were applied using an ABI Prism 7500 Fast system (Applied Biosystems, Germany) with SYBR Green detection. The primer and qPCR conditions used are listed in Table 10. Each SYBR Green reaction contained 7.5 µL of Power SYBR® Green PCR master mix (Applied Biosystems, Germany), 0.75 µL of each primer (5 µM), 0.375 µL of T4gp32 (MP Biomedicals, Germany), 3.625 µL water and 2 µL diluted template DNA or cDNA (3 ng µL^{-1}) for functional genes (*tfdA* and *cadA*). For 16S rRNA, 1 µL diluted template DNA or cDNA (3 ng µL^{-1}) and 4.625 µL of water was used. For quantification, standard plasmid DNA was used with a dilution series from 10^8 to 10^1 copies µL^{-1} according to Ditterich et al. (2013b). *CadA* showed no response to MCPA addition and was therefore not considered during the study.

6.4.8 Gene-centric modeling of MCPA biodegradation

We used a recently developed modeling approach (ref. to Chavez Rodriguez et al. (2020)) to simulate MCPA mineralization (C_P [mmol g^{-1}]), *tfdA* genes and transcripts [copies g^{-1}], and carbon use efficiency (CUE). The original modeling approach was extended to account for constitutive gene expression and to include a temperature response function as follows:

1. We assumed gene expression to be in quasi-steady state described by the Hill function, including constitutive gene expression that is potentially important at low concentrations:

$$\widehat{mRNA} = f_T \cdot \left(\frac{(C_P^L)^{n_H}}{(C_P^L)^{n_H} + (K_G)^{n_H}} + \frac{\alpha}{f_T} \right) \tag{12}$$

   where f_T represents the number of transcripts per gene, n_H [-] and K_G [mmol cm^{-3}] are the Hill exponent and Hill constant respectively, α is the constitutive gene expression coefficient set to $1.2 \cdot 10^{-5}$ transcripts per gene (Leveau et al., 1999b),

and C_P^L [mmol cm^{-3}] is the solution phase concentration of MCPA.

2. We used the temperature response function $f_R(T)$ from Sierra et al. (2015), which influences microbial growth, but also decay rate, exogenous and endogenous maintenance rates, and decay rate of non-extractable residues, and is defined as:

$$f_R(T) = (Q_{10})^{\left(\frac{T - 10°C}{10°C}\right)} \tag{13}$$

where Q_{10} [-] is the temperature function constant, and T is the temperature in °C.

The full model description, process formulations and model equations can be found in the Supplementary Information, section 8.1.8 Model parameter ranges are found in Table 11 in the Supplementary Information.

6.4.9 Model calibration

We performed a hierarchical model calibration using the parameter ranges from Table 11. Model calibration was achieved by minimizing the sum of squared error (SSE) with the optimization algorithm Simulated Annealing from MATLAB:

$$SSE = \sum_{i=1}^{n} \frac{(y^i_{measured} - y^i_{simulated})^2}{\sigma_i^2} \tag{14}$$

where $y_{measured}$ is the mean value of the i^{th} observation, $y_{simulated}$ is the corresponding i^{th} simulated value, and σ^2 is the standard deviation of the corresponding observations.

The hierarchy of parameter groups was formed by assuming: i) different bacterial subpopulations under the two different initial concentrations of MCPA (C), ii) possible physiological and morphological bacterial changes under different moisture levels (W) that were not well captured by moisture functions found in the literature, and iii) specific soil-dependent parameters (S). Thus, parameters for calibration were grouped according to the proposed hierarchy (Table 11).

Model outputs corresponding to the measured data for model calibration are the following:

$$\text{Mineralization [\%]} = \frac{^{14}\text{CO}_2 \cdot 100\%}{^{14}C^0_{MCPA}} \quad (15)$$

$$\text{Genes [copies g}^{-1}\text{]} = \frac{C_B}{f_1} \quad (16)$$

$$\text{Transcripts [copies g}^{-1}\text{]} = \frac{\widehat{mRNA} \cdot C_B}{f_1} \quad (17)$$

$$\text{Residual MCPA [mg kg}^{-1}\text{]} = C^L_P \cdot \frac{\theta}{\rho} + K_P \cdot \left(C^L_P\right)^{n_P} \quad (18)$$

$$\text{DT}_{50\text{RES}}\ [\text{d}^{-1}] = Time[(\text{Residual MCPA} = 0.5 \cdot C^0_{MCPA})] \quad (19)$$

where f_1 [mmol gene^{-1}] is the conversion factor cell to carbon (Table 11). Incorporation of ^{14}C into the microbial biomass (C_{mic}) as well as CUE were not used for model calibration.

We complemented our model calibration with a local sensitivity analysis of our parameter fits through the sensitivity coefficient (Ingalls, 2008; Zi, 2011), identifiability score (Yao et al., 2003; Malwade et al., 2017) and error (Malwade et al., 2017) of estimated parameters.

6.4.10 Carbon use efficiency (CUE)

We derived CUE both experimentally and with two model-based CUE_S:

1. CUE_M: experiment-based CUE used for labeled substances (Sinsabaugh et al., 2013).

$$CUE_M = \frac{^{14}C_{mic}}{^{14}C_{mic} + R_{cum}} \quad (20)$$

where: $^{14}C_{mic}$ is the C uptake in microbial biomass, and R_{cum} is the cumulative respiration rate.

2. CUE_E: environmental model-based CUE adapted from Geyer et al. (2016).

$$CUE_E = \frac{C_B^{14}}{C_B^{14} + {}^{14}CO_2} \tag{21}$$

3. CUE_C: community model-based CUE adapted from Geyer et al. (2016) and Manzoni et al. (2018).

$$CUE_C = 1 - \frac{r^{14}_{respiration} + r^{14}_{m-endogenous} + r^{14}_{m-exogenous} + r^{NER}_{decay}}{r^{14}_{respiration} + r^{14}_{growth} + r^{14}_{m-exogenous}} \tag{22}$$

6.4.11 Statistical analysis

A linear model with mixed effects as part of the "nlme" package using the lme function (Pinheiro et al., 2020) implemented in R version 3.5.2 was applied, specifying concentration, soil moisture, temperature and their interactions as fixed effects, with microcosms as random effects. Response variables were ^{14}C mineralization rate, ^{14}C uptake, CUE, *tfdA* gene expression, and *tfdA* abundance. Model assumptions from ANOVA were visually confirmed by residual diagnostic plots (Kozak and Piepho, 2018). For specification of contrasts between the influencing factors relevant for the verification of our hypothesis, a post-hoc comparison was conducted using the package “emmeans” (Lenth et al., 2020). With this package, the estimated marginal means were calculated, and interaction plots were made by using the “emmip” function to display the interactions between the variables soil moisture, temperature, and concentration. The influences of the variables were compared pairwise with the Tukey method, and the standard error (SE) and p-value for each result was simultaneously computed.

6.5 Results and discussion

Pesticide degradation studies often fail to consider the possibility that the efficiency of microbial C utilization can shift in response to environmental factors (Allison et al.,

2010; Manzoni et al., 2012a). Our study, therefore, analyzed microbial utilization of the pesticide MCPA in response to limiting (10°C/pF 3.5) and optimal (20°C/pF 1.8) environmental conditions. In addition to estimating the mineralization of ^{14}C-labeled MCPA and the dynamics of specific degraders, we calculated the CUE of MCPA turnover to evaluate microbial C allocation to catabolic and anabolic processes. We complemented our analyses with a mechanistic gene-based biodegradation model, which was fitted to the experimental data (Table 12).

6.5.1 Enhanced MCPA mineralization by elevated temperature and moisture

Maximum microbial MCPA mineralization among treatments was determined by accumulated $^{14}CO_2$ production at the end of the incubation period (Figure 10 A, B, C, D). Under optimal soil conditions (20°C, pF 1.8) and 20 mg kg^{-1}, nearly 70% of the initially applied ^{14}C-labeled MCPA was mineralized. Under limiting conditions (10°C, pF 3.5) and 1 mg kg^{-1}, mineralization was significantly reduced and peaked at only 23%. These results were confirmed by our model simulations, which accurately depicted the measured mineralization (Figure 10 A, B, C, D).

As a single factor, a temperature increase from 10 to 20°C resulted in an increase in $^{14}CO_2$ mineralization of 10.5% ($F_{1,16} = 73.9$, $p < 0.01$). However, the effect was significantly more pronounced at high MCPA concentrations (+17.7%) than at low MCPA concentrations (+3.4%, $F_{1,16} = 35.2$, $p < 0.001$; Figure 10 A, B, C, D). Comparable temperature-dependent increases in mineralization were demonstrated in studies by Nowak et al. (2020a) and Muskus et al. (2020) for glyphosate, Helweg (1993b) for mecoprop (MCPP), and Bouseba et al. (2009) for 2,4-D. These increases in ^{14}C mineralization appeared to be independent of the chemical properties and associated behaviours of those pesticides in soils. In our experiment, an explanation could be found in the temperature sensitivity of the enzyme-catalyzed reactions of MCPA degradation, which are associated with inherent kinetic properties (intrinsic temperature sensitivity) and

a concentration-dependent response of mineralization rates to temperature (apparent temperature sensitivity, (Davidson and Janssens, 2006)).

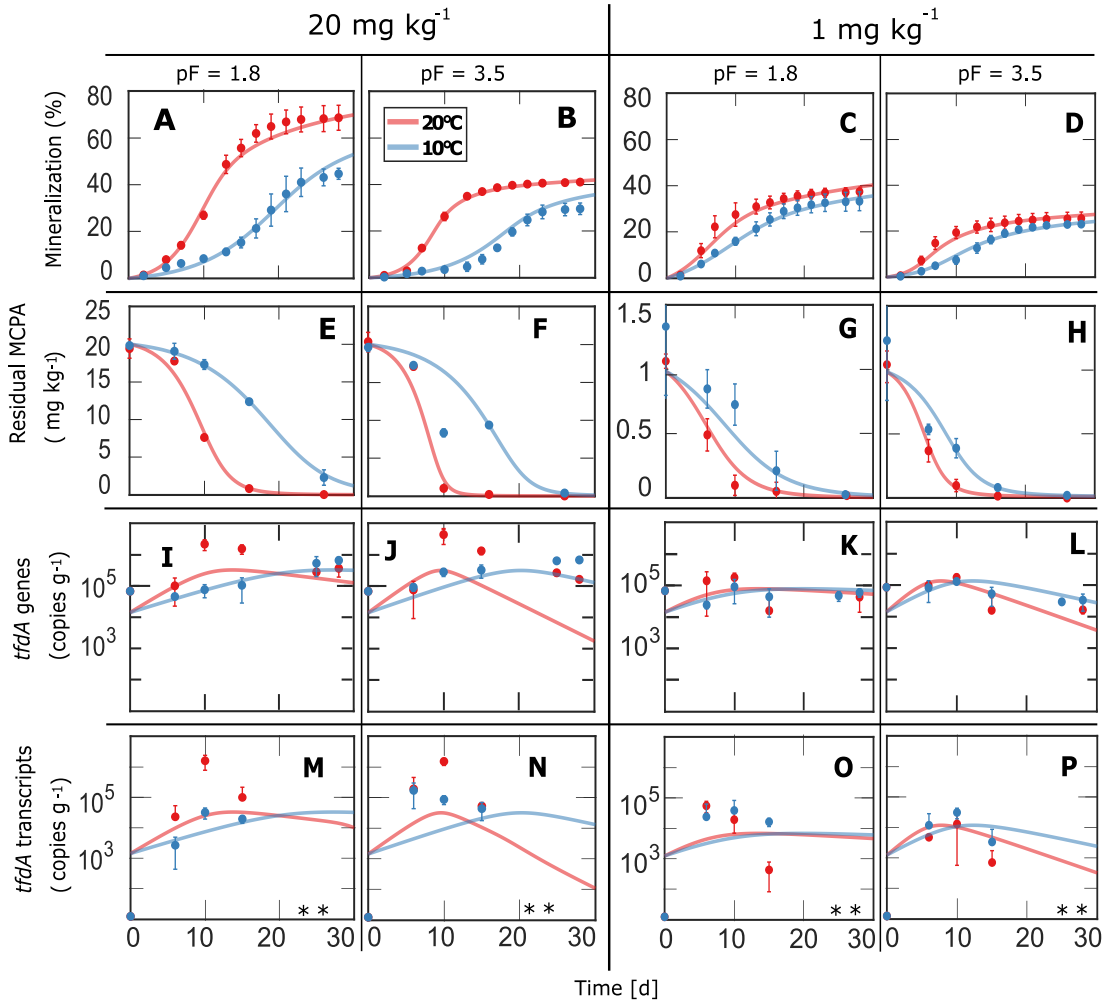

Figure 10: Measured (dots) and simulated (lines) of cumulative $^{14}CO_2$ mineralization at two MCPA concentrations as a function of temperature and soil moisture over time (A, B, C, D), Residual MCPA expressed as mg kg^{-1} over time (E, F, G, H), *tfdA* genes during the MCPA biodegradation experiment expressed as gene copies g^{-1} dw (I, J, K, L), *tfdA* transcripts quantities during MCPA degradation expressed as copies g^{-1} dw (M, N, O, P). *tfdA* genes and transcripts are expressed at log-scale. Error bars represent standard errors of the mean values for soil triplicates (see M&M). *tfdA* transcript abundances at days 25 and 28 (* in panels M to P) were below the detection limit and therefore were not included in the model calibration.

Additionally, we evaluated the effect of water content as a sole factor, in which a reduction from pF 1.8 to 3.5 resulted in the strongest decrease in $^{14}CO_2$ mineralization (-16.2 % $F_{1,16} = 136$, $p < 0.01$). This effect was most pronounced at the high MCPA concentration ($F_{1,16} = 17.9$, $p < 0.001$), where total mineralization was 21.3% higher at pF 1.8 as compared to pF 3.5 (Figure 10 A,B). At the low MCPA concentrations, this increase was only 11.0% (Figure 10 C, D). Microbial activity tipically decreases with increasing osmotic potential, as demonstrated by Sparling et al. (1989). According to Ilstedt et al. (2000), the reason a reduction in water content also reduces the maximum mineralizable ^{14}C fraction of MCPA is related to substrate diffusion limitation due to reduced thickness of the water film on soil particles as osmotic potential declines (Papendick and Campbell, 1981). Schroll et al. (2006) determined a water potential for aerobically degradable chemicals of -0.015 MPa, which corresponds to a pF value of about 2.2, slightly below the pF-value of 1.8.

Evaluation of MCPA residues (Figure 10 E-H) indicated almost complete degradation, especially in the 1 mg kg^{-1} treatment at 20°C, in which MCPA was no longer detectable after 10 to 15 days. Ten percent of the initial applied MCPA remained in the soil only under the treatment combination of 20 mg mg kg^{-1}, 10°C and pF 1.8. In the treatment combination pF 3.5 and 20°C, no MCPA could be extracted after 20 days. If the incubation took place at 10°C, MCPA was no longer detectable after 25 days. Similar detection times for MCPA were reported by Baelum et al. (2006), Jacob et al. (2006), Hiller et al. (2009), and Peña et al. (2015).

6.5.2 Invariable microbial dynamics under limiting temperature and moisture

Potential of MCPA degradation and microbial activity were measured through *tfdA* gene (Figure 10 I-L) and transcript abundances (Figure 10 M-P), respectively. The *tfdA* gene abundance responded only to the 20 mg kg^{-1} and 20°C treatment (Figure 10 I, J). The abundance of *tfdA* genes reached a maximum 10 days after MCPA application; with

significantly higher copy numbers at pF 3.5 ($4.3 \cdot 10^6$ copies g^{-1} dry weight (dw)) than at pF 1.8 ($2.2 \cdot 10^6$ copies g^{-1} dw; day:pF; $F_{1,24} = 16.48$, $p < 0.01$). After the peak, a slow decline followed until day 28, after which the initial level of 10^4 copies g^{-1} dw was reached again. The concentration-dependent proliferation of *tfdA*-harboring microorganisms is consistent with the study by Bælum et al. (2008b), which demonstrated a similar increase from $1 \cdot 10^4$ to $3 \cdot 10^6$ copies g^{-1} dw during the degradation of 20 mg kg^{-1} MCPA.

Below 20 mg kg^{-1}, *tfdA* DNA remained at a consistently low level, indicating no growth occurred during mineralization (Nicolaisen et al., 2008b). The response of *tfdA* transcripts to concentration and temperature mirrored the patterns of *tfdA* gene abundance (concentration:day:temperature; $F_{1,96} = 30.01$, $p < 0.001$), with a clear response to the treatment of 20 mg kg^{-1} MCPA at 20°C. However, soil moisture had no effect on gene transcription ($F_{1,24} = 1.51$, $p = 0.90$). We also observed a correlation between the detected levels of *tfdA* mRNA (Figure 10 M-P) and the mineralized pesticide (Figure 10 A-D). For example, no *tfdA* mRNA was detected in the control treatments (data not shown), and *tfdA* mRNA was only detected once mineralization of MCPA could be measured.

After a lag phase of approximately 5 days, there was a slow increase in $^{14}CO_2$-mineralization accompanied by an increase in *tfdA* mRNA from an average of 10^1 on day 0 to a peak of 10^6 copies g^{-1} dw on day 10. At this time, the inflection point of the sigmoidal $^{14}CO_2$ mineralization curve was attained: i.e., the maximum degradation intensity. Subsequently, $^{14}CO_2$-mineralization decreased again, coinciding with a drop in *tfdA* transcript abundance, which fell below our detection limit (10^3 copies g^{-1} dw) for mRNA quantification at day 28 (Figure 10 M,N).

Similar results were obtained by Vieublé Gonod (2002) and Bælum et al. (2008b), where an initial "lag" period (0 - 8d) with minor mineralization indicated limited microbial pesticide turnover. In a second phase characterized by a sharp increase in mineralization (after day eight), Bælum et al. (2008b) detected a maximum *tfdA* level of 10^4 transcripts

per gram soil on day 16, followed by a decline to approximately 10^3 copies on day 24.

The observed patterns of *tfdA* gene and transcript dynamics were well captured by gene-based mechanistic model simulation. According to Gözdereliler et al. (2013), different degrader subpopulations are adapted to different MCPA concentrations. Therefore, we allowed the parameters f_1 (conversion factor cell to carbon), m (maintenance coefficient), and Y_P (yield coefficient) to take different values at 1 and 20 $\mathrm{mg\,kg^{-1}}$. Calibrated parameters (Table 12) suggested populations with bigger cells, higher maintenance demands and lower yield efficiencies at 20 $\mathrm{mg\,kg^{-1}}$ than at 1 $\mathrm{mg\,kg^{-1}}$, which is in accordance with Gözdereliler et al. (2013). Additionally, within each concentration level, slightly smaller cells with low maintenance demands and high yield efficiencies might be expected at pF 3.5.

6.5.3 CUE dependency on temperature, moisture, and MCPA concentration

We determined CUE_M based on measured ^{14}C incorporation into microbial biomass (Sinsabaugh et al., 2013). Additionally, and taking advantage of our mechanistic gene-centric model, we derived two model-based carbon use efficiencies - CUE_E and CUE_C. While CUE_M accounts for pesticide-derived C incorporation into the entire microbial community, the two model-based carbon use efficiencies exclusively consider C utilization by specific pesticide degraders. CUE_M and CUE_E measure effects of pesticide-C stabilization on carbon utilization over a longer period, taking into account the effects of biomass turnover, substrate recycling, and potential cross-feeding (Geyer et al., 2016). CUE_C is calculated from simulated process rates and measures the immediate carbon utilization after MCPA uptake.

The prerequisite for CUE_M assessment is quantification of ^{14}C incorporation into the biomass ($^{14}C_{mic}$). Soil moisture did not affect $^{14}C_{mic}$ (Table 20). In contrast, a temperature reduction to 10°C significantly increased $^{14}C_{mic}$ during the first five days after MCPA application by 3 percentage points to 10% ($F_{1,16} = 4.9$, $p < 0.05$), compared

to the 20°C treatment. Microbial uptake of MCPA can occur very quickly, according to Nowak et al. (2011a), who found a peak in 2,4-D derived ^{13}C after only two days. They identified bacteria as the main degraders of 2,4-D in the soil. However, an initial high $^{14}C_{mic}$ is followed by ^{14}C losses, since the ^{14}C is assimilated to form precursor compounds (PreC) for further biosynthesis or is dissimilated for maintenance respiration (Geyer et al., 2016).

This short-term metabolic reaction of degraders is represented by the CUE_C (Figure 14). On average, CUE_C increased by 0.2 at 1 mg kg^{-1} compared to 20 mg kg^{-1}. The CUE_C in relation to the remaining MCPA concentration reached zero at 1 mg kg^{-1} and pF 1.8 after about 99% of the initially applied MCPA was degraded; this was in contrast to the 20 mg kg^{-1} treatment, where this point was reached earlier (90%, Figure 14). These findings indicate a more efficient utilization of MCPA-derived C at low initial concentrations and longer-lasting gross production. Gross production is defined as total pesticide uptake minus pesticide-C that is mineralized and used for further biosynthesis processes (Geyer et al., 2016). Therefore, in contradiction to the constant metabolic flux analysis of Geyer et al. (2019), in which no change in the biochemical processes was detected during the incubation of different glucose concentrations, we can confirm a decrease in CUE_C for MCPA at 20 mg kg^{-1}. Lower CUE_C under higher MCPA concentration is likely attributable to two different fitted values of growth yield parameters for each initial MCPA concentration (Table 12). This finding supports the inherent model assumption made in accordance with Gözdereliler et al. (2013) that two subpopulations of pesticide degraders with different physiologies trigger concentration-dependent shifts in pesticide-C metabolism. Metabolic regulations leading to increased nutrient-mobilizing extracellular enzymes or carbon-wasting respiratory mechanisms under nutrient limitations could also be responsible for lower CUE_C (Manzoni et al., 2017). However, these processes can be ruled out in fertilized soils; in addition, we used the same homogenized soil for all treatments ruling out any differences in nutrient

availability between treatments. Short term differences in CUE_C should affect the long-

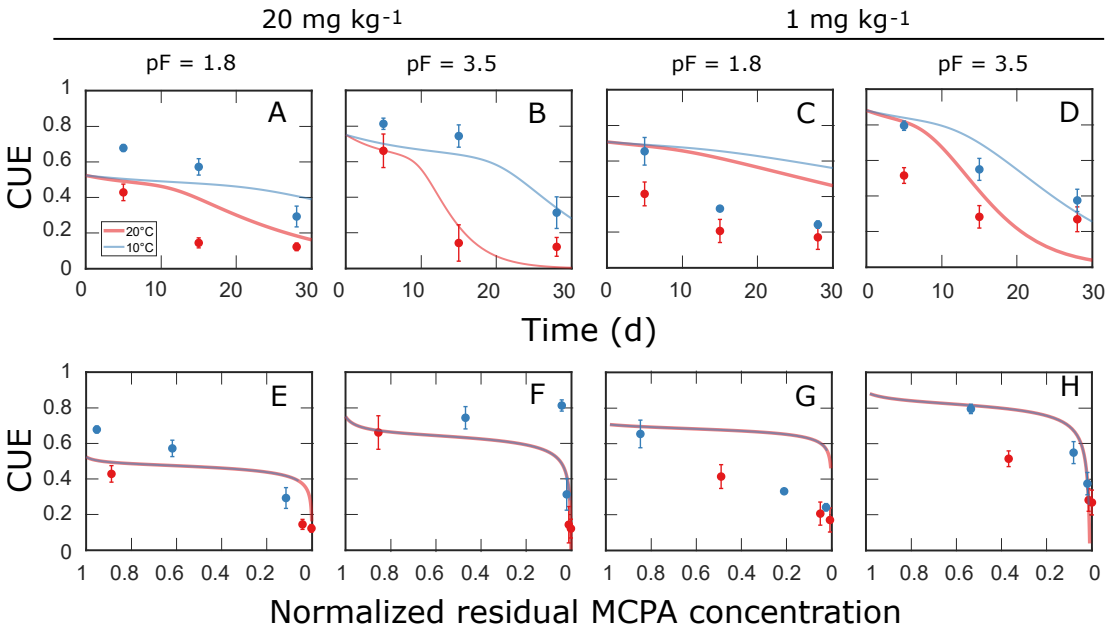

Figure 11: CUE vs. time (d) showed in panels A to D, and CUE vs normalized residual MCPA concentration in soil showed in panels E to H. CUE_M (Eq. 20) is presented as points and CUE_E (Eq. 21) as lines. Note that the CUE_M were not used for model calibration (see M&M).

term fate of the MCPA-C, as measured by CUE_M and CUE_E. CUE_M was significantly higher during the MCPA degradation at 20 mg kg^{-1} compared to 1 mg kg^{-1} (+ 0.06; $F_{1,16} = 5.8$, $p < 0.05$) during the first 15 days (Figure 11 A, B, C, D). CUE_M can only be statistically evaluated by comparison at each time point. But, comparing CUE_M over time is misleading, as different states of degradation dynamics are being compared. To eliminate this deviation, CUE_E was considered as a function of the relative decrease in MCPA concentration (Figure 11 E, F, G, H). The simulated CUE_E is about 0.2 higher at low concentrations than at high concentrations, indicating greater carbon stabilization at the ecosystem level at low concentrations. For CUE_M, this effect was only evident at the end of the incubation ($CUE = 0.21$; $F_{1,16} = 4.3$, $p = 0.05$).

We observed an increase in CUE_M with decreasing temperature (Figure 11 A, B, C, D),

which also has previously been reported (Frey et al., 2013; Domeignoz-Horta et al., 2020; Dacal et al., 2021), and is associated with higher growth efficiencies (Domeignoz-Horta et al., 2020; Pold et al., 2020) and lower energy costs to maintain existing biomass (Sinsabaugh et al., 2013; Gözdereliler et al., 2013). An additional temperature effect is that increased microbial activity at 20°C leads to increased MCPA turnover especially at 20 $mg\,kg^{-1}$, which is in agreement with the Arrhenius equation (Laidler, 1984). The substrate concentration was therefore present longer at 10°C and as a result, maintained a higher CUE_M for a longer time (Figure 11 E, F, G, H). The simulated carbon use efficiencies did not indicate the temperature effect (Figure 11 E, F, G, H), because the model assumptions for CUE_E and CUE_C assign the same temperature sensitivity to microbial growth, maintenance and turnover (see Eq. 25, 26, 27, 28 and 29 in the Supplementary Information, Section 8.1.8).

In addition to concentration and temperature, CUE_M was increased by the reduction in soil water content (+ 0.15; $F_{1,16} = 40.3$, $p < 0.01$), especially at the first time point (fifth day). Similarly, CUE_E and CUE_C were 0.25 higher at pF 3.5 (Figure 11). Consistent with this finding of our study, Jones et al. (2018) found an upward trend in microbial CUE under the following aridity levels: hyper-arid > arid > semi-arid, with the subsequent finding that even under hyper-dry conditions, very low microbial activity and C turnover occurred with altered C allocation. The reason given was reduced catalytic activity related to a decline in motility of organisms and enzymes across a water film that loses thickness as drought increases.

Interestingly, increased CUE with reduced temperature and water content was not accompanied by any response of *tfdA* transcript and gene copy numbers in our study. This imbalance may be explained by the fact that microbial use of the substrate is more complex than simple conversion to biomass (Schimel and Schaeffer, 2012). Rather, bacterial degraders synthesize a variety of products, e.g., to maintain basic functions, such as extracellular enzymes, extracellular polysaccharides, cell wall polymers, but also

stress response compounds, such as osmolytes, to survive under dry conditions (Schimel et al., 2007). This formation of stress compounds could explain a slight increase in carbon use efficiencies during MCPA degradation under drier conditions compared to the near optimal water content at pF 1.8.

6.5.4 Effect of temperature and soil moisture on pesticide DT_{50}

Differences in MCPA mineralization were also reflected in DT_{50}-values, describing the time required to mineralize 50% of the applied MCPA (Table 6). We determined two different DT_{50}-values; i) a DT_{50MIN} derived from the mineralization kinetics and typically calculated in dissipation experiments of pesticides, and ii) a DT_{50RES} derived from the residual MCPA concentration. Under limiting conditions, we observed longer DT_{50RES} and DT_{50MIN}-values, with temperature exerting a stronger influence than soil moisture.

We observed that lowering the temperature to 10°C at 1 mg kg^{-1} and pF 3.5 increased the residence time of MCPA by a factor of 1.9 based on mineralization kinetics (Table 6). In contrast, the DT_{50RES}-value differed only by a factor of 1.6. This may be explained by an altered temperature-dependent C allocation, namely a disproportionate increase in ^{14}C incorporation at 10°C versus an increase in mineralization at 20°C. Consequently, this resulted in almost equal MCPA-utilization rates (Steinweg et al., 2008). It is, therefore, important to consider total MCPA turnover, as DT_{50RES} theoretically includes the dynamics of ^{14}C incorporation and mineralization, whereas DT_{50MIN} captures only the contribution of mineralization. At pF 1.8, both DT_{50} values were identical (Table 6). However, at pF 1.8 the CUE_C and CUE_E were on average 0.2 lower than at pF 3.5 (Figure 11, Eqs. 22 and 21) reflecting a reduced contribution of ^{14}C incorporation to MCPA-derived C turnover.

Compared to the concentration of 1 mg kg^{-1}, the effect of a temperature reduction at 20 mg kg^{-1} was independent of both soil moisture and the DT_{50} approach, increasing half-lives by a factor of 2 (Table 6). In this case, degradation was initially limited by the

number of microorganisms, in contrast to degradation at 1 mg kg^{-1}, where degradation potential was provided by the autochthonous microbial abundance; here, rapid first-order degradation could be initiated immediately (Baelum et al., 2006; Wirsching et al., 2020a). According to Babey et al. (2017), degradation of 2,4-D is most efficient when the ratio of degraders to instantaneous pesticide concentrations favors degraders. This was the case for the treatment at 20°C and high initial pesticide concentration after relatively lower mineralization was observed in the first phase of the experiment (0-5d). In the absence of growth at 10°C, as indicated by the lack of any increase in *tfdA* copy numbers, DT_{50MIN} and DT_{50RES} values were significantly higher, indicating slower degradation.

Table 6: Half-life DT_{50RES} derived from the residual MCPA concentration in soils and DT_{50MIN} derived from mineralization kinetics as a function of soil water content, concentration, and temperature

	DT_{50RES}						DT_{50MIN}					
	pF 1.8			pF 3.5			pF 1.8			pF 3.5		
	10°C	20°C	10°C/20°C	10°C	20°C	10°C/20°C	10°C	20°C	10°C/20°C	10°C	20°C	10°C/20°C
20 mg kg^{-1}	18.4	9.3	**2.0**	15.6	7.4	**2.1**	18.5	9.9	**1.9**	17.6	8.8	**2.0**
1 mg kg^{-1}	9.6	6.5	**1.5**	8.5	5.4	**1.6**	10.3	6.7	**1.5**	12.2	6.3	**1.9**

Our results partially contradict previous findings (Parker and Doxtader, 1983; Cattaneo et al., 1997; Castillo and Torstensson, 2007; Bouseba et al., 2009) that claim a decrease in temperature and soil moisture during MCPA biodegradation is always accompanied by a significant increase in half-life. The extent to which the residence time of MCPA was affected by a change in temperature and soil moisture depended solely on initial concentration and associated degradation dynamics. This study shows, that ^{14}C incorporation is not necessarily proportional to mineralization, confirming the hypothesis that under limiting conditions assimilation can be enhanced to support anabolic processes. Dissimilation including non-growth maintenance activities (Geyer et al., 2016) increased with temperature, as energy costs became more important regulators of motility or molecular turnover of proteins (Russell and Cook, 1995). As a result, the MCPA-derived carbon will be used more efficiently by microorganisms at low temperatures and reduced soil moisture. Applying this principle to pesticide degradation, estimating DT_{50}-values from cumulative

mineralization curves alone could, under certain circumstances, imply a systematic overestimation of pesticide persistence.

6.6 Conclusion

We expect that our findings for MCPA are valid for other pesticides with similar degradation pathways such as 2,4-Dichlorophenol (2,4-D) or 4-Chloro-2-methylphenol (mecoprop). However, pesticides with other properties may behave differently. For example, the temperature sensitivity of pesticide degradation may be strongly influenced by the sorption affinity of the pesticide. Under conditions of lower availability of highly sorptive pesticides such as glyphosate, the measured or apparent temperature sensitivity may be lower than expected and reduce the variation in residence time compared to MCPA. Further research is needed to determine the validity of the proposed mechanisms for pesticides with different properties.

6.7 Acknowledgement

The authors acknowledge support by the State of Baden-Württemberg through bwHPC. We would like to thank Stephanie Nowak from the Environmental Analytical Chemistry Department in Tübingen for measuring the MCPA concentrations and Kathleen Regan for the English corrections.

6.8 Funding

This study was financially supported by the German Research Foundation (DFG) within the Research Training Group "Integrated Hydrosystem modeling" (RTG 1829) and the Collaborative Research Center 1253 CAMPOS (DFG Grant Agreement SFB 1253/1 2017) as well as by the Ellrichshausen Foundation.

6.9 Declaration

Conflict of interest: The authors have no conflicts of interest related to this article.

7 Appendices

7.1 Supplementary Information for Chapter 8 (Study II)

7.1.1 Experimental Design

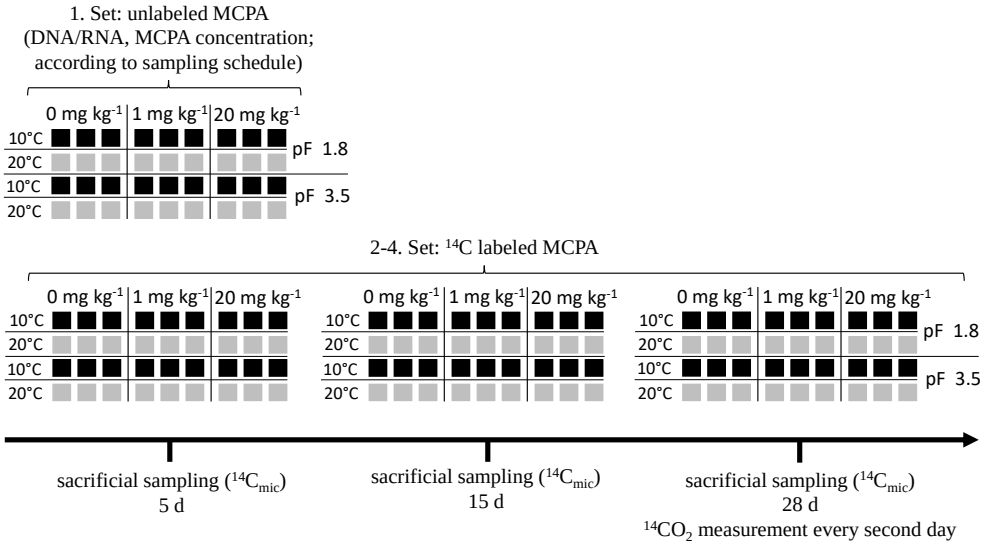

Figure 12: Schematic representation of the experimental design

7.1.2 Sampling schedule

Table 7: Sampling schedule

Analyses	Sampling time
^{14}C mineralization	1, 2, 5, 7, 10, 13, 15, 17, 19, 21, 23, 26, and 28 d
$^{14}C_{mic}$	5, 15, and 28 d
MCPA concentration	0, 6, 10, 16, and 28 d
DNA/RNA measurement	0, 6, 10, 16, 25 and 28 d

7.1.3 MCPA dissipation analysis

A soil suspension of 2 g soil mixed with 10mL methanol/water (1:1) was homogenized on a horizontal shaker at 200 rev min^{-1} for 10 min, then heated in a water bath for 60 min at 50 °C. After shaking again at 200 rev min^{-1} for 10 min, the mixture was centrifuged at 2500 g for 10 min, and 2 mL of the supernatant was removed and filtered (0.45 µm pore size). The extraction recovery of MCPA was >98% (20 $mg\,kg^{-1}$ MCPA was added to a soil sample. After one hour, MCPA was extracted and the MCPA concentration was determined again to obtain the recovery level). Before the HPLC-MS/MS analysis, the extracts were sonicated and homogenized for 5 min by vortexing. On a 1260-Infinity system from Agilent Technologies, one µL of the sample was injected onto a reversed-phase column (Agilent Poroshell 120 C18, 2.1 mm internal diameter, 100 mm length, 2.7 µL particle size) at a temperature of 40°C. MCPA was eluted isocratically within 5 min using 50% water and acetonitrile (both acidified with 0.1% formic acid) at a flow rate of 0.4 $mL\,min^{-1}$. After chromatographic separation, MCPA was detected by tandem mass spectrometry using an Agilent 6490 iFunnel Triple Quadrupole (QqQ) instrument. The analyte was ionized using negative electrospray ionization (ESI-) by applying 12 $L\,min^{-1}$ sheath gas (N_2) at 400°C, 16 $L\,min^{-1}$ drying gas (N_2) at 150°C, 30 psi nebulizer pressure, 4.2 kV capillary voltage, and 1.2 kV nozzle voltage. MS/MS experiments were conducted by MRM (Multi Reaction Monitoring), using N_2 as collision gas and collision energy (CE) dependent mass transitions (MCPA: quantifier 198.9/140.9 at 10 eV, qualifier: 198.9/34.9 at 45 eV). The limit of quantification (LOQ) was defined as 13 $\mu g\,kg^{-1}$ MCPA in soil.

7.1.4 MCPA mineralization ($^{14}CO_2$)

The overall CO_2 evolution from the microcosms was determined via titration (DIN EN ISO 16072:2011-09). First, a 0.5 mL aliquot was taken from a CO_2 trap containing 2 mL 1M NaOH which was set up in the microcosm. The actual respiration measurement was carried out by adding 0.5 mL of 1 M $BaCl_2$ and two drops of phenolphthalein. In

the following titration with 0.1 M HCl, the end point of the neutralization reaction was indicated by a color change to transparency. To determine the specific $^{14}CO_2$ content, an aliquot of 1 mL was taken from the same $^{14}CO_2$ trap and mixed with 4 ml scintillation liquid (Rotiszint Eco Plus, Carl Roth GmbH + Co. KG) in a 5 mL scintillation vial (LDPE). The decay rate in Bequerel (Bq) was measured using a scintillation counter (Wallac 1411, liquid scintillation counter, USA). To account for interfering substances, a quenching adjustment with ^{14}C aqueous standards was used to improve the accuracy of the actual counts per second (cps) for the entire energy band.

7.1.5 Microbial biomass (C_{mic})

Microbial biomass was estimated using the chloroform fumigation extraction method (CFE) developed by Vance et al. (1987), adapted by Poll et al. (2010a) for an additional ^{14}C determination. Prior to extraction, 10 g soil was first weighed to ensure the release of the microbially bound C after a 24-hour fumigation with ethanol-free chloroform. After removal of the chloroform, 40 mL of 0.5 M K_2SO_4 solution was added, shaken on a horizontal shaker at 250 rev min^{-1} for 30 min and centrifuged at 4420 g for 30 min. The clear supernatant was then passed through a 20 µm filter, diluted 1:4 with deionized water to avoid high salinity during detection, and measured with a Multi-N/C 2100S TOC-TNb analyzer (AnalytikJena, Jena, Germany). A second subsample of 10 g soil was not fumigated with chloroform to determine only the amount of extractable organic carbon. C content of the control (non-fumigated) samples was subtracted from the C content of the fumigated samples to determine C_{mic} content. The k_{EC} factor of 0.45 was used to estimate the extractable portion of microbial biomass C. To obtain the ^{14}C content in C_{mic}, 1 mL of the CFE supernatant was mixed with 4 mL scintillation liquid (Rotiszint Eco Plus, Carl Roth GmbH+Co. KG) in a 5 mL scintillation vial (LDPE). Calculation of the incorporated ^{14}C was performed as described for the C_{mic} content, here using the activity difference between the fumigated and non-fumigated samples. For

the non-fumigated samples, the undiluted supernatant was used. Total ^{14}C utilization was estimated by adding the $^{14}CO_2$ mineralization and ^{14}C incorporation on days 5, 15 and 28.

7.1.6 DNA/RNA co-extraction

For RNA and DNA extraction, 2 g frozen soil was weighed into 15 mL bead-beating tubes and extracted using the RNAeasy PowerSoil Total RNA Kit for soil (Qiagen, Germany) and the RNAeasy PowerSoil DNA Elution Kit (Qiagen, Germany) in a co-extraction method following the user manual. After extraction, the RNA and DNA samples were aliquoted and stored at -80°C (RNA samples) or at -20°C (DNA samples) for further use. The DNA and RNA concentrations were measured using a fluorescent dye and microplate reader (Synergy HTX Multi-Mode Reader, Bio-Tek Instruments Inc., Germany). For DNA and RNA quantification, the Quant-iT™ PicoGreen™ dsDNA Assay Kit and the Quant-iT™ RNA Assay Kit (Thermo Fisher Scientific, Germany), respectively were used following the user manuals. Before using the RNA-samples for Real-Time quantitative PCR (qPCR), possible remaining DNA in the RNA samples was digested using the TURBO DNA-free™ Kit (Invitrogen, Thermo Fisher Scientific, Germany) following the manufacturer´s protocol (Table 8). After digestion, RNA samples were divided in two subsamples of 11 µL each and labeled as + and - subsamples. For the following reverse transcription, the SuperScript™ III Reverse Transcriptase Kit with Random Primers and RNase (Invitrogen, Thermo Fisher Scientific, Germany), and dNTPs (10mM; Genaxxon, Germany) were used. The reaction was carried out according to the user manual of SuperScript™ III Reverse Transcriptase from Invitrogen. Reaction conditions and temperature program are described in Table 9. The + subsamples served as cDNA, whereas the - subsample served as a negative control for the remaining DNA after digestion.

Table 8: Digestion

Procedure	Reaction mixture	Temperature profile
Incubation	20 µL RNA sample	30 min at 37 °C
	2.4 µL 10x Turbo DNA buffer	
	1.6 µL Turbo DNase	
DNase Inactivation	0.16 Vol Inactivation reagent	5 min at room temperature

Table 9: Reverse transcription

Reaction	Mixture	Temperature profile
reaction 1	11 µl DNA digestion sample	5 min at 65°C
(+ and - sample)	1µl random primer	>= 1 min at 4°C
	1 µl dNTPs	
reaction 2	• Preparation (+ samples):	5 min at 25°C
	4 µl 5x First Strand Buffer	60 min at 50°C
	1 µl 0.1 M DTT (100mM)	15 min at 70°C
	1 µl RNase OUT	Cool down at 4°C
	1 µl reverse transcriptase (200 U/l)	
	13 µl reaction 1	
	• Preparation (- samples):	
	4 µl 5x First Strand Buffer	
	1 µl 0.1 M DTT (100mM)	
	1 µl RNase OUT	
	1 µl DEPC water	
	13 µl reaction 1	

Table 10: Primer sequence

Target sequence	Primer	qPCR conditions
16S rRNA genes*	341F: CCT ACG GGA GGC AGC AG	600 s at 95°C,
	515R: ATT ACC GCG GCT GCT GGC A	Cycle (35): 15 s at 95 °C , 30 s at 60°C, 30 s at 72°C, 30 s at 75°C (m.o.f) melting curve
*tfdA***	F: GAG CAC TAC GCR CTG AAY TCC CG	600 s at 95°C,
	R: GTC GCG TGC TCG AGA AG	Cycle (40): 15 s at 95 °C , 30 s at 64°C, 30 s at 72°C, 30 s at 81°C (m.o.f) melting curve
*cadA****	F: AAG CTG CAR TTT GAR AAY GG	600 s at 95°C,
	R: MGG ATT GAA ATC CTG RTA	Cycle (40): 15 s at 95 °C , 30 s at 55°C, 30 s at 72°C, 30 s at 80°C (m.o.f) melting curve

m.o.f - measurement of fluorescence; *López-Gutiérrez et al. (2004), **Baelum et al. (2006), ***(Kitagawa et al., 2002b)

7.1.7 Gene-centric modeling of MCPA biodegradation

We used a recently developed modeling approach (ref. to Chavez Rodriguez et al. (2020)) to simulate MCPA mineralization (C_P [mmol g^{-1}]), *tfdA* genes (proxy for active bacterial biomass C_B [mmol g^{-1}]) and transcripts, and CUE. The original modeling approach was extended to account for constitutive gene expression and to include a temperature response function.

7.1.8 Model description

We assumed gene expression to be in quasi-steady state described by the Hill function, including constitutive gene expression that is potentially important at low concentrations:

$$\widehat{mRNA} = f_T \cdot \left(\frac{(C_P^L)^{n_H}}{(C_P^L)^{n_H} + (K_G)^{n_H}} + \frac{\alpha}{f_T} \right) \tag{23}$$

where f_T represents the number of transcripts per gene, n_H [-] and K_G [mmol cm^{-3}] are the Hill exponent and constant respectively, α is the constitutive gene expression coefficient set to $1.2 \cdot 10^{-5}$ transcripts per gene Leveau et al. (1999b), and C_P^L [mmol cm^{-3}] is the solution phase concentration of MCPA.

Microbial growth is regulated in three ways (Eq. 24) by: i) MCPA-dependent *tfdA* gene transcription (mRNA, Eq. 23), ii) MCPA-dependent reaction kinetics (Monod term in Eq. 24), and iii) a Q_{10} temperature response function (Eq. 25).

$$r_{growth} = \mu_{max} \cdot C_B \cdot \left(\frac{(C_P^L)^{n_H}}{(C_P^L)^{n_H} + (K_G)^{n_H}} + \frac{\alpha}{f_T} \right) \cdot \left(\frac{C_P^L}{C_P^L + K_M} \right) \cdot f_R(T) \tag{24}$$

where μ_{max} [d^{-1}] is the maximum growth rate coefficient, K_M [mmol cm^{-3}] is the Monod constant, and $f_R(T)$ [-] is the temperature response function.

The temperature response function $f_R(T)$ from Sierra et al. (2015) not only influences microbial growth, but also decay rate (Eq. 26), maintenance rate (exogenous (Eq. 27) and endogenous (Eq. 28), and decay rate of non-extractable residues (Eq. 29), and is

defined as:

$$f_R(T) = (Q_{10})^{\left(\frac{T - 10°C}{10°C}\right)} \tag{25}$$

where Q_{10} [-] is the temperature function constant, and T is the temperature in °C.

The decay rate is defined as:

$$r_{death} = C_B \cdot a_a \cdot f_R(T) \tag{26}$$

where a_a [d^{-1}] is the decay rate coefficient.

The total maintenance rate is partitioned into two different maintenance fluxes: exogenous and endogenous (Wang and Post, 2012). The exogenous flux describes the fraction of the total maintenance demand that can be met with the available MCPA in the system. We modeled this flux using a simple Michaelis Menten expression Pagel et al. (2020):

$$r_{m-exogenous} = \left(\frac{m \cdot C_P^L}{C_P^L + K_M}\right) \cdot C_B \cdot \left(\frac{\rho}{\theta}\right) \cdot f_R(T) \tag{27}$$

where m [d^{-1}] is the maintenance rate coefficient.

The endogenous maintenance flux describes the fraction of the demand that is met by the biomass under insufficient MCPA levels in the system (Wang and Post, 2012), and it is modeled by subtracting the exogenous maintenance flux from the total maintenance demand.

$$r_{m-endogenous} = C_B \cdot m \cdot \left(1 - \frac{C_P^L}{C_P^L + K_M}\right) \cdot f_R(T) \tag{28}$$

We introduced a non-extractable residues pool to account for the delayed release of CO_2 coming from the decaying biomass:

$$r_{decay}^{NER} = C_B^{NER} \cdot a_{CO_2} \cdot f_R(T) \tag{29}$$

where: C_B^{NER} [$mmol\,cm^{-3}$] is the non-extractable residues pool, and a_{CO_2} [d^{-1}] is the

decay rate coefficient of the C_B^{NER}.

To describe the ^{14}C dynamics, we incorporated a ^{14}C pool, which accounts for only the ^{14}C portion of labeled MCPA. Processes described for the ^{14}C pool are: growth, maintenance, and respiration. Additionally, the C_B^{NER} pool traces only the ^{14}C-C_B^{NER} formed. We calculated each ^{14}C flux by multiplying the corresponding total flux by the current mass fraction (α_{14}) of the source pool (Pagel et al., 2016). The α_{14} was in turn derived from the total activity of ^{14}C per g of soil (A_S = 15 kBq per 100 g of soils) and the mean specific activity of MCPA (α_{MCPA}= 55 mCi mmol^{-1}) in relation to the initial MCPA (C^0_{MCPA}) applied (either 1 or 20 mg kg^{-1}).

The full ODE equations used are:

$$\frac{dC_B}{dt} = r_{growth} - r_{m-endogenous} - r_{decay} \tag{30}$$

$$\frac{d^{14}C_B}{dt} = r^{14}_{growth} - r^{14}_{m-endogenous} - r^{14}_{decay} \tag{31}$$

$$\frac{dC_B^{NER}}{dt} = r^{14}_{decay} - r^{NER}_{decay} \tag{32}$$

$$\frac{dC_P^L}{dt} = -\frac{r_{uptake} + r_{m-exogenous}}{R_F} \tag{33}$$

$$\frac{d^{14}CO_2}{dt} = r^{14}_{respiration} + r^{14}_{m-endogenous} + r^{14}_{m-exogenous} + r^{NER}_{decay} \tag{34}$$

R_F is the retardation factor (ref. to Chavez Rodriguez et al. (2020)) introduced to account for nonlinear equilibrium sorption using the Freundlich isotherm:

$$RF := 1 + \frac{\rho}{\theta} \cdot K_P \cdot n_P \cdot (C_P^L)^{(n_P - 1)} \tag{35}$$

where K_P [mmol$^{(1-\mathrm{nP})}$g^{-1}cm$^{(3\mathrm{n_P})}$] and n_P [-] are the Freundlich coefficient and exponent fixed to 0.09 and 0.8576 (adapted from Gawlik et al. (2003)), θ [cm^3 cm^{-3}] is the soil water content, and ρ [g cm^{-3}] is the soil bulk density.

The uptake rate r_{uptake} (ref. Chavez Rodriguez et al. (2020)) depends on the bioavailable fraction of pesticide as follows:

$$r_{uptake} = \mu_{max} \cdot C_B \cdot \left(\frac{\rho}{\theta}\right) \cdot \left(\frac{(C_P^L)^{n_H}}{(C_P^L)^{n_H} + (K_G)^{n_H}} + \frac{\alpha}{f_T}\right) \cdot \left(\frac{C_P^L}{C_P^L + K_M}\right) \cdot \left(\frac{1}{Y_P}\right) \cdot f_R(T) \quad (36)$$

7.1.9 Model parameters

Table 11: Model Parameters

Hierarchy	Parameters	Units	Description	Range
C	f_T	transcripts gene^{-1}	Conversion factor transcripts per gene	[10^{-3}–10^{3}]
C	n_H	-	Hill exponent	[1-10]
	K_G	mmol cm^{-3}	Hill constant	[10^{-10}–10^{3}]
C	μ_{max}	d^{-1}	Maximum growth rate coefficient	[0.1–5]
W	a_a	d^{-1}	Decay rate coefficient	[10^{-3}–0.1]
	Y_P	-	Yield coefficient	[0.1–0.9]
	m	d^{-1}	Maintenance coefficient	[10^{-5}–0.1]
	K_M	mmol cm^{-3}	Monod constant	[10^{-5}–10^{3}]
W	a_{CO_2}	d^{-1}	Decay rate coefficient of the NER	[10^{-5}–0.1]
	f_1	mmol gene^{-1}	Conversion factor cell to carbon	[10^{-12}–10^{-9}]
	Q_{10}	-	Temperature function constant	[1.1–3]
S	C_B^o	gene g^{-1}	Initial biomass	[10^{4}–10^{6}]

C = concentration specific; W = water level specific; S = soil/sample specific

Table 12: Best fits for model parameters after Simulated Annealing parameter calibration

		1 mg		20 mg	
Hierarchy	e Parameters	pF = 1.8	pF = 3.5	pF = 1.8	pF = 3.5
C.S	f_T	0.09	0.09	0.10	0.10
C.S	n_H	8.3	8.3	6.7	6.7
	K_G	$2.6 \cdot 10^{-8}$	$1.7 \cdot 10^{-7}$	$1.5 \cdot 10^{-6}$	$2.4 \cdot 10^{-6}$
C.S	μ_{max}	0.8	0.8	0.4	0.4
WL.S	a_a	0.01	0.1	0.01	0.1
	Y_P	0.7	0.9	0.5	0.8
	m	0.007	0.02	0.02	0.03
	K_M	0.0002	$7.3.0 \cdot 10^{-5}$	0.002	0.0005
WL.S	a_{CO_2}	0.0011	0.0015	0.0011	0.0015
	f_1	$3.3 \cdot 10^{-10}$	$1.4 \cdot 10^{-10}$	$9.9 \cdot 10^{-10}$	$9.8 \cdot 10^{-10}$
	Q_{10}	1.5	1.6	2.0	2.1
S.S	Initial Biomass	14159.2	14159.2	14159.2	14159.2

C.S = concentration specific; WL.S = water level specific; S.S = soil/sample specific.

Only 10 out of 35 parameters were poorly constrained and had an estimation error higher than 100% (Table 13). These parameters are mainly related to the gene expression

(hill exponent (n_H) and hill coefficient (n_G), as well decay ratio of NER components (a_{CO_2}). Interestingly, these parameters also have a low sensitivity score and identifiability coefficient for the given data, suggesting a potential for reduction of processes that are not supported by this data.

Table 13: Local sensitivity analysis and estimation error of the parameter fits

Parameter	Best Fit	Sensitivity coefficient	Identifiability score	Estimation Error (%)
f_T (C.S)	0.1	12.0	9.0	61.1
n_H (C.S)	6.7	$5.2 \cdot 10^{-3}$	$2.8 \cdot 10^{-5}$	$3.4 \cdot 10^{4}$
K_G	$1.5 \cdot 10^{-6}$	$2.1 \cdot 10^{-5}$	$6.1 \cdot 10^{-6}$	$4.3 \cdot 10^{4}$
μ_{max} (C.S)	0.4	815.0	815.0	9.4
a_a (WL.S)	0.01	4.7	0.2	228.6
Y_P	0.5	60.3	44.2	16.1
m	0.02	3.6	0.8	88.1
K_M	$1.6 \cdot 10^{-3}$	109.6	23.0	37.4
a_{CO_2} (WL.S)	$1.1 \cdot 10^{-3}$	$4.6 \cdot 10^{-4}$	$2.4 \cdot 10^{-5}$	$4.2 \cdot 10^{3}$
f_1	$9.9 \cdot 10^{-10}$	21.2	3.3	36.7
Q_{10}	2.0	95.1	60.5	5.7
K_G	$2.4 \cdot 10^{-6}$	0.1	0.1	$7.6 \cdot 10^{3}$
a_a (WL.S)	0.1	141.8	84.0	25.2
Y_P	0.8	193.9	147.9	5.8
m	0.03	6.1	0.8	37.4
K_M	$4.8 \cdot 10^{-4}$	109.2	6.7	22.0
a_{CO_2} (WL.S)	$1.5 \cdot 10^{-3}$	0.1	0.0	118.1
f_1	$9.8 \cdot 10^{-10}$	35.1	4.9	29.5
Q_{10}	2.1	228.8	163.7	2.6
f_T (C.S)	0.1	12.0	10.3	16.9
n_H (C.S)	8.3	$4.8 \cdot 10^{-9}$	$1.1 \cdot 10^{-12}$	$3.7 \cdot 10^{7}$
K_G	$2.6 \cdot 10^{-8}$	$2.8 \cdot 10^{-19}$	$1.1 \cdot 10^{-19}$	$1.5 \cdot 10^{11}$
µ_max (C.S)	0.8	285.0	251.9	32.6
Y_P	0.7	147.3	131.4	10.7
m	$7.1 \cdot 10^{-3}$	0.8	0.2	188.3
K_M	$2.1 \cdot 10^{-4}$	84.9	33.5	46.2
f_1	$3.3 \cdot 10^{-10}$	17.0	5.6	49.6
Q_{10}	1.5	44.2	18.9	13.1
K_G	$1.7 \cdot 10^{-7}$	$5.0 \cdot 10^{-9}$	$1.8 \cdot 10^{-9}$	$3.6 \cdot 10^{7}$
Y_P	0.9	550.3	550.3	3.6
m	0.02	4.8	1.1	26.2
K_M	$7.3 \cdot 10^{-5}$	94.7	1.1	47.5
f_1	$1.4 \cdot 10^{-10}$	24.1	7.2	24.6
Q_{10}	1.6	73.6	51.6	7.9
Biomass (S.S)	$1.4 \cdot 10^{4}$	74.6	11.9	23.0

Highlighted rows showed parameter estimations with an error higher than 100%.

Model codes available under: DOI: 10.5281/zenodo.5081655.

7.1.10 Cumulative $^{14}CO_2$ respiration

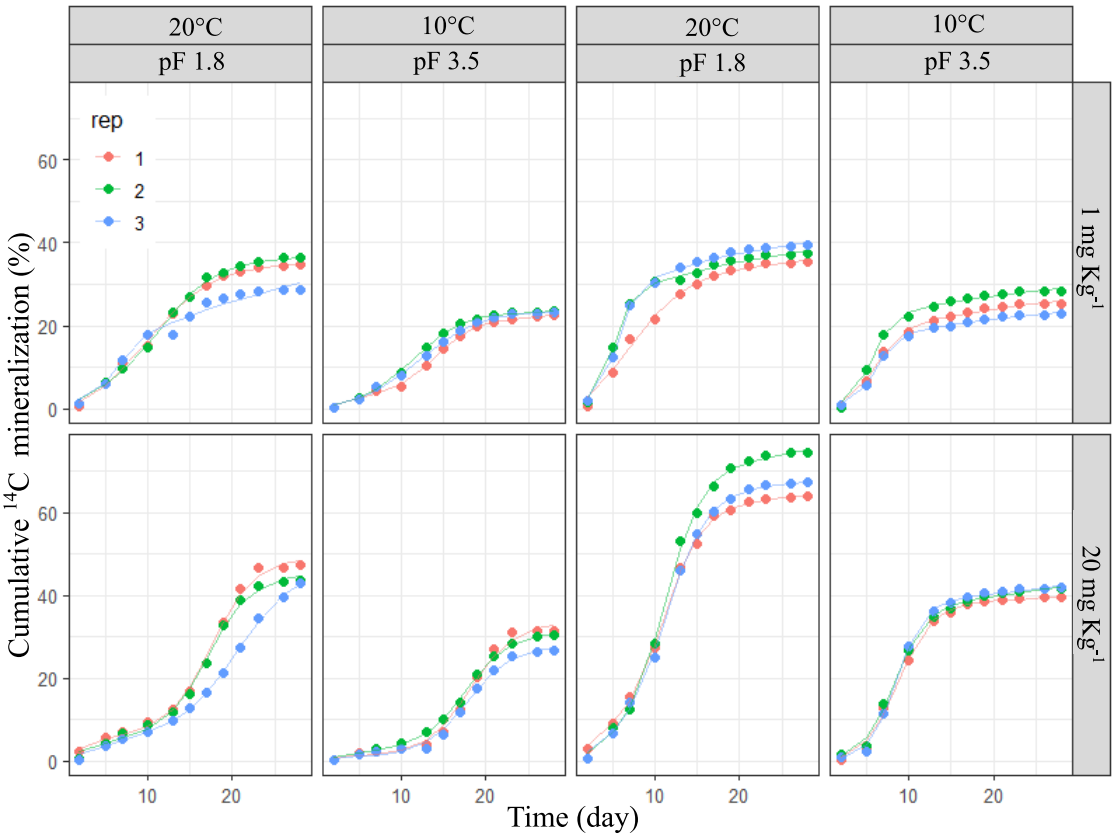

Figure 13: Cumulative $^{14}CO_2$ mineralization of two MCPA concentrations as a function of soil temperature and soil moisture over time. Mineralization of MCPA is represented by the percentage of initial ^{14}C-MCPA. Curves were fitted to the data points via a logistic model.

7.1.11 Estimated marginal means

Table 14: Contrast of the estimated marginal means of mineralization on day 28 as a function of temperature (the contrast function setting interaction = "tukey")

temp_treatment_tukey	Estimate	SE	df	t.ratio	p.value
1 - 20°C	-10.5	1.2	16	-8.7	$1.9 \cdot 10^{-7}$

Table 15: Interaction contrast of the estimated marginal means of mineralization on day 28 as a function of temperature and MCPA concentration (the contrast function setting interaction = "tukey")

temp_treatment_tukey	Concentration	Estimate	SE	df	t.ratio	p.value
1 - 20°C	1	-3.3	1.7	16	-1.9	0.07
1 - 20°C	20	-17.7	1.7	16	-10.3	$1.7 \cdot 10^{-8}$

Table 16: Contrast of the estimated marginal means of mineralization on day 28 as a function of soil moisture (the contrast function setting interaction = "tukey")

water_treatment_tukey	Estimate	SE	df	t.ratio	p.value
pF_1.8 - pF_3.5	16.2	1.2	16	13.4	$4.2 \cdot 10^{-10}$

Table 17: Interaction contrast of the estimated marginal means of mineralization on day 28 as a function of soil moisture and MCPA concentration (the contrast function setting interaction = "tukey")

water_treatment_tukey	Concentration	Estimate	SE	df	t.ratio	p.value
pF_1.8 - pF_3.5	1	11.1	1.7	16	6.5	$7.8 \cdot 10^{-6}$
pF_1.8 - pF_3.5	20	21.3	1.7	16	12.4	$1.2 \cdot 10^{-9}$

Table 18: Interaction contrast of the estimated marginal means of *tfdA* copies g^{-1} as a function of temperature, MCPA concentration, time and soil moisture (the contrast function setting interaction = "tukey")

Temp_tukey	MCPA	Day	pF	Estimate	SE	df	t.ratio	p.value
1 - 20°C	0	0	1.8	$-1.1 \cdot 10^{-12}$	91.8	24	$-1.1 \cdot 10^{-14}$	1.00
1 - 20°C	1000	0	1.8	$2.6 \cdot 10^{-13}$	91.8	24	$2.9 \cdot 10^{-15}$	1.00
1 - 20°C	20000	0	1.8	$6.6 \cdot 10^{-13}$	91.8	24	$7.2 \cdot 10^{-15}$	1.00
1 - 20°C	0	6	1.8	-51.7	91.8	24	-0.6	0.58
1 - 20°C	1000	6	1.8	-180.1	91.8	24	-2.0	0.06
1 - 20°C	20000	6	1.8	-85.2	91.8	24	-0.9	0.36
1 - 20°C	0	10	1.8	-138.2	91.8	24	-1.5	0.15
1 - 20°C	1000	10	1.8	-130.8	91.8	24	-1.4	0.17
1 - 20°C	20000	10	1.8	$-1.2 \cdot 10^{-3}$	91.8	24	-12.8	$3.0 \cdot 10^{-12}$
1 - 20°C	0	15	1.8	277.6	91.8	24	3.0	0.01
1 - 20°C	1000	15	1.8	98.0	91.8	24	1.1	0.30
1 - 20°C	20000	15	1.8	-915.8	91.8	24	-10.0	$5.2 \cdot 10^{-10}$
1 - 20°C	0	26	1.8	-2.3	91.8	24	0.0	0.98
1 - 20°C	1000	26	1.8	4.9	91.8	24	0.1	0.96
1 - 20°C	20000	26	1.8	-0.4	91.8	24	0.0	1.00
1 - 20°C	0	0	3.5	$-2.9 \cdot 10^{-15}$	91.8	24	$-3.2 \cdot 10^{-15}$	1.00
1 - 20°C	1000	0	3.5	$1.2 \cdot 10^{-13}$	91.8	24	$1.3 \cdot 10^{-15}$	1.00
1 - 20°C	20000	0	3.5	$1.2 \cdot 10^{-13}$	91.8	24	$1.3 \cdot 10^{-15}$	1.00
1 - 20°C	0	6	3.5	74.9	91.8	24	0.8	0.42
1 - 20°C	1000	6	3.5	-33.4	91.8	24	-0.4	0.72
1 - 20°C	20000	6	3.5	55.4	91.8	24	0.6	0.55
1 - 20°C	0	10	3.5	-18.7	91.8	24	-0.2	0.84
1 - 20°C	1000	10	3.5	-55.6	91.8	24	-0.6	0.55
1 - 20°C	20000	10	3.5	$-1.5 \cdot 10^{-3}$	91.8	24	-16.4	$1.6 \cdot 10^{-14}$
1 - 20°C	0	15	3.5	44.0	91.8	24	0.5	0.64
1 - 20°C	1000	15	3.5	130.0	91.8	24	1.4	0.17
1 - 20°C	20000	15	3.5	-580.9	91.8	24	-6.3	$1.5 \cdot 10^{6}$
1 - 20°C	0	26	3.5	-0.6	91.8	24	0.0	0.99
1 - 20°C	1000	26	3.5	4.5	91.8	24	0.0	0.96
1 - 20°C	20000	26	3.5	2.3	91.8	24	0.0	0.98

Table 19: Interaction contrast of the estimated marginal means of *tfdA* gene transcript as a function of temperature, MCPA concentration, time and soil moisture (the contrast function setting interaction = "tukey")

Temp_tukey	MCPA	Day	pF	Estimate	SE	df	t.ratio	p.value
1 - 20°C	0	0	1.8	$2.0 \cdot 10^{-10}$	$1.0 \cdot 10^{5}$	24	$2.0 \cdot 10^{-15}$	1.00
1 - 20°C	1000	0	1.8	$9.5 \cdot 10^{-11}$	$1.0 \cdot 10^{5}$	24	$9.5 \cdot 10^{-16}$	1.00
1 - 20°C	20000	0	1.8	$-1.1 \cdot 10^{-10}$	$1.0 \cdot 10^{5}$	24	$-1.1 \cdot 10^{-15}$	1.00
1 - 20°C	0	6	1.8	-346.1	$1.0 \cdot 10^{5}$	24	$-3.5 \cdot 10^{-3}$	1.00
1 - 20°C	1000	6	1.8	$-3.1 \cdot 10^{4}$	$1.0 \cdot 10^{5}$	24	-0.3	0.76
1 - 20°C	20000	6	1.8	$-2.0 \cdot 10^{4}$	$1.0 \cdot 10^{5}$	24	-0.2	0.84
1 - 20°C	0	10	1.8	-70.3	$1.0 \cdot 10^{5}$	24	$-7.0 \cdot 10^{-4}$	1.00
1 - 20°C	1000	10	1.8	$1.9 \cdot 10^{4}$	$1.0 \cdot 10^{5}$	24	0.2	0.85
1 - 20°C	20000	10	1.8	$-2.0 \cdot 10^{6}$	$1.0 \cdot 10^{5}$	24	-15.3	$6.8 \cdot 10^{-14}$
1 - 20°C	0	15	1.8	$5.0 \cdot 10^{3}$	$1.0 \cdot 10^{5}$	24	0.05	0.96
1 - 20°C	1000	15	1.8	$1.6 \cdot 10^{4}$	$1.0 \cdot 10^{5}$	24	0.2	0.87
1 - 20°C	20000	15	1.8	$-8.0 \cdot 10^{4}$	$1.0 \cdot 10^{5}$	24	-0.8	0.44
1 - 20°C	0	26	1.8	-519.9	$1.0 \cdot 10^{5}$	24	$-5.2 \cdot 10^{-3}$	1.00
1 - 20°C	1000	26	1.8	18.2	$1.0 \cdot 10^{5}$	24	$1.8 \cdot 10^{-4}$	1.00
1 - 20°C	20000	26	1.8	$1.5 \cdot 10^{5}$	$1.0 \cdot 10^{5}$	24	1.5	0.16
1 - 20°C	0	0	3.5	$1.5 \cdot 10^{-10}$	$1.0 \cdot 10^{5}$	24	$1.5 \cdot 10^{-15}$	1.00
1 - 20°C	1000	0	3.5	$1.2 \cdot 10^{-10}$	$1.0 \cdot 10^{5}$	24	$1.2 \cdot 10^{-15}$	1.00
1 - 20°C	20000	0	3.5	$3.9 \cdot 10^{-11}$	$1.0 \cdot 10^{5}$	24	$3.9 \cdot 10^{-16}$	1.00
1 - 20°C	0	6	3.5	$-2.6 \cdot 10^{-10}$	$1.0 \cdot 10^{5}$	24	$-2.6 \cdot 10^{-15}$	1.00
1 - 20°C	1000	6	3.5	$7.1 \cdot 10^{3}$	$1.0 \cdot 10^{5}$	24	0.07	0.94
1 - 20°C	20000	6	3.5	$-2.1 \cdot 10^{4}$	$1.0 \cdot 10^{5}$	24	-0.2	0.84
1 - 20°C	0	10	3.5	971.3	$1.0 \cdot 10^{5}$	24	$9.7 \cdot 10^{-3}$	0.99
1 - 20°C	1000	10	3.5	$1.8 \cdot 10^{4}$	$1.0 \cdot 10^{5}$	24	0.2	0.86
1 - 20°C	20000	10	3.5	$-1.4 \cdot 10^{6}$	$1.0 \cdot 10^{5}$	24	-14.1	$4.4 \cdot 10^{-13}$
1 - 20°C	0	15	3.5	-25.7	$1.0 \cdot 10^{5}$	24	$-2.6 \cdot 10^{-4}$	1.00
1 - 20°C	1000	15	3.5	$2.6 \cdot 10^{3}$	$1.0 \cdot 10^{5}$	24	0.03	0.98
1 - 20°C	20000	15	3.5	$-9.4 \cdot 10^{3}$	$1.0 \cdot 10^{5}$	24	-0.09	0.93
1 - 20°C	0	26	3.5	-10.6	$1.0 \cdot 10^{5}$	24	$-1.1 \cdot 10^{-4}$	1.00
1 - 20°C	1000	26	3.5	12.4	$1.0 \cdot 10^{5}$	24	$1.2 \cdot 10^{-4}$	1.00
1 - 20°C	20000	26	3.5	$4.7 \cdot 10^{3}$	$1.0 \cdot 10^{5}$	24	0.05	0.96

Table 20: Contrast of the estimated marginal means of ^{14}C incorporation as a function of soil moisture (the contrast function setting interaction ="tukey")

Water_treatment_tukey	mcpa	Estimate	SE	df	t.ratio	p.value
pF 1.8 - pF 3.5	1 $mg\,kg^{-1}$	-1.2	1.5	16	-0.8	0.4
pF 1.8 - pF 3.5	20 $mg\,kg^{-1}$	2.7	1.5	16	1.8	0.1

Table 21: Contrast of the estimated marginal means of ^{14}C incorporation as a function of temperature (the contrast function setting interaction ="tukey")

Temp_treatment_tukey	Day	estimate	SE	df	t.ratio	p.value
1 - 20°C	5	2.9	1.3	16	2.2	0.04
1 - 20°C	15	8.0	1.3	16	6.0	$1.8 \cdot 10^{-5}$
1 - 20°C	28	6.5	1.4	16	4.8	$2.0 \cdot 10^{-4}$

Table 22: Contrast of the estimated marginal means of CUE_M as a function of temperature (the contrast function setting interaction = "tukey")

temp_treatment_tukey	day	Estimate	SE	df	t.ratio	p.value
1 - 20°C	5	0.2	0.0239	16	9.6	$4.8 \cdot 10^{-8}$
1 - 20°C	15	0.4	0.0252	16	13.9	$2.3 \cdot 10^{-10}$
1 - 20°C	28	0.1	0.0246	16	5.5	$5.2 \cdot 10^{-5}$

Table 23: Contrast of the estimated marginal means of CUE_M as a function of soil moisture (the contrast function setting interaction = "tukey")

water_treatment_tukey	day	Estimate	SE	df	t.ratio	p.value
pF_1.8 - pF_3.5	5	-0.15	0.024	16	-6.3	$9.7 \cdot 10^{-6}$
pF_1.8 - pF_3.5	15	-0.12	0.025	16	-4.8	$2.2 \cdot 10^{-4}$
pF_1.8 - pF_3.5	28	-0.06	0.025	16	-2.5	0.02

7.1.12 CUE_C

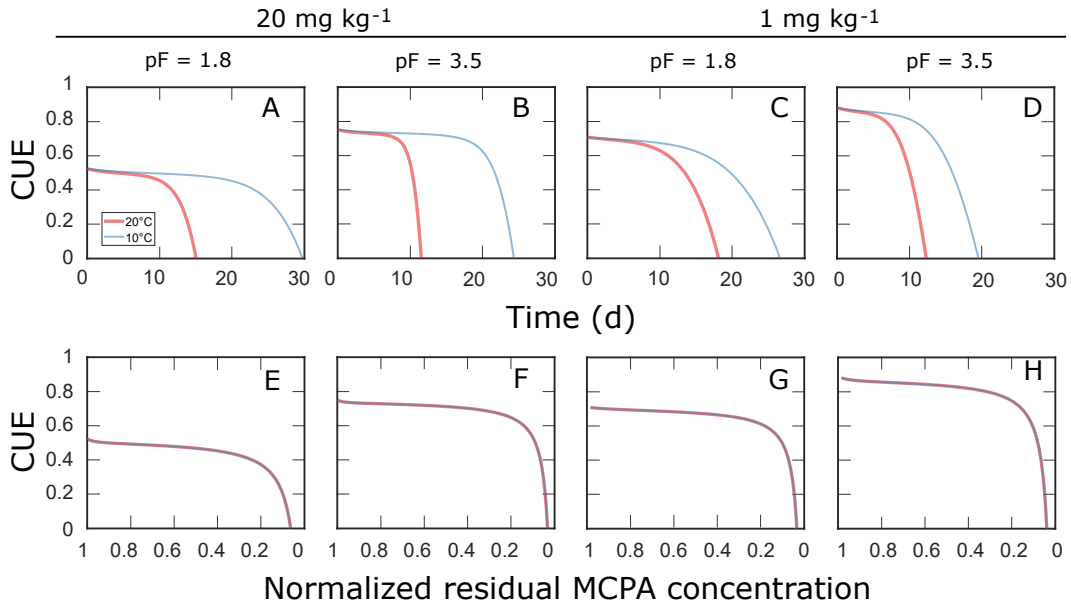

Figure 14: CUE_C (eq. 22) vs. time (d) showed in panels A to D, and CUE_C vs normalized residual MCPA concentration in soils showed in panels E to H.

8 ^{13}C assimilation as well as functional gene abundance and expression elucidate the biodegradation of glyphosate in a field experiment

This chapter includes the following publication:

1. Wirsching, J., Wimmer, B., Ditterich, F., Schlögl, J., Martin-Laurent, F., Huhn, C., Haderlein, S., Kandeler, E., & Poll, C. (2022). "^{13}C assimilation as well as functional gene abundance and expression elucidate the biodegradation of glyphosate in a field experiment." Environmental Pollution 306, 119382.

   https://doi.org/10.1016/j.envpol.2022.119382

8.1 Graphical abstract

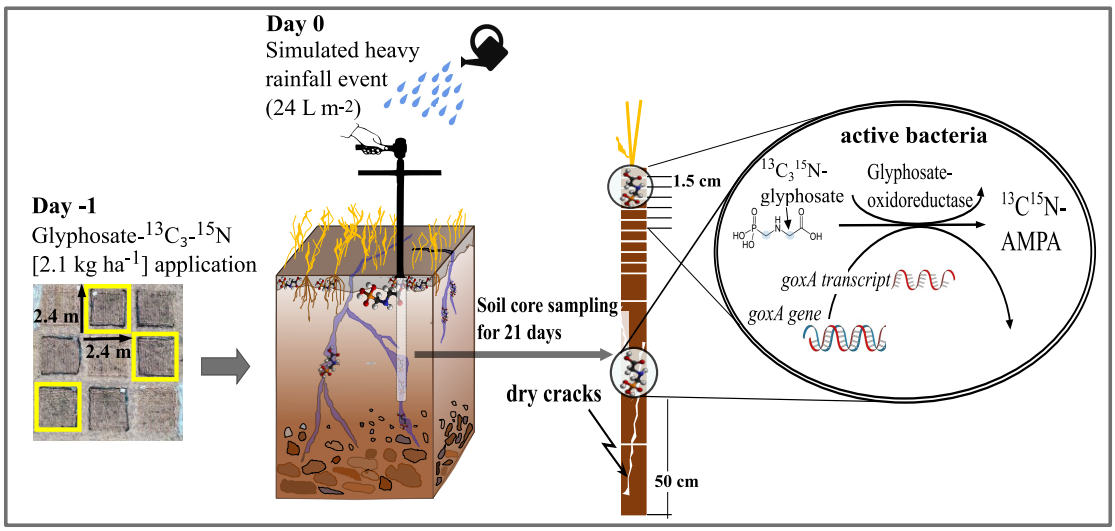

8.2 Abstract

Glyphosate (*N*-phosphonomethylglycine; GLP) and its main metabolite AMPA (aminomethylphosphonic acid), are frequently detected in relatively high concentrations in

European agricultural topsoils. Glyphosate has a high sorption affinity, yet it can be detected occasionally in groundwater. We hypothesized that shrinkage cracks occurring after dry periods could facilitate GLP transport to greater depths where subsoil conditions slow further microbial degradation. To test this hypothesis, we simulated a heavy rain event on a clay-rich arable soil. We applied 2.1 kg ha^{-1} of 100% $^{13}C_3$,^{15}N-labeled GLP one day before the simulated rainfall event. Microbial degradation of translocated GLP over a 21-day period was assessed by quantifying ^{13}C incorporation into phospholipid fatty acids. Microbial degradation potential and activity were determined by quantifying the abundance and expression of functional genes involved in the two known degradation pathways of GLP; to AMPA (*goxA*) or sarcosine (*sarc*). We confirmed that *goxA* transcripts were elevated in the range of $4.23 \cdot 10^5$ copy numbers g^{-1} soil only one day after application. The increase in AMPA associated with a rise in *goxA* transcripts and *goxA*-harboring microorganisms indicated that the degradation pathway to AMPA dominated. Based on ^{13}C-enrichment three hours after the HRE, fungi appeared to initiate glyphosate degradation. At later time points, Gram$^+$ bacteria proved to be the main degraders due to their higher ^{13}C-incorporation. Once GLP reached the subsoil, degradation continued but more slowly. By comparing GLP distribution and its microbial degradation in macropores and in the bulk soil, we demonstrated different time- and depth-dependent GLP degradation dynamics in macropores. This indicates the need for field studies in which soil properties relevant to GLP degradation are related to limiting environmental conditions, providing a realistic assessment of GLP fate in soils.

8.3 Introduction

Glyphosate (GLP) is applied intensively in both conventional and no-tillage farming (Silva et al., 2018). Recommended application rates range from 0.72 to 2.88 kg ha^{-1} for a single treatment (EFSA et al., 2015) applied one to three times per year (Silva et al., 2018). After application, only a fraction of the pesticide amount applied actually

reaches the target plants; up to 50% are distributed on the soil surface (Fenner et al., 2013). GLP application accounted for the largest proportion of pesticide residues in European topsoil in 2015 (Silva et al., 2019a). The magnitude of detected GLP residues contradicts a number of laboratory studies demonstrating complete and rapid degradation of GLP, with half-lives of only a few days to weeks (Rueppel et al., 1977; Grunewald et al., 2001; Simonsen et al., 2008; Singh et al., 2019). The discrepancy between the complete degradation of pesticides under laboratory conditions and their persistence in the field has not been resolved. When GLP has been defined as immobile in lab experiments, possible advective or particle-facilitated translocation under natural conditions has not been accounted for, and half-lives derived from degradation kinetics have often ignored the rate-limiting bioavailability in heterogeneous soils (Dechesne et al., 2010). Therefore, in situ studies of GLP fate are needed in highly structured soils where heterogeneous distribution of GLP and degraders are to be expected.

During summer months and dry periods, soils with high clay content have a tendency to form shrinkage cracks (Boivin et al., 2004), which may be especially prone to GLP transport along preferential flow pathways to greater depths. Studies addressing GLP transport behavior have confirmed GLP translocation across macropores, with increasing GLP and AMPA concentrations measured in seepage water shortly after storm events (Veiga et al., 2001; Kjær et al., 2005).

Of importance here is also precipitation intensity, as large events can promote more rapid transport of GLP into microbially inactive zones and, to a greater extent, to deeper soil horizons than low-intensity precipitation events (Manzoni et al., 2011). In general, subsoil is characterized by reduced microbial density (Preusser et al., 2021), lower O_2 availability, and a generally slower carbon turnover rate compared to topsoil (Rumpel and Kögel-Knabner, 2011). Since stable carbon-phosphorus (C-P) bonds are virtually impossible to break by physicochemical means (Sviridov et al., 2012), GLP degradation depends entirely on microbial degradation; limited microbial efficiency under suboptimal

conditions may result in a longer GLP residence time.

Degradation of GLP to AMPA or sarcosine are known to be its major degradation pathways (Sviridov et al., 2015). The AMPA degradation pathway involves GLP oxidoreductase (GOXA)-catalyzed cleavage of the carboxymethylene-nitrogen (C-N) bond in the first degradation step to yield AMPA and glyoxylate. GOXA-encoding genes have been identified in a variety of bacteria (Zhan et al., 2018). In the sarcosine-mediated degradation pathway, C-P lyase catalyzes the cleavage of the C-P bond to yield sarcosine and inorganic phosphorus (Zhan et al., 2018). The C-P lyase complex, *phn* (*phnCDEFGHIJKLMNOP*) has been well studied in *E.coli* and its ability to metabolize a wide range of different phosphonates has been confirmed (Zhan et al., 2018). González-Valenzuela and Dussán (2018) identified a sarcosine oxidase gene (*sarcF*, *sarcR*) in *L. sphaericus* that encodes the conversion of sarcosine to glycine in the second degradation step.

While the degradation pathways and rates of GLP degradation under laboratory conditions are well known, less is known about the microbial degradation of GLP in heterogeneous soil where environmental factors such as drought can greatly alter soil structure and conditions for GLP degradation. To date, field studies of GLP degradation have been based primarily on the chemical analysis of GLP residues and metabolite formation. The recent development of molecular approaches based on direct soil nucleic acids (both DNA and RNA), followed by qPCR and RT-qPCR assays, allows quantification of the abundance and activity of different pesticide-degrading microbial guilds (e.g., for the oxamyl-degrading bacterial guild, see Gallego et al. (2019)). To our knowledge, glyphosate-degrading genes are known (see Huang et al., 2017), but these approaches have not yet been applied to track the abundance and activity of glyphosate-degrading microbial guilds in soils. Combined with monitoring the incorporation of ^{13}C and^{15}N from $^{13}C_3$,^{15} N-labeled glyphosate, these approaches will provide unique insight into the microbial processes involved in glyphosate transformation in soil and determine its fate

in the environment.

In a field experiment, we aimed to relate, for the first time, the fate of isotopically labeled GLP to microbiological indices of GLP degradation after a simulated heavy rain event. We were specifically interested in the depth distribution of GLP in the bulk soil and along shrinkage cracks, and the consequences of this distribution on i) microbial degradation dynamics and ii) preferential degradation pathways of different microbial groups. Furthermore, we compared microbial GLP degradation rates in top- and subsoil. By quantifying the abundances of the two functional genes *goxA* and *sarc*, we were able to determine the genetic potential for GLP degradation, and determine transcript abundances indicating fluctuations in microbial degradation activity. Determination of ^{13}C incorporation into phospholipid fatty acids (PLFAs) allowed us to follow the flux of GLP-derived C into major microbial groups during GLP degradation.

8.4 Materials and Methods

8.4.1 Field site

The investigated arable field is located in the Ammer catchment in southern Germany (N48°52.126′, E8°97.268′). The area is characterized by mean annual temperature and precipitation of 9.4°C and 718 mm respectively (Deutscher Wetterdienst, 2016). Dry conditions and temperatures above 20°C prevailed during the 21-day experiment in July 2019 (Agrarmeteorologie Baden-Württemberg; wetter-bw.de, latest access 14.10.21). The arable soil is a fluvial sediment-derived Gleysol (WRB) with a silty loam-texture (9% sand, 69% silt and 22% clay; Schlögl et al., submitted), organic C content between 2 and 2.5 g kg^{-1} dry weight (dw), and average pH of 6.8.

8.4.2 Experimental Design

The experimental plot was laid out in a Latin square (3x3) in the field. Three treatments were assigned in triplicate to the total of nine subplots with a sampling area of 4 m^2

((Schlögl et al., 2022), submitted; schematic illustration of the treatment setup Figure 18). The barley was harvested just before the experiment, and only the stubble remained.

The experiment began with application of 2.1 kg ha^{-1} (manual sprayer; Schachtner, Ludwigsburg, Germany) GLP (free acid dissolved in deionized water, 100% labelled, purity 95%; CIL, Andover, MA, USA) to G plots (210 mg m^{-2}), which was below the highest single treatment allowed in Germany of 2.9 kg ha^{-1} and slightly above the recommended concentration of 1.8 kg ha^{-1} (LfL, 2020). One day later, the heavy rain event was simulated (HRE, 24 L m^{-2}; 24 mm h^{-1}) using watering cans with a sprinkler head. Followed by a simulated wet period analogous to light precipitation of 5 L m^{-2} (5 mm h^{-1}) over a 14-day period. Natural precipitation was not controlled by roofing. Once, between the 10th and 11th day, it rained 24.7 mm h^{-1} (Figure 18).

Three hours after the HRE, undisturbed 50-cm soil cores were collected using a HUMAX soil sampling probe (GreenGround, Switzerland). To differentiate the facilitated transport of GLP along preferential flow paths from the matrix flux, we collected bulk soil samples and samples taken from shrinkage cracks that had formed in the highly structured soil during the dry period preceding the field study. During the two weeks prior to the experiment, temperatures were above 20 °C for all but two days, and light precipitation occurred on three days (Figure 18). The infrequent occurrence of such shrinkage cracks resulted in only 4 sampling days. Bulk samples were collected at 6 time points (sampling schedule Table 24). In the field, soil cores were stored on dry ice, then transferred to -80°C to ensure RNA integrity. In the laboratory, the frozen soil cores were cut into segments. Topsoil (0-20 cm) was divided into 10 x 1.5 cm-segments for GLP/AMPA quantification and combined into 3 cm-segments for subsequent analyses requiring a larger soil volume, followed by 5 cm-segments to a depth of 20 cm. The subsoil from 20 cm downwards was divided into segments from 20-30, 30-40, and 40-50 cm depths.

8.4.3 GLP and AMPA residue analysis

GLP-$^{13}C_3$,^{15}N and AMPA-^{13}C,^{15}N residues in soil samples were quantified using an extraction protocol with subsequent CE-MS analysis as described by Wimmer et al. (2020, 2022), detailed information in the Supplement). Supernatants were then analyzed for GLP and AMPA without derivatization using capillary electrophoresis-mass spectrometry. Limits of detection (LOD) were 7.6 and 25.5 µg kg^{-1} for GLP and AMPA, respectively; analyte recovery >80 %. Final concentrations were calculated as the ratio of signal areas of analyte to standard, multiplied with the standard concentrations and the liquid-solid extraction ratio.

8.4.4 GLP-derived ^{13}C in phospholipid fatty acids (PLFAs)

We used PLFAs as biomarkers to study the differential contributions to GLP degradation of Gram positive (Gr^+) and Gram negative (Gr^-) bacteria and fungi. The branched fatty acids i15:0, a15:0, i16:0, and i17:0 are all indicators of Gr^+ bacteria, and the cy17:0 and cy19:0 are indicative of Gr^- bacteria (Zelles, 1999). The biomarker 18:2ω6.9c was used as a fungal indicator (Frostegård and Bååth, 1996). PLFAs were extracted from 4 g of field-fresh soil according to Bligh and Dyer (Bligh and Dyer, 1959).

To determine the δ^{13}C content in the PLFA samples, a four-step fractionation in Ag^+-SPE cartridges (6 mL, Supelco, Palo Alto, USA) was carried out using elution steps with *n*-hexane and increasing concentration of acetone (99:1, *v*/*v*; 96:4, *v*/*v*; 90:10, *v*/*v* and 0:100, *v*/*v*) according to Kramer et al. (2008) (detailed information in the Supplement).

8.4.5 DNA/RNA assay

For DNA and RNA co-extraction the FastDNATM Spin Kit for Soil (MP Biomedical, Germany) and the RNaid Kit (MP Biomedical, Germany) were used following the protocol from Tournier et al. (2015) with minor modifications (see supplementary material). On Day 6, we had difficulties extracting DNA/cDNA from the soil samples (Figure 16, Day

6). All values are in the range or just above the detection limit (Table 38; detailed information in the Supplement).

8.4.6 GoxA primer design

Five GLP oxidoreductase gene sequences (*goxA*) were retrieved from GenBank (accession numbers: GU214711.1, GU479462, GU479463.1, KF711750.1 and CP015007.1). Primer pairs were designed with Primer3Web version 4.1.0 ($GoxA_{fd}$ ATC GGC TT[T/C] GA[G/A] ACT GAA GG and $GoxA_{rd}$ CC[A/G] TTT CCA T[A/C]G G[T/C/G]G T[T/A]G CG); detailed information in the Supplement).

8.4.7 Real-time quantitative PCR

To quantify the total bacterial community (16S rRNA gene) and the functional genes involved (*goxA* and *sarc*) a real-time quantitative PCR (qPCR) assay was established using an ABI Prism 7500 Fast Analyzer (Applied Biosystems, Germany) with SYBR Green detection. The qPCR conditions and the primer used are summarized in Table 26 (detailed information in the Supplement).

8.4.8 Statistical analysis

An anisotropic exponential model was realized that assumes and estimates a different correlation slope for each coordinate due to the different depth and time intervals. Depth and time were specified as fixed factors, plot replicates nested in time as random effect, and depth and time as residuals (error components). Response variables were GLP decline over time for each soil depth, evolution of *goxA* and *sarc* abundance and gene expression, and dynamics of ^{13}C incorporation. Pseudo-analysis of variance with incremental Wald statistics (Kenward and Roger, 1997) was then performed, and model assumptions were visually confirmed by residual diagnostic plots (Kozak and Piepho, 2018; Schöpfer et al., 2020). The significance of pairwise differences was determined by calculating half least

significant error intervals implemented in the asremlPlus-package.

8.5 Results and Discussion

Using mRNA-based analysis as an activity index and quantifying GLP- derived ^{13}C enrichment in PLFAs, we examined microbial GLP degradation activity along a soil depth profile over a 21-day period after a simulated heavy rainfall to determine field-scale GLP degradation. As a prerequisite for understanding the role of GLP degraders and their activities, we quantified residues of GLP as well as AMPA during a period of 21 days in the bulk soil and in shrinkage cracks (Wimmer et al., 2022).

8.5.1 Shrinkage cracks facilitate deeper GLP transport

In the bulk soil samples taken immediately after GLP application and a heavy rainfall simulation of 24 L m^{-2}, we detected on average 69.2% (21 µmol kg^{-1}) of the applied GLP (recovery rate of 86% for GLP and 75% for AMPA) in the first 0-1.5 cm. A significant concentration drop ($p < 0.001$) was measured in the next 1.5-3 cm. At this depth, we found only 6.4% (2.3 µmol kg^{-1}) of the applied GLP, indicating that most of the GLP was retained in the first, near-surface segment. Despite this near-surface retention, 21.9% (6.8 µmol kg^{-1}) of the applied GLP had been detected at depths of 3-20 cm and 2.5% (0.8 µmol kg^{-1}) in the remaining 30 cm (Figure 15 A, Day 0). This relative distribution along the soil profile remained close to stable even after 21 days and daily irrigation with water rate of 5 L m^{-2} (Figure 15 A, Day 21). In depth sections of 0-1.5, 1.5-20, and 20-50 cm, 3.7% (1.2 µmol kg^{-1}), 1.1% (0.38 µmol kg^{-1}), and 0.28% (0.07 µmol kg^{-1}) of the originally applied GLP could be detected at Day 21 (Figure 15 A).

This limited mobility, is attributed to the strong binding of GLP to the soil matrix, a finding also noted in the majority of studies (Glass, 1987; Piccolo et al., 1994; Autio et al., 2004) as illustrated by relatively high Freundlich adsorption coefficients (K_f) ranging from 56 to 166 for silty loam soils (Vereecken, 2005).

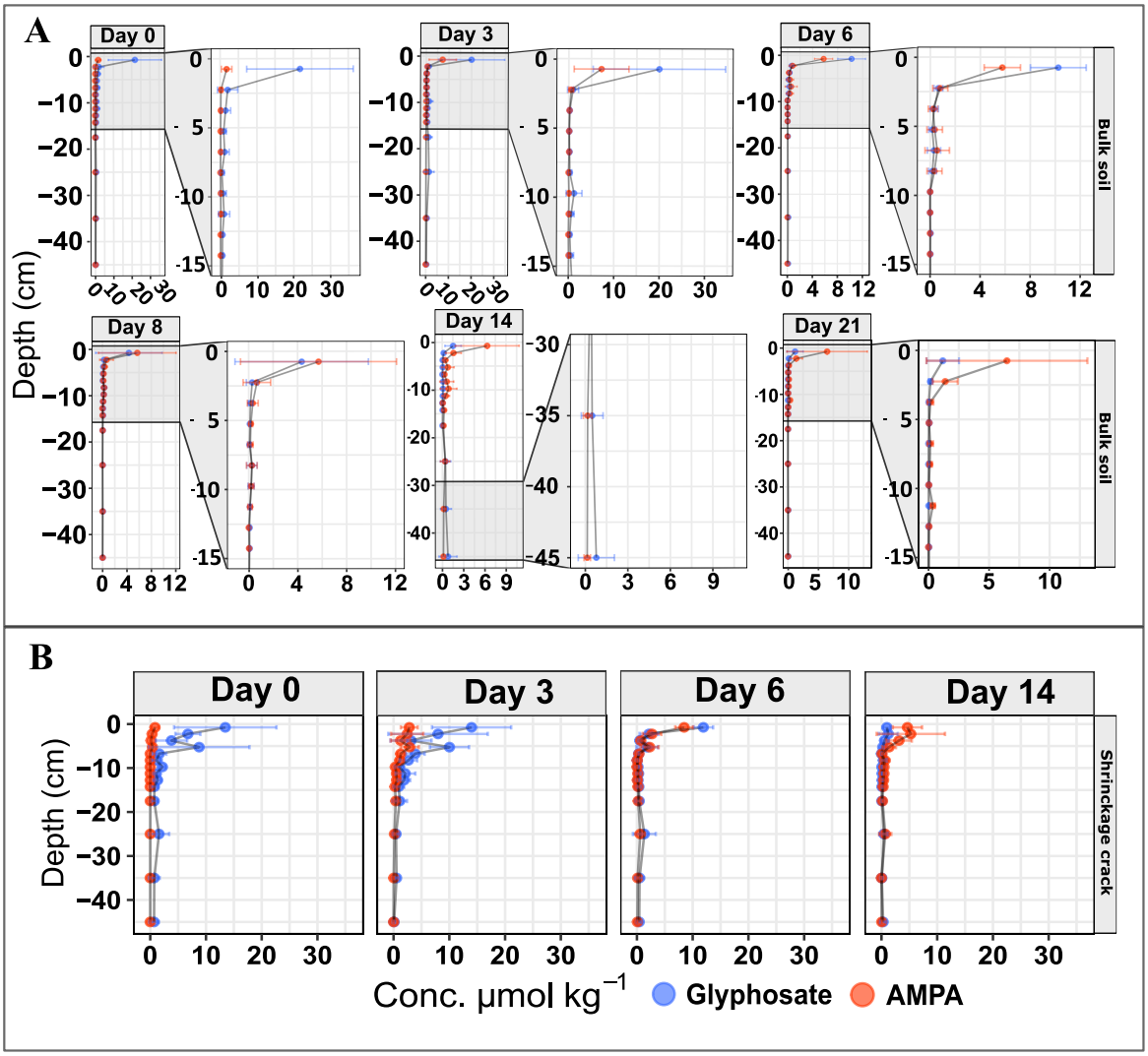

Figure 15: **(A)** Concentration (µmol kg^{-1}) distribution in bulk soil cores for GLP (blue) and AMPA (red) over the depth profile on different sampling days. **(B)** Concentration (µmol kg^{-1}) distribution in shrinkage crack cores. Mean values of three replicates (n = 3) are shown. Error bars indicate the standard deviation.

In our study, the transport behavior of newly formed AMPA in all soil cores was comparable to GLP, as indicated by the congruent AMPA distribution. On Day 21, 74.4% (6.5 µmol kg^{-1}), 25.6% (2.2 µmol kg^{-1}), and 0% AMPA were found in the 0-1.5, 1.5-15, and 15-50 cm segments, respectively, if the total AMPA concentration in the soil profile is used as a reference. The discrepancy of 5.5% GLP to 0% AMPA in the subsoil

(15 - 50 cm) can possibly be explained by lower degradation rates of GLP, which will be discussed later in more detail.

The coexistence of GLP and AMPA in soil samples has been frequently observed (Aparicio et al., 2013; Battaglin et al., 2014; Lupi et al., 2015; Haberkon et al., 2020). In the study by Battaglin et al. (2014), on the spatial distribution of GLP and AMPA, GLP but no AMPA was detected in only 2.3% of 3732 water and sediment samples; conversely, AMPA without GLP residues was detected in 17.9% of the samples. Therefore, as described in the literature, we will treat AMPA and GLP transport together, which will allow us to determine AMPA formation in situ based on the already displaced GLP.

Another important observation is that lateral inflow that bypasses the soil matrix along preferential flow pathways could contribute to an increase in concentration even at deeper soil horizons, e.g., at Day 14 (Figure 15 A). Here, we observed a sudden concentration peak in a depth range of 35-50 cm (1.07 µmol kg^{-1}). The GLP concentration was almost as high as in the upper soil segment (1.53 µmol kg^{-1}) of 0-1.5 cm. This finding is consistent with Borggaard and Gimsing (2008), who also emphasized the importance of preferential flows for transport of GLP and AMPA deeper into the soil profile associated with heavy rainfall shortly after application. (Napoli et al., 2015) demonstrated the potential for translocation of both GLP and AMPA over one meter in the case of a silty clay soil. They found that 0.2% and 0.58% of the applied application amount was recovered at a depth of one meter.

The potential for systematic leaching of GLP in structured soils was illustrated by shrinkage crack sampling. In shrinkage cracks that were visible at the surface, GLP distribution extended to a depth of 7.5 cm (Figure 15 B, Day 0). Over this range, a significant increase in GLP concentration, on average 4.73 µmol ($p < 0.05$), was observed as compared to the bulk soil. Daily irrigation during the first 14 days of the experiment allowed the clayey soil to swell, which closed the shrinkage cracks and reduced further translocation.

8.5.2 GLP degradation via the AMPA pathway in the bulk soil

One day after application and based on the presence of the target DNA sequence *goxA*, the topsoil (0-20 cm) was abundant in microorganisms that degrade GLP via the AMPA pathway. At this soil depth, *goxA* concentration averaged $2.27 \cdot 10^6$ copy numbers g^{-1} soil (Figure 16 A, Day 0). Over the course of the experiment, the number of microorganisms carrying the *goxA* gene continued to increase. The maximum of $4.1 \cdot 10^6$ copy numbers g^{-1} soil was reached on Day 8, followed by a decrease to $7.2 \cdot 10^5$ copy numbers g^{-1} soil until Day 21 (Figure 16 A).

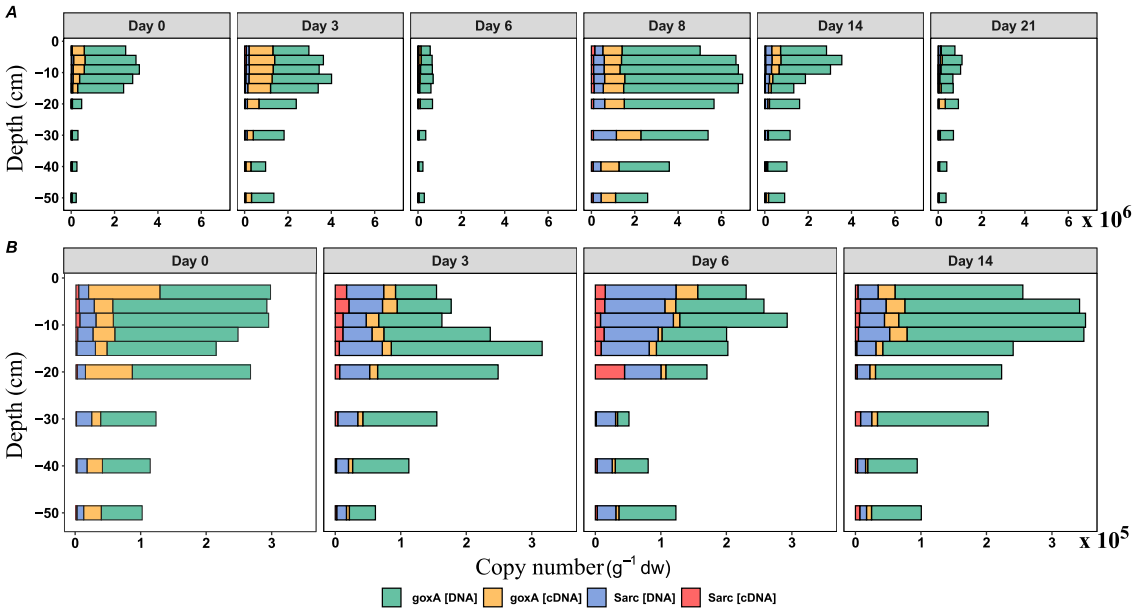

Figure 16: (A) Gene abundance (DNA) and gene transcript (cDNA) of *goxA* for bulk soil cores initiating degradation of GLP to AMPA, and *sarc* abundance (DNA) and *sarc* expression (cDNA) initiating degradation to sarcosine. (B) Quantification of gene abundance and gene transcription in shrinkage crack cores. Mean copies g^{-1} dw of three field replicates are shown.

The proliferation of *goxA* gene sequences in conjunction with the increase in AMPA concentration to approximately 7 µmol kg^{-1} (Figure 16 A, Day 21) indicates active bacterial GLP degradation to AMPA in which the C-N bond is cleaved to produce equimolar amounts of AMPA and glyoxylate. In most known GLP-degrading bacteria,

glyoxylate enters the glyoxylate cycle as a favorable energy substrate (Firdous et al., 2020), which bypasses the CO_2 generating steps of the TCA cycle (tricarboxylic acid cycle) (Dunn et al., 2009), while AMPA is exported to the extracellular space (Balthazor and Hallas, 1986; Jacob et al., 1988). In this respect, our results are consistent with the study by Sun et al. (2019b), where AMPA also began to accumulate and appeared to be 3 to 6 times more resistant to degradation than GLP, and with the study by Simonsen et al. (2008), in which GLP had a half-life of 9 and AMPA of 32 days in the same soil. Few bacterial strains, such as *Arthrobacter atrocyaneus ATCC 13752* (Pipke and Amrhein, 1988), *Arthrobacter sp. GLP-1* (Jacob et al., 1988), and *Pseudomonas sp. LBr*, use AMPA mainly as a phosphorus source after AMPA is catalyzed by a C-P lyase into methylamine and phosphate.

In addition to DNA analysis, including not only active but also dormant microorganisms and traces of bacterial DNA remaining in the soil, transcription of *goxA* genes as an activity index also showed a clear response to GLP application. Elevated *goxA* transcripts in the topsoil of $4.23 \cdot 10^5$ copy numbers g^{-1} soil together with the conversion of GLP to stoichiometric amounts of 2.5 µmol kg^{-1} AMPA three hours after the HRE indicated an immediate response to the application of GLP. Following the time course of GLP degradation activity based on the *goxA* transcripts, the peak value of $8.6 \cdot 10^5$ copy numbers g^{-1} soil was reached on Day 8. Maximum microbial activity coincided with the inflection point of the remaining GLP concentration relative to the newly formed AMPA (Figure 15 A, Day 8). As GLP concentrations gradually declined, transcript abundance returned to baseline levels of $5.4 \cdot 10^4$ copy numbers g^{-1} soil by Day 21. These field-determined dynamics of *goxA* expression are consistent with the results of laboratory degradation studies (Rueppel et al., 1977; Gimsing et al., 2004; Li et al., 2016), all of which found a rapid initial degradation rate followed by a gradual slowdown approaching a saturation phase after most of the available GLP was consumed. A microbial adaptation phase to the sudden appearance of GLP, as has often been demonstrated for other

herbicides such as phenoxy acetic acids (Bælum et al., 2008a; Nowak et al., 2020b), was not detected.

8.5.3 GLP degradation via the sarcosine pathway in the bulk soil

Microorganisms harboring the *sarc* gene had copy numbers in the range of 10^4 to 10^5 g^{-1} soil, an order of magnitude below the average *goxA* of 10^5 to 10^6 g^{-1} soil. The *sarc* abundance significantly ($p < 0.05$) increased to $1.3 \cdot 10^5$ copy numbers g^{-1} soil compared to the first sampling after only three days (Figure 16 A), followed by a slight increase in copy number to $4.6 \cdot 10^5$ copy numbers g^{-1} soil by Day 8. After reaching the maximum around 8 days, copy number declined to $7.1 \cdot 10^4$ g^{-1} soil after 21 days.

According to Borggaard and Gimsing (2008), the C-P lyase complex is activated only in the presence of an intracellular phosphate deficit. Sviridov et al. (2015) and Villamar-Ayala et al. (2019) discovered that bacterial strains growing on mineral media or under isolated conditions generally displayed a strong tendency to degrade via the sarcosine pathway. In agricultural soils, the sarcosine pathway can be down-regulated when phosphorus levels are high (Pipke and Amrhein, 1988).

Also, compared to the average transcript abundance of *goxA* ($\sim 10^5$ to 10^6), the *sarc* transcripts of $\sim 10^4$ were lower by an order of magnitude. Nevertheless, we detected a significant increase from an initial 10^4 to 10^5 copy numbers g^{-1} soil by Day 8. Parallel to its degradation to AMPA, a small amount of GLP is also converted to sarcosine. Jacob et al. (1988) proposed that the necessary partitioning of the two degradation pathways, a capability demonstrated in *Pseudomonas sp. LBr* in his study, depends on the need for additional phosphorus for microbial growth. Therefore, not only can the sarcosine pathway be activated or deactivated by phosphorus deficiency, but the phosphorus requirement of anabolic processes could induce transcription of *sarc* genes at a comparatively low level that is, however, analogous to *goxA* expression dynamics (Jacob et al., 1988).

8.5.4 GLP-derived ^{13}C enrichment in microorganisms of bulk soil samples

Three hours after HRE, fungi in the topsoil appear to have initiated GLP degradation; as the relative ^{13}C to the group specific PLFA C content of 1.1% and the absolute ^{13}C content of 7.6 ng g^{-1} dw were significantly higher as compared with Gr$^+$ bacteria (0%, 1.9 ng g^{-1} dw, Figure 17, Figure 44). Compared with Gr$^-$ bacteria (0.7%, 6.7 ng g^{-1} dw), ^{13}C incorporation was higher in fungi, but not statistically significant.

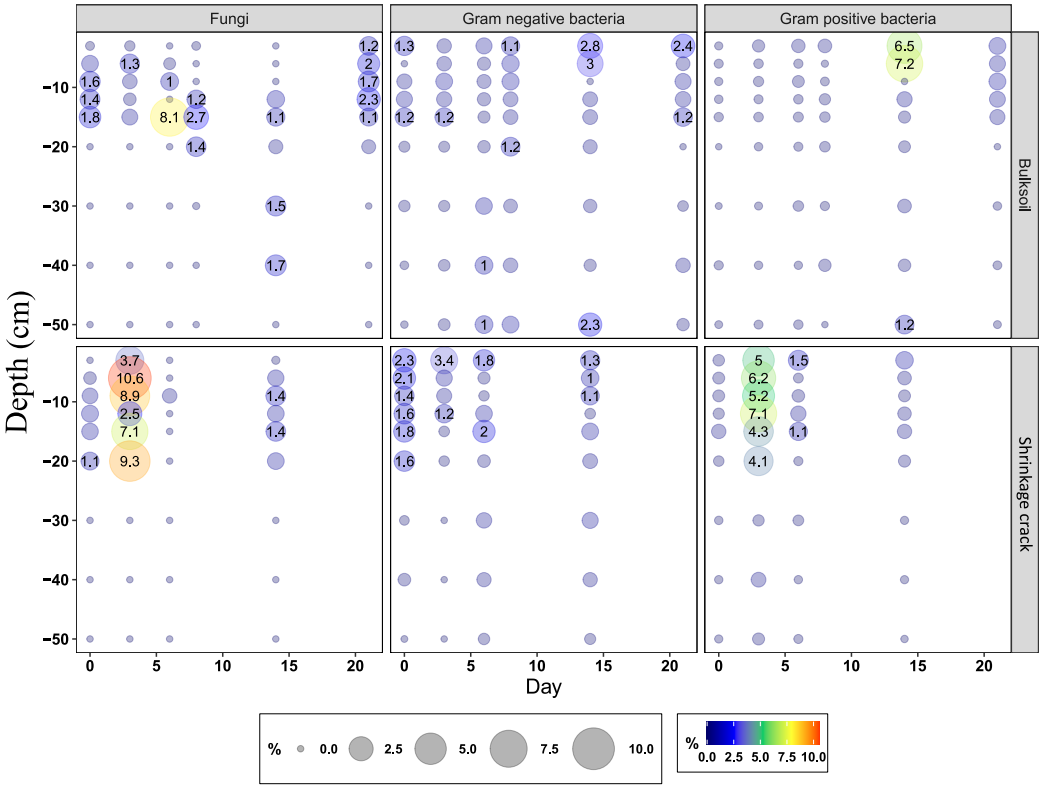

Figure 17: Relative (%; to the total PLFA group specific C) incorporation of GLP-derived ^{13}C into Gr$^+$-, Gr$^-$-bacteria and fungi along the soil depth profile and as a function of time. Small numbers indicate the percentage. Only values above 1% are displayed.

Fungi are known to be initial degraders of complex molecules such as lignin (Boer et al., 2005), and there is also evidence of their predominant role in cleaving C-P bonds, which are increasing in the environment through cleaning, medical, and household products (Krzyśko-Lupicka et al., 1997). In a previous study by Krzyśko-Lupicka et al. (1997), three

fungal strains; *T. harzianum, Scopulariopsis sp.* and *A. niger* were identified as effective utilizers of GLP in liquid medium serving as the sole source of phosphorus. Consistent with the surprisingly rapid ^{13}C incorporation in our study (Figure 17), immediate degradation participation of the aforementioned fungal strains was reported by these authors. In a batch experiment with isolated *Fusarium* strains, Castro Jr et al. (2007) confirmed this immediate response by demonstrating a GLP reduction of up to 40% after 20 days.

The incorporation of ^{13}C also confirmed that this is not just a co-metabolic degradation or detoxification of GLP, commonly associated with fungal degradation of organic pollutants (Harms et al., 2017). GLP can also serve as a carbon or perhaps energy source; a recent study by Spinelli et al. (2021), found that *P. lilacinum* degraded GLP to a greater extent via the sarcosine pathway as a nutrient, not only a P_i source. The quick response of fungi to GLP application (Figure 17) suggests that fungi, as the first step in a successive GLP degradation process, can assist bacteria in the further conversion of GLP through the release of extracellular enzymes like laccases or Mn-peroxidases (Pizzul et al., 2009).

The ^{13}C enrichment in bacterial biomass in the topsoil samples increased with time. However, the total ^{13}C content in Gr^- bacteria of about 15 ng g^{-1} dw compared to Gr^+ bacteria (9.2 ng g^{-1} dw) was significantly higher ($p < 0.05$) until Day 8. From Day 14, the total enrichment of ^{13}C (166 ng g^{-1} dw) in Gr^+ bacteria was significantly higher ($p < 0.01$) than in Gr^- bacteria (15.2 ng g^{-1} dw) or fungi (0.3 ng g^{-1} dw), within the first 6 cm (Figure S25). Gr^- bacteria continuously incorporated ^{13}C at a fairly constant level, while the Gr^+ bacteria only took up ^{13}C after some time, but then to a greater extent. At later time points in the field experiment, it was difficult to distinguish whether the GLP-derived ^{13}C was taken up directly or indirectly via cross-feeding.

Sviridov et al. (2012) indicated a strong similarity between the composition of C-P lyases in Gr^- and Gr^+ bacteria, suggesting similar GLP degradation ability in both bacterial groups. In a separate study by Fan et al. (2012), *Bacillus cereus CB4* (Gr^+

bacteria) was able to degrade 94.47% via the AMPA and sarcosine pathways in a GLP-contaminated soil in China after only 5 days. Comparable degradation was reached by *Ochrobactrum intermedium Sq20* (Gr^- bacteria) in GLP-contaminated soil with GLP utilization as the sole carbon source and complete degradation (500 $mg\,L^{-1}$ GLP) within 4 days (Firdous et al., 2018). One explanation for the observed disparities in degradation participation by Gr^- and Gr^+ bacteria when degradation potential was comparable can be found in the study by Muskus et al. (2022), which confirmed an increasing contribution of Gr^+ bacteria to GLP degradation with increasing total organic carbon (TOC). An increase in TOC or decreasing pH resulted in higher levels of ^{13}C-enriched PLFAs indicative for the starvation of Gr^- bacteria. Muskus et al. (2022) concluded that Gr^- bacteria were involved in the GLP degradation in earlier stages and under different soil conditions. Therefore, a physiological condition unique to Gr^+ or Gr^- bacteria under different environmental and soil conditions may also determine carbon utilization and the timing and extent of GLP degradation.

8.5.5 GLP biodegradation in the topsoil compared to subsoil

When microbial abundance and degradation activity in the topsoil was compared to the subsoil, there was more intense degradation in the first 0-20 cm at the beginning of the experiment (Figure 16 A, Days 0 and 3). When GLP was present in deeper soil layers, microbial activity and growth of degraders were also observed in the subsoil. At Day 8, at a depth of 20-50 cm, transcripts and gene abundances of *goxA* increased significantly ($p < 0.001$) to $8.8 \cdot 10^5$ and $4.5 \cdot 10^6$ copy numbers g^{-1} soil, respectively. The increase in *goxA* gene expression was accompanied by a significant ($p < 0.05$) increase in *sarc* transcripts from $7.4 \cdot 10^2$ to $8.4 \cdot 10^4$ copy number g^{-1} soil at Day 8. Enrichment with ^{13}C demonstrated that bacterial GLP degradation also occurred to a small degree in the subsoil (Figure 17). On Day 14, elevated GLP concentration was observed at a depth of 40 to 50 cm. At this depth, the incorporation of ^{13}C into Gr^+ bacteria increased

from an average of 5 ng g^{-1} dw at 30 to 40 cm to 13.4 ng g^{-1} dw at 50 cm. Combining this increase with the increased gene abundance confirms actual degradation and rules out a translocation of ^{13}C enriched bacteria from topsoil to subsoil. This temporary response of microbial GLP degradation was observed despite limiting conditions expected in the subsoil, such as the possible spatial separation between substrate and degraders (Dechesne et al., 2010, 2014; Pinheiro et al., 2015a), and fluctuating redox potentials during the experimental period (Schlögl et al., 2022). It is likely that the degradation rate was slower than in the topsoil, however. This is indicated by the reduced gene expression of *goxA* and *sarc* in the subsoil compared to the topsoil and by the reduced AMPA formation.

The simulated heavy rainfall event could have had two opposing regulatory functions. First, it may have promoted leaching and transport of GLP into microbially inactive zones, inhibiting further degradation (Flury, 1996). At the same time, a short-term increase in soil moisture leads to more dissolution of GLP, which also increases the likelihood of contact between GLP and degraders, perhaps facilitating effective biodegradation (Manzoni et al., 2011). Low intensity, prolonged precipitation that changes redox conditions in the subsoil from oxic to moderately or even strongly reducing may further inhibit aerobic oxidation of GLP to AMPA and glyoxylate (Schlögl et al., 2022). Since the redox state is subject to strong fluctuations, especially in August, this situation could reverse very quickly and slow degradation only temporarily (Kanissery et al., 2015).

8.5.6 Microbial GLP degradation in shrinkage crack sampling

The most notable difference in the topsoil between the shrinkage cracks and the bulk soil was the order of magnitude lower gene and transcript abundance in the shrinkage cracks (Figure 16, B). This difference was evident not only in the absolute abundances of GLP degraders ($\sim 10^5$ vs. $\sim 10^6$ copy numbers g^{-1} soil in the bulk soil), but also in the relative abundances when *goxA* was related to 16S rRNA genes (Figure S22).

However, this is in contrast to the study by Vinther et al. (2001), who did not find significant differences in degradation potential in macropores vs. soil matrix based on ^{14}C mineralization for mecoprop and isoproturon.

In flow paths of non-biological origin, the emergence of microbial activity gradients correlates directly with flow velocity (Rubol et al., 2014). Macropores that are smaller in size ($\sim$ 30-300 µm Ø) can provide beneficial microbial habitat conditions compared to larger macropores (Franklin et al., 2021). Lower flow velocities, and moderate water retention, and quick oxygenation allow biofilm formation associated with an increase in the expression of microbial functions (Bouckaert et al., 2013). Even when compared directly to bulk soil, smaller macropores can exhibit higher carbon mineralization rates (Hagedorn et al., 2015) and provide important microbial hotspots for biogeochemical processes (Bundt et al., 2001). From a microbial perspective, large macropores such as shrinkage cracks (>300 µm Ø, (Kravchenko et al., 2019)) provide less favorable environments due to their extreme wetting and drying regimes and the easy loss of nutrients by leaching (Franklin et al., 2021). Leaching, particle transport, and further degradation of GLP appear confined exclusively to macropores that comprise only a small fraction of the soil volume, and are therefore controlled by the local sorption and degradation conditions along pore walls (Köhne et al., 2009).

After GLP application, *goxA* was initially elevated in the topsoil and remained nearly constant over time (Figure 41 B). *Sarc* was present in low copy numbers of $2.3 \cdot 10^4$ g^{-1} soil at the beginning of the experiment (Figure 16 B). Subsequently, *sarc* gene and transcript abundances increased significantly ($p < 0.05$) to a peak of $9.3 \cdot 10^4$ and $1.2 \cdot 10^4$ copy numbers g^{-1} of soil, respectively, then fell back to baseline when the substrate in the form of GLP was no longer able to sustain growth and enzyme synthesis was no longer induced. In fact, on Day 6, there was no longer a significant difference between the detected copy or transcript abundances of *sarc* and *goxA*, although *goxA* was more abundant in the bulk soil at each time point (Figure 16 A). The sarcosine pathway seems

to have become more important in shrinkage cracks (Figure 16 B, Day 3 and 8). It is possible that GLP and phosphate compete for sorption sites (Gimsing et al., 2004; Borggaard and Gimsing, 2008). GLP retention at a depth of 10 cm could therefore have displaced and remobilized phosphate, and subsequent leaching could have resulted in an in-situ phosphate depletion. Such a local phosphate deficit could explain the promoted sarcosine pathway in shrinkage cracks.

The highest relative ^{13}C enrichment in shrinkage cracks was observed in fungi at the beginning of the experiment (Day 3). By this date, fungi would have used GLP as a relevant substrate source (about 10% of its PLFA C originated from GLP, Figure 17). The maximum of 152 $ng\,g^{-1}$ dw in Gr^+ bacteria averaged over a depth of 20 cm was reached after only three days. This is a significant ($p < 0.01$) increase compared to the enrichment in Gr^- bacteria (7.1 $ng\,g^{-1}$ dw) and fungi (2.5 $ng\,g^{-1}$ dw). Interestingly, the ^{13}C enrichment of PLFAs observed in shrinkage cracks indicates altered and more rapid incorporation dynamics than in the bulk soil (Figure 17), similar to the observed shift in *goxA* to *sarc* gene and transcript abundances (Figure 16 B). There is evidence that microbial communities are unique in pores of different sizes (Treves et al., 2003). Shaped by the structural properties of macropores and their atmospheric connectivity (Treves et al., 2003; Rabbi et al., 2016) the presence of distinct microbial communities could explain the predominant sarcosine pathway in addition to the phosphate deficit that may have occurred. To date, it is not known how the distribution and interactions of bacteria and fungi in different aggregates regulate their functional (gene) expression or what consequences there may be for overall soil functions (Rabbi et al., 2016) or GLP degradation.

8.6 Conclusion

Against the background of increasing GLP residues in soils, it seems necessary to investigate the structural conditions in soils and the influence on microbial degradation of

increased vertical translocation of GLP after rain events. Examination of shrinkage cracks formed during a drought period following a simulated rain event revealed a systematic relocation of recently applied GLP along shrinkage cracks. In these shrinkage cracks, GLP degradation to sarcosine was more important than in the bulk soil. In both soil compartments, a significant involvement of fungi over Gram$^+$ bacteria was observed during the initial phase of glyphosate degradation, potentially facilitating glyphosate degradation for bacteria. Finally, the degradation of GLP in the subsoil seemed to slow down, but is still present. These results highlight the need to consider GLP transport behavior and microbial degradation at the field scale to gain a comprehensive understanding of the fate of pesticides where they are applied, i.e., on arable fields. Further research should focus on the fate of AMPA under environmental conditions that occur during the spray season in structured soils. Degradation rates, slowing of microbial activity with increasing soil depth, influence of changing redox conditions, and consideration of drought and unpredictable storm events as a result of climate change should also be investigated.

8.7 Acknowledgement

We thank Wolfgang Armbruster for isotope analyses and Sabine Rudolph for assistance during PLFA extraction. We would also like to thank Kathleen Regan for the English correction. We thank Marie Uksa for information on qPCR conditions and primer selection. We thank Heike Haselwimmer for the subsequent qPCR assay runs and Dr. Waqas Ahmed Malik and Professor Dr. Piepho for assistance in statistical analysis.

8.8 Funding

This study was financially supported by the German Research Foundation (DFG) under the Collaborative Research Center 1253 CAMPOS (DFG grant SFB 1253/1 2017).

9 Appendices

9.1 Supplementary Information for Chapter 10 (Study III)

9.1.1 Experimental Design

The plots were separated by above-ground plastic barriers buried 20 cm deep and extending 30 cm high above ground, to exclude boundary effects. The entire plot had an area of 5.76 m^2

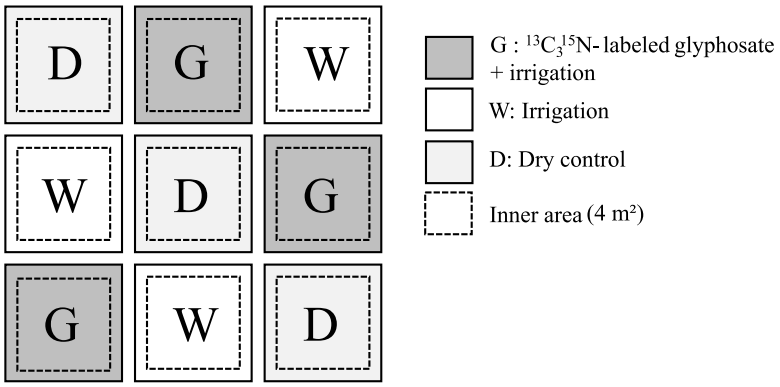

Figure 18: Illustration of the experimental design: dark gray plots were treated with GLP (G), white plots were irrigated with water only (W), and the light gray were left dry (D) and used as controls.

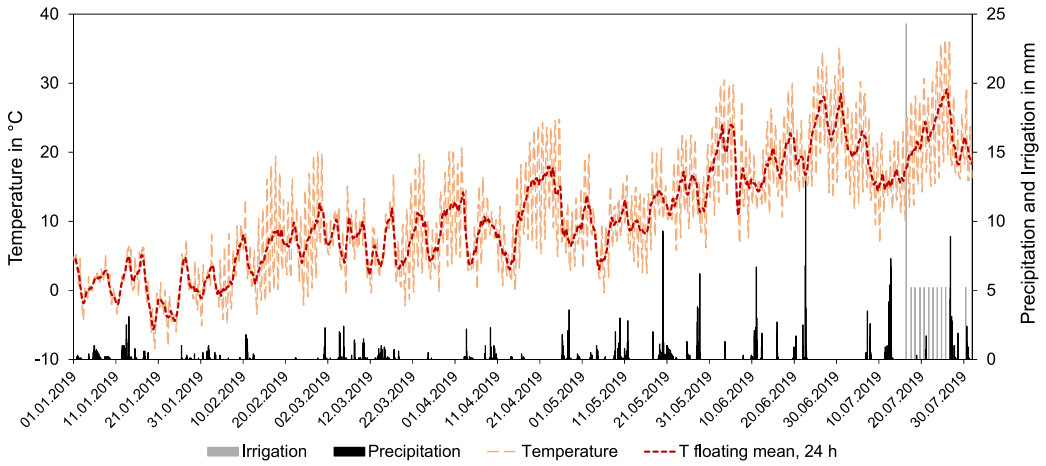

Figure 19: Hourly data on irrigation (grey bars) and natural precipitation (black bars) in mm as well as temperature (T) in °C from 01.01.2019 until 31.07.2019 (experiment duration 16.07.2019 – 06.08.2019; adapted from Schlögl et al., 2022).

9.1.2 Sampling schedule

Table 24: Sampling schedule

Date	Sampling Date	Application	Irrigation	Shrinkage crack	Bulksoil
15.07.2019	Day -1	X			
16.07.2019	Day 0		X (30 L m²)	X	X
17.07.2019	Day 1				
18.07.2019	Day 2				
19.07.2019	Day 3		X (5 L m²)	X	X
20.07.2019	Day 4		X (5 L m²)		
21.07.2019	Day 5		X (5 L m²)		
22.07.2019	Day 6		X (5 L m²)	X	X
23.07.2019	Day 7		X (5 L m²)		
24.07.2019	Day 8		X (5 L m²)		X
25.07.2019	Day 9		X (5 L m²)		
26.07.2019	Day 10		X (5 L m²)		
27.07.2019	Day 11				
28.07.2019	Day 12				
29.07.2019	Day 13				
30.07.2019	Day 14		X (5 L m²)	X	X
31.07.2019	Day 15				
01.08.2019	Day 16				
02.08.2019	Day 17				
03.08.2019	Day 18				
04.08.2019	Day 19				
05.08.2019	Day 20				
06.08.2019	Day 21				X

9.1.3 GLP and AMPA residue analysis

GLP-$^{13}C_3$,^{15}N and AMPA-^{13}C,^{15}N residues in soil samples were quantified using an extraction protocol with subsequent CE-MS analysis as described by Wimmer et al. (2020). In short, duplicates of 0.2 g lyophilized soil were suspended in 0.5 mL aqueous Na_3PO_4 solution (0.05 mol L^{-1}) containing GLP and AMPA standards for quantification (0.5 g L^{-1}). Suspensions were sonicated for 0.5 h, then centrifuged for 15 min. Supernatant was collected, acidified with HCl, vortexed, and again centrifuged. Supernatants were then analyzed for GLP and AMPA without derivatization using capillary electrophoresis-mass spectrometry (described in Wimmer et al. (2020)). For separation, a bare fused silica capillary of 68 cm length and 50 µm inner diameter was used. The background electrolyte was formic acid (0.175 mmol L^{-1}) at pH 2.8. The separation voltage was -30 kV with additional 50 mbar pressure. Both analytes were detected in negative ionization mode; limits of detection were 8 and 36 µg kg^{-1} for GLP and AMPA, respectively; analyte recovery >80 %. Final concentrations were calculated as the ratio of signal areas of analyte to standard, multiplied with the standard concentrations and the liquid-solid extraction ratio.

9.1.4 GLP-derived ^{13}C in phospholipid fatty acids

We used PLFAs as biomarkers to study the differential contributions to GLP degradation of Gram positive (Gr^+) and Gram negative (Gr^-) bacteria and fungi. The branched fatty acids i15:0, a15:0, i16:0, and i17:0 are all indicators of Gr^+ bacteria, and the cy17:0 and cy19:0 are indicative of Gr^- bacteria (Zelles, 1999). The biomarker 18:2ω6.9c was used as a fungal indicator (Frostegård and Bååth, 1996).

PLFAs were extracted from 4 g of field-fresh soil with a mixture of chloroform, methanol and citrate buffer (citric acid monohydrate, 0.15 mol L^{-1}, pH = 4; 1:2:0.8; $v/v/v$) according to Bligh and Dyer (Bligh and Dyer, 1959). The extract was purified using silica gel SPE cartridges (Bond Elut SI, 500 mg, 3 mL, Agilent Technologies, Santa Clara, CA,

USA) following the procedure of Frostegård et al. (1993) and separated into glyco- and neutral lipids as well as phospholipid fatty acids. Subsequent methanolysis of PLFAs was performed with 0.2 mol L^{-1} methanolic KOH as described by Ruess et al. (2007). Fatty acid methyl esters (FAMEs) were quantified and identified by gas chromatography (GC; Perkin-Elmer Corporation, Norwalk, CT, USA).

To determine the δ^{13}C content in the PLFA samples, a four-step fractionation in Ag^{+}-SPE cartridges (6 mL, Supelco, Palo Alto, USA) was carried out using elution steps with *n*-hexane and increasing concentration of acetone (99:1, *v*/*v*; 96:4, *v*/*v*; 90:10, *v*/*v* and 0:100, *v*/*v*) according to Kramer et al. (2008). Monoenoic trans- and cis-FAMEs (2nd and 3rd fractions) were removed and only the saturated (1st fraction) and dienoic FAMEs (4th fraction) were kept. The δ^{13}C-values of FAMEs were determined using a gas chromatograph (6890 series, Agilent Technologies, Santa Clara, CA, USA) coupled to a gas chromatography incinerator III Interphase (Thermo Finnigan, Waltham, MA, USA) connected to a Delta Plus XP mass spectrometer (Thermo Finnigan MAT, Bremen, Germany). δ^{13}C-values of all FAMEs were corrected for the addition of a methyl group according to Denef et al. (2007). The determination of GLP-derived ^{13}C (% C_{GLP}; related to the total, group-specific PLFA-derived C) was calculated using Equation 1:

$$\% \; C_{GLP} = \frac{\delta_{sample} - \delta_{soil}}{\delta_{reference} - \delta_{soil}} \cdot 100 \tag{37}$$

where δ_{Sample} is the δ^{13}C-value of GLP from the sample, δ_{Soil} is the δ^{13}C-value of a blank sample from a corresponding soil depth taken from the wet plots, irrigated with water only. $\delta_{\mathrm{reference}}$ is the δ^{13}C-value of the labeled GLP (100‰). In addition, the absolute quantity of GLP-derived ^{13}C in PLFAs was calculated (^{13}C ng g^{-1} dry weight).

9.1.5 DNA/RNA assay

As a pre-test we compared DNA and RNA extraction from 250 mg and 500 mg of the studied soil and decided to use 500 mg for further analyses. Shaking of samples to bind DNA to the binding matrix was done manually (12 min on a rotary shaker were also tested). The guanidine thiocyanate step was omitted. The final volume of the DNA or RNA extracts was 100 µL. Samples were stored at -20°C (DNA) or -80°C (RNA) for further use. By using a NanoDrop ND 2000 spectrophotometer (Thermo Fisher Scientific, Germany) DNA and RNA concentrations were measured at wavelength 260 nm. Purity of the DNA and RNA extracts was determined by calculating the quotients of 260/280 and 260/230. Digestion of potential DNA residues and subsequent reverse transcription were performed according to Wirsching et al. (2020b).

9.1.6 GoxA primer design

Two primer pairs were designed with Primer3Web version 4.1.0.: one specific for the *goxA* sequence of *Ochrobactrum sp. G-1*, accession number GU214711.1 ($GoxA_f$ ATC GGC TTT GAG ACT GAA GG and $GoxA_r$ CCA TTT CCA TAG GTG TCG CG) and another one degenerated to target the five goxA sequences ($GoxA_{fd}$ ATC GGC TT[T/C] GA[G/A] ACT GAA GG and $GoxA_{rd}$ CC[A/G] TTT CCA T[A/C]G G[T/C/G]G T[T/A]G CG).

Table 25: GenBank accession numbers for nucleotide sequences

Deposition number	Primer	sequence number
BankIt2535179	GOXA243-5 SP6 9	OM105670
BankIt2535179	GOXA243-16 SP6 10	OM105671
BankIt2535179	GOXA243D-3 SP6 11	OM105672
BankIt2535179	GOXA243D-7 SP6 12	OM105673
BankIt2535085	GOXA529-BB-1 SP6 1	OM105674
BankIt2535085	GOXA529-BB-9 SP6 2	OM105675
BankIt2535085	GOXA529-ICE-2 SP6 3	OM105676
BankIt2535085	GOXA529-ICE-10 SP6 4	OM105677

These two primer pairs generated an amplicon of 243 pb. A third primer pair

targeting goxA and generating an amplicon of 529 bp was also designed ($GoxA_f2$ GCAGACTTCGCCAAGGAC and $GoxA_r2$ CAGTTAGGAGCGGCTGTGAG). These three primer pairs were checked in silico using Primer3Web. In addition, their specificities for *goxA* sequences were determined by cloning and sequencing the *goxA* amplicons obtained from DNA extracted from GLP-exposed arable soils. All amplicons sequences were similar to *goxA* sequences (sequence deposited in the Genbank database under deposition numbers 2535179 and 2535179 for the 243 and 529 bp amplicons (Table 25).

9.1.7 Real-time quantitative PCR

For each SYBR Green reaction 7.5 µL of Power SYBR Green PCR master mix (Applied Biosystems, Germany), 0.75 µL of each primer solution containing 5 µmol primer, 0.375 µL of T4gp32 solution (MP Biomedicals, Germany), 3.625 µL water and 2 µL diluted template DNA or cDNA solution (5 ng µL^{-1}) for functional genes (*goxA* and *sarc*) were mixed. For quantification of the 16S rRNA gene 1 µL diluted template DNA or cDNA (5 ng µL^{-1}) and 4.625 µL water were used. According to Ditterich et al. (2013a) standard plasmid DNA was used for quantification with a dilution series from 10^8 to 10^1 copies µL^{-1}.

Table 26: Primer sequence used in this study

Target sequence	Primer	qPCR conditions
16S rRNA genes*	341F: CCT ACG GGA GGC AGC AG 515R: ATT ACC GCG GCT GCT GGC A	600 s at 95°C Cycle (35): 15 s at 95°C , 30 s at 60°C 30 s at 72°C, 30 s at 75°C (m.o.f)
goxA	F: ATC GGC TT[T/C] GA[G/A] ACT GAA GG R: CC[A/G] TTT CCA T[A/C]G G[T/C/G]G T[T/A]G CG	600 s at 95°C Cycle (40): 15 s at 95°C , 30 s at 56°C, 30 s at 72°C, 30 s at 79°C (m.o.f)
*sarc***	F: CGT GTG AAA CCT GGA AAA CGT GGT R: TAG CGG CTA CAT GAA CAC CTG CT	600 s at 95°C Cycle (40): 15 s at 95 °C , 30 s at 60°C, 30 s at 72°C (m.o.f)

m.o.f - measurement of fluorescence; *López-Gutiérrez et al. (2004), **González-Valenzuela and Dussán (2018)

9.1.8 Statistical analysis

For two-dimensional models using the licensed R package ASReml-R version 4, the special functions require two arguments specifying the (x,y) coordinates of each observation. In the present study, the depth profile was implemented as an x-coordinate and in the temporal dimension as a y-coordinate. An anisotropic exponential model was realized that assumes and estimates a different correlation slope for each coordinate due to the different depth and time intervals. Depth and time were specified as fixed factors, plot replicates nested in time as random effect, and depth and time as residuals (error components). Response variables were GLP decline over time for each soil depth, evolution of *goxA* and *sarc* abundance and gene expression, and dynamics of ^{13}C incorporation. Pseudo-analysis of variance with incremental Wald statistics (Kenward and Roger, 1997) was then performed, and model assumptions were visually confirmed by residual diagnostic plots (Kozak and Piepho, 2018; Schöpfer et al., 2020). The significance of pairwise differences was determined by calculating half least significant error intervals implemented in the asremlPlus-package.

9.1.9 GLP dissipation

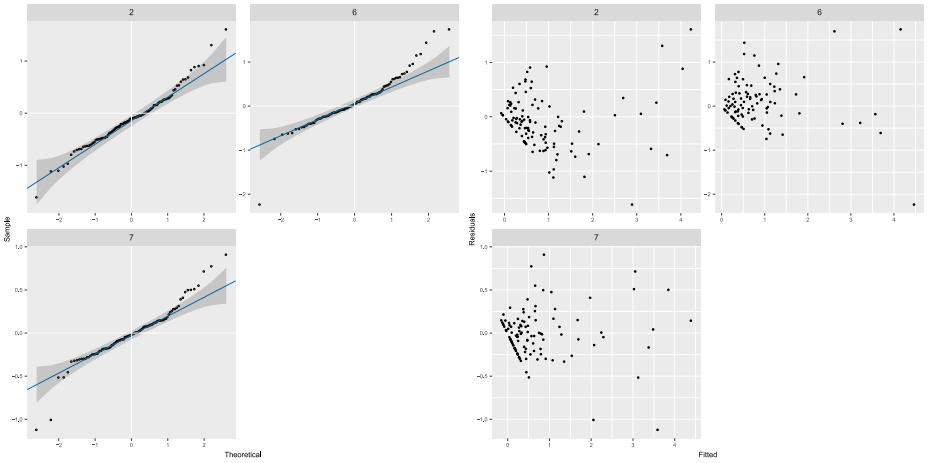

Figure 20: Model assumptions for Wald test were visually confirmed by residual diagnostic plots. Normal Q-Q plot to test for normality (left sight panels). Tests for Homogeneity of Variance (reight sight panels).

Table 27: Wald tests for fixed effects. Response: GLP concentration

	Df	Sum of Sq	Wald statistic	Pr(Chisq)
(Intercept)	1	67.69	67.69	2.220e-16 ***
Depth	13	480.29	480.29	<2.2e-16***
Day	3	20.34	20.34	0.0001445 ***
Sampling	1	23.31	23.31	1.381e-06 ***
Depth:Day	39	131.19	131.19	6.636e-12 ***
Depth:Sampling	13	68.2	68.2	1.726e-09 ***
Day:Sampling	3	11.1	11.1	0.0112565 *
Depth:Day:Sampling	39	61.3	61.3	0.0128000 *
residual (MS)		1.0		

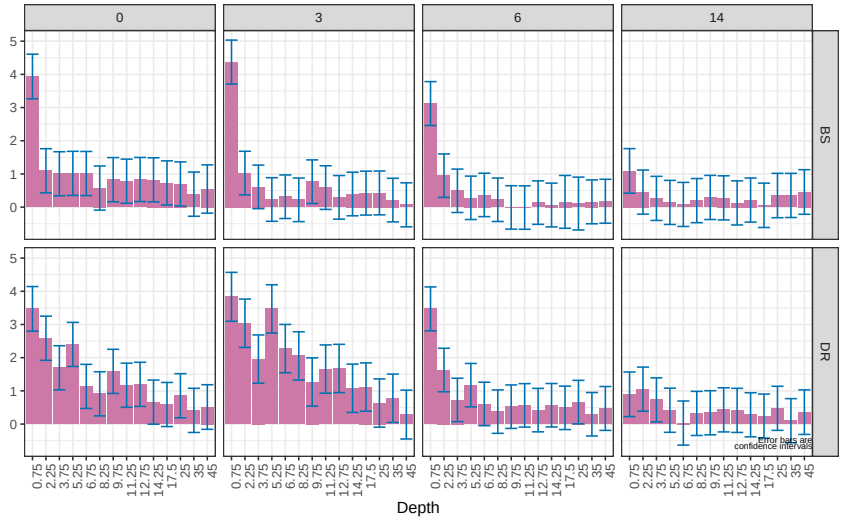

Figure 21: Predictions for GLP dissipation from Sampling:Day:Depth (square-root transformed); Least Significant Difference (LSD) being added and subtracted to the predictions, the LSD being calculated using the square root of the mean of the variances of all or a subset of pairwise differences between the predictions.

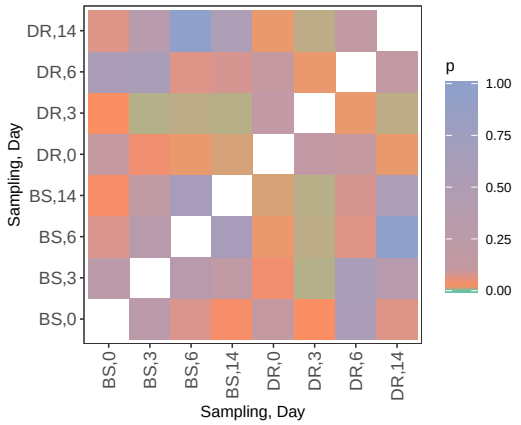

Figure 22: p values for all pairwise differences between predicted values (Sampling:Day; GLP concentration)

9.1.10 GoxA and sarc quantification - shrinkage crack

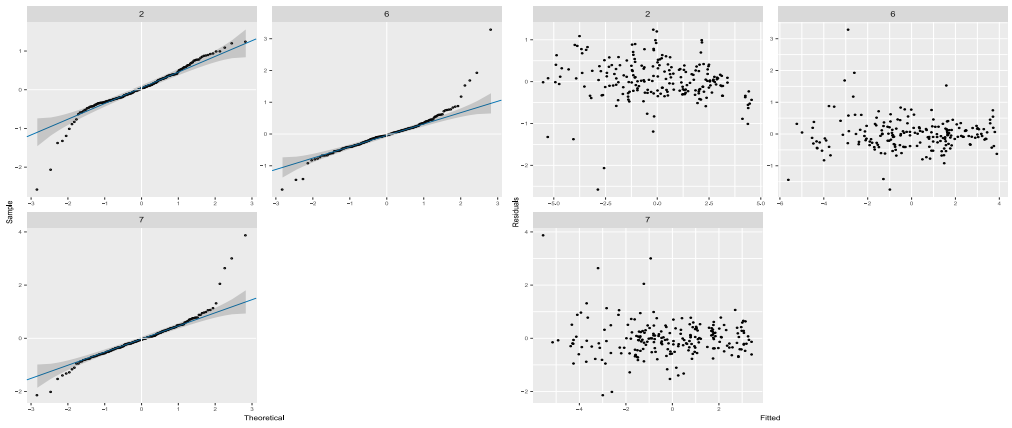

Figure 23: Model assumptions for Wald test were visually confirmed by residual diagnostic plots.Normal Q-Q plot to test for normality (left sight panels). Tests for Homogeneity of Variance (right sight panels).

Table 28: Wald tests for fixed effects (shrinkage cracks). Response: DNA/cDNA

	Df	Sum of Sq	Wald statistic	Pr(Chisq)
(Intercept)	1	194.8	194.8	< 2.2e-16***
Depth	8	28.2	28.2	0.00042***
Day	3	9.17	9.17	0.027*
Analysis	3	180.6	180.6	< 2.2-16***
Depth:Day	24	31.04	31.04	0.15
Depth:Analysis	24	49.7	49.7	0.0015**
Day:Analysis	9	61.9	61.9	5.7e-10***
Depth:Day:Analysis	72	65.9	61.9	0.67
residual (MS)		1.0		

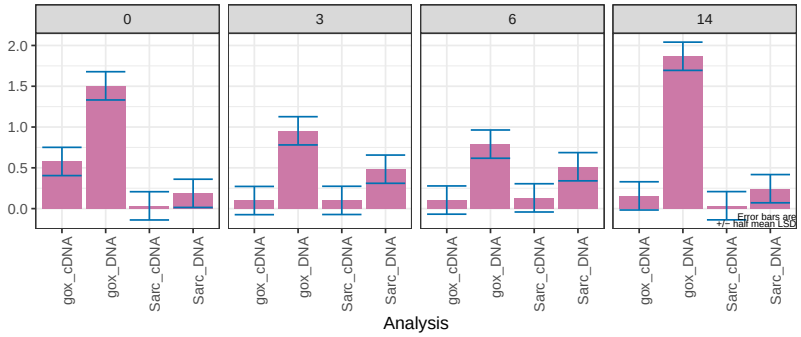

Figure 24: Predictions for DNA/cDNA abundance from Analysis:Day (Shrinkage crack, square-root transformed); LSD values, minimum LSD = 0.4192772, mean LSD = 0.4576249, maximum LSD = 0.4760428 , (sed range / mean sed = 0.124)

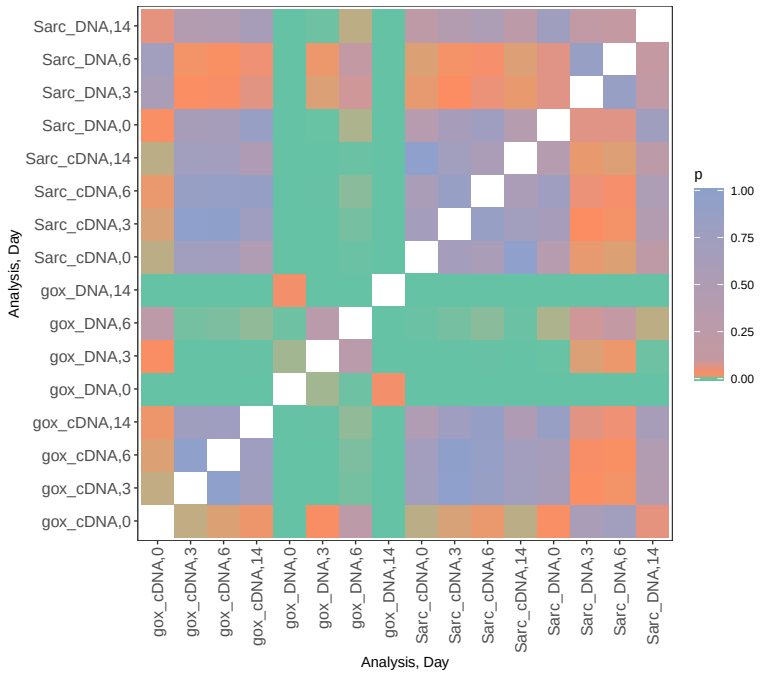

Figure 25: p values for all pairwise differences between predicted values (Analysis:Day; DNA)

Table 29: Mean values and standard deviation of DNA/cDNA data in the topsoil (shrinkage crack)

Topsoil	Day	Analysis	MW	SD
0-20 cm	0	gox_DNA	2.00E+05	4.97E+04
	3	gox_DNA	1.27E+05	5.41E+04
	6	gox_DNA	1.16E+05	1.96E+04
	14	gox_DNA	2.43E+05	1.64E+04
	0	gox_cDNA	4.32E+04	5.54E+04
	3	gox_cDNA	1.82E+04	1.60E+03
	6	gox_cDNA	1.52E+04	1.86E+02
	14	gox_cDNA	2.26E+04	1.24E+03
	0	Sarc_DNA	2.30E+04	3.81E+03
	3	Sarc_DNA	5.07E+04	8.09E+03
	6	Sarc_DNA	9.34E+04	4.83E+03
	14	Sarc_DNA	3.70E+04	5.94E+03
	0	Sarc_cDNA	3.96E+03	9.10E+02
	3	Sarc_cDNA	1.45E+04	1.20E+03
	6	Sarc_cDNA	1.20E+04	2.76E+03
	14	Sarc_cDNA	4.89E+03	1.39E+03

Table 30: Mean values and standard deviation of DNA/cDNA data in the subsoil (shrinkage crack)

Subsoil	Day	Analysis	MW	SD
20-50 cm	0	gox_DNA	7.37E+04	2.30E+03
	3	gox_DNA	7.95E+04	1.91E+04
	6	gox_DNA	5.16E+04	4.40E+04
	14	gox_DNA	1.07E+05	2.58E+04
	0	gox_cDNA	2.15E+04	1.14E+04
	3	gox_cDNA	6.15E+03	1.41E+03
	6	gox_cDNA	4.07E+03	1.17E+02
	14	gox_cDNA	6.55E+03	2.77E+03
	0	Sarc_DNA	1.64E+04	5.83E+03
	3	Sarc_DNA	2.12E+04	1.47E+03
	6	Sarc_DNA	2.70E+04	5.37E+02
	14	Sarc_DNA	1.32E+04	4.40E+03
	0	Sarc_cDNA	1.34E+03	2.73E+02
	3	Sarc_cDNA	2.71E+03	8.17E+02
	6	Sarc_cDNA	2.36E+03	1.02E+03
	14	Sarc_cDNA	5.93E+03	3.32E+03

9.1.11 GoxA and sarc quantification - bulk soil

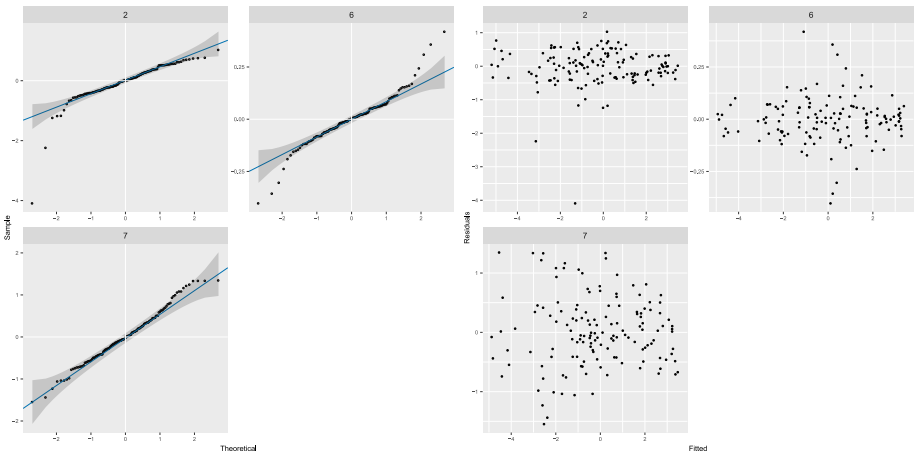

Figure 26: Model assumptions for Wald test were visually confirmed by residual diagnostic plots. Normal Q-Q plot to test for normality (left sight panels). Tests for Homogeneity of Variance (right sight panels).

Table 31: Wald tests for fixed effects (bulk soil). Response: DNA/cDNA

	Df	Sum of Sq	Wald statistic	Pr(Chisq)
(Intercept)	1	358.83	358.83	< 2.2e-16***
Depth	8	152.10	152.10	< 2.2e-16***
Day	5	68.27	68.27	< 2.2e-16***
Analysis	3	1901.00	1901.00	< 2.2-16***
Depth:Day	40	147.92	147.92	2.709e-14 ***
Depth:Analysis	24	84.69	84.69	1.072e-08 ***
Day:Analysis	15	345.06	345.06	< 2.2-16***
Depth:Day:Analysis	120	154.28	154.28	0.01906 *
residual (MS)		1.0		

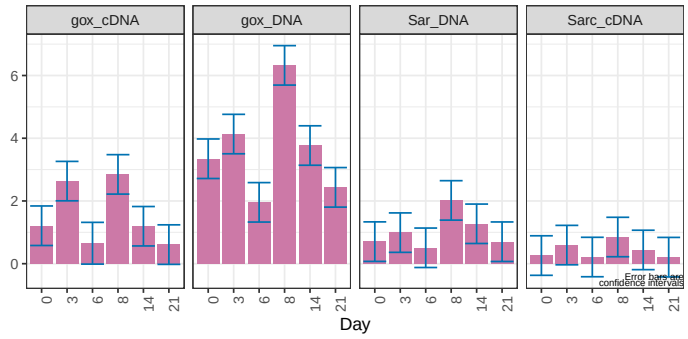

Figure 27: Predictions for DNA/cDNA abundance from Analysis:Day (bulk soil, square-root transformed); LSD values: minimum LSD = 0.4789915, mean LSD = 0.8499834, maximum LSD = 0.9182752 (sed range / mean sed = 0.517)

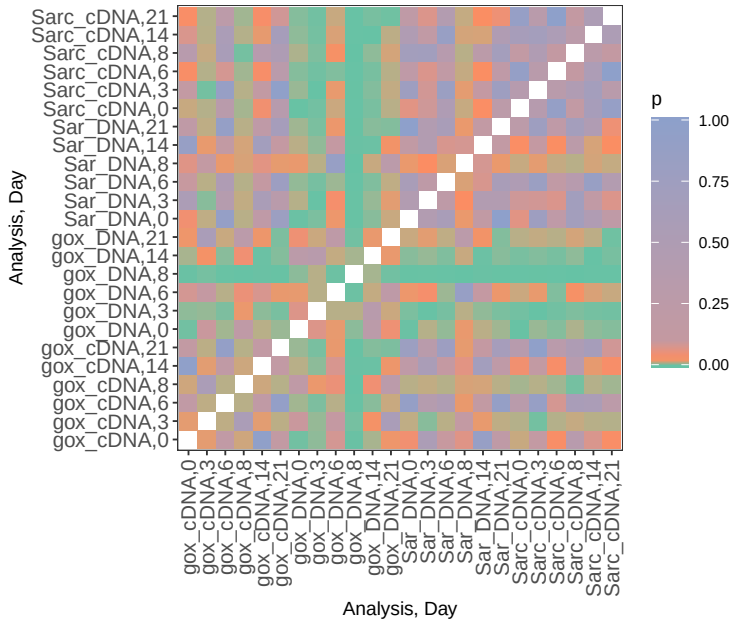

Figure 28: p values for all pairwise differences between predicted values (Analysis:Day; DNA; bulk soil)

Table 32: Mean values and standard deviation of DNA/cDNA data in the topsoil (bulksoil)

Topsoil	Day	Analysis	MW	SD
0-20 cm	0	gox_DNA	2.27E+06	1.41E+05
	3	gox_DNA	2.19E+06	2.48E+05
	6	gox_DNA	5.19E+05	3.69E+04
	8	gox_DNA	4.10E+06	2.55E+05
	14	gox_DNA	1.97E+06	1.31E+05
	21	gox_DNA	7.23E+05	9.65E+04
	0	gox_cDNA	4.23E+05	6.52E+04
	3	gox_cDNA	1.10E+06	6.00E+04
	6	gox_cDNA	9.23E+04	2.86E+04
	8	gox_cDNA	8.56E+05	1.64E+05
	14	gox_cDNA	2.88E+05	1.04E+04
	21	gox_cDNA	5.39E+04	3.01E+04
	0	Sarc_DNA	6.77E+04	1.58E+04
	3	Sarc_DNA	1.34E+05	1.23E+04
	6	Sarc_DNA	3.58E+04	7.55E+03
	8	Sarc_DNA	4.56E+05	7.14E+04
	14	Sarc_DNA	2.40E+05	7.06E+03
	21	Sarc_DNA	7.10E+04	2.89E+04
	0	Sarc_cDNA	1.47E+04	5.09E+03
	3	Sarc_cDNA	6.15E+04	8.35E+03
	6	Sarc_cDNA	4.29E+03	1.95E+03
	8	Sarc_cDNA	1.18E+05	3.65E+04
	14	Sarc_cDNA	3.09E+04	5.70E+03
	21	Sarc_cDNA	6.81E+03	5.93E+03

Table 33: Mean values and standard deviation of DNA/cDNA data in the subsoil (bulksoil)

Subsoil	Day	Analysis	MW	SD
	0	gox_DNA	2.30E+05	1.01E+04
	3	gox_DNA	1.04E+06	2.47E+05
	6	gox_DNA	2.45E+05	9.97E+04
	8	gox_DNA	4.40E+06	2.34E+05
	14	gox_DNA	8.78E+05	1.10E+05
	21	gox_DNA	4.17E+05	1.21E+05
	0	gox_cDNA	7.99E+03	3.27E+03
	3	gox_cDNA	2.60E+05	4.80E+04
	6	gox_cDNA	3.03E+04	1.38E+03
	8	gox_cDNA	8.76E+05	2.55E+05
	14	gox_cDNA	6.80E+04	3.80E+04
	21	gox_cDNA	3.62E+04	1.61E+04
20- 50 cm	0	Sarc_DNA	3.03E+04	1.87E+03
	3	Sarc_DNA	6.29E+04	2.22E+04
	6	Sarc_DNA	1.49E+04	3.38E+03
	8	Sarc_DNA	5.95E+05	5.53E+05
	14	Sarc_DNA	8.20E+04	3.06E+04
	21	Sarc_DNA	3.18E+04	8.25E+03
	0	Sarc_cDNA	7.44E+02	2.29E+02
	3	Sarc_cDNA	1.59E+04	3.09E+03
	6	Sarc_cDNA	1.24E+03	1.90E+02
	8	Sarc_cDNA	8.41E+04	1.29E+04
	14	Sarc_cDNA	6.98E+03	1.25E+03
	21	Sarc_cDNA	2.85E+03	4.26E+02

9.1.12 Absolute ^{13}C enrichment in PLFA - bulk soil

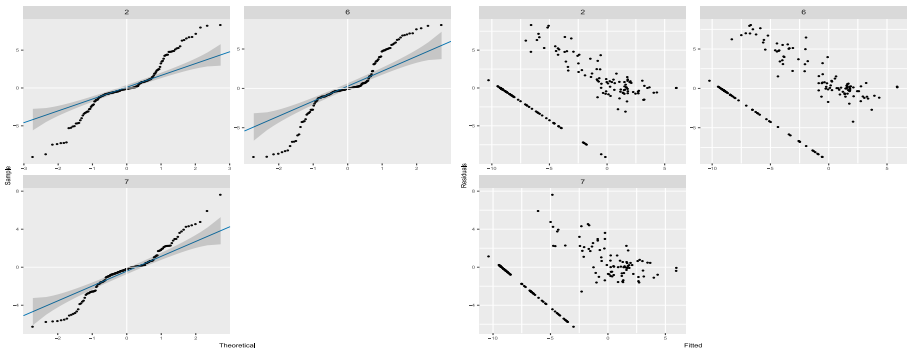

Figure 29: Model assumptions for Wald test were visually confirmed by residual diagnostic plots. Normal Q-Q plot to test for normality (left sight panels). Tests for Homogeneity of Variance (right sight panels).

Table 34: Wald tests for fixed effects (bulk soil). Response: log(PLFA).

	Df	Sum of Sq	Wald statistic	Pr(Chisq)
(Intercept)	1	210.476	210.476	< 2.2e-16***
Depth	8	83.0	83.0	< 2.2e-16***
Day	5	62.9	62.9	< 2.2e-16***
Microorganism	2	86.1	86.1	< 2.2-16***
Depth:Day	40	182.2	182.2	< 2.2-16***
Depth:Microorganism	16	28.4	28.4	0.02804 *
Day:Microorganism	10	36.7	36.7	6.161e-05 ***
Depth:Day:Microorganism	80	191.7	191.7	3.666e-11 ***
residual (MS)		1.0		

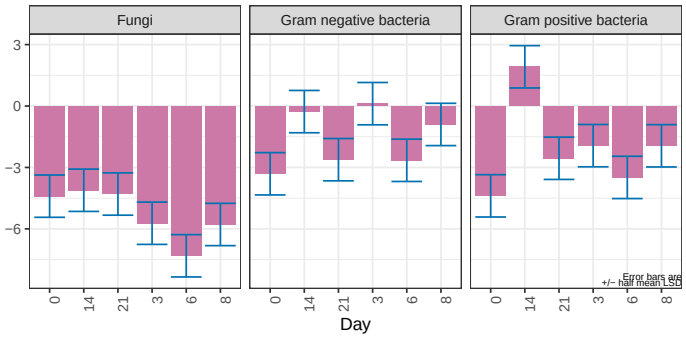

Figure 30: Predictions for PLFA ^{13}C enrichment from Day:Microorganism (bulk soil, log transformed); LSD values: minimum LSD = 1.911059, mean LSD = 2.066311, maximum LSD = 2.270447, (sed range / mean sed = 0.174)

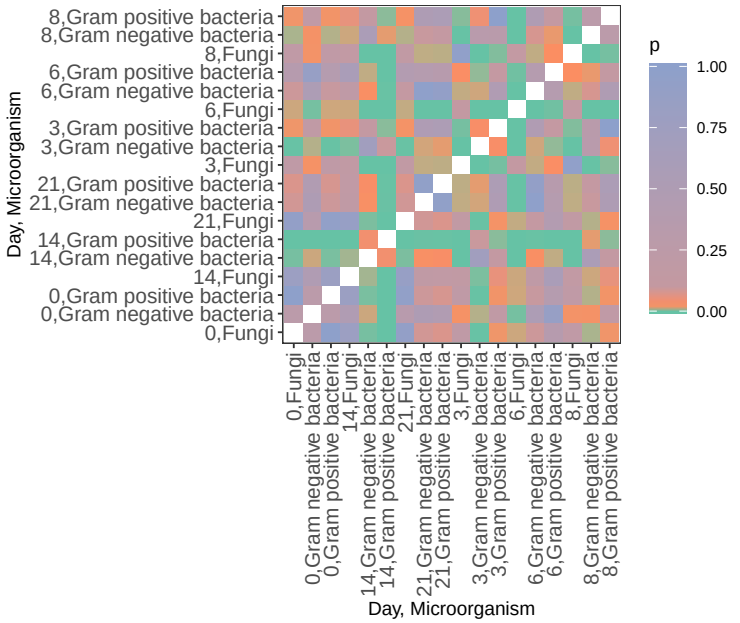

Figure 31: p values for all pairwise differences between predicted values (Day:Microorganism; PLFA ^{13}C enrichment; bulk soil)

9.1.13 Absolute ^{13}C enrichment in PLFA - shrinkage crack

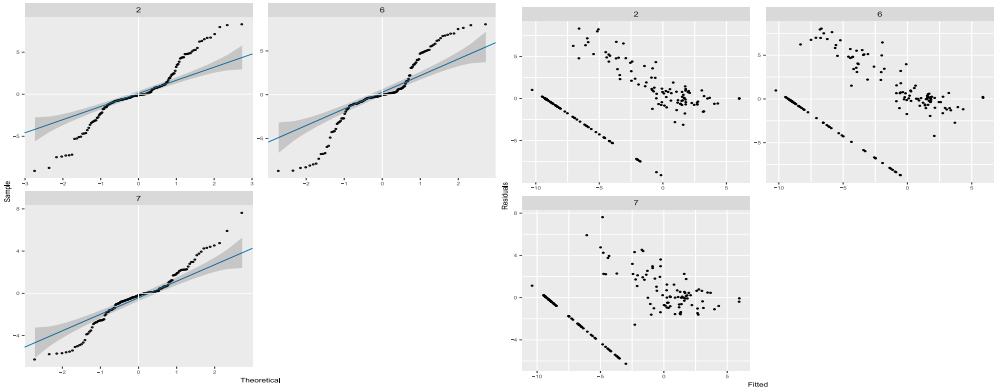

Figure 32: Model assumptions for Wald test were visually confirmed by residual diagnostic plots. Normal Q-Q plot to test for normality (left sight panels). Tests for Homogeneity of Variance (right sight panels).

Table 35: Wald tests for fixed effects (shrinkage crack). Response: log(PLFA).

	Df	Sum of Sq	Wald statistic	Pr(Chisq)
(Intercept)	1	32.2	32.2	1.387e-08 **
Depth	8	278.4	278.4	< 2.2e-16***
Day	3	4.7	4.7	0.19163
Microorganism	2	200.6	200.6	< 2.2-16***
Depth:Day	24	117.3	117.3	2.875e-14 ***
Depth:Microorganism	16	100.1	100.1	3.197e-14 ***
Day:Microorganism	6	105.1	105.1	< 2.2e-16***
Depth:Day:Microorganism	48	63.1	63.1	0.06959 .
residual (MS)		1.0		

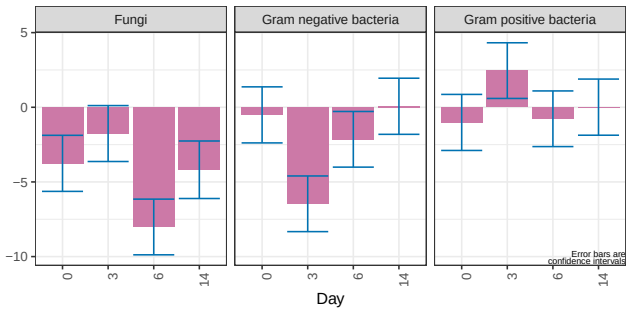

Figure 33: Predictions for PLFA ^{13}C enrichment from Day:Microorganism (shrinkage crack, log transformed); LSD values: minimum LSD = 1.745362 , mean LSD = 2.521157, maximum LSD = 2.823601, (sed range / mean sed = 0.428)

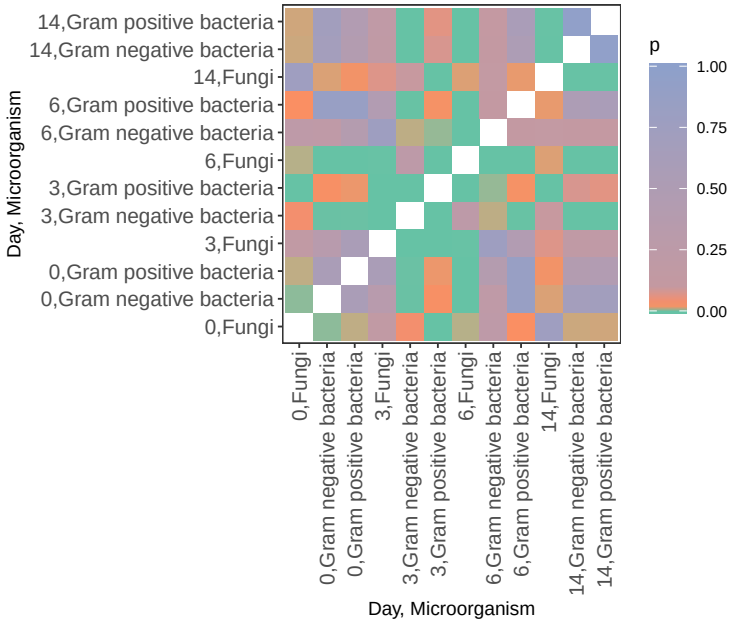

Figure 34: p values for all pairwise differences between predicted values (Day:Microorganism; PLFA ^{13}C enrichment; shrinkage crack)

9.1.14 Relative ^{13}C enrichment in PLFA - bulksoil

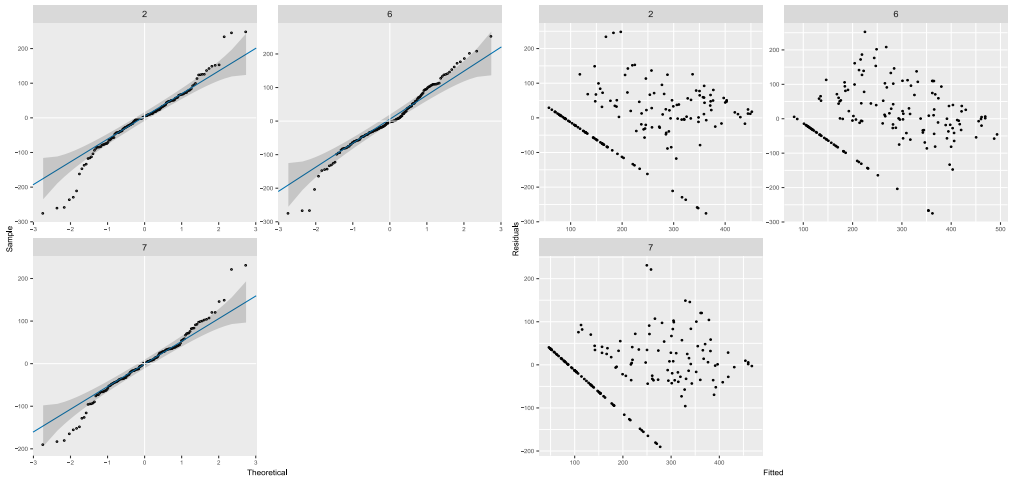

Figure 35: Model assumptions for Wald test were visually confirmed by residual diagnostic plots. Normal Q-Q plot to test for normality (left sight panels). Tests for Homogeneity of Variance (right sight panels).

Table 36: Wald tests for fixed effects (bulksoil). Response: rank(PLFA).

	Df	Sum of Sq	Wald statistic	Pr(Chisq)
(Intercept)	1	281.2	281.2	< 2.2e-16***
Depth	8	102.0	102.0	< 2.2e-16***
Day	5	37.8	37.8	2.2e-16***
Microorganism	2	44.4	44.4	< 4.122e-07 ***
Depth:Day	40	126.3	126.3	6.916e-11 ***
Depth:Microorganism	16	64.6	64.6	8.340e-08 ***
Day:Microorganism	10	29.9	29.9	0.000881 ***
Depth:Day:Microorganism	80	188.2	188.2	1.020e-10 ***
residual (MS)		1.0		

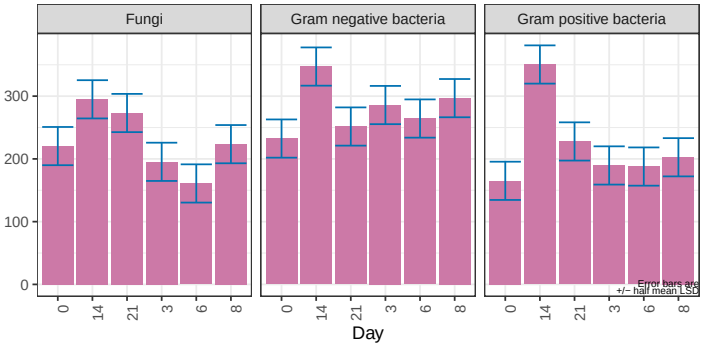

Figure 36: Predictions for relative ^{13}C enrichment in PLFA; Day:Microorganism (bulksoil, rank-transformed); LSD values: minimum LSD = 49.31971, mean LSD = 60.93282, maximum LSD = 63.59253 (sed range / mean sed = 0.234)

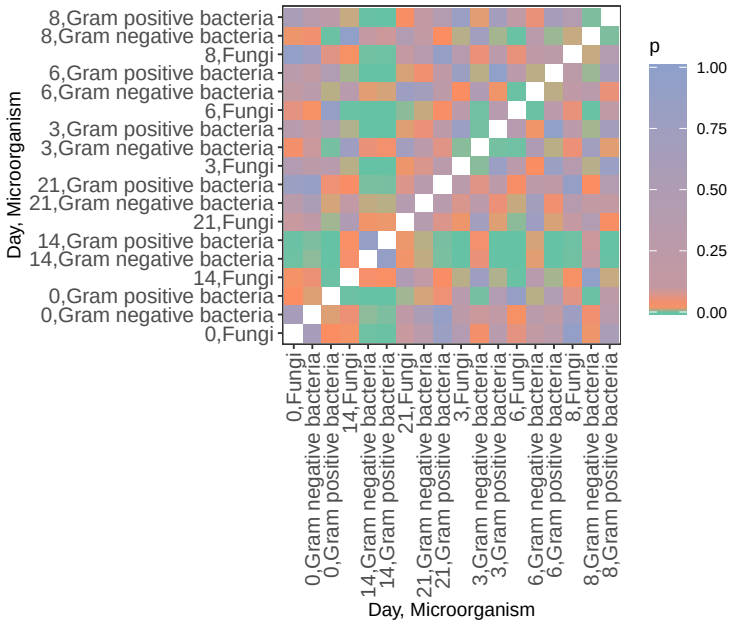

Figure 37: p values for all pairwise differences between predicted values (Day:Microorganism; relative ^{13}C enrichment in PLFA; bulksoil)

9.1.15 Relative ^{13}C enrichment in PLFA - shrinkage crack

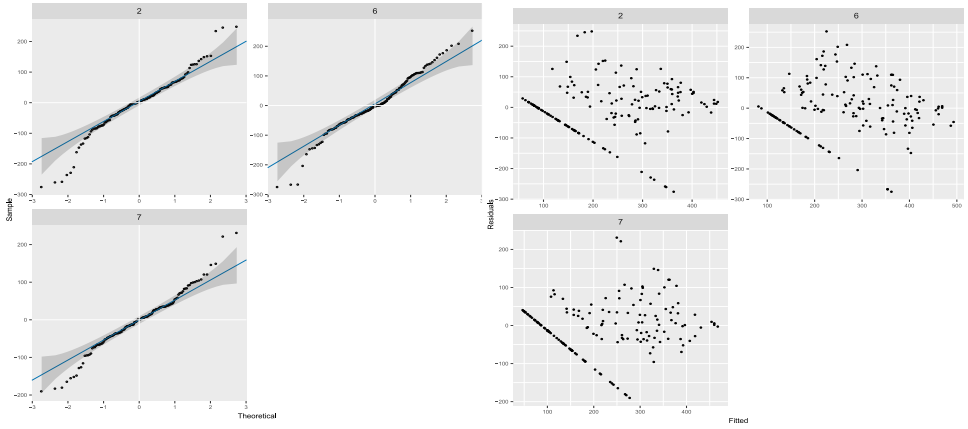

Figure 38: Model assumptions for Wald test were visually confirmed by residual diagnostic plots. Normal Q-Q plot to test for normality (left sight panels). Tests for Homogeneity of Variance (right sight panels).

Table 37: Wald tests for fixed effects (shrinkage crack). Response: rank(PLFA).

	Df	Sum of Sq	Wald statistic	Pr(Chisq)
(Intercept)	1	419.3	419.3	< 2.2e-16***
Depth	8	155.0	155.0	< 2.2e-16***
Day	3	7.4	7.4	0.06017 .
Microorganism	2	8.2	8.2	0.01645 *
Depth:Day	24	98.2	98.2	6.023e-11 ***
Depth:Microorganism	16	51.1	51.1	1.492e-05 ***
Day:Microorganism	6	100.8	100.8	< 2.2e-16***
Depth:Day:Microorganism	48	71.1	71.1	0.01677 *
residual (MS)		1.0		

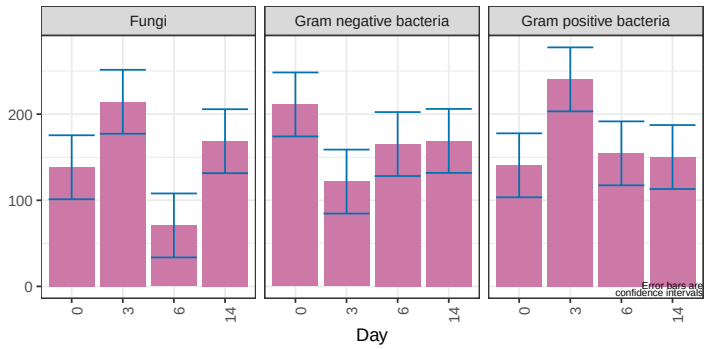

Figure 39: Predictions for relative ^{13}C enrichment in PLFA; Day:Microorganism (shrinkage crack, rank-transformed); LSD values: minimum LSD = 49.31971, mean LSD = 60.93282, maximum LSD = 63.59253 (sed range / mean sed = 0.234)

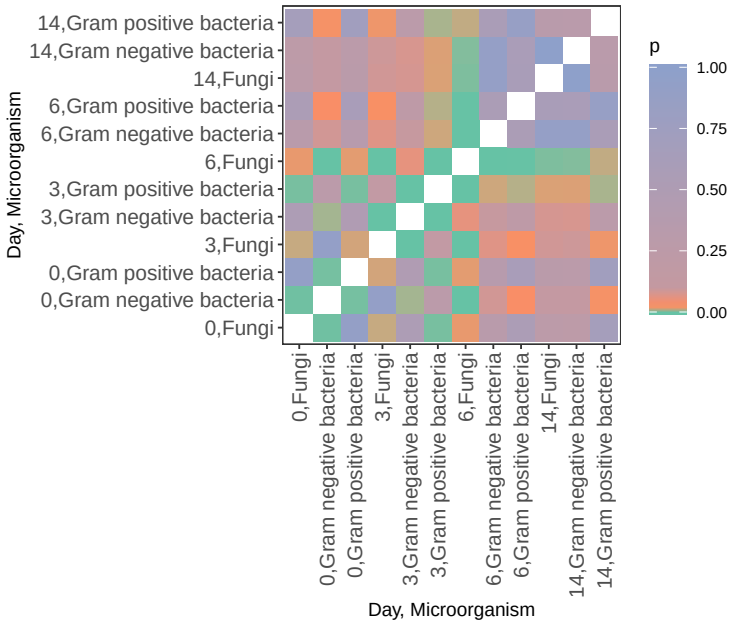

Figure 40: p values for all pairwise differences between predicted values (Day:Microorganism; relative ^{13}C enrichment in PLFA; shrinkage crack)

9.1.16 Total microbial abundance - 16S rRNA

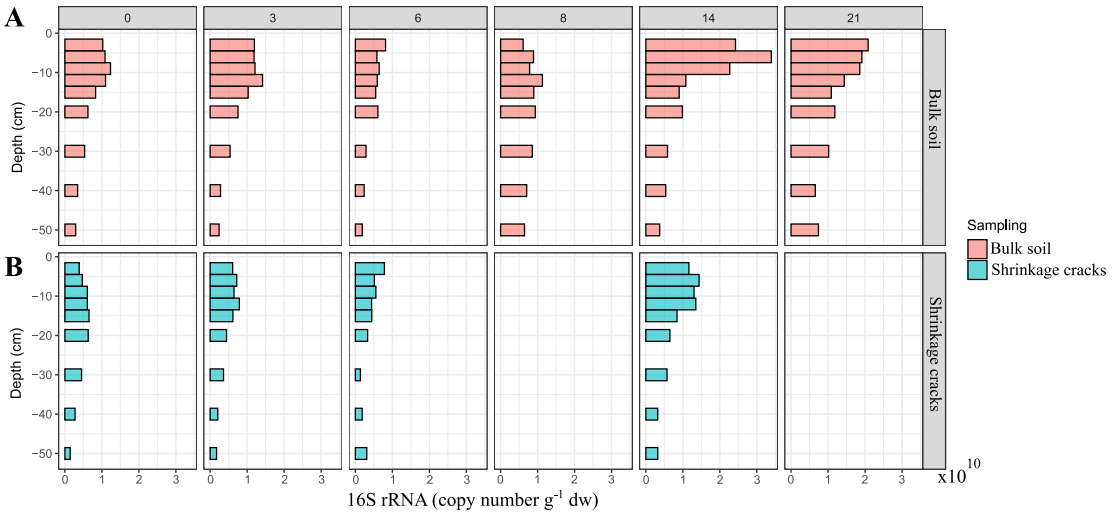

Figure 41: Total microbial abundance (16S rRNA copy number per g^{-1} soil) (A) in bulk soil samples and (B) in shrinkage cracks along the soil profile and over time.

9.1.17 Standard curves of qPCR runs for goxA and sarc

Table 38: CT (Cycle Threshold)-values *goxA*

Plate	e8	e7	e6	e5	e4	e3	e2	e1
1	9.07	12.78	16.25	19.70	22.64	25.16	27.18	below the NTC
2	9.29	12.98	16.44	19.81	23.17	25.88		
3	10.44	14.05	18.46	21.83	24.26	27.48	28.53	
4	10.18	13.94	18.14	21.46	24.27	27.75	29.04	
5	9.86	13.86	18.05	21.61	24.49	27.93	29.21	
6	9.80	13.75	17.88	21.40	24.27	27.69	29.01	
7	10.00	14.05	18.11	21.75	24.58	28.13	29.22	
8	6.81	10.97	14.33	17.73	21.21	23.94	26.18	
9	8.82	13.62	17.20	20.13	23.56	26.63	28.60	
10	9.46	12.82	16.30	19.78	23.47	26.85	28.38	
11	6.26	11.36	15.05	18.53	22.30	25.56	28.12	28.64066823
12	8.61	12.60	15.99	19.82	23.83	27.49	29.63	30.54885419
13	8.91	12.92	16.15	20.02	23.81	26.79	29.74	30.55282784
14		12.43	16.25	20.82	23.71	27.77	30.63	31.65379588
15		12.70	16.65	22.42	24.83	29.47	31.13	31.97332001
16		11.36	15.29	21.24	23.46	27.92	29.80	30.27410316
17	calculated							
18	calculated							
19	calculated							
20	7.22	11.18	14.47	17.76	21.23	24.94	28.12	29.43568865
MW	8.91	12.79	16.53	20.34	23.48	26.90	28.91	30.44
StabW.N	1.25	1.01	1.26	1.37	1.05	1.36	1.18	1.08
StabW	1.29	1.04	1.29	1.41	1.08	1.40	1.22	1.16
dilution step	100000000	10000000	1000000	100000	10000	1000	100	10

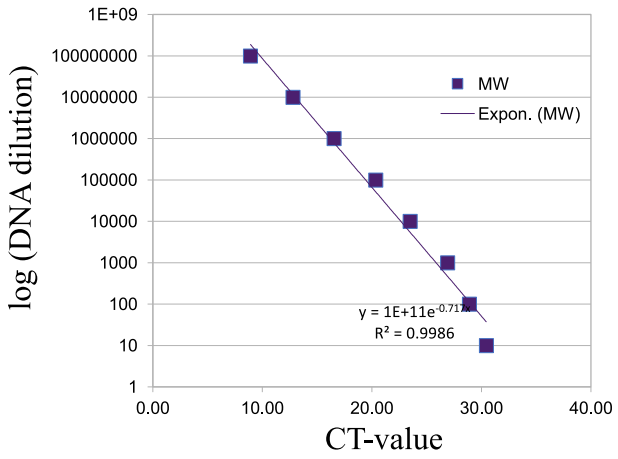

Figure 42: Standard curve; log DNA dilution vs. CT-values

9.1.18 *sarc*

Table 39: CT (Cycle Threshold)-values *sarc*

Plate	e8	e7	e6	e5	e4	e3	e2	e1
1	7.55	11.09	14.44	17.58	20.98	24.12	26.14	
2	9.59	13.15	16.47	19.84	23.15	26.25	27.71	
3	9.93	13.33	16.66	20.00	23.40	26.61	28.51	
4	9.13	12.67	15.93	19.26	22.69	25.85	27.63	29.3997065
5	9.76	13.18	16.59	19.94	23.27	26.52	28.24	
6	9.44	12.91	16.38	19.78	23.05	26.29	28.96	29.8360653
7	9.73	13.11	16.65	19.95	23.24	26.61	28.07	
8	9.01	12.43	15.94	18.92	22.36	25.68	28.48	
9	7.12	11.42	14.89	18.21	21.64	24.92	27.76	29.1915092
10	9.75	13.01	15.97	19.40	23.12	26.14	29.48	30.7356103
11	9.33	12.94	15.76	19.61	23.06	25.92	29.53	31.156833
12	9.33	12.94	15.76	19.61	23.06	25.92	29.53	31.156833
13	9.54	13.29	16.10	20.03	23.58	26.53	30.33	31.8690058
14	8.98	12.63	16.04	19.51	23.16	26.34	28.72	30.819198
15	9.07	12.76	16.01	19.49	23.04	26.22	28.52	30.0821908
16	9.53	13.04	16.33	19.92	23.55	26.67	29.10	30.7512786
17	8.90	12.37	15.77	19.44	22.90	26.13	28.57	30.2931175
18	8.85	12.45	15.83	19.49	23.00	26.15	29.02	31.3389301
19	7.94	11.70	14.89	18.70	22.34	25.42	27.90	29.4507974
20								
MW	9.08	12.65	15.92	19.40	22.87	26.01	28.54	30.47
StabW.N	0.75	0.61	0.59	0.63	0.63	0.62	0.90	0.80
StabW	0.77	0.63	0.61	0.65	0.65	0.64	0.93	0.83
dilution step	100000000	10000000	1000000	100000	10000	1000	100	10

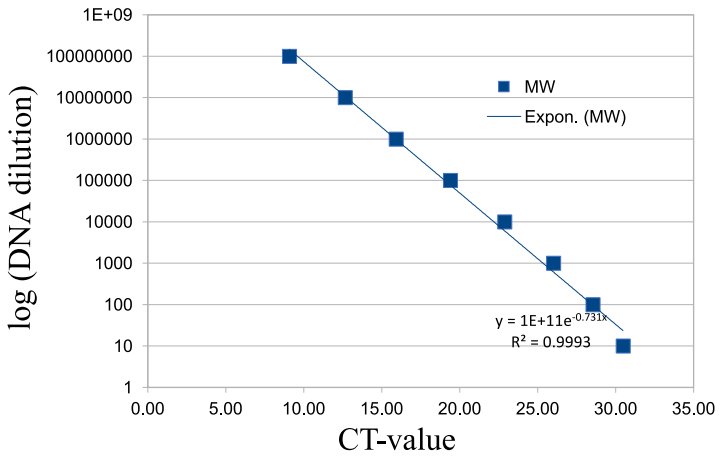

Figure 43: Standard curve; log DNA dilution vs. CT-values

9.1.19 Absolute (ng g^{-1}) ^{13}C incorporation of GLP-derived C

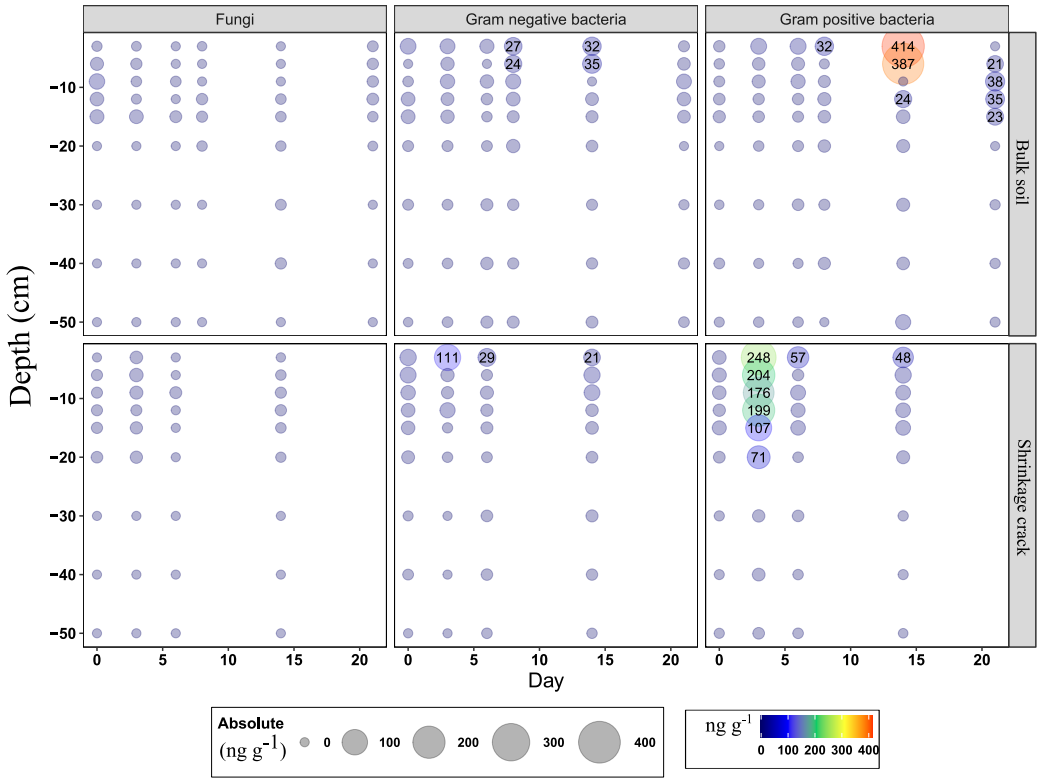

Figure 44: Absolute (ng g^{-1}) ^{13}C incorporation of GLP-derived ^{13}C into Gr^{+}-, Gr^{-}-bacteria and fungi along the soil profile and as a function of time. Bulk soil vs. Shrinkage crack.

Table 40: Mean values and standard deviation for PLFA in the topsoil (bulk soil)

Topsoil	Day	Microorganism	MW_%13C	SD_%13	MW_ng_g_13C	SD_ng_g_13C
	0	Fungi	1.14642313	0.295779748	7.616561153	5.5826164
	0	Gram negative bacteria	0.69078185	0.423853949	5.690626432	6.53635967
	0	Gram positive bacteria	0.03857238	0.034192961	1.835698643	1.55358935
	3	Fungi	0.61641716	0.29845148	2.245581104	5.70295483
	3	Gram negative bacteria	0.73495202	0.188039919	8.310157331	1.39132173
	3	Gram positive bacteria	0.11986939	0.138607455	6.302435194	9.12828468
	6	Fungi	1.88249604	5.796631474	0.749311704	1.88112796
	6	Gram negative bacteria	0.44010998	0.106810207	3.829921197	3.13825184
0-20 cm	6	Gram positive bacteria	0.172825	0.179117848	7.252624583	9.36128694
	8	Fungi	0.77361197	0.487798731	0.692789095	0.12031635
	8	Gram negative bacteria	0.81763284	0.223917067	15.10230989	10.3077042
	8	Gram positive bacteria	0.15652525	0.253582585	9.220994411	22.1913325
	14	Fungi	0.48063991	0.167173657	0.349708974	0.09695658
	14	Gram negative bacteria	1.63506164	0.599643616	17.31353568	13.2799366
	14	Gram positive bacteria	3.39625768	0.523512777	193.1750387	33.1218569
	21	Fungi	1.63871168	0.172988838	1.675940519	0.32605678
	21	Gram negative bacteria	1.08123314	1.3762888	6.126804749	1.23675386
	21	Gram positive bacteria	0.75896204	0.257345217	23.33020149	5.74947414

Table 41: Mean values and standard deviation for PLFA in the subsoil (bulk soil)

Subsoil	Day	Microorganism	MW_%13C	SD_%13	MW_ng_g_13C	SD_ng_g_13C
	0	Fungi	0	0	0	0
	0	Gram negative bacteria	0.08137212	0.06206729	0.49341713	0.37995262
	0	Gram positive bacteria	0.02603318	0.02802287	0.46533042	0.49521568
	14	Fungi	1.15256073	0.72081604	1.18906315	0.87705754
	14	Gram negative bacteria	0.97544543	0.94729586	1.98571646	1.30683572
	14	Gram positive bacteria	0.64116587	0.23039987	7.94483221	1.69601695
	21	Fungi	0	0	0	0
	21	Gram negative bacteria	0.3115575	0.28432523	0.97946583	0.80509427
20-50 cm	21	Gram positive bacteria	0.03088678	0.01089533	0.4062763	0.09491061
	3	Fungi	0	0	0	0
	3	Gram negative bacteria	0.21050609	0.06334409	0.91415305	0.15258394
	3	Gram positive bacteria	0.03294372	0.02082158	0.48725672	0.21284884
	6	Fungi	0	0	0	0
	6	Gram negative bacteria	0.97003298	0.26310742	3.44739961	1.22911528
	6	Gram positive bacteria	0.07814537	0.04207185	1.1476966	0.89262836
	8	Fungi	0.00091469	0.0033608	0	0
	8	Gram negative bacteria	0.61035469	0.46660493	2.21673201	1.70505948
	8	Gram positive bacteria	0.11338455	0.14486705	1.61994747	1.2384435

Table 42: Mean values and standard deviation for PLFA in the topsoil (shrinkage crack)

Topsoil	Day	Microorganism	MW_%13C	SD_%13	MW_ng_g_13C	SD_ng_g_13C
0-20 cm	0	Fungi	0.54047465	0.25205589	1.1912854	0.42633663
	0	Gram negative bacteria	1.83033722	0.17304791	12.5680622	1.64848047
	0	Gram positive bacteria	0.27279186	0.24177792	7.49572184	2.76609341
	3	Fungi	6.97924034	3.19210635	4.57248128	1.91743972
	3	Gram negative bacteria	1.21008737	1.15483693	27.0553467	81.3834319
	3	Gram positive bacteria	5.58297938	0.91748667	186.640126	65.0206702
	6	Fungi	0.1047691	0.25858972	0.59150567	1.78233474
	6	Gram negative bacteria	1.00294975	0.90617735	8.55660758	7.98546433
	6	Gram positive bacteria	0.71964417	0.5033097	18.3746682	35.7023894
	14	Fungi	0.98740642	0.19862566	1.09081499	0.32749638
	14	Gram negative bacteria	0.88960568	0.28489267	13.1733489	5.11730023
	14	Gram positive bacteria	0.50735071	0.07085199	20.4788761	3.31410993

Table 43: Mean values and standard deviation for PLFA in the subsoil (shrinkage crack)

Subsoil	Day	Microorganism	MW_%13C	SD_%13	MW_ng_g_13C	SD_ng_g_13C
20-50 cm	0	Fungi	0	0	0	0
	0	Gram negative bacteria	0.13134079	0.05844578	0.45494975	0.16176813
	0	Gram positive bacteria	0.02799279	0.02507561	0.35540179	0.33560948
	3	Fungi	0	0	0	0
	3	Gram negative bacteria	0	0	0	0
	3	Gram positive bacteria	0.33102675	0.37219362	3.77089922	3.48605276
	6	Fungi	0	0	0	0
	6	Gram negative bacteria	0.44612871	0.28980239	1.75769597	0.87315349
	6	Gram positive bacteria	0.07675554	0.04071384	1.22502823	0.37573337
	14	Fungi	0	0	0	0
	14	Gram negative bacteria	0.47125774	0.25760477	1.88770895	1.16700218
	14	Gram positive bacteria	0.01894367	0.01630655	0.30404491	0.33661059

10 General discussion

To evaluate the impact of pesticides on soil life and water resources, their fate in soils as primary sinks must be quantified. Pesticides are subject to complex transport, retention, and degradation processes, making it difficult to determine whether soils serve as sinks for pesticides or as secondary sources of inputs to groundwater following continuous pesticide accumulation. The objective of this thesis was to identify additional limiting factors to the known degradation processes in order to bridge the gap between the persistence determined in laboratory experiments and the often much longer residence times in soils.

10.1 Concentration thresholds for pesticide degradation

In a microcosm experiment (Chapter 4), ^{14}C-labeled MCPA concentrations increasing from 30 to 20000 µg kg^{-1} were incubated for a short time (37 days) to study the microbial degradation of MCPA at low and high concentrations. The most striking results were that in a concentration range between 1,000 and 5,000 µg kg^{-1}, *tfdA* mRNA-based activity increased but growth of *tfdA*-containing microorganisms was observed only at a threshold value of 20,000 µg kg^{-1}. Degradation of MCPA $\leq$ 1000 µg kg^{-1} began immediately without a lag phase and followed first-order degradation kinetics, whereas $\geq$ 1000 µg kg^{-1}, sigmoidal mineralization was observed. Similar to the study by Fomsgaard (1997b), a concentration-dependent degradation rate was confirmed, but using a molecular approach based on direct soil nucleic acids followed by qPCR assay we could indirectly interpret the underlying energetic requirements for growth and degradation activity via an increase in *tfdA* DNA or *tfdA* mRNA. Probably the greatest obstacle to microbial growth arises from the thermodynamics of metabolism (Großkopf and Soyer, 2016). Since microbial growth depends on the energy derived from substrates converted into end products, it is subject to the thermodynamics of such metabolic transformations (Großkopf and Soyer, 2016). A relationship between dissipated energy and growth stoichiometry has already been established, which made it possible to predict and calculate the energy and

mass balances of microbial growth (Quéméner et al., 2014). This relationship between microbial growth rate and catabolic energy density leads to the well-known dependence of microbial growth rate on substrate concentration. Quéméner et al. (2014) introduced a flux-force relationship between microbial growth rate and catabolic energy density and considered an apparent threshold substrate concentration for growth; this was confirmed by a degradation experiment in which the relationship between growth rate and increasing glucose concentration was examined. Indeed, the correct circumscription of microbial growth rate dependency can be achieved with any empirical equation that has a sigmoid form, as described by Monod (1942). The bioenergetic growth restriction, whose concentration threshold for MCPA is about 20,000 $\mu g\,kg^{-1}$, can only be extended to pesticides used as a sole energy and carbon source, as in the case of MCPA or other phenoxy herbicides such as 2,4-dichlorophenol (2,4-D) or 4-chloro-2-methylphenol (mecoprop; (Chavez Rodriguez et al., 2020; Ugalde-Salas et al., 2020)). This is an assumption justified not only by the observed *tfdA* increase at 20,000 $\mu g\,kg^{-1}$, but also in the significant increase in CUE in the 5,000 and 20,000 $\mu g\,kg^{-1}$ range, indicating microbial carbon allocation to biomass formation. However, by applying this concept of transition state theory to the degradation of atrazine, Chavez Rodriguez et al. (2020) was able to demonstrate that bioenergetic mechanisms cannot be responsible for the persistence of atrazine or hydroxyatrazine (the first metabolite of atrazine degradation) at low concentrations. The decisive factor here is the microbial mode of utilization. Atrazine, which is used primarily as a nitrogen source, or glyphosate, which is co-metabolized to obtain phosphorus, are not subject to energetic concentration-dependent growth limitations. This co-metabolic degradation is sustained by the utilization of soil organic matter, and according to stoichiometric theory (Creamer et al., 2014), actual substrate degradation can be maximized by the additional yield of N and P from the pesticide molecules. It seems unlikely, therefore, that the pesticide residues would remain at low molar concentrations due to bioenergetic limitations. However, co-metabolic

degradation of pesticides is often associated with incomplete degradation, where the resulting metabolites, such as hydroxyatrazine or AMPA from atrazine or glyphosate degradation, persist at low concentrations (Silva et al., 2019b; Riedo et al., 2021) if not further utilized (Zhan et al., 2018). In the case of MCPA, its low-molecular-weight degradation can be attributed to the constitutive *tfd* gene expression mentioned in Chapter 4, which in the study by Leveau et al. (1999b) progressed continuously in pure cultures in the presence of fructose, aided by energy recovery from this secondary carbon source. Therefore, the hypothesis that microbial degradation of MCPA at low molar concentrations ceases when functional gene expression is no longer induced must be rejected. However, the hypotheses that there are different concentration thresholds for microbial activity and microbial growth using MCPA as a C and energy source and that a decline in microbial growth with decreasing concentration is reflected in CUE, can be confirmed.

Pesticide concentration affects microbial degradation, but at very low concentrations, degradation is unlikely to cease completely. Secondary carbon sources and, in the case of MCPA, constitutive gene expression, support further degradation. It should be clarified whether this gene regulation applies to other compounds. In the context of degradation of low molar concentrations of pesticides, practical limitations must also be mentioned. The detection limit for MCPA and glyphosate in the two studies presented was 13 and 7.5 $\mu g\,kg^{-1}$, respectively, with a recovery of 80 to 95%. For atrazine, a detection limit of > 3 $\mu g\,kg^{-1}$ soil at a recovery rate of 80% was reported (Singh et al., 2018). As concentrations approach the detection limit, statements about the presence of pesticide residues become uncertain, and we cannot simply apply the proposed mechanisms of gene regulation and progressive MCPA degradation to the concentration gap between the EU proposed limit of 0.1 $\mu g\,L^{-1}$ (Cosgrove et al., 2019) for pesticide residues in drinking water and our lowest concentration of 30 $\mu g\,kg^{-1}$.

10.2 Temperature, soil moisture, and pesticide concentration in relation to microbial degradation

To identify further limiting factors for microbial pesticide degradation, the second study examined MCPA degradation of 1 and 20 mg kg^{-1} under limiting (pF 3.5 and 10°C) and favorable (pF 1.8 and 20°C) conditions in a 28-day incubation experiment. The concentration ranges of 1 and 20 mg kg^{-1} were chosen according to the results from Chapter 4 and were intended to include first-order degradation and degradation associated with microbial growth. Consistent with previous studies (Helweg, 1987a; Castillo and Torstensson, 2007; Bouseba et al., 2009; Muskus et al., 2019b), the degradation rate derived from DT_{50}-values decreased significantly at lower temperatures, and less MCPA was converted overall under drought. However, a new finding was that the magnitude of the effect of temperature and soil moisture content depended on the initial concentration and that microorganisms utilized MCPA-derived carbon more efficiently, as indicated by the increased CUE value under limiting conditions. This redistribution of carbon is not accounted for in ^{14}C mineralization. During first-order degradation of 1 mg kg^{-1} without microbial growth, consistent with the first study (Chapter 4, Figure 6), this difference is evident from the ^{14}C mineralization curves´ derived DT_{50}-values and the actual MCPA degradation that occurs more quickly. In the range of 20°C, the first-order degradation dynamics at 1 mg kg^{-1} of Chapter 4 (Figure 6) and Chapter 6 (Figure 10) agreed. However, at 10 °C, all degradation curves in Chapter 6 (Figure 10) showed a lag phase of about 5 days, even at 1 mg kg^{-1}. Thus, Chapter 6 supplements Chapter 4 by emphasizing the importance of the climatic conditions under which MCPA degradation took place. At 1 mg kg^{-1} and 10°C, the sigmoidal degradation dynamics were not due to growth of the MCPA-degrading microorganisms, which was evident from the lack of increase in *tfdA* DNA content (Chapter 6, Figure 10). The observed reduction in pesticide degradation was explained mainly by reduced microbial activity, especially in the initial phase of degradation, and the simultaneous increase in CUE indicated

non-growth-related anabolic C utilization (Chapter 6, Figure 11). By introducing CUE into temperature- and soil moisture-dependent pesticide degradation, presented for the first time in this thesis, the underlying microbial constraints and adaptive mechanisms to changing environmental conditions can also be applied to pesticide degradation, in agreement with results of numerous studies (Manzoni et al., 2011, 2012b; Zhang et al., 2018) investigating carbon (C) metabolism as the core of ecosystem functions. Considering pesticides, such as MCPA in our case, as simple sources of carbon and transferring our understanding of how soil microorganisms partition carbon between respiration and biomass growth - and ultimately storage (Manzoni et al., 2012b) - also allows us to make statements about the pesticide fractions present in the soil. According to the ^{13}C-mass balance of Muskus et al. (2019a), at the end of glyphosate degradation, there is a nearly constant ^{13}C-biomass formation, a strong decrease in respiration, and an increased fraction of non-extractable residues at 10 °C compared to 20 °C. A decrease in mineralization compared to assimilation would be reflected in increased CUE. In pesticide degradation studies, temperature-dependent pesticide degradation is usually described by the Arrhenius equation, which gives the degradation rate coefficient as a function of temperature and activation energy E_a. The ratio between the degradation rates at 20° and 10°C is usually given as the Q_{10} value. This value is used in environmental exposure assessments to account for the effects of different temperatures (EFSA, 2008). However, if simultaneous growth begins during pesticide degradation, the relationship between reaction rate and temperature is no longer meaningful. The activity is then distributed among multiple individuals and no longer represents the increased activity of the original degradation population, as indicated by the analogous increase in *tfdA* DNA as growth and *tfdA* mRNA activity indices in Chapters 4 (Figure 6) and 6 (Figure 10). In addition, the CUE determined in Chapters 4 and 6 indicates some concentration dependence and the possibility of more efficient C utilization, which may be necessary for the maintenance of tolerance mechanisms such as the synthesis of osmolytes or extracellular enzymes.

The questionable application of the Arrhenius equation, already pointed out by Helweg (1987a), puts into perspective the proposal of the European Food Safety Authority (EFSA, 2008) for an environmental exposure assessment that takes into account the effects of different temperatures but does not distinguish between degradation rates derived from mineralization and total pesticide dissipation. In addition, the apparent Q_{10} value from field observations should be related to the observed ecosystem response to temperature and water content, which results from the combination of several processes, each of which has its own temperature sensitivity to pesticide degradation (Niu et al., 2021). The modeling of the temperature response function $f_R(T)$ from Chapter 6 underscores the need to assign a specific temperature sensitivity to mineralization and assimilation. This thesis is primarily concerned with factors limiting microbial degradation of pesticides, and only the temperature and soil moisture range as determined during the spraying season in central Europe has been studied. Previous studies have found that under extreme conditions, e.g., at 0°C or below -0.015 MPa, degradation stops completely (Helweg, 1987a; Schroll et al., 2006; Moyano et al., 2013). The effects of temperature and soil water content on pesticide degradation presented here cannot be extrapolated to colder or drier latitudes without considering microbial adaptation mechanisms. For each extreme environmental condition studied, a variety of microorganisms have shown that not only can they tolerate these conditions, but that they often require these extreme conditions for survival (Rampelotto, 2010). To thrive successfully in low-temperature environments, psychrophiles have evolved a complex array of structural and functional adaptations (Margesin and Miteva, 2011). Consequently, there is evidence of a wide range of metabolic activities in cold ecosystems, even at subfreezing temperatures (Margesin and Miteva, 2011). Thus, it is understandable that cold-adapted microorganisms with modified enzymes that exhibit high catalytic activity at cold temperatures still degrade pesticides under psychrophilic conditions (Bajaj and Singh, 2015). A shift in microbial efficiency to the psychrophilic range will also result in a somewhat different pattern of CUE than

our results suggest. Notwithstanding the potential adaptation mechanisms identified in Chapter 6, under drier and colder conditions, and based on altered C allocation, pesticide degradation will be slower in cold than in temperate climates (Stenrød et al., 2008). Leaching during cold climate periods (fall, winter, and spring) in this temporarily frozen soil may result in translocation of pesticides to deeper soil layers with lower biological activity and generally lower sorption capacity for pesticides due to lower soil organic carbon content (Stenrød et al., 2008). Therefore, pesticides may reappear in deeper soil layers one year after spraying. Risk assessment methods for pesticide leaching under cold climate conditions should consider winter/spring processes. More attention needs to be paid to the influence of climate on the degradation of pesticides in soil and the risk of leaching to surface and groundwater. In colder climates, the focus is on the influence of temperature on microbial degradation of pesticides, while in Mediterranean climates, for example, low precipitation is becoming increasingly important. Again, the effects of extreme drought on pesticide degradation are not addressed in this thesis, and the focus, as in the case of the temperature range, is on climatic conditions in central Europe during the spray season. However, the water content-dependent change in CUE under drought conditions shown in Chapter 6 (Figure 11) may represent the onset of more general microbial drought tolerance strategies in the form of increased anabolic C utilization that could be transferable to drier climate zones. In studies of carbon turnover on the rate and temperature sensitivity of heterotrophic respiration (Rh) under altered precipitation, it was confirmed that Rh in ecosystems respond strongly to precipitation and increasing drought, both annually and during the growing season (Suseela et al., 2012). Limiting moisture can suppress microbial activity regardless of temperature, which should reduce the temperature sensitivity of Rh (Davidson and Janssens, 2006). In this thesis it is reflected in reduced MCPA mineralization in Chapter 6 (Figure 10) under pF 3.5. Once again, this evidence raises concerns about the use of a fixed Q_{10} value for risk assessment of pesticides under different boundary conditions. It is clear that Rh,

temperature sensitivity, and the apparent Q_{10} value are affected by soil moisture, but it is unclear how this interaction is maintained between soils (Craine and Gelderman, 2011) or even climate zones. Suseela et al. (2012) noted that for an ecosystem, it is not known if these interactions are consistent over time or vary seasonally, although seasonal variation might be expected. For example, microbial community composition and extracellular enzyme production, as well as temperature sensitivity of microbial enzymes, could vary with seasonal changes in substrate and nutrient availability (Wallenstein et al., 2009). An indication of this seasonal variability was given by Suseela et al. (2012) on soil organic matter decomposition and CO_2 flux, where apparent Q_{10} increased with warming (3.5°C) in spring and fall. However, due to limited soil moisture, warming and precipitation in summer had no effect on apparent Q_{10}. Bouseba et al. (2009) confirmed that soil moisture not only affects the microbial activity of 2,4-D mineralization in an Algerian soil, but that limiting the water content in the soil leads to a structural change in the bacterial community. This finding reveals a blind spot in current risk assessments. Few studies address temperature- and water-content-dependent changes in microbial composition and link them to specific microorganisms and intrinsic degradation pathways. A study by Reedich et al. (2017) demonstrates that transformation products of pesticides produced by soil microbial degradation networks can vary in toxicity, such that a pesticide applied at 10°C in the spring may produce different transformation products with different toxicological effects than the pesticide sample applied at 22°C in the same location. The impact of interactions between the soil microbiome and pesticides under seasonal variability in temperature and soil water content (Reedich et al., 2017) is complemented in this work by evidence of a possible microbial guild at low and elevated MCPA concentrations and a specific C use efficiency presented in Chapter 6. This in turn may be partially responsible for the difference in degradation kinetics in Chapter 4 (Figure 6) at ≤ 1 and ≥ 1 mg kg^{-1}. The initial hypotheses were also confirmed; under limiting conditions CUE increases and non-linearity of mineralization and actual MCPA

decline may lead to an overestimation of its half-life. However, the hypothesis that the effect size will be more pronounced at higher concentrations could not be confirmed. In this case, temperature- and soil moisture-dependent C allocation plays a subordinate role and only the onset of microbial growth is decisive for effective degradation, which did not occur at 10°C. To summarize, environmental factors do play a role in pesticide degradation, but are unlikely to control long-term pesticide persistence under temperate climate conditions. To confirm these results, pesticides different from and more persistent than MCPA should be prioritized in further studies.

10.3 Pesticide degradation at the field scale

For this reason, the third study investigated glyphosate degradation at the field scale. Prevailing drought conditions and the formation of shrinkage cracks in a clayey soil, followed by simulated precipitation events, resulted in transport and microbial degradation processes that were distinctly different in the bulk soil than in shrinkage cracks. The overarching question of this thesis, whether processes relevant to pesticide degradation occur only at the field scale and cannot be identified in laboratory experiments, leading to an incomplete assessment of residence time in soil, can be partially justified in Chapter 8. Solute transport through the soil is enhanced by precipitation events and soil heterogeneity, such as wormholes or shrinkage cracks, which facilitate the transport of pollutants into the subsoil. All these processes are embedded in a spatio-temporal hierarchy (Richter et al., 2008). Long-term processes of microbial and target populations at the evolutionary level with regular pesticide application are often associated with enhanced biodegradation (Biederbeck et al., 1987; Kumar Singh et al., 2002) and the development of resistance (Ramakrishnan et al., 2019). When moving from the laboratory scale to larger spatial scales, it is important to consider the dependency of pesticide degradation rates on soil properties. The spatial distribution of soil properties has both a deterministic (soil type) and a random component (land use, environmental conditions, etc. (Richter et al., 2008)).

Nevertheless, laboratory studies such as those in Chapters 4 and 6 are necessary to develop a simplified understanding of the processes that breaks down the field-scale complexity into discrete fragments, and despite the simplification, the degradation and breakthrough curves can be described very well by mathematical models of varying sophistication (Richter et al., 2008). The demonstration of the initial concentration dependence of the degradation rate in Chapter 4 (Figure 6) and the temperature- and water content dependent degradation kinetics for MCPA in Chapter 6 (Figure 10) become apparent in the field-scale degradation in Chapter 8 as well. The sharp decrease in concentration observed for glyphosate with increasing soil depth somewhat mirrors the concentration gradient studied in Chapter 4. In Chapter 8, an increase in glyphosate degraders based on the *goxA* and *sarc* gene abundances occured mainly in the topsoil. Analogously, only at an MCPA concentration of 20 mg^{-1} could an increase in *tfdA*-harboring microorganisms be observed. By contrast, with increasing soil depth and reduced glyphosate concentration, the degradation activity decreased, whereas low MCPA concentrations in chapter 4 were converted very quickly (Figure 6). Soil structure, microbial biomass distribution, and the fact that microbial communities are more exposed to pesticide contamination at the surface than in the subsoil, clearly take precedence despite the pesticide used, and may obscure the concentration-dependent degradation kinetics determined in homogenized soil samples. A steady decrease in the average pesticide degradation rate with increasing soil depth was observed for several compounds (Larsen et al., 2000; Rodríguez-Cruz et al., 2006; Cruz et al., 2008; Badawi et al., 2013). This decline in mineralization potential is detectable over relatively short vertical distances from the plow layer to the subsoil, as observed in Chapter 8 (Figure 16), and follows a trend similar to the distribution of microbial biomass in soil profiles, confirming our hyphothesis of a vertical decline in microbial degradation capability at greater soil depth (Holden and Fierer, 2005). Vertical variability in microbial pesticide degradation is also influenced by the history of pesticide application (Dechesne et al.,

2014) and can extend to underlying aquifer sediments Batıoğlu-Pazarbaşı et al. (2012).

In Chapter 8, in addition to its physiological importance and influence on solute movement presented in Chapter 6, soil moisture played an even greater role in pesticide degradation (Figure 10). Precipitation events determined the translocation of even highly sorptive pesticides such as glyphosate to the subsoil, bypassing the highly active first 30 cm of topsoil. This preferential transport mechanism was also demonstrated for atrazine (Edwards et al., 1993), a pesticide that also displays a relatively high sorption capacity in soils (Sun et al., 2019a). Thus, biodegradation of pesticides in the subsoil occurs in the proximity of these macropores (Dechesne et al., 2014), a soil characteristic that may remain hidden in laboratory experiments and is difficult to reproduce in its variability even in undisturbed soil column experiments. The accumulation of pesticide-degrading microorganisms on pore walls could be the result of favorable conditions, such as significant oxygen flux or the availability of earthworm exudates. To date, few studies have distinguished macropores (e.g., macropores with evidence of current or recent earthworm activity versus only hydraulically active macropores) and examined their influence on spatial distribution and biodegradation of pesticides in the subsoil (Dechesne et al., 2014). Based on the confirmed hypothesis that preferential flow pathways determine the transport of pesticides in structured soils, this work emphasizes the interrelationship with prevailing environmental factors, suggesting the need for application time and substance-specific concentration ranges in agricultural applications to be of great importance in assessing environmental risk and water protection.

The most important results in terms of a more realistic assessment of the fate of pesticides in soils derive from the study of soil structure in conjunction with simulated rainfall events. Soil heterogeneity and macropore formation determine the depth distribution of pesticides and whether degradation occurs in a high- or low-activity microbial zone, and therefore may explain the inconsistencies in results of residence times under laboratory and field conditions. As a final recommendation, systematically

designed field studies should be conducted to collect solid data on the status quo of pesticide contamination in agricultural soils and on biodegradability under regional seasonal environmental conditions, with emphasis on rainfall distribution. Recognizing the multitude of other soil and environmental conditions that control pesticide degradation, we examined underrepresented variables such as concentration dependence, the combination of concentration, temperature, and soil water content, and soil structure as a stand-alone feature related to heavy rainfall events on pesticide degradation. More comprehensive long-term studies are needed to evaluate the risk of pesticide residence time in soil in different agricultural soils.

11 General conclusion and outlook

In this thesis, the degradation of two selected pesticides - a highly mobile (MCPA) and an immobile (glyphosate) herbicide - was systematically investigated at both laboratory and field scales to obtain a basic mechanistic understanding of pesticide degradation and to verify the latter under realistic conditions and extend it to field-scale processes. The following key findings of this thesis may provide an initial explanation for the divergence between actual and predicted residence times of pesticides in soils. They do provide a basis for directing future pesticide studies toward a more realistic assessment of their residence times in soils.

In the future, the risk of pesticide impairment of soil functions should not be considered as an isolated problem; rather, it should be considered in interaction with other environmental stressors. In particular, the role of the recently emerged pollutant class microplastics (MPs) as a transport vehicle for chemical pollutants in soil organisms has not yet been adequately studied in soils (Zhang and Xu, 2022). Ecosystem responses to climate change may not be additive or linear (Gill et al., 2002; Burkett et al., 2005; Suseela et al., 2012), and microbes may exhibit threshold responses (Porporato et al., 2004; Suseela et al., 2012). Identification of these nonlinearities and thresholds can reduce

some uncertainties in pesticide use in the context of ongoing climate change and support decision making for substance approval (Zhou et al., 2008) and can be most convincingly identified when pesticide degradation experiments include multiple stages of each climate factor, such as increasing drought or heavy local precipitation (Suseela et al., 2012).

12 Acknowledgements

I would like to thank all my colleagues, family and friends for their support during my PhD. Not to leave anyone unmentioned, I would like to express my general gratitude to all the people who helped me.

13 Curriculum Vitae

Johannes Wirsching

Date of birth: 21.02.1989

Place of birth: Waiblingen, Germany

https://orcid.org/0000-0003-3843-4114

EDUCATION

2018-2023	PhD student at the Institute of Soil Science and Land Evaluation, Soil biology (Prof. Ellen Kandeler), University of Hohenheim
2014-2018	Master degree in Soil science, University of Hohenheim, Germany
2007-2014	Bachelor degree in Environmental science, Albert Ludwigs University Freiburg, Germany

WORK EXPERIENCE

2019 – 2022	Lecturer of the module Environmental Pollution and soil microorganism for the Master Programs ENVIROFOOD, ENVIRO and Landscape Ecology, University of Hohenheim, Germany, summer semester 2019-2022
2014-2014	Engineering office Wehrstein Geotechnik, Fellbach (January-September)

Place, Date

Signature of the student

14 Declaration

Annex 3

Declaration in lieu of an oath on independent work according to Sec. 18(3) sentence 5 of the University of Hohenheim's Doctoral Regulations for the Faculties of Agricultural Sciences, Natural Sciences, and Business, Economics and Social Sciences

1. The dissertation submitted on the topic

Constraints on microbial pesticide degradation in Soils

is work done independently by me.

2. I only used the sources and aids listed and did not make use of any impermissible assistance from third parties. In particular, I marked all content taken word-for-word or paraphrased from other works.

3. I did not use the assistance of a commercial doctoral placement or advising agency.

4. I am aware of the importance of the declaration in lieu of oath and the criminal consequences of false or incomplete declarations in lieu of oath.

I confirm that the declaration above is correct. I declare in lieu of oath that I have declared only the truth to the best of my knowledge and have not omitted anything.

Place, Date	Signature of the student

15 Reference

Allison, S.D., Wallenstein, M.D., Bradford, M.A., 2010. Soil-carbon response to warming dependent on microbial physiology. Nature Geoscience 3, 336–340. URL: https://doi.org/10.1038/ngeo846.

Aparicio, V.C., De Gerónimo, E., Marino, D., Primost, J., Carriquiriborde, P., Costa, J.L., 2013. Environmental fate of glyphosate and aminomethylphosphonic acid in surface waters and soil of agricultural basins. Chemosphere 93, 1866–1873. URL: https://doi.org/10.1016/j.chemosphere.2013.06.041.

Arora, P.K., Bae, H., 2014. Bacterial degradation of chlorophenols and their derivatives. Microbial Cell Factories 13, 1–17.

Audus, L.J., 1952. The decomposition of 2:4-dichlorophenoxyacetic acid and 2-methyl-4-chlorophenoxyacetic acid in the soil. Journal of the Science of Food and Agriculture 3, 268–274. URL: https://doi.org/10.1002/jsfa.2740030607.

Authority, E.F.S., Medina-Pastor, P., Triacchini, G., 2020. The 2018 european union report on pesticide residues in food. EFSA Journal 18.

Autio, S., Siimes, K., Laitinen, P., Rämö, S., Oinonen, S., Eronen, L., 2004. Adsorption of sugar beet herbicides to finnish soils. Chemosphere 55, 215–226. URL: https://doi.org/10.1016/j.chemosphere.2003.10.015.

Babey, T., Vieublé-gonod, L., Rapaport, A., Pinheiro, M., Garnier, P., Dreuzy, J.r.D., 2017. Spatiotemporal simulations of 2 , 4-D pesticide degradation by microorganisms in 3D soil-core experiments. Ecological Modelling 344, 48–61. URL: http://dx.doi.org/10.1016/j.ecolmodel.2016.11.006.

Badawi, N., Johnsen, A.R., Sørensen, J., Aamand, J., 2013. Centimeter-scale spatial variability in 2-methyl-4-chlorophenoxyacetic acid mineralization increases with depth in agricultural soil. Journal of environmental quality 42, 683–689.

Baelum, J., Henriksen, T., Hansen, H.C.B., Jacobsen, C.S., 2006. Degradation of 4-chloro-2-methylphenoxyacetic acid in top- and subsoil is quantitatively linked to the class III tfdA gene. Applied and environmental microbiology 72, 1476–1486. doi:10.1128/AEM.72.2.1476-1486.2006.

Bælum, J., Henriksen, T., Hansen, H.C.B., Jacobsen, C.S., 2006. Degradation of 4-chloro-2-methylphenoxyacetic acid in top-and subsoil is quantitatively linked to the class iii tfda gene. Applied and Environmental Microbiology 72, 1476–1486.

Bælum, J., Nicolaisen, M.H., Holben, W.E., Strobel, B.W., Sørensen, J., Jacobsen, C.S., 2008a. Direct analysis of tfda gene expression by indigenous bacteria in phenoxy acid amended agricultural soil. The ISME journal 2, 677–687.

Bælum, J., Nicolaisen, M.H., Holben, W.E., Strobel, B.W., Sørensen, J., Jacobsen, C.S., 2008b. Direct analysis of tfdA gene expression by indigenous bacteria in phenoxy acid amended agricultural soil. ISME Journal 2, 677–687. doi:10.1038/ismej.2008.21.

Bailey, G.W., White, J.L., 1970. Factors influencing the adsorption, desorption, and movement of pesticides in soil. Single Pesticide Volume: The Triazine Herbicides , 29–92.

Bailey, V.L., Smith, A.P., Tfaily, M., Fansler, S.J., Bond-Lamberty, B., 2017. Differences in soluble organic carbon chemistry in pore waters sampled from different pore size domains. Soil Biology and Biochemistry 107, 133–143. doi:10.1016/j.soilbio.2016.11.025.

Bajaj, S., Singh, D.K., 2015. Biodegradation of persistent organic pollutants in soil,

water and pristine sites by cold-adapted microorganisms: Mini review. International biodeterioration & biodegradation 100, 98–105.

Balthazor, T.M., Hallas, L.E., 1986. Glyphosate-degrading microorganisms from industrial activated sludge. Applied and Environmental Microbiology 51, 432–434.

Barja, B., dos Santos Afonso, M., 2005. Aminomethylphosphonic acid and glyphosate adsorption onto goethite: a comparative study. Environmental science & technology 39, 585–592.

Barrett, K., McBride, M., 2005. Oxidative degradation of glyphosate and aminomethylphosphonate by manganese oxide. Environmental science & technology 39, 9223–9228.

Batıoğlu-Pazarbaşı, M., Bælum, J., Johnsen, A.R., Sørensen, S.R., Albrechtsen, H.J., Aamand, J., 2012. Centimetre-scale vertical variability of phenoxy acid herbicide mineralization potential in aquifer sediment relates to the abundance of tfda genes. FEMS Microbiology Ecology 80, 331–341.

Battaglin, W.A., Meyer, M., Kuivila, K., Dietze, J., 2014. Glyphosate and its degradation product ampa occur frequently and widely in us soils, surface water, groundwater, and precipitation. JAWRA Journal of the American Water Resources Association 50, 275–290. URL: https://doi.org/10.1111/jawr.12159.

Baumgarten, C., Bilharz, M., Döring, U., Eisold, A., Friedrich, B., Frische, T., Gather, C., Günther, D., Wichtrup, W.G., Hofmeier, K., Hofmeier, M., Jering, A., Langner, M., Leujak, W., Marx, M., Matthey, A., Mohaupt, V., Osiek, D., Penn-Bressel, G., Plambeck, N.O., Pohl, M., Rechenber, J, Scheuschner, T, Seven, J, Ullrich, A, Vogel, I., Walter, AB, Wolter, R, Zimmermann, A., 2008. Daten zur umwelt ausgabe 2018, umwelt und landwirtschaft .

Bevan, R., Brown, T., Matthies, F., Sams, C., Jones, K., Hanlon, J., La Vedrine, M., 2017. Human biomonitoring data collection from occupational exposure to pesticides. EFSA Supporting Publications 14, 1185E.

Biederbeck, V., Campbell, C., Smith, A., 1987. Effects of long-term 2, 4-D field applications on soil biochemical processes. Technical Report. Wiley Online Library.

Blake, L., Goulding, K., 2002. Effects of atmospheric deposition, soil ph and acidification on heavy metal contents in soils and vegetation of semi-natural ecosystems at rothamsted experimental station, uk. Plant and soil 240, 235–251.

Bligh, E.G., Dyer, W.J., 1959. A rapid method of total lipid extraction and purification. Canadian journal of biochemistry and physiology 37, 911–917. URL: https://doi.org/10.1139/o59-099.

Boer, W.d., Folman, L.B., Summerbell, R.C., Boddy, L., 2005. Living in a fungal world: impact of fungi on soil bacterial niche development. FEMS microbiology reviews 29, 795–811.

Boivin, P., Garnier, P., Tessier, D., 2004. Relationship between clay content, clay type, and shrinkage properties of soil samples. Soil Science Society of America Journal 68, 1145–1153.

Borggaard, O.K., Gimsing, A.L., 2008. Fate of glyphosate in soil and the possibility of leaching to ground and surface waters: a review. Pest Management Science: formerly Pesticide Science 64, 441–456. URL: https://doi.org/10.1002/ps.1512.

Bouckaert, L., Sleutel, S., Van Loo, D., Brabant, L., Cnudde, V., Van Hoorebeke, L., De Neve, S., 2013. Carbon mineralisation and pore size classes in undisturbed soil cores. Soil Research 51, 14–22.

Bouseba, B., Zertal, A., Beguet, J., Rouard, N., Devers, M., Martin, C., Martin-Laurent,

F., 2009. Evidence for 2,4-D mineralisation in Mediterranean soils. Pest Management Science 65, 1021–1029. doi:10.1002/ps.1789.

Brunner, W., Focht, D.D., 1984. Deterministic three-half-order kinetic model for microbial degradation of added carbon substrates in soil. Applied and Environmental microbiology 47, 167–172.

Bundt, M., Widmer, F., Pesaro, M., Zeyer, J., Blaser, P., 2001. Preferential flow paths: biological 'hot spots' in soils. Soil Biology and Biochemistry 33, 729–738.

Burkett, V.R., Wilcox, D.A., Stottlemyer, R., Barrow, W., Fagre, D., Baron, J., Price, J., Nielsen, J.L., Allen, C.D., Peterson, D.L., et al., 2005. Nonlinear dynamics in ecosystem response to climatic change: case studies and policy implications. Ecological complexity 2, 357–394.

Cakmak, I., Yazici, A., Tutus, Y., Ozturk, L., 2009. Glyphosate reduced seed and leaf concentrations of calcium, manganese, magnesium, and iron in non-glyphosate resistant soybean. European Journal of Agronomy 31, 114–119.

Carvalho, F.P., 2017. Pesticides, environment, and food safety. Food and energy security 6, 48–60.

Casado, J., Brigden, K., Santillo, D., Johnston, P., 2019. Screening of pesticides and veterinary drugs in small streams in the european union by liquid chromatography high resolution mass spectrometry. Science of the total environment 670, 1204–1225.

Castillo, M.d.P., Torstensson, L., 2007. Effect of Biobed Composition, Moisture, and Temperature on the Degradation of Pesticides. Journal of Agricultural and Food Chemistry 55, 5725–5733. doi:10.1021/jf0707637.

Castro Jr, J.V., Peralba, M.C., Ayub, M.A., 2007. Biodegradation of the herbicide glyphosate by filamentous fungi in platform shaker and batch bioreactor. Journal of Environmental Science and Health, Part B 42, 883–886.

Cattaneo, M.V., Masson, C., Greer, C.W., 1997. The influence of moisture on microbial transport, survival and 2,4-D biodegradation with a genetically marked Burkholderia cepacia in unsaturated soil columns. Biodegradation 8, 87–96. URL: https://doi.org/10.1023/A:1008236401342TS-CrossRef.

Chavez Rodriguez, L., Ingalls, B., Schwarz, E., Streck, T., Uksa, M., Pagel, H., 2020. Gene-Centric Model Approaches for Accurate Prediction of Pesticide Biodegradation in Soils. Environmental Science & Technology 54, 13638–13650. doi:10.1021/acs.est.0c03315.

Choi, J.S., Fermanian, T.W., Wehner, D.J., Spomer, L.A., 1988. Effect of Temperature, Moisture, and Soil Texture on DCPA Degradation. Agronomy Journal 80, 108. doi:10.2134/agronj1988.00021962008000010024x.

Chowdhury, A., Pradhan, S., Saha, M., Sanyal, N., 2008. Impact of pesticides on soil microbiological parameters and possible bioremediation strategies. Indian Journal of Microbiology 48, 114–127. doi:10.1007/s12088-008-0011-8.

Coche, A., Babey, T., Rapaport, A., Vieublé-Gonod, L., Garnier, P., de Dreuzy, J.R., 2018. Interaction of porosity structures and microbial uptake dynamics in the degradation of pesticides at μm and mm scales, in: Computational Methods in Water Resources XXII (CMWR), pp. 2–p.

Cooper, J., Dobson, H., 2007. The benefits of pesticides to mankind and the environment. Crop Protection 26, 1337–1348.

Cosgrove, S., Jefferson, B., Jarvis, P., 2019. Pesticide removal from drinking water sources by adsorption: a review. Environmental Technology Reviews 8, 1–24.

Craine, J.M., Gelderman, T.M., 2011. Soil moisture controls on temperature sensitivity of soil organic carbon decomposition for a mesic grassland. Soil Biology and Biochemistry 43, 455–457.

Creamer, C.A., Jones, D.L., Baldock, J.A., Farrell, M., 2014. Stoichiometric controls upon low molecular weight carbon decomposition. Soil Biology and Biochemistry 79, 50–56.

Cruz, M.S.R., Jones, J.E., Bending, G.D., 2008. Study of the spatial variation of the biodegradation rate of the herbicide bentazone with soil depth using contrasting incubation methods. Chemosphere 73, 1211–1215.

Dacal, M., Delgado-Baquerizo, M., Barquero, J., Berhe, A.A., Gallardo, A., Maestre, F.T., García-Palacios, P., 2021. Temperature Increases Soil Respiration Across Ecosystem Types and Soil Development, But Soil Properties Determine the Magnitude of This Effect. Ecosystems doi:10.1007/s10021-021-00648-2.

Danganan, C.E., Ye, R.W., Daubaras, D.L., Xun, L., Chakrabarty, A., 1994. Nucleotide sequence and functional analysis of the genes encoding 2, 4, 5-trichlorophenoxyacetic acid oxygenase in pseudomonas cepacia ac1100. Applied and environmental microbiology 60, 4100–4106.

Davidson, E.A., Janssens, I.A., 2006. Temperature sensitivity of soil carbon decomposition and feedbacks to climate change. Nature 440, 165–173. doi:10.1038/nature04514.

Dechesne, A., Badawi, N., Aamand, J., Smets, B.F., 2014. Fine scale spatial variability of microbial pesticide degradation in soil: scales, controlling factors, and implications. Frontiers in microbiology 5, 667.

Dechesne, A., Owsianiak, M., Bazire, A., Grundmann, G.L., Binning, P.J., Smets, B.F., 2010. Biodegradation in a partially saturated sand matrix: compounding effects of water content, bacterial spatial distribution, and motility. Environmental science & technology 44, 2386–2392.

Denef, K., Bubenheim, H., Lenhart, K., Vermeulen, J., Cleemput, O.V., Boeckx, P., Müller, C., 2007. Community shifts and carbon translocation within metabolically-

active rhizosphere microorganisms in grasslands under elevated co 2. Biogeosciences 4, 769–779. URL: https://doi.org/10.5194/bg-4-769-2007.

Dideriksen, K., Stipp, S., 2003. The adsorption of glyphosate and phosphate to goethite: a molecular-scale atomic force microscopy study. Geochimica et Cosmochimica Acta 67, 3313–3327.

Ditterich, F., Poll, C., Pagel, H., Babin, D., Smalla, K., Horn, M.A., Streck, T., Kandeler, E., 2013a. Succession of bacterial and fungal 4-chloro-2-methylphenoxyacetic acid degraders at the soil–litter interface. FEMS microbiology ecology 86, 85–100.

Ditterich, F., Poll, C., Pagel, H., Babin, D., Smalla, K., Horn, M.A., Streck, T., Kandeler, E., 2013b. Succession of bacterial and fungal 4-chloro-2-methylphenoxyacetic acid degraders at the soil – litter interface. FEMS Microbiology Ecology 86, 85–100. doi:10.1111/1574-6941.12131.

Dollinger, J., Dagès, C., Voltz, M., 2015. Glyphosate sorption to soils and sediments predicted by pedotransfer functions. Environmental chemistry letters 13, 293–307.

Domeignoz-Horta, L.A., Pold, G., Liu, X.J.A., Frey, S.D., Melillo, J.M., DeAngelis, K.M., 2020. Microbial diversity drives carbon use efficiency in a model soil. Nature Communications 11, 3684. doi:10.1038/s41467-020-17502-z.

Dörfler, U., Haala, R., Matthies, M., Scheunert, I., 1996. Mineralization kinetics of chemicals in soils in relation to environmental conditions. Ecotoxicology and environmental safety 34, 216–222. URL: https://doi.org/10.1006/eesa.1996.0066.

Duke, S.O., 2018. The history and current status of glyphosate. Pest management science 74, 1027–1034.

Dunn, M., Ramirez-Trujillo, J., Hernández-Lucas, I., 2009. Major roles of isocitrate

lyase and malate synthase in bacterial and fungal pathogenesis. Microbiology 155, 3166–3175.

Duo-Sen, L., Shui-Ming, Z., 1987a. Kinetic model for degradative processes of pesticides in soil. Ecological modelling 37, 131–138.

Duo-Sen, L., Shui-Ming, Z., 1987b. Kinetic model for degradative processes of pesticides in soil. Ecological Modelling 37, 131–138. doi:10.1016/0304-3800(87)90021-4.

EC, 2020a .

Edwards, W.M., Shipitalo, M., Owens, L., Dick, W., 1993. Factors affecting preferential flow of water and atrazine through earthworm burrows under continuous no-till corn. Journal of environmental quality 22, 453–457.

EFSA, 2008. Opinion on a request from efsa related to the default q10 value used to describe the temperature effect on transformation rates of pesticides in soil-scientific opinion of the panel on plant protection products and their residues (ppr panel). EFSA Journal 6, 622.

EFSA, et al., 2015. Conclusion on the peer review of the pesticide risk assessment of the active substance ferric phosphate. EFSA Journal 13.

Egli, T., 2010. How to live at very low substrate concentration. Water Research 44, 4826–4837.

Fan, J., Yang, G., Zhao, H., Shi, G., Geng, Y., Hou, T., Tao, K., 2012. Isolation, identification and characterization of a glyphosate-degrading bacterium, bacillus cereus cb4, from soil. The Journal of general and applied microbiology 58, 263–271.

FAO, I., 2017. Global assessment of the impact of plant protection products on soil functions and soil ecosystems. FAO, Rome .

Fenner, K., Canonica, S., Wackett, L.P., Elsner, M., 2013. Evaluating pesticide degradation in the environment: blind spots and emerging opportunities. science 341, 752–758.

Firdous, S., Iqbal, S., Anwar, S., 2020. Optimization and modeling of glyphosate biodegradation by a novel comamonas odontotermitis p2 through response surface methodology. Pedosphere 30, 618–627.

Firdous, S., Iqbal, S., Anwar, S., Jabeen, H., 2018. Identification and analysis of 5-enolpyruvylshikimate-3-phosphate synthase (epsps) gene from glyphosate-resistant ochrobactrum intermedium sq20. Pest management science 74, 1184–1196.

Flury, M., 1996. Experimental evidence of transport of pesticides through field soils—a review. Journal of environmental quality 25, 25–45.

Fomsgaard, I.S., 1997a. Modelling the mineralization kinetics for low concentrations of pesticides in surface and subsurface soil. Ecological Modelling 102, 175–208.

Fomsgaard, I.S., 1997b. Modelling the mineralization kinetics for low concentrations of pesticides in surface and subsurface soil. Ecological Modelling 102, 175–208. doi:10.1016/S0304-3800(97)01982-0.

Fomsgaard, I.S., Kristensen, K., 1999a. Influence of microbial activity, organic carbon content, soil texture and soil depth on mineralisation rates of low concentrations of 14c-mecoprop—development of a predictive model. Ecological Modelling 122, 45–68.

Fomsgaard, I.S., Kristensen, K., 1999b. Influence of microbial activity, organic carbon content, soil texture and soil depth on mineralisation rates of low concentrations of 14C-mecoprop—development of a predictive model. Ecological Modelling 122, 45–68. doi:10.1016/S0304-3800(99)00118-0.

Franklin, S.M., Kravchenko, A.N., Vargas, R., Vasilas, B., Fuhrmann, J.J., Jin, Y., 2021.

The unexplored role of preferential flow in soil carbon dynamics. Soil Biology and Biochemistry , 108398.

Fredslund, L., Vinther, F.P., Brinch, U.C., Elsgaard, L., Rosenberg, P., Jacobsen, C.S., 2008. Spatial Variation in 2-Methyl-4-chlorophenoxyacetic Acid Mineralization and Sorption in a Sandy Soil at Field Level. Journal of Environmental Quality 37, 1918–1928. doi:10.2134/jeq2006.0208.

Frey, S.D., Lee, J., Melillo, J.M., Six, J., 2013. The temperature response of soil microbial efficiency and its feedback to climate. Nature Climate Change 3, 395–398. doi:10.1038/nclimate1796.

Frostegård, A., Bååth, E., 1996. The use of phospholipid fatty acid analysis to estimate bacterial and fungal biomass in soil. Biology and Fertility of soils 22, 59–65. URL: https://doi.org/10.1007/BF00384433.

Frostegård, Å., Bååth, E., Tunlio, A., 1993. Shifts in the structure of soil microbial communities in limed forests as revealed by phospholipid fatty acid analysis. Soil Biology and Biochemistry 25, 723–730. URL: https://doi.org/10.1016/0038-0717(93)90113-P.

Funke, T., Han, H., Healy-Fried, M.L., Fischer, M., Schönbrunn, E., 2006. Molecular basis for the herbicide resistance of roundup ready crops. Proceedings of the National Academy of Sciences 103, 13010–13015.

Gallego, S., Devers-Lamrani, M., Rousidou, K., Karpouzas, D.G., Martin-Laurent, F., 2019. Assessment of the effects of oxamyl on the bacterial community of an agricultural soil exhibiting enhanced biodegradation. Science of the Total Environment 651, 1189–1198.

Gavrilescu, M., 2005. Fate of pesticides in the environment and its bioremediation. Engineering in life sciences 5, 497–526.

Gawlik, B.M., Lamberty, A., Pauwels, J., Blum, W.E.H., Mentler, A., Bussian, B., Eklo, O., Fox, K., Kördel, W., Hennecke, D., Maurer, T., Perrin-Ganier, C., Pflugmacher, J., Romero-Taboada, E., Szabo, G., Muntau, H., 2003. Certification of the European reference soil set (IRMM-443—EUROSOILS). Part I. Adsorption coefficients for atrazine, 2,4-D and lindane. Science of The Total Environment 312, 23–31. doi:10.1016/S0048-9697(03)00193-1.

Geissen, V., Silva, V., Lwanga, E.H., Beriot, N., Oostindie, K., Bin, Z., Pyne, E., Busink, S., Zomer, P., Mol, H., et al., 2021. Cocktails of pesticide residues in conventional and organic farming systems in europe–legacy of the past and turning point for the future. Environmental Pollution 278, 116827.

Geyer, K.M., Dijkstra, P., Sinsabaugh, R., Frey, S.D., 2019. Clarifying the interpretation of carbon use efficiency in soil through methods comparison. Soil Biology and Biochemistry 128, 79–88. doi:10.1016/j.soilbio.2018.09.036.

Geyer, K.M., Kyker-Snowman, E., Grandy, A.S., Frey, S.D., 2016. Microbial carbon use efficiency: accounting for population, community, and ecosystem-scale controls over the fate of metabolized organic matter. Biogeochemistry 127, 173–188. doi:10.1007/s10533-016-0191-y.

Gill, R.A., Polley, H.W., Johnson, H.B., Anderson, L.J., Maherali, H., Jackson, R.B., 2002. Nonlinear grassland responses to past and future atmospheric co2. Nature 417, 279–282.

Gimsing, A., Borggaard, O., Bang, M., 2004. Influence of soil composition on adsorption of glyphosate and phosphate by contrasting danish surface soils. European Journal of Soil Science 55, 183–191.

Gimsing, A.L., Borggaard, O.K., 2001. Effect of kcl and cacl2 as background electrolytes

on the competitive adsorption of glyphosate and phosphate on goethite. Clays and Clay Minerals 49, 270–275.

Glass, R.L., 1987. Adsorption of glyphosate by soils and clay minerals. Journal of Agricultural and Food Chemistry 35, 497–500.

Goebel, M., Bachmann, J., Reichstein, M., Janssens, I.A., Guggenberger, G., 2011. Soil water repellency and its implications for organic matter decomposition–is there a link to extreme climatic events? Global Change Biology 17, 2640–2656.

González-Valenzuela, L.E., Dussán, J., 2018. Molecular assessment of glyphosate-degradation pathway via sarcosine intermediate in lysinibacillus sphaericus. Environmental Science and Pollution Research 25, 22790–22796.

Goverde, M., van der Heijden, M., Wiemken, A., Sanders, I., Erhardt, A., 2000. Arbuscular mycorrhizal fungi influence life history traits of a lepidopteran herbivore. Oecologia 125, 362–369.

Gözdereliler, E., Boon, N., Aamand, J., De Roy, K., Granitsiotis, M.S., Albrechtsen, H.J., Sørensen, S.R., 2013. Comparing metabolic functionalities, community structures, and dynamics of herbicide-degrading communities cultivated with different substrate concentrations. Applied and environmental microbiology 79, 367–375. doi:10.1128/AEM.02536-12.

Greer, L.E., Shelton, D.R., 1992. Effect of inoculant strain and organic matter content on kinetics of 2, 4-dichlorophenoxyacetic acid degradation in soil. Applied and Environmental Microbiology 58, 1459–1465.

Griffin, D.M., 1969. Soil water in the ecology of fungi. Annual Review of Phytopathology , 289–310doi:10.1146/annurev.py.07.090169.001445.

Griffin, D.M., 1981. Water Potential as a Selective Factor in the Microbial Ecology of Soils, in: Parr, J.F., Gardner, W.R., Elliott, L.F. (Eds.), Water Potential Relations in

Soil Microbiology. SSSA, [S.l.]. SSSA Special Publications TS - CrossRef, pp. 141–151. doi:10.2136/sssaspecpub9.c5.

Großkopf, T., Soyer, O.S., 2016. Microbial diversity arising from thermodynamic constraints. The ISME journal 10, 2725–2733.

Grunewald, K., Schmidt, W., Unger, C., Hanschmann, G., 2001. Behavior of glyphosate and aminomethylphosphonic acid (ampa) in soils and water of reservoir radeburg ii catchment (saxony/germany). Journal of Plant Nutrition and Soil Science 164, 65–70.

Guengerich, F.P., 2015. Introduction: Metals in biology: α-ketoglutarate/iron-dependent dioxygenases. Journal of Biological Chemistry 290, 20700–20701.

Haberkon, N.B.R., Aparicio, V.C., Buschiazzo, D.E., De Geronimo, E., Aimar, S.B., Costa, J.L., Mendez, M.J., 2020. Glyphosate and ampa concentrations in the respirable dust emitted experimentally by soil aggregates, shortly after herbicide application. Geoderma 369, 114334. URL: https://doi.org/10.1016/j.geoderma.2020.114334.

Hagedorn, F., Bruderhofer, N., Ferrari, A., Niklaus, P.A., 2015. Tracking litter-derived dissolved organic matter along a soil chronosequence using 14c imaging: biodegradation, physico-chemical retention or preferential flow? Soil Biology and Biochemistry 88, 333–343.

Hamamoto, S., Moldrup, P., Kawamoto, K., Komatsu, T., 2010. Excluded-volume expansion of Archie's law for gas and solute diffusivities and electrical and thermal conductivities in variably saturated porous media. Water Resources Research 46. doi:10.1029/2009WR008424.

Harms, H., Wick, L., Schlosser, D., 2017. The fungal community in organically polluted systems. The fungal community: its organization and role in the ecosystem, 4th edn. CRC, Boca Raton, FL , 459–469.

Hedlund, J., Longo, S.B., York, R., 2020. Agriculture, pesticide use, and economic development: a global examination (1990–2014). Rural Sociology 85, 519–544.

Helweg, A., 1987a. Degradation and adsorption of 14c-mcpa in soil—influence of concentration, temperature and moisture content on degradation. Weed research 27, 287–296.

Helweg, A., 1987b. Degradation and adsorption of 14C-MCPA in soil—influence of concentration, temperature and moisture content on degradation. Weed Research 27, 287–296. doi:10.1111/j.1365-3180.1987.tb00765.x.

Helweg, A., 1993a. Degradation and adsorption of 14c-mecoprop (mcpp) in surface soils and in subsoil. influence of temperature, moisture content, sterilization and concentration on degradation. Science of the Total Environment 132, 229–241.

Helweg, A., 1993b. Degradation and adsorption of 14C-mecoprop (MCPP) in surface soils and in subsoil. Influence of temperature, moisture content, sterilization and concentration on degradation. Science of The Total Environment 132, 229–241. doi:10.1016/0048-9697(93)90134-R.

Helweg, A., Fomsgaard, I.S., Reffstrup, T.K., S rensen, H., 1998a. Degradation of mecoprop and isoproturon in soil influence of initial concentration. International journal of environmental analytical chemistry 70, 133–148.

Helweg, A., Fomsgaard, I.S., Reffstrup, T.K., Srensen, H., 1998b. Degradation of Mecoprop and Isoproturon in Soil Influence of Initial Concentration. International Journal of Environmental Analytical Chemistry 70, 133–148. doi:10.1080/03067319808032610.

Herrero-Hernández, E., Marín-Benito, J., Andrades, M., Sánchez-Martín, M., Rodríguez-Cruz, M., 2015. Field versus laboratory experiments to evaluate the fate of azoxystrobin in an amended vineyard soil. Journal of environmental management 163, 78–86.

Hiller, E., Bartaľ, M., Milička, J., Čerňanský, S., 2009. Environmental Fate of the Herbicide MCPA in Two Soils as Affected by the Presence of Wheat Ash. Water, Air, and Soil Pollution 197, 395–402. doi:10.1007/s11270-008-9820-y.

Hiller, E., Khun, M., Zemanová, L., Jurkovic, L., Bartal, M., 2006. Laboratory study of retention and release of weak acid herbicide mcpa by soils and sediments and leaching potential of mcpa. Plant Soil and Environment 52, 550.

Hiller, E., Tatarková, V., Šimonovičová, A., et al., 2012. Sorption, desorption, and degradation of (4-chloro-2-methylphenoxy) acetic acid in representative soils of the danubian lowland, slovakia. Chemosphere 87, 437–444.

Holden, P.A., Fierer, N., 2005. Microbial processes in the vadose zone. Vadose Zone Journal 4, 1–21.

Hornsby, A.G., Wauchope, R.D., Herner, A., 1995. Pesticide properties in the environment. Springer Science & Business Media.

Huang, W., Chang, Y., 1998. A thermodynamic analysis of the ni al system. Intermetallics 6, 487–498.

Ilstedt, U., Nordgren, A., Malmer, A., 2000. Optimum soil water for soil respiration before and after amendment with glucose in humid tropical acrisols and a boreal mor layer. Soil Biology and Biochemistry 32, 1591–1599. doi:10.1016/S0038-0717(00)00073-0.

Ingalls, B., 2008. Sensitivity Analysis : from model parameters to system behaviour Local Sensitivity Analysis : Derivation. Essays in biochemistry 45, 177–193.

Jacob, B., Trine, H., Bruun, H.H.C., Suhr, J.C., 2006. Degradation of 4-Chloro-2-Methylphenoxyacetic Acid in Top- and Subsoil Is Quantitatively Linked to the Class III tfdA Gene. Applied and Environmental Microbiology 72, 1476–1486. doi:10.1128/AEM.72.2.1476-1486.2006.

Jacob, G., Garbow, J., Hallas, L., Kimack, N., Kishore, G., Schaefer, J., 1988. Metabolism of glyphosate in pseudomonas sp. strain lbr. Applied and environmental microbiology 54, 2953–2958.

Jacobsen, C.S., van der Keur, P., Iversen, B.V., Rosenberg, P., Barlebo, H.C., Torp, S., Vosgerau, H., Juhler, R.K., Ernstsen, V., Rasmussen, J., et al., 2008. Variation of mcpa, metribuzine, methyltriazine-amine and glyphosate degradation, sorption, mineralization and leaching in different soil horizons. Environmental pollution 156, 794–802.

Jacobsen, C.S., Pedersen, J.C., 1991. Mineralization of 2, 4-dichlorophenoxyacetic acid (2, 4-d) in soil inoculated with pseudomonas cepacia dbo1 (pro101), alcaligenes eutrophus aeo106 (pro101) and alcaligenes eutrophus jmp134 (pjp4): effects of inoculation level and substrate concentration. Biodegradation 2, 253–263.

Jensen, P.H., Hansen, H.C.B., Rasmussen, J., Jacobsen, O.S., 2004. Sorption-controlled degradation kinetics of mcpa in soil. Environmental science & technology 38, 6662–6668.

Joergensen, R.G., 1996. The fumigation-extraction method to estimate soil microbial biomass: calibration of the kec value. Soil Biology and Biochemistry 28, 25–31.

Johnsen, A.R., Binning, P.J., Aamand, J., Badawi, N., Rosenbom, A.E., 2013. The gompertz function can coherently describe microbial mineralization of growth-sustaining pesticides. Environmental science & technology 47, 8508–8514.

Johnson, T.A., Ellsworth, T.R., Hudson, R.J., Sims, G.K., 2013. Diffusion limitation for atrazine biodegradation in soil .

Jones, D.L., Olivera-Ardid, S., Klumpp, E., Knief, C., Hill, P.W., Lehndorff, E., Bol, R., 2018. Moisture activation and carbon use efficiency of soil microbial communities

along an aridity gradient in the Atacama Desert. Soil Biology and Biochemistry 117, 68–71. doi:10.1016/j.soilbio.2017.10.026.

Jury, W.A., Spencer, W.F., Farmer, W.J., 1987. Behavior Assessment Model for Trace Organics in Soil: I. Model Description. Journal of Environmental Quality 16, 448. doi:10.2134/jeq1987.00472425001600040027x.

Kaestner, M., Nowak, K.M., Miltner, A., Trapp, S., Schaeffer, A., 2014. Classification and modelling of nonextractable residue (ner) formation of xenobiotics in soil–a synthesis. Critical Reviews in Environmental Science and Technology 44, 2107–2171.

Kah, M., Brown, C., 2006. Adsorption of ionisable pesticides in soils. Reviews of environmental contamination and toxicology , 149–217.

Kanissery, R.G., Welsh, A., Sims, G.K., 2015. Effect of soil aeration and phosphate addition on the microbial bioavailability of carbon-14-glyphosate. Journal of environmental quality 44, 137–144.

Karanasios, E., Karpouzas, D.G., Tsiropoulos, N.G., 2012. Key parameters and practices controlling pesticide degradation efficiency of biobed substrates. Journal of Environmental Science and Health, Part B 47, 589–598. doi:10.1080/03601234.2012.665753.

Karpouzas, D.G., Papadopoulou, E., Ipsilantis, I., Friedel, I., Petric, I., Udikovic-Kolic, N., Djuric, S., Kandeler, E., Menkissoglu-Spiroudi, U., Martin-Laurent, F., 2014. Effects of nicosulfuron on the abundance and diversity of arbuscular mycorrhizal fungi used as indicators of pesticide soil microbial toxicity. Ecological Indicators 39, 44–53.

Kästner, M., Nowak, K.M., Miltner, A., Schäffer, A., 2016. (multiple) isotope probing approaches to trace the fate of environmental chemicals and the formation of non-extractable 'bound'residues. Current opinion in biotechnology 41, 73–82.

Keesstra, S.D., Geissen, V., Mosse, K., Piiranen, S., Scudiero, E., Leistra, M., van Schaik, L., 2012. Soil as a filter for groundwater quality. Current Opinion in Environmental Sustainability 4, 507–516.

Kenward, M., Roger, J., 1997. The precision of fixed effects estimates from restricted maximum likelihood. Biometrics 53, 983–997.

Kitagawa, W., Takami, S., Miyauchi, K., Masai, E., Kamagata, Y., Tiedje, J.M., Fukuda, M., 2002a. Novel 2, 4-dichlorophenoxyacetic acid degradation genes from oligotrophic bradyrhizobium sp. strain hw13 isolated from a pristine environment. Journal of Bacteriology 184, 509–518.

Kitagawa, W., Takami, S., Miyauchi, K., Masai, E., Kamagata, Y., Tiedje, J.M., Fukuda, M., 2002b. Novel 2,4-dichlorophenoxyacetic acid degradation genes from oligotrophic Bradyrhizobium sp. strain HW13 isolated from a pristine environment. Journal of bacteriology 184, 509–518. doi:10.1128/jb.184.2.509-518.2002.

Kjær, J., Olsen, P., Ullum, M., Grant, R., 2005. Leaching of glyphosate and amino-methylphosphonic acid from danish agricultural field sites. Journal of Environmental Quality 34, 608–620.

Köhne, J.M., Köhne, S., Šimnek, J., 2009. A review of model applications for structured soils: b) pesticide transport. Journal of contaminant hydrology 104, 36–60.

Koricheva, J., Gange, A.C., Jones, T., 2009. Effects of mycorrhizal fungi on insect herbivores: a meta-analysis. Ecology 90, 2088–2097.

Kozak, M., Piepho, H.P., 2018. What's normal anyway? residual plots are more telling than significance tests when checking anova assumptions. Journal of Agronomy and Crop Science 204, 86–98.

Kramer, J.K., Hernandez, M., Cruz-Hernandez, C., Kraft, J., Dugan, M.E., 2008. Combining results of two gc separations partly achieves determination of all cis and

trans 16: 1, 18: 1, 18: 2 and 18: 3 except cla isomers of milk fat as demonstrated using ag-ion spe fractionation. Lipids 43, 259–273. URL: https://doi.org/10.1007/s11745-007-3143-4.

Kravchenko, A., Guber, A., Razavi, B., Koestel, J., Blagodatskaya, E., Kuzyakov, Y., 2019. Spatial patterns of extracellular enzymes: combining x-ray computed micro-tomography and 2d zymography. Soil Biology and Biochemistry 135, 411–419.

Krzyśko-Lupicka, T., Strof, W., Kubś, K., Skorupa, M., Wieczorek, P., Lejczak, B., Kafarski, P., 1997. The ability of soil-borne fungi to degrade organophosphonate carbon-to-phosphorus bonds. Applied microbiology and biotechnology 48, 549–552.

Kumar Singh, B., Walker, A., Wright, D., 2002. Persistence of chlorpyrifos, fenamiphos, chlorothalonil, and pendimethalin in soil and their effects on soil microbial characteristics. Bulletin of Environmental Contamination and Toxicology 69, 181–188.

Kuzyakov, Y., 2010. Priming effects: interactions between living and dead organic matter. Soil Biology and Biochemistry 42, 1363–1371.

Kuzyakov, Y., Blagodatskaya, E., 2015. Microbial hotspots and hot moments in soil: concept & review. Soil Biology and Biochemistry 83, 184–199.

Laidler, K.J., 1984. The development of the Arrhenius equation. Journal of Chemical Education 61, 494. doi:10.1021/ed061p494.

Larsen, L., Sørensen, S.R., Aamand, J., 2000. Mecoprop, isoproturon, and atrazine in and above a sandy aquifer: vertical distribution of mineralization potential. Environmental science & technology 34, 2426–2430.

Ledger, T., Pieper, D., González, B., 2006. Chlorophenol hydroxylases encoded by plasmid pjp4 differentially contribute to chlorophenoxyacetic acid degradation. Applied and Environmental Microbiology 72, 2783–2792.

Lenth, R., Buerkner, P., Herve, M., Love, J., Riebl, H., Singmann, H., 2020. emmeans. URL: https://github.com/rvlenth/emmeansM4-Citavi.

Leveau, J.H., KoÈnig, F., FuÈchslin, H., Werlen, C., Van Der Meer, J.R., 1999a. Dynamics of multigene expression during catabolic adaptation of ralstonia eutropha jmp134 (pjp4) to the herbicide 2, 4-dichlorophenoxyacetate. Molecular microbiology 33, 396–406.

Leveau, J.H., Zehnder, A.J., van der Meer, J.R., 1998. The tfdk gene product facilitates uptake of 2, 4-dichlorophenoxyacetate by ralstonia eutropha jmp134 (pjp4). Journal of Bacteriology 180, 2237–2243.

Leveau, J.H.J., König, F., Füchslin, H., Werlen, C., Van Der Meer, J.R., 1999b. Dynamics of multigene expression during catabolic adaptation of Ralstonia eutropha JMP134 (pJP4) to the herbicide 2 , 4-dichlorophenoxyacetate. Molecular Microbiology 33, 396–406. doi:10.1046/j.1365-2958.1999.01483.x.

LfL, 2020. Information zum wirkstoff glyphosat. Bayerische Landesanstalt für Landwirtschaft .

Li, H., Joshi, S.R., Jaisi, D.P., 2016. Degradation and isotope source tracking of glyphosate and aminomethylphosphonic acid. Journal of agricultural and food chemistry 64, 529–538.

López-Gutiérrez, J.C., Henry, S., Hallet, S., Martin-Laurent, F., Catroux, G., Philippot, L., 2004. Quantification of a novel group of nitrate-reducing bacteria in the environment by real-time pcr. Journal of microbiological methods 57, 399–407.

López-Gutiérrez, J.C., Henry, S., Hallet, S., Martin-Laurent, F., Catroux, G., Philippot, L., 2004. Quantification of a novel group of nitrate-reducing bacteria in the environment by real-time PCR. Journal of Microbiological Methods 57, 399–407. doi:10.1016/j.mimet.2004.02.009.

Lupi, L., Miglioranza, K.S., Aparicio, V.C., Marino, D., Bedmar, F., Wunderlin, D.A., 2015. Occurrence of glyphosate and ampa in an agricultural watershed from the southeastern region of argentina. Science of the total environment 536, 687–694. URL: https://doi.org/10.1016/j.scitotenv.2015.07.090.

Mackay, D., Shiu, W.Y., Lee, S.C., 2006. Handbook of physical-chemical properties and environmental fate for organic chemicals. CRC press.

Malwade, A., Nguyen, A., Sadat-Mousavi, P., Ingalls, B.P., 2017. Predictive modeling of a batch filter mating process. Frontiers in Microbiology 8, 1–11. doi:10.3389/fmicb.2017.00461.

Manzoni, S., Čapek, P., Mooshammer, M., Lindahl, B.D., Richter, A., Šantrůčková, H., 2017. Optimal metabolic regulation along resource stoichiometry gradients. Ecology Letters 20, 1182–1191. doi:10.1111/ele.12815.

Manzoni, S., Čapek, P., Porada, P., Thurner, M., Winterdahl, M., Beer, C., Brüchert, V., Frouz, J., Herrmann, A.M., Lindahl, B.D., et al., 2018. Reviews and syntheses: Carbon use efficiency from organisms to ecosystems–definitions, theories, and empirical evidence. Biogeosciences 15, 5929–5949. URL: https://doi.org/10.5194/bg-15-5929-2018.

Manzoni, S., Molini, A., Porporato, A., 2011. Stochastic modelling of phytoremediation. Proceedings of the Royal Society A: Mathematical, Physical and Engineering Sciences 467, 3188–3205. URL: https://doi.org/10.1098/rspa.2011.0209.

Manzoni, S., Porporato, A., 2009. Soil carbon and nitrogen mineralization: Theory and models across scales. Soil Biology and Biochemistry 41, 1355–1379. doi:https://doi.org/10.1016/j.soilbio.2009.02.031.

Manzoni, S., Schaeffer, S.M., Katul, G., Porporato, A., Schimel, J.P., 2014. A theoretical analysis of microbial eco-physiological and diffusion limitations to carbon cycling in

drying soils. Soil Biology and Biochemistry 73, 69–83. doi:10.1016/j.soilbio.2014.02.008.

Manzoni, S., Schimel, J.P., Porporato, A., 2012a. Responses of soil microbial communities to water stress: results from a meta-analysis. Ecology 93, 930–938. doi:10.1890/11-0026.1.

Manzoni, S., Taylor, P., Richter, A., Porporato, A., Ågren, G.I., 2012b. Environmental and stoichiometric controls on microbial carbon-use efficiency in soils. New Phytologist 196, 79–91.

Margesin, R., Miteva, V., 2011. Diversity and ecology of psychrophilic microorganisms. Research in microbiology 162, 346–361.

McManus, S.L., Richards, K.G., Grant, J., Mannix, A., Coxon, C.E., 2014. Pesticide occurrence in groundwater and the physical characteristics in association with these detections in ireland. Environmental monitoring and assessment 186, 7819–7836.

Miglioranza, K.S., Sagrario, M.d.l.A.G., de Moreno, J.E.A., Moreno, V.J., Escalante, A.H., Osterrieth, M.L., 2002. Agricultural soil as a potential source of input of organochlorine pesticides into a nearby pond. Environmental Science and Pollution Research 9, 250–256.

Monod, J., 1942. Recherches sur la croissance des cultures bacteriennes .

Morales, M., Allegrini, M., Basualdo, J., Villamil, M., Zabaloy, M., 2020. Primer design to assess bacterial degradation of glyphosate and other phosphonates. Journal of Microbiological Methods 169, 105814.

Morton, P.A., Fennell, C., Cassidy, R., Doody, D., Fenton, O., Mellander, P.E., Jordan, P., 2020. A review of the pesticide mcpa in the land-water environment and emerging research needs. Wiley Interdisciplinary Reviews: Water 7, e1402.

Moyano, F.E., Manzoni, S., Chenu, C., 2013. Responses of soil heterotrophic respiration to moisture availability: An exploration of processes and models. Soil Biology and Biochemistry 59, 72–85. doi:10.1016/j.soilbio.2013.01.002.

Mueller, T.C., Moorman, T.B., Snipes, C.E., 1992. Effect of concentration, sorption, and microbial biomass on degradation of the herbicide fluometuron in surface and subsurface soils. Journal of agricultural and food chemistry 40, 2517–2522.

Muskus, A.M., Krauss, M., Miltner, A., Hamer, U., Nowak, K.M., 2019a. Effect of temperature, pH and total organic carbon variations on microbial turnover of 13C315N-glyphosate in agricultural soil. Science of The Total Environment 658, 697–707. doi:https://doi.org/10.1016/j.scitotenv.2018.12.195.

Muskus, A.M., Krauss, M., Miltner, A., Hamer, U., Nowak, K.M., 2019b. Effect of temperature, ph and total organic carbon variations on microbial turnover of 13c315n-glyphosate in agricultural soil. Science of the Total Environment 658, 697–707.

Muskus, A.M., Krauss, M., Miltner, A., Hamer, U., Nowak, K.M., 2020. Degradation of glyphosate in a Colombian soil is influenced by temperature, total organic carbon content and pH. Environmental Pollution 259, 113767. doi:10.1016/j.envpol.2019.113767.

Muskus, A.M., Miltner, A., Hamer, U., Nowak, K.M., 2022. Microbial community composition and glyphosate degraders of two soils under the influence of temperature, total organic carbon and ph. Environmental Pollution , 118790.

Napoli, M., Cecchi, S., Zanchi, C.A., Orlandini, S., 2015. Leaching of glyphosate and aminomethylphosphonic acid through silty clay soil columns under outdoor conditions. Journal of environmental quality 44, 1667–1673. URL: https://doi.org/10.2134/jeq2015.02.0104.

Newman, M.M., Lorenz, N., Hoilett, N., Lee, N.R., Dick, R.P., Liles, M.R., Ramsier, C., Kloepper, J.W., 2016. Changes in rhizosphere bacterial gene expression following glyphosate treatment. Science of the Total Environment 553, 32–41.

Nicolaisen, M.H., Bælum, J., Jacobsen, C.S., Sørensen, J., 2008a. Transcription dynamics of the functional tfda gene during mcpa herbicide degradation by cupriavidus necator aeo106 (pro101) in agricultural soil. Environmental Microbiology 10, 571–579.

Nicolaisen, M.H., Bælum, J., Jacobsen, C.S., Sørensen, J., 2008b. Transcription dynamics of the functional tfdA gene during MCPA herbicide degradation by Cupriavidus necator AEO106 (pRO101) in agricultural soil. Environmental Microbiology 10, 571–579. doi:10.1111/j.1462-2920.2007.01476.x.

Niu, B., Zhang, X., Piao, S., Janssens, I.A., Fu, G., He, Y., Zhang, Y., Shi, P., Dai, E., Yu, C., et al., 2021. Warming homogenizes apparent temperature sensitivity of ecosystem respiration. Science Advances 7, eabc7358.

Nivelle, E., Verzeaux, J., Chabot, A., Roger, D., Chesnais, Q., Ameline, A., Lacoux, J., Nava-Saucedo, J.E., Tétu, T., Catterou, M., 2018. Effects of glyphosate application and nitrogen fertilization on the soil and the consequences on aboveground and belowground interactions. Geoderma 311, 45–57.

Nowak, K.M., Miltner, A., Gehre, M., Schäffer, A., Kästner, M., 2011a. Formation and Fate of Bound Residues from Microbial Biomass during 2,4-D Degradation in Soil. Environmental Science & Technology 45, 999–1006. doi:10.1021/es103097f.

Nowak, K.M., Miltner, A., Gehre, M., Schaffer, A., Kastner, M., 2011b. Formation and fate of bound residues from microbial biomass during 2, 4-d degradation in soil. Environmental science & technology 45, 999–1006.

Nowak, K.M., Miltner, A., Poll, C., Kandeler, E., Streck, T., Pagel, H., 2020a. Plant litter enhances degradation of the herbicide MCPA and increases formation of biogenic

non-extractable residues in soil. Environment international 142, 105867. doi:10.1016/j.envint.2020.105867.

Nowak, K.M., Miltner, A., Poll, C., Kandeler, E., Streck, T., Pagel, H., 2020b. Plant litter enhances degradation of the herbicide mcpa and increases formation of biogenic non-extractable residues in soil. Environment International 142, 105867.

Obojska, A., Lejczak, B., Kubrak, M., 1999. Degradation of phosphonates by streptomycete isolates. Applied microbiology and biotechnology 51, 872–876.

Ockleford, C., Adriaanse, P., Berny, P., Brock, T., Duquesne, S., Grilli, S., Hernandez-Jerez, A., Bennekou, S., Klein, M., Kuhl, T., et al., 2017. Scientific opinion addressing the state of the science on risk assessment of plant protection products for in-soil organisms. efsa j.

Oh, K.H., Ahn, S.K., Yoon, K.H., Kim, Y.S., 1995. Biodegradation of the phenoxy herbicide MCPA by microbial consortia isolated from a rice field. Bulletin of Environmental Contamination and Toxicology 55. doi:10.1007/BF00196033.

Padgette, S.R., Kolacz, K.H., Delannay, X., Re, D., LaVallee, B., Tinius, C., Rhodes, W., Otero, Y., Barry, G., Eichholtz, D., et al., 1995. Development, identification, and characterization of a glyphosate-tolerant soybean line. Crop science 35, 1451–1461.

Pagel, H., Kriesche, B., Uksa, M., Poll, C., Kandeler, E., Schmidt, V., Streck, T., 2020. Spatial Control of Carbon Dynamics in Soil by Microbial Decomposer Communities. URL: https://www.frontiersin.org/article/10.3389/fenvs.2020.00002.

Pagel, H., Poll, C., Ingwersen, J., Kandeler, E., Streck, T., 2016. Modeling coupled pesticide degradation and organic matter turnover: From gene abundance to process rates. Soil Biology and Biochemistry 103, 349–364. doi:10.1016/j.soilbio.2016.09.014.

Pallud, C., Dechesne, A., Gaudet, J., Debouzie, D., Grundmann, G., 2004. Modification of spatial distribution of 2, 4-dichlorophenoxyacetic acid degrader microhabitats during growth in soil columns. Applied and Environmental Microbiology 70, 2709–2716.

Papendick, R.I., Campbell, G.S., 1981. Theory and Measurement of Water Potential. doi:10.2136/sssaspecpub9.c1.

Parker, L.W., Doxtader, K.G., 1983. Kinetics of the Microbial Degradation of 2,4-D in Soil. Journal of Environmental Quality 12, 553–558. doi:10.2134/jeq1983.00472425001200040024x.

Parr, J.F., Gardner, W.R., Elliott, L.F., 1981. Water Potential Relations in Soil Microbiology. SSSA, [S.l.]. doi:10.2136/sssaspecpub9.

Paszko, T., 2011. Adsorption and desorption processes of mcpa in polish mineral soils. Journal of Environmental Science and Health, Part B 46, 569–580.

Paszko, T., Muszyński, P., Materska, M., Bojanowska, M., Kostecka, M., Jackowska, I., 2016. Adsorption and degradation of phenoxyalkanoic acid herbicides in soils: a review. Environmental Toxicology and Chemistry 35, 271–286.

Patfield, D., Matheson, G., 2008. Robust non-linear regression using aic scores .

Patzko, T., 2009. Degradation of MCPA in soil horizons of polish agricultural soils. Polish Journal of Environmental Studies , 1083–1091.

Pemberton, J., 1979. Evolution and spread of pesticide degrading ability among soil micro-organisms. Plasmids of medical, environmental and commercial importance .

Peña, D., López-Piñeiro, A., Albarrán, Á., Becerra, D., Sánchez-Llerena, J., 2015. Environmental fate of the herbicide MCPA in agricultural soils amended with fresh and aged de-oiled two-phase olive mill waste. Environmental Science and Pollution Research 22, 13915–13925. doi:10.1007/s11356-015-4622-4.

Pereira, J.L., Antunes, S.C., Castro, B.B., Marques, C.R., Gonçalves, A.M., Gonçalves, F., Pereira, R., 2009. Toxicity evaluation of three pesticides on non-target aquatic and soil organisms: commercial formulation versus active ingredient. Ecotoxicology 18, 455–463.

Peterson, G.E., 1967. The discovery and development of 2, 4-d. Agricultural history 41, 243–254.

Piccolo, A., Celano, G., Arienzo, M., Mirabella, A., 1994. Adsorption and desorption of glyphosate in some european soils. Journal of Environmental Science & Health Part B 29, 1105–1115. URL: https://doi.org/10.1080/03601239409372918.

Pinheiro, J., Bates, D., DebRoy, S., Sarkar, D., 2020. Linear and Nonlinear Mixed Effects Models URL: https://cran.r-project.org/package=nlme.

Pinheiro, M., Garnier, P., Beguet, J., Laurent, F.M., Gonod, L.V., 2015a. The millimetre-scale distribution of 2, 4-d and its degraders drives the fate of 2, 4-d at the soil core scale. Soil Biology and Biochemistry 88, 90–100.

Pinheiro, M., Garnier, P., Beguet, J., Martin Laurent, F., Vieublé Gonod, L., 2015b. The millimetre-scale distribution of 2,4-D and its degraders drives the fate of 2,4-D at the soil core scale. Soil Biology and Biochemistry 88, 90–100. doi:10.1016/j.soilbio.2015.05.008.

Pinheiro, M., Pagel, H., Poll, C., Ditterich, F., Garnier, P., Streck, T., Kandeler, E., Gonod, L.V., 2018. Water flow drives small scale biogeography of pesticides and bacterial pesticide degraders-a microcosm study using 2, 4-d as a model compound. Soil Biology and Biochemistry 127, 137–147.

Pipke, R., Amrhein, N., 1988. Degradation of the phosphonate herbicide glyphosate by arthrobacter atrocyaneus atcc 13752. Applied and Environmental Microbiology 54, 1293–1296.

Pizzul, L., del Pilar Castillo, M., Stenström, J., 2009. Degradation of glyphosate and other pesticides by ligninolytic enzymes. Biodegradation 20, 751–759.

Pold, G., Domeignoz-Horta, L.A., Morrison, E.W., Frey, S.D., Sistla, S.A., DeAngelis, K.M., 2020. Carbon use efficiency and its temperature sensitivity covary in soil bacteria. mBio 11, e02293–19. doi:10.1128/mBio.02293-19.

Poll, C., Pagel, H., Devers-Lamrani, M., Martin-Laurent, F., Ingwersen, J., Streck, T., Kandeler, E., 2010a. Regulation of bacterial and fungal mcpa degradation at the soil–litter interface. Soil Biology and Biochemistry 42, 1879–1887.

Poll, C., Pagel, H., Devers-Lamrani, M., Martin-Laurent, F., Ingwersen, J., Streck, T., Kandeler, E., 2010b. Regulation of bacterial and fungal MCPA degradation at the soil–litter interface. Soil Biology and Biochemistry 42, 1879–1887. doi:10.1016/j.soilbio.2010.07.013.

Popp, J., Pető, K., Nagy, J., 2013. Pesticide productivity and food security. a review. Agronomy for sustainable development 33, 243–255.

Porporato, A., Daly, E., Rodriguez-Iturbe, I., 2004. Soil water balance and ecosystem response to climate change. The American Naturalist 164, 625–632.

Preusser, S., Liebmann, P., Stucke, A., Wirsching, J., Müller, K., Mikutta, R., Guggenberger, G., Don, A., Kalbitz, K., Bachmann, J., et al., 2021. Microbial utilization of aboveground litter-derived organic carbon within a sandy dystric cambisol profile. Frontiers in Soil Science 1, 3.

Priestman, M.A., Funke, T., Singh, I.M., Crupper, S.S., Schönbrunn, E., 2005. 5-enolpyruvylshikimate-3-phosphate synthase from staphylococcus aureus is insensitive to glyphosate. FEBS letters 579, 728–732.

Quéméner, D.L., Bouchez, T., et al., 2014. A thermodynamic theory of microbial growth. The ISME journal 8, 1747–1751.

Rabbi, S.M.F., Daniel, H., Lockwood, P.V., Macdonald, C., Pereg, L., Tighe, M., Wilson, B.R., Young, I.M., 2016. Physical soil architectural traits are functionally linked to carbon decomposition and bacterial diversity. Scientific reports 6, 1–9.

Ramakrishnan, B., Venkateswarlu, K., Sethunathan, N., Megharaj, M., 2019. Local applications but global implications: Can pesticides drive microorganisms to develop antimicrobial resistance? Science of the Total Environment 654, 177–189.

Rampelotto, P.H., 2010. Resistance of microorganisms to extreme environmental conditions and its contribution to astrobiology. Sustainability 2, 1602–1623.

Reedich, L.M., Millican, M.D., Koch, P.L., 2017. Temperature Impacts on Soil Microbial Communities and Potential Implications for the Biodegradation of Turfgrass Pesticides. Journal of Environmental Quality 46, 490–497. doi:10.2134/jeq2017.02.0067.

Reffstrup, T.K., Sørensen, H., Helweg, A., 1998. Degradation of mecoprop at different concentrations in surface and sub-surface soil. Pesticide science 52, 126–132.

Richter, O., Diekkrüger, B., Nörtersheuser, P., 2008. Environmental fate modelling of pesticides: from the laboratory to the field scale. John Wiley & Sons.

Riedo, J., Wettstein, F.E., Rosch, A., Herzog, C., Banerjee, S., Buchi, L., Charles, R., Wachter, D., Martin-Laurent, F., Bucheli, T.D., et al., 2021. Widespread occurrence of pesticides in organically managed agricultural soils—the ghost of a conventional agricultural past? Environmental Science & Technology 55, 2919–2928.

Rodríguez-Cruz, M.S., Bælum, J., Shaw, L.J., Sørensen, S.R., Shi, S., Aspray, T., Jacobsen, C.S., Bending, G.D., 2010. Biodegradation of the herbicide mecoprop-p with soil depth and its relationship with class iii tfda genes. Soil Biology and Biochemistry 42, 32–39.

Rodríguez-Cruz, M.S., Jones, J.E., Bending, G.D., 2006. Field-scale study of the

variability in pesticide biodegradation with soil depth and its relationship with soil characteristics. Soil Biology and Biochemistry 38, 2910–2918.

Rosenbom, A.E., Binning, P.J., Aamand, J., Dechesne, A., Smets, B.F., Johnsen, A.R., 2014. Does microbial centimeter-scale heterogeneity impact mcpa degradation in and leaching from a loamy agricultural soil? Science of the total environment 472, 90–98.

Rubol, S., Freixa, A., Carles-Brangarí, A., Fernandez-Garcia, D., Romaní, A.M., Sanchez-Vila, X., 2014. Connecting bacterial colonization to physical and biochemical changes in a sand box infiltration experiment. Journal of hydrology 517, 317–327.

Rueppel, M.L., Brightwell, B.B., Schaefer, J., Marvel, J.T., 1977. Metabolism and degradation of glyphosate in soil and water. Journal of Agricultural and Food Chemistry 25, 517–528.

Ruess, L., Schütz, K., Migge-Kleian, S., Häggblom, M.M., Kandeler, E., Scheu, S., 2007. Lipid composition of collembola and their food resources in deciduous forest stands—implications for feeding strategies. Soil Biology and Biochemistry 39, 1990–2000. URL: https://doi.org/10.1016/j.soilbio.2007.03.002.

Rumpel, C., Kögel-Knabner, I., 2011. Deep soil organic matter—a key but poorly understood component of terrestrial c cycle. Plant and soil 338, 143–158.

Russell, J.B., Cook, G.M., 1995. Energetics of bacterial growth: balance of anabolic and catabolic reactions. Microbiological Reviews 59, 48–62. doi:10.1128/mr.59.1.48-62.1995.

Sarmah, A.K., Müller, K., Ahmad, R., 2004. Fate and behaviour of pesticides in the agroecosystem—a review with a new zealand perspective. Soil Research 42, 125–154.

Schimel, J., Balser, T.C., Wallenstein, M., 2007. Microbial stress-response physiology and its implications for ecosystem function. Ecology 88, 1386–1394. doi:10.1890/06-0219.

Schimel, J.P., Schaeffer, S.M., 2012. Microbial control over carbon cycling in soil. Frontiers in microbiology 3, 348. doi:10.3389/fmicb.2012.00348PM-23055998.

Schlögl, J., Wimmer, B., Cramaro, L., Wirsching, J., Poll, C., Pagel, H., Kandeler, E., Huhn, C., Griebler, C., Stumpp, C., Haderlein, S.B., 2022. Heavy rainfall following a summer drought stimulates soil redox dynamics and facilitates rapid and deep translocation of glyphosate in floodplain soils. Environ. Sci.: Processes Impacts URL: http://dx.doi.org/10.1039/D1EM00527H.

Schoen, S., Winterlin, W., 1987. The effects of various soil factors and amendments on the degradation of pesticide mixtures. Journal of Environmental Science and Health, Part B 22, 347–377. doi:10.1080/03601238709372561.

Schöpfer, L., Menzel, R., Schnepf, U., Ruess, L., Marhan, S., Brümmer, F., Pagel, H., Kandeler, E., 2020. Microplastics effects on reproduction and body length of the soil-dwelling nematode caenorhabditis elegans. Frontiers in Environmental Science 8, 41.

Schroll, R., Becher, H.H., Dörfler, U., Gayler, S., Grundmann, S., Hartmann, H.P., Ruoss, J., 2006. Quantifying the effect of soil moisture on the aerobic microbial mineralization of selected pesticides in different soils. Environmental Science & Technology 40, 3305–3312. doi:10.1021/es052205j.

Selinger, D.W., Saxena, R.M., Cheung, K.J., Church, G.M., Rosenow, C., 2003. Global rna half-life analysis in escherichia coli reveals positional patterns of transcript degradation. Genome research 13, 216–223.

Sharma, A., Kumar, V., Shahzad, B., Tanveer, M., Sidhu, G.P.S., Handa, N., Kohli, S.K., Yadav, P., Bali, A.S., Parihar, R.D., et al., 2019. Worldwide pesticide usage and its impacts on ecosystem. SN Applied Sciences 1, 1–16.

Sheals, J., Sjöberg, S., Persson, P., 2002. Adsorption of glyphosate on goethite: molecular characterization of surface complexes. Environmental science & technology 36, 3090–3095.

Sierra, C.A., Trumbore, S.E., Davidson, E.A., Vicca, S., Janssens, I., 2015. Sensitivity of decomposition rates of soil organic matter with respect to simultaneous changes in temperature and moisture. Journal of Advances in Modeling Earth Systems 7, 335–356. doi:https://doi.org/10.1002/2014MS000358.

Silva, V., Mol, H.G., Zomer, P., Tienstra, M., Ritsema, C.J., Geissen, V., 2019a. Pesticide residues in european agricultural soils–a hidden reality unfolded. Science of the Total Environment 653, 1532–1545.

Silva, V., Mol, H.G.J., Zomer, P., Tienstra, M., Ritsema, C.J., Geissen, V., 2019b. Pesticide residues in European agricultural soils – A hidden reality unfolded. Science of The Total Environment 653, 1532–1545. doi:10.1016/j.scitotenv.2018.10.441.

Silva, V., Montanarella, L., Jones, A., Fernández-Ugalde, O., Mol, H.G., Ritsema, C.J., Geissen, V., 2018. Distribution of glyphosate and aminomethylphosphonic acid (ampa) in agricultural topsoils of the european union. Science of the Total Environment 621, 1352–1359.

Simonsen, L., Fomsgaard, I.S., Svensmark, B., Spliid, N.H., 2008. Fate and availability of glyphosate and ampa in agricultural soil. Journal of Environmental Science and Health, Part B 43, 365–375.

Singh, S., Kumar, V., Chauhan, A., Datta, S., Wani, A.B., Singh, N., Singh, J., 2018. Toxicity, degradation and analysis of the herbicide atrazine. Environmental chemistry letters 16, 211–237.

Singh, S., Kumar, V., Singh, J., 2019. Kinetic study of the biodegradation of glyphosate

by indigenous soil bacterial isolates in presence of humic acid, fe (iii) and cu (ii) ions. Journal of Environmental Chemical Engineering 7, 103098.

Sinsabaugh, R.L., Manzoni, S., Moorhead, D.L., Richter, A., 2013. Carbon use efficiency of microbial communities. Ecology Letters 16, 930–939. doi:10.1111/ele.12113.

Socías-Viciana, M., Fernández-Pérez, M., Villafranca-Sánchez, M., González-Pradas, E., Flores-Céspedes, F., 1999. Sorption and leaching of atrazine and mcpa in natural and peat-amended calcareous soils from spain. Journal of Agricultural and Food Chemistry 47, 1236–1241.

Sørensen, S.R., Schultz, A., Jacobsen, O.S., Aamand, J., 2006. Sorption, desorption and mineralisation of the herbicides glyphosate and mcpa in samples from two danish soil and subsurface profiles. Environmental Pollution 141, 184–194.

Sparling, G.P., West, A.W., Reynolds, J., 1989. Influence of soil moisture regime on the respiration response of soils subjected to osmotic stress. Soil Research 27, 161–168. doi:10.1071/SR9890161.

Spinelli, V., Ceci, A., Dal Bosco, C., Gentili, A., Persiani, A.M., 2021. Glyphosate-eating fungi: Study on fungal saprotrophic strains' ability to tolerate and utilise glyphosate as a nutritional source and on the ability of purpureocillium lilacinum to degrade it. Microorganisms 9, 2179.

Steinweg, J.M., Plante, A.F., Conant, R.T., Paul, E.A., Tanaka, D.L., 2008. Patterns of substrate utilization during long-term incubations at different temperatures. Soil Biology and Biochemistry 40, 2722–2728. doi:10.1016/j.soilbio.2008.07.002.

Stenrød, M., Perceval, J., Benoit, P., Almvik, M., Bolli, R.I., Eklo, O.M., Sveistrup, T.E., Kværner, J., 2008. Cold climatic conditions: Effects on bioavailability and leaching of the mobile pesticide metribuzin in a silt loam soil in norway. Cold Regions Science and Technology 53, 4–15.

Sun, J., Ma, X.l., Wang, W., Zhang, J., Zhang, H., Wang, Y.j., Feng, J., 2019a. The adsorption behavior of atrazine in common soils in northeast china. Bulletin of environmental contamination and toxicology 103, 316–322.

Sun, K., Gao, B., Zhang, Z., Zhang, G., Zhao, Y., Xing, B., 2010. Sorption of atrazine and phenanthrene by organic matter fractions in soil and sediment. Environmental Pollution 158, 3520–3526.

Sun, M., Li, H., Jaisi, D.P., 2019b. Degradation of glyphosate and bioavailability of phosphorus derived from glyphosate in a soil-water system. Water research 163, 114840.

Suseela, V., Conant, R.T., Wallenstein, M.D., Dukes, J.S., 2012. Effects of soil moisture on the temperature sensitivity of heterotrophic respiration vary seasonally in an old-field climate change experiment. Global Change Biology 18, 336–348.

Sviridov, A., Shushkova, T., Ermakova, I., Ivanova, E., Epiktetov, D., Leontievsky, A., 2015. Microbial degradation of glyphosate herbicides. Applied Biochemistry and Microbiology 51, 188–195.

Sviridov, A.V., Shushkova, T.V., Zelenkova, N.F., Vinokurova, N.G., Morgunov, I.G., Ermakova, I.T., Leontievsky, A.A., 2012. Distribution of glyphosate and methylphosphonate catabolism systems in soil bacteria ochrobactrum anthropi and achromobacter sp. Applied microbiology and biotechnology 93, 787–796.

Thirunarayanan, K., Zimdahl, R.L., Smika, D.E., 1985. Chlorsulfuron Adsorption and Degradation in Soil. Weed Science 33, 558–563. doi:10.1017/S0043174500082849.

Tournier, E., Amenc, L., Pablo, A.L., Legname, E., Blanchart, E., Plassard, C., Robin, A., Bernard, L., 2015. Modification of a commercial dna extraction kit for safe and rapid recovery of dna and rna simultaneously from soil, without the use of harmful solvents. MethodsX 2, 182–191.

Treves, D., Xia, B., Zhou, J., Tiedje, J., 2003. A two-species test of the hypothesis that spatial isolation influences microbial diversity in soil. Microbial Ecology 45, 20–28.

Ugalde-Salas, P., Quéméner, D.L., Harmand, J., Rapaport, A., Bouchez, T., et al., 2020. Insights from microbial transition state theory on monod's affinity constant. Scientific reports 10, 1–4.

Van Bruggen, A.H., He, M.M., Shin, K., Mai, V., Jeong, K., Finckh, M., Morris Jr, J., 2018. Environmental and health effects of the herbicide glyphosate. Science of the total environment 616, 255–268.

Van Der Heijden, M.G., Bruin, S.d., Luckerhoff, L., Van Logtestijn, R.S., Schlaeppi, K., 2016. A widespread plant-fungal-bacterial symbiosis promotes plant biodiversity, plant nutrition and seedling recruitment. The ISME journal 10, 389–399.

Vance, E.D., Brookes, P.C., Jenkinson, D.S., 1987. An extraction method for measuring soil microbial biomass C. Soil Biology and Biochemistry 19, 703–707. doi:10.1016/0038-0717(87)90052-6.

Veiga, F., Zapata, J., Marcos, M.F., Alvarez, E., 2001. Dynamics of glyphosate and aminomethylphosphonic acid in a forest soil in galicia, north-west spain. Science of the Total Environment 271, 135–144.

Vereecken, H., 2005. Mobility and leaching of glyphosate: a review. Pest Management Science: formerly Pesticide Science 61, 1139–1151. URL: https://doi.org/10.1002/ps.1122.

Veresoglou, S.D., Chen, B., Rillig, M.C., 2012. Arbuscular mycorrhiza and soil nitrogen cycling. Soil Biology and Biochemistry 46, 53–62.

Vieublé Gonod, L., 2002. Variabilité spatiale de la minéralisation de substrats carbonés (2,4-D, leucine, lysine) dans la matrice solide du sol. Theses. Université Claude Bernard Lyon 1. URL: https://hal.inrae.fr/tel-02831087.

Vieublé Gonod, L., Chadoeuf, J., Chenu, C., 2006. Spatial distribution of microbial 2, 4-dichlorophenoxy acetic acid mineralization from field to microhabitat scales. Soil Science Society of America Journal 70, 64–71.

Villamar-Ayala, C.A., Carrera-Cevallos, J.V., Vasquez-Medrano, R., Espinoza-Montero, P.J., 2019. Fate, eco-toxicological characteristics, and treatment processes applied to water polluted with glyphosate: A critical review. Critical Reviews in Environmental Science and Technology 49, 1476–1514.

Vink, J.P., Van Der Zee, S.E., 1997. Effect of oxygen status on pesticide transformation and sorption in undisturbed soil and lake sediment. Environmental Toxicology and Chemistry: An International Journal 16, 608–616.

Vinther, F.P., Elsgaard, L., Jacobsen, O.S., 2001. Heterogeneity of bacterial populations and pesticide degradation potentials in the unsaturated zone of loamy and sandy soils. Biology and fertility of soils 33, 514–520.

Wallenstein, M.D., McMahon, S.K., Schimel, J.P., 2009. Seasonal variation in enzyme activities and temperature sensitivities in arctic tundra soils. Global Change Biology 15, 1631–1639.

Wang, G., Post, W.M., 2012. A theoretical reassessment of microbial maintenance and implications for microbial ecology modeling. FEMS Microbiology Ecology 81, 610–617.

Wang, S., Seiwert, B., Kästner, M., Miltner, A., Schäffer, A., Reemtsma, T., Yang, Q., Nowak, K.M., 2016. (bio) degradation of glyphosate in water-sediment microcosms–a stable isotope co-labeling approach. Water research 99, 91–100.

Wang, X., Lu, Z., Miller, H., Liu, J., Hou, Z., Liang, S., Zhao, X., Zhang, H., Borch, T., 2020. Fungicide azoxystrobin induced changes on the soil microbiome. Applied Soil Ecology 145, 103343.

Werner, D., Garratt, J.A., Pigott, G., 2013. Sorption of 2, 4-d and other phenoxy herbicides to soil, organic matter, and minerals. Journal of Soils and Sediments 13, 129–139.

Wimmer, B., Neidhardt, H., Schwientek, M., Haderlein, S.B., Huhn, C., 2022. Phosphate addition enhances alkaline extraction of glyphosate from highly sorptive soils and aquatic sediments. Pest Management Science .

Wimmer, B., Pattky, M., Zada, L.G., Meixner, M., Haderlein, S.B., Zimmermann, H.P., Huhn, C., 2020. Capillary electrophoresis-mass spectrometry for the direct analysis of glyphosate: method development and application to beer beverages and environmental studies. Analytical and bioanalytical chemistry 412, 4967–4983. URL: https://doi.org/10.1007/s00216-020-02751-0.

Wirsching, J., Pagel, H., Ditterich, F., Uksa, M., Werneburg, M., Zwiener, C., Berner, D., Kandeler, E., Poll, C., 2020a. Biodegradation of Pesticides at the Limit: Kinetics and Microbial Substrate Use at Low Concentrations. Frontiers in Microbiology 11, 1476. doi:10.3389/fmicb.2020.02107.

Wirsching, J., Pagel, H., Ditterich, F., Uksa, M., Werneburg, M., Zwiener, C., Berner, D., Kandeler, E., Poll, C., 2020b. Biodegradation of pesticides at the limit: Kinetics and microbial substrate use at low concentrations. Frontiers in microbiology 11, 2107.

Wolińska, A., Stępniewska, Z., 2012. Dehydrogenase activity in the soil environment. Dehydrogenases 10, 183–210.

Yao, K.Z., Shaw, B.M., Kou, B., Mcauley, K.B., Bacon, D.W., 2003. Modeling Ethylene / Butene Copolymerization with Multi-site Catalysts : Parameter Estimability and Experimental Design. Polymer Reaction Engineering 11, 563–588. doi:10.1081/PRE-120024426.

Zeglin, L.H., Bottomley, P.J., Jumpponen, A., Rice, C.W., Arango, M., Lindsley, A., McGowan, A., Mfombep, P., Myrold, D.D., 2013. Altered precipitation regime affects the function and composition of soil microbial communities on multiple time scales. Ecology 94, 2334–2345. doi:10.1890/12-2018.1.

Zelles, L., 1999. Fatty acid patterns of phospholipids and lipopolysaccharides in the characterisation of microbial communities in soil: a review. Biology and fertility of soils 29, 111–129. URL: https://doi.org/10.1007/s003740050533.

Zertal, A., Sehili, T., Boule, P., 2001. Photochemical behaviour of 4-chloro-2-methylphenoxyacetic acid: influence of ph and irradiation wavelength. Journal of Photochemistry and Photobiology A: Chemistry 146, 37–48.

Zhan, H., Feng, Y., Fan, X., Chen, S., 2018. Recent advances in glyphosate biodegradation. Applied microbiology and biotechnology 102, 5033–5043.

Zhang, M., Xu, L., 2022. Transport of micro-and nanoplastics in the environment: Trojan-horse effect for organic contaminants. Critical Reviews in Environmental Science and Technology 52, 810–846.

Zhang, Q., Phillips, R.P., Manzoni, S., Scott, R.L., Oishi, A.C., Finzi, A., Daly, E., Vargas, R., Novick, K.A., 2018. Changes in photosynthesis and soil moisture drive the seasonal soil respiration-temperature hysteresis relationship. Agricultural and Forest Meteorology 259, 184–195.

Zhou, X., Weng, E., Luo, Y., 2008. Modeling patterns of nonlinearity in ecosystem responses to temperature, co2, and precipitation changes. Ecological Applications 18, 453–466.

Zi, Z., 2011. Sensitivity analysis approaches applied to systems biology models. IET Systems Biology 5, 336–346. doi:10.1049/iet-syb.2011.0015.

Zobiole, L., Kremer, R., Oliveira Jr, R., Constantin, J., 2011. Glyphosate affects micro-organisms in rhizospheres of glyphosate-resistant soybeans. Journal of applied microbiology 110, 118–127.